TECHNIQUES FOR SIGNAL TO NOISE RATIO ADAPTATION IN INFARED OPTICAL WIRELESS FOR OPTIMISATION OF RECEIVER PERFORMANCE

MOHAMMAD FAIZ LIEW ABDULLAH

A thesis submitted in partial fulfilment of the requirements for the degree of Doctor of Philosophy

The University Of Warwick
Division of Electrical & Electronic Engineering,
School Of Engineering,
December 2006

CONTENTS **Pages**

List of Tables Pages

List of Figures Pages

GLOSSARY

AGC	Automatic gain control
BJT	Bipolar junction transistor
BTA	Bootstrapped transimpedance amplifier
CFA	Current feedback amplifier
EMI	Electro-magnetic interference
FET	Field effect transistor
FTTH	Fibre-to-the-home
IrDA	Infrared data association
LAN	Local Area Network
NF	Noise figure
QoS	Quality-of-service
SNR	Signal-to-noise ratio
VCR	Variable resistor
VFA	Voltage feedback amplifier
VFIR	Very Fast IR
VGA	Variable gain amplifier
USB	Universal serial bus

Acknowledgements

First of all I would like to thank God and the many people that had helped me to make this study and thesis possible. I am indebted to my supervisor, Prof Roger Green, for being my mentor for the last four years, for his keen guidance, encouragement and valuable comments throughout my research. I wish to thank my second supervisor, Dr. Mark Leeson for his valuable comments and suggestions throughout the research and thesis. I endeavour to pass on to future students that which I have experienced from them. I wish to express my gratitude to the Ministry of Science and Technology Malaysia and College University Technology Tun Hussein Onn for their financial support of this study.

I would also like to express my thanks to all the technical staff of the University of Warwick, Jonathan and Ian for their technical support.

I wish to thank my friends in the Communications and Signal Processing Research Group, my friends back in Malaysia and my friends who are venturing the same journey in other universities in United Kingdom for providing valuable support over the years.

Special gratitude to my loving wife, Anika Zafiah: for being a wonderful wife and for your tireless support of our family, even though you are striving for your PhD research studies at the same time. To you I wish you the very best of luck in your viva and I owe everything to you with compound interest. I wish to thank my parents, Gwi Peng for her support. A special thanks goes to my brother-in law, Akmal for his invaluable support. To our three loving children, Zu Arasy (6), Sadrina (5) and Syakib (3), who was born 4 months after we began our PhD studies, for constantly bringing joy, excitement and always testing our parenting skill. Finally this thesis is also dedicated to our "baby" who is going to be born at the end of March 2007.

DECLARATION

The work described in this thesis is entirely original and my own, except where otherwise indicated.

Parts of this work were presented at conferences, namely

"Optical Wireless Front-Ends", 2nd Malaysian Research Group Annual Conference, Manchester, Sept 2003.
(www.mrg-online.org/conference/02/mohdabdullah.htm)

"Optical Wireless Communication Front-Ends" High Frequency Postgraduate Student Colloquium, pp. 3-8, Manchester, 6-7 Sept 2004.

Signed

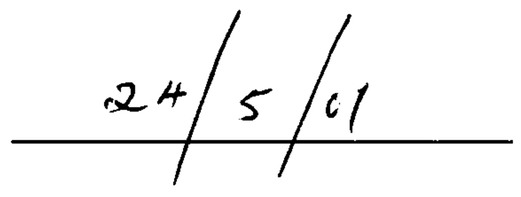

Date

ABSTRACT

The challenge of creating a new environment of links for wireless infrared and optical local area networks (LANs) is driving new innovations in the design of optical transceivers. This thesis is concerned with a systematic approach to the design of receivers for indoor optical wireless communication. In particular, it is concerned with how to offer bandwidth adjustment capability in a receiver according to the dynamic service quality of the incoming signals. Another part of the discussion of the thesis is how one can properly choose the front-end preamplifier and biasing circuitry for the photodetector. Also, comparison is made between different types of amplifier, and the methods of bandwidth enhancement.

The designs of six different techniques of integrating transimpedance amplifiers, with photodetectors to adapt an adjustable bandwidth control receiver are discussed. The proposed topologies provide an adjustable range of bandwidths for different frequency ranges, typically between 52Hz to 115MHz. The composite technique designs were used to incorporate into a system with an automatic gain control to study its effect, on an optical wireless receiver which had bandwidth adjustment and automatic gain adjustment. Theoretical analysis of noise performance for all the designed circuits is also presented. The theory and design of obstacles of indoor optical wireless receiver delivery, in addition to techniques for mitigating these effects, are discussed. This shows that infrared is a viable alternative to radio for certain applications.

Chapter 1

Introduction

1.1 Overview

Trends in the telecommunications and computer industries suggest that the network of the future will consist of a high capacity backbone network with short range communication links providing network access to portable communicators and portable computers. In this vision of the future, mobile users will have access to similar grade high-speed network services available to wired terminals. For this purpose, some parts of communication links

need to be constructed wirelessly. This situation is illustrated in Fig. 1.1. During the last decade, therefore, wireless communication technology, such as optical local area networks (LANs) and wireless infrared (IR) communication systems has grown rapidly [1.1 – 1.5]. Optical LANs use fibre as the physical transmission medium for networks serving resources within a small geographic area, while wireless IR uses free space as a communication channel for short-range, localised networks. Optical wireless communications is becoming one of the cornerstones of today's revolution in information technology because of its benefits of high speed transmission and isolation from electromagnetic interference. With the drive towards portable and multimedia communications, we are faced with the challenge of bringing the capacity of our communications infrastructure directly to the user, providing seamless access to large quantities of information anywhere and at any time. To accomplish this however, will require mid-range or short-range wireless communication links with extremely high capacity. In an extreme case, for example, uncompressed high-definition video can require a data rate of in excess of 100 Mbit/s.

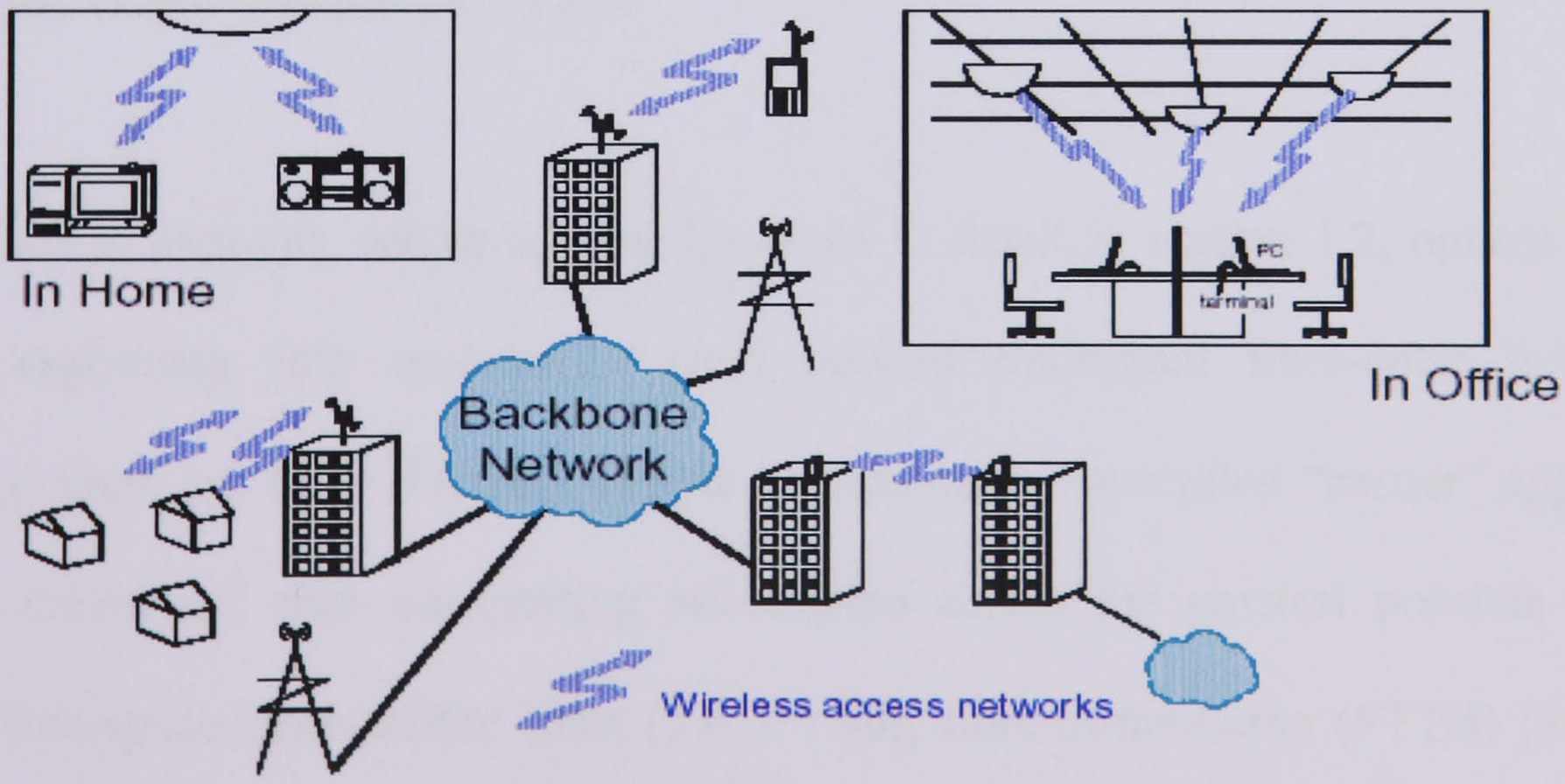

Figure 1.1 Wired backbone and wireless access network [1.1]

Light offers great advantages as a medium of communication. It enjoys unequalled channel bandwidth and is capable of data rates in the terabits per second range, whether traveling through free space or through optical fibre. This tremendous capacity is due to the nature of the photons that constitute an optical signal. Unlike electrons, photons react weakly to their environment and to one another as such optical signals neither generate nor are sensitive to electromagnetic interference (EMI), parasitic coupling and other problems faced by electrical signals [1.6]. In comparison, from IR to radio frequencies, the technology suffers from electro-magnetic interference (EMI) problems as the radio spectrum gets increasingly crowded. Now that personal communications and wireless computer networks are evolving rapidly, the available spectrum is considered to be a scarce resource. Simultaneously, there is an increase in the interference level caused by switched node power supplies and other high-frequency equipment. Particularly in hospitals and industrial environments, the applicability of radio systems is already seriously limited by these problems. Extensive frequency allocation regulations can only partly solve them. Eventually although EMI aspects will become an integral part of every system design, future applications require the exploration of new wavelength ranges.

Given their advantages, which will be discussed in detail in section 1.2, optical links are rapidly expanding into application areas beyond traditional fibre-optic links [1.7]. Basically, there are three different sample applications of so-called "carrier" applications that are concerned with transporting information across the greatest possible distance, namely free-space intersatellite links [1.8 – 1.10], fibre-to-the-home (FTTH) [1.11-1.12]

and terrestrial free-space links for inter-building communications [1.13]. Current optical LANs, represented by the Gigabit Ethernet and ATM-PON network specifications, can be used to realise high data rate systems that find their application in parallel processing environments, newspaper and magazine production, and medical imaging networks [1.14]. The immunity of fibre optic LANs to electromagnetic radiation makes this technology an attractive choice for implementation in sensitive environments, such as in aircraft and vehicles [1.15-1.16]. Furthermore, broadband requirements to connect central office locations to customer premises benefit from the high bandwidths made feasible through the use of FTTH technology. Today, the limiting factor in the deployment of advanced optical LANs is the prohibitive cost of the transmitter and receiver [1.17]. However, novel integrated circuit design techniques are helping drive down the cost of implementation, in order for these LAN solutions to become more common. Finally, so called "optical wireless links" provide a communications solution for portable applications [1.18]. In particular, short range "point-and-shoot" systems in accordance with the infrared Data Association (IrDA) standard provide a simple solution for transferring information to and from portable devices, offering high data rates at low cost and with a small form factor that is not prone to mechanical wear [1.19].

The success of such short range systems is particularly showing how optical communication systems are likely to proliferate in the future, where IrDA wireless links have overshadowed both the Universal Serial Bus (USB) and IEEE 1394 FireWire to become the leading serial port alternative for connectivity [1.20]. A new technology has been proposed for indoor, short range wireless communication, called IrGate. IrGate core

technology is based on a method of diffused-infrared (DIR) communication links, performing at high bit rates reaching up to 10Mbps [1.21]. IrDA is also extending its IR-PHY standard to 16Mbps, a new high speed extension called Very Fast IR (VFIR). VFIR is designed as an extension to the current 4Mbps FIR, where the much higher throughput enables wider applications beyond the current perception of a "wire replacement" [1.22].

Figure 1.2 and Figure 1.3 show the main features of the IrDA standards and the IR transmission speed, time and coverage area of the current implementations.

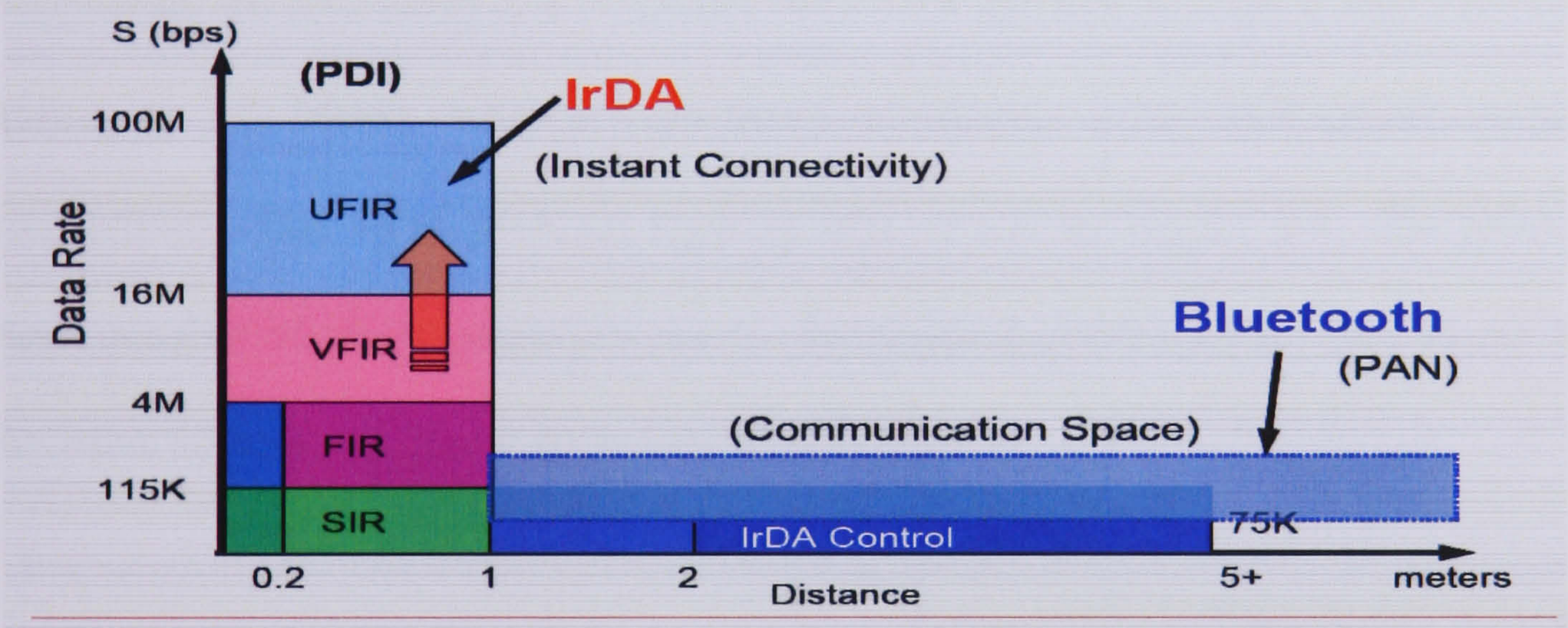

Figure 1.2 The main features of IrDA [1.23]

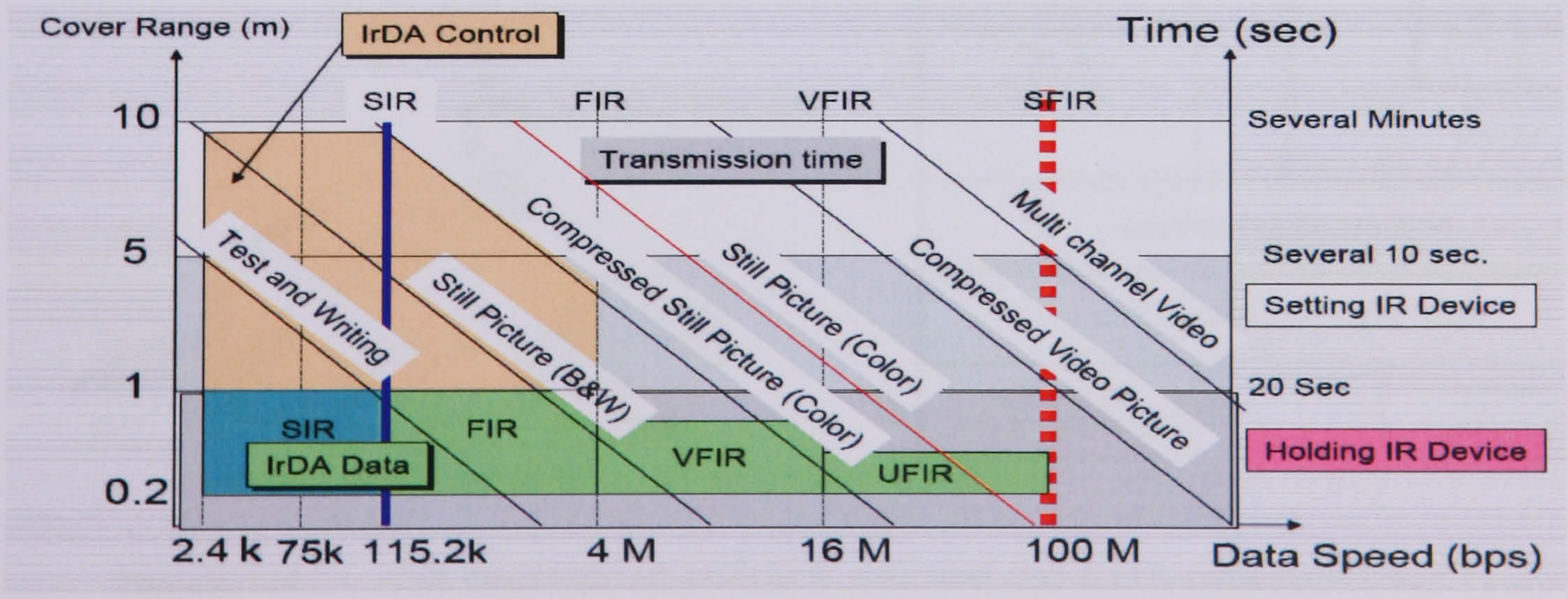

Figure 1.3 Infrared transmission speed, time and coverage area [1.23]

1.2 Wireless Infrared Medium – Advantages and Drawbacks

The infrared data association (IrDA) was established in 1993 as a collaboration between major industrial organisations in order to establish an open standard for infrared (IR) data communication [1.20] [1.24-1.28]. The resulting IrDA protocol aimed to provide a simple, low-cost, reliable means of IR communication between devices such as portable computers, desktop computers, printers, other peripherals and LANs using directed point-to-point connectivity. Figure 1.4 illustrates an example image of an IrDA link with which PC peripherals are connected to a PC. IrDA links can currently provide a baud rate up to 115.2 kbit/s, or 16 Mbit/s with a high-speed extension, using half-duplex point-to-point connectivity. The IrDA protocol stack is also shown in Figure. 1.4. The IrDA protocol stack consists of three mandatory layers: the physical (IrPHY) layer, the IrLAP layer, and the IrDA Link Management Protocol (IrLMP) layer.

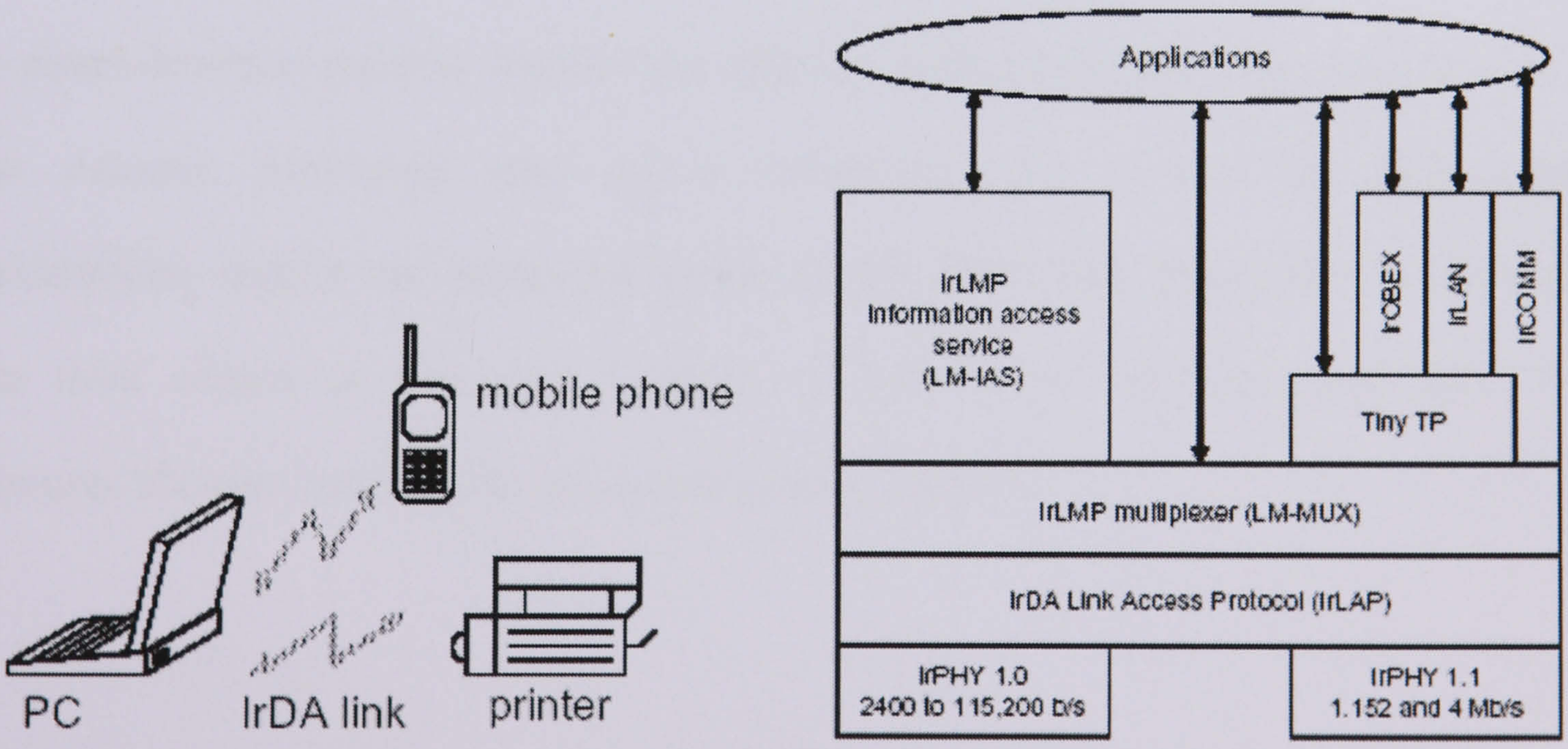

Figure 1.4 An example of an IrDA link and the IrDA protocol stack [1.20]

Therefore, one of the prime motivators for considering the use of an optical carrier in the wireless context is the demand for greater transmission bandwidths. As previously discussed, the radio frequency spectrum has already exceedingly become congested and frequency allocations of sufficient bandwidths are extremely hard to obtain [1.29]. As a medium for short-range wireless communication, IR radiation has several advantages over radio. The primary advantage is an abundance of unregulated bandwidth, with a range of more than 130THz. In addition, being similar in wavelength, part of the infrared spectrum shares many of the features of visible light; in particular, infrared radiation does not pass through walls or other opaque barriers, so that an infrared signal is confined to the room in which it originates. More importantly, it allows neighbouring rooms to use independent infrared links without interference. Furthermore, infrared links using intensity modulation and direct detection receivers do not suffer from multipath fading [1.30].

Nevertheless, IR does have some drawbacks as well, offering a limited range because the noise from ambient light is high, as shown in Figure 1.5 [1.30]. Also, the square-law nature of a direct-detection receiver doubles the effective path loss in dB when compared to a linear detector. Moreover, strict power limitations, due to eye and skin safety considerations, restrict the transmitter output power. IR is also susceptible to blocking, either from objects or personnel, resulting in loss of the communication link. The differences between radio and IR are summarised in Table 1.

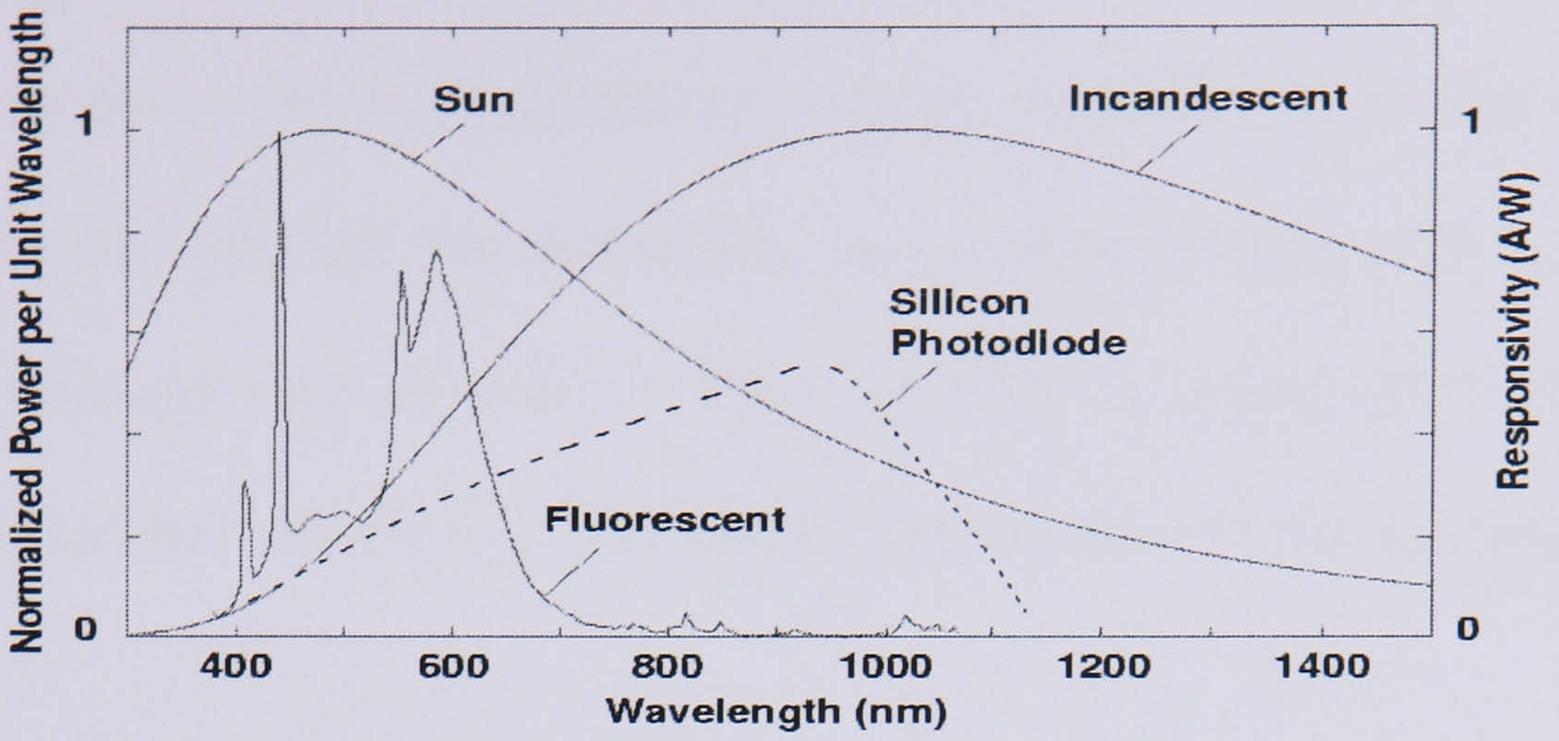

Figure 1.5 Ambient Light Noises and Silicon Photodiode Responsivity [1.30]

Table 1 Properties of Infrared and Radio Channels [1.30]

Property	***Infrared***	***Radio***
Multipath Fading	No	Yes
Multipath Dispersion	Yes	Yes
Source of Bandwidth Limitation	High Photodiode capacitance, Multipath dispersion	Regulatory
Source of Dominant Noise	Ambient background light	Interference from other users
Security	High	Low
Range	Low	High
Input X(t) Represents	Power	Amplitude
Path Loss	High	High

Thus, it is likely that wireless IR technology will be successful in a range of applications, where the benefits outweigh the drawbacks, and it demonstrates clear advantages over competing technology such as radio or wired systems. It is important that the wireless designer or researcher develops a user model appropriate to the envisaged application scenario.

1.3 Recent Wireless Infrared Communication Systems

In the 1990s, practical applications using optical wireless communication were realised, and some products and their standards were completed. Optical wireless systems are classified into two categories, depending on where the system is utilised. In this section, these applications will be introduced, from this point of view.

1.3.1 Indoor Application

There is a growing interest in indoor wireless networks as a consequence of the large-scale utilisation of personal computers and mobile communicators. In this application, an optical wireless communication system is a candidate for the medium of wireless networks. IR is preferred as the wavelength in these applications. A large total transmission bandwidth is possible, facilitating fast transmission systems due to the very high frequency involved in the optical carrier. Moreover, because of the short wavelength, optical radiation is confined

within a room, since the radiation is either reflected or absorbed by the walls, as shown Figure 1.6 [1.31]. Therefore, cell planning in networks is simple.

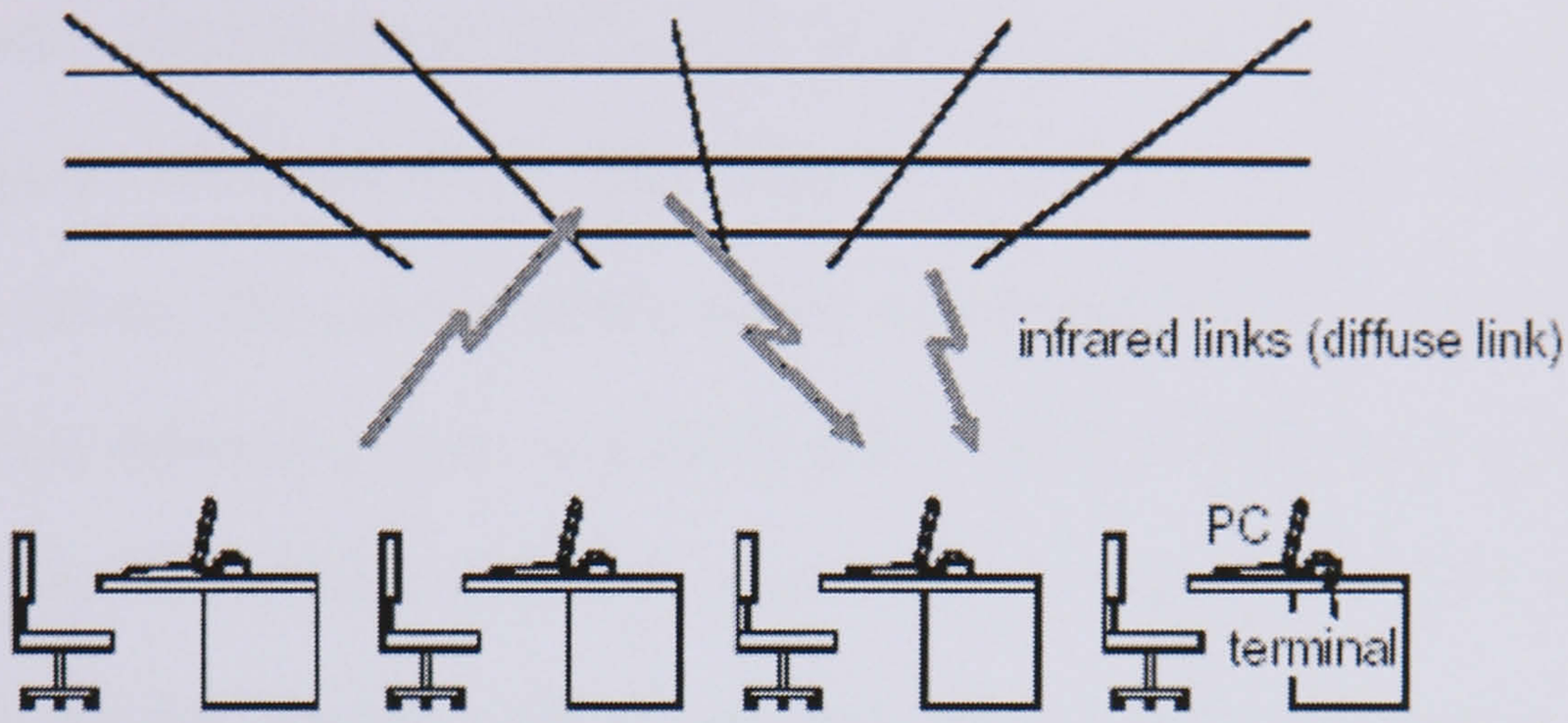

Figure 1.6 Example of an IEEE 802.11 network with infrared transmission [1.31]

1.3.2 Outdoor Application

There are many situations where an optical fibre is not always suitable for a fixed link, examples including temporary links, rapid deployment requirements and extremely cost sensitive links, such as those from the kerb to the house. The cost problem in the links, such as those from the kerb to the house, is called the "last one mile problem,". Radio and microwave links currently solve some of these issues, however such systems are not without some serious drawbacks, notably a high cost, large physical size, the need for regulatory approval and spectrum allocation, and the low bandwidth available. Optical wireless systems can be utilised in these situations, as a viable alternative to RF.

Over shorter distance, less than 500 m, permanent systems with very high availabilities can be designed. Moreover, the intrinsically low cost of near IR components, which couple into

free space, can be exploited to produce a lower cost alternative to fibre for some fixed applications, such as broadband signals. An example of an information-offering system using LED traffic lights has been proposed in Japan via optical beam networking [1.32-1.34]. This system utilises a traffic light consisting of LEDs, which can offer traffic information to drivers. The concept of this system is shown in Figure 1.7. This information contains real-time information such as a traffic jam, a traffic restriction, an accident and a parking lot, or local information such as an event and stay information. These systems offer information to moving objects, such as cars and other vehicles. Therefore, an optical wireless communication system is suitable as an access network. Moreover, the required optical devices can be made cheaply when manufactured in large quantities when used for an optical wireless communication system.

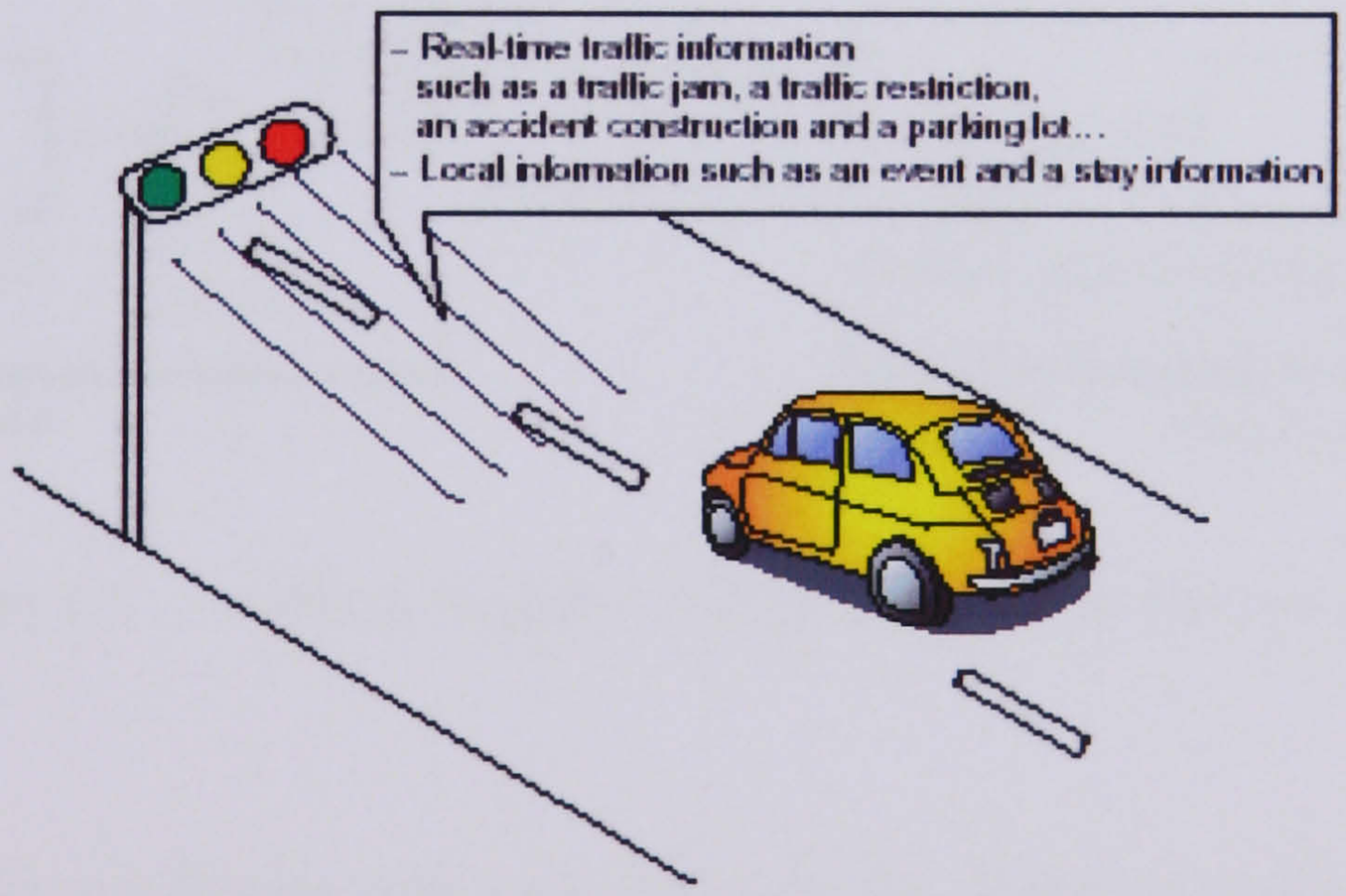

Figure 1.7 System image of a traffic information offering system using Infrared traffic light [1.32]

1.4 Optical Wireless Link Design

Figure 1.8 shows the basic elements of a wireless optical link. On the transmit side, an information source produces a data stream that is encoded and sent to the appropriate drive circuitry used to modulate the optical signal, generated by either a light emitting diode (LED) or a laser. The signal propagates through free space, or through a waveguide such as an optical fibre, until it reaches the photodetector at the receiver end. The photodetector converts the optical signal into an electric current that is sensed by the preamplifier and regenerated to a sufficiently strong voltage signal, from which the original data can be recovered by the demodulator and sent downstream for further processing.

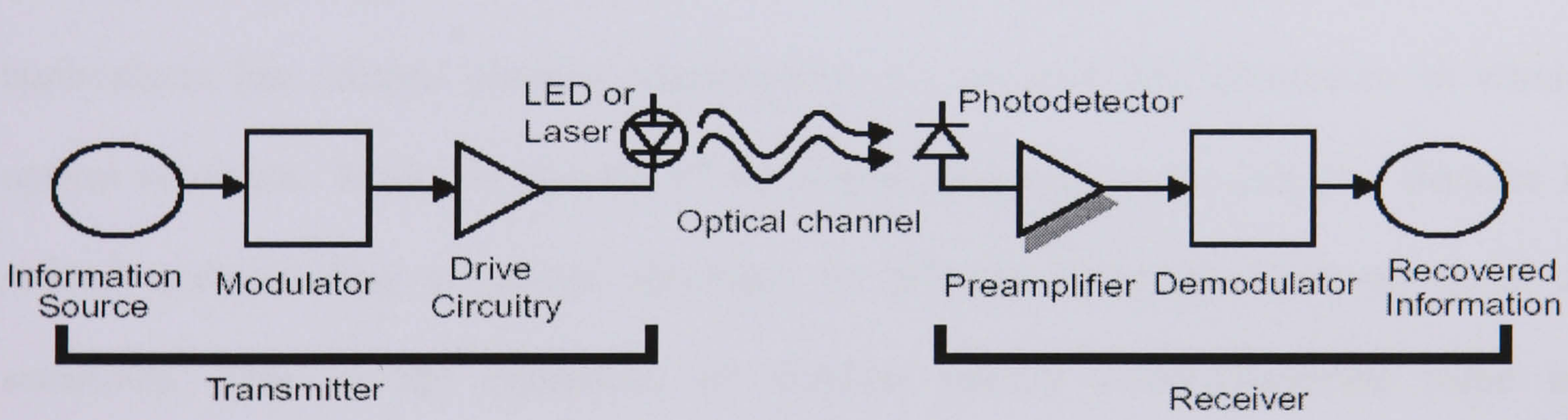

Figure 1.8 Block diagram of a typical optical wireless link.

Varying link lengths are driving new innovations in the design of transmitter and receiver technology for optical communication systems. In wireless LAN technologies, some end users may be located a short distance away from each other, while others could be on a different floor or in another building. IrDA has established standards for wireless links that

specify that receivers must resolve signals transmitted over link distances that can vary between zero and one metre. Since photocurrent amplitude is directly proportional to received signal intensity, this range of channel distances translates to a preamplifier signal current that can vary through five orders of magnitude [1.35]. Furthermore, as inexpensive optical links become widespread, the low cost and high potential for integrated circuit technology has made it an advantageous choice for realising receivers. For the preamplifier in particular, transimpedance amplifiers have become popular for realising bandwidth enhancement and amplification.

1.5 Motivation

Despite the disadvantage, outlined above the expansion of optical communications into new applications has created exciting opportunities for research and innovation in wireless optical receivers. While the growth of fibre-optic networks in the last few decades has refined understanding of optical receivers, its primary focus has been on speed and sensitivity. Due to the expansion of wireless optical communications come new requirements for receiver designs.

Probably the most widespread trend has been that referred to, is increased system integration, and the drive to reduce system components, cost and size. Traditionally, optical receivers have not been subject to many system level constraints, since optical receivers for long-haul fibre-optic networks are principally designed for performance, rather than down

to a cost. As such, they have typically used advanced high-speed semiconductor technologies, such as GaAs and Si bipolar processes [1.35]. Increasingly, new optical receiver designs are being implemented in low-cost, high-integration circuit technologies such as composite or hybrid combination [1.36]. However, the desire to implement these techniques implies a need to design receivers that keep pace with developments in advanced technology. An emerging trend in optical receivers is the desire for greater dynamic range, where this is defined as a measure of the variation in signal strength that can be tolerated by the receiver whilst still meeting performance requirements, such as the bit error rate. The minimum signal is determined by the receiver's noise, whilst the maximum signal is determined by the overload or saturation point of the receiver. Traditionally, receivers for long-haul fibre-optic networks have not required as wide a dynamic range because the received signal levels have been optimised to be small so as to maximise link distance and to minimise the need for repeaters. With many of the new applications, more flexibility is required, and the link distance plus associated path losses, are less stringently controlled. In such cases, the receiver must compensate by having an increased dynamic range. If the requirement is modest, the increase can be achieved through additional bandwidth or gain control stages at the front end of the receiver. However, if the required increase is great, additional steps must be taken at the preamplifier stage. For instance, current IrDA standards for optical wireless systems allow a variable link distance from 0 cm up to 100 cm. Over this distance, the irradiance may, vary over fiver orders of magnitude, 500 mW/cm^2 down to 4$\mu W/cm^2$ [1.20].

For many applications, optical wireless is operated in the presence of intense infrared and visible background illumination. While received background light can be minimised by optical filtering, it stills add shot noise, which is usually the limiting noise source in a well-designed receiver. Due to its high intensity, this shot noise can be modeled as additive, white, Gaussian, and independent of the required transmitted signal. When little or no ambient light is present, the dominant noise source is receiver pre-amplifier noise, which is also signal independent and Gaussian. Figure 1.9 shows a model link of a direct detection optical wireless channel using an intensity modulation technique.

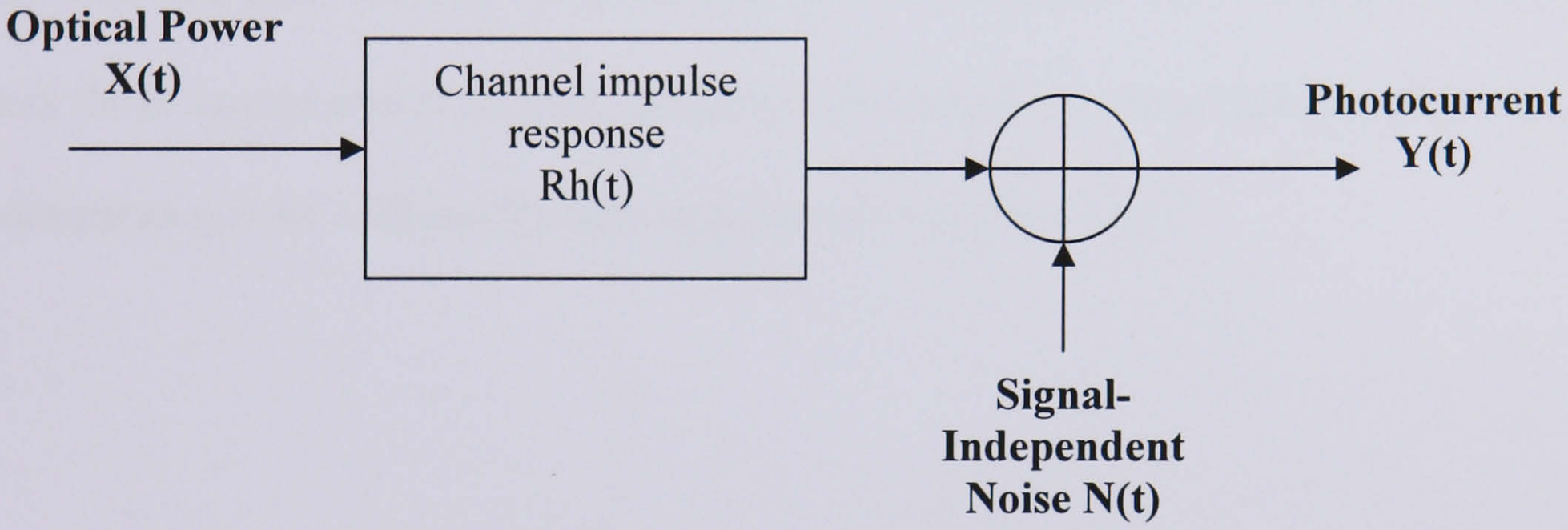

Figure 1.9 Modeling a link as a baseband filter and time-invariant system having an impulse response $h(t)$, with signal-independent, additive noise $N(t)$. The photodetector has responsivity R. [1.30]

The performance of a wireless optical link at bit rate is related to the received electrical signal-to-noise ratio (SNR). Achieving a high electrical SNR is the biggest problem facing the designer of such a link. This is due to the directional nature of both the signal and the noise, meaning that the SNR at the receiver can vary significantly. These imply that

wireless network environment required an adaptable system, in order to provide a better dynamic quality of service (QoS). The dynamic QoS approach centres on the notion of providing QoS support at some point within a frequency range requested by the user or depends on the signal being transmitted. To utilise dynamic QoS, the receiver system must be capable of adapting to the level of signal provided by the network, which may vary during the course of transmission.

In summary, due to the advances in wireless communication, new receiver requirements are needed, namely wide dynamic range, and an adaptable receiver system with automatic bandwidth and gain control. One application in particular, IR wireless communications, pushes these requirements to their extreme, motivating the investigation of how these new requirements can be addressed at the receiver preamplifier stage.

1.6 Organisation of the Thesis

This thesis constitutes an extended study of receiver preamplifier circuits designed to address the emerging requirements placed on IR optical wireless receivers. The primary focus will be on the IR optical wireless application where these requirements are most clearly needed. In general, IR optical wireless receivers have more modest bandwidths than fibre-optic receivers. This is because: (i) infrared optical wireless is a low cost application and (ii) the large path losses that are incurred through free-space transmission require the use of large LED's and photodiodes that are innately slow. Such devices typically have

active areas on the order of a few square millimeters. Current industry standards support data rates of 16Mb/s, but higher rates of 64Mb/s and above are being investigated.

In this thesis, the objectives are to optimise the optical wireless receiver concept using adaptable bandwidth adjustment control methods. This technique allows low noise photodetection and amplification to achieve better service quality. The following are the main contributions of the thesis :

- Six different technique circuit configurations of variable bandwidth transimpedance amplifier as shows in Table 2.

Table 2 : Receivers designed

Technique	**Bandwidth Range**	**BW Adjustment**	**Effective component**	**Gain**
Transimpedance amplifier with FET voltage control	700kHz – 4.5MHz	3.8MHz	Transistor (FET & BJT)	80dB
Bootstrap Transimpedance amplifier with adjustable capacitor	52Hz – 233MHz	232MHz	Transistor (BJT)	48dB
Transimpedance amplifier with external voltage control	4.7MHz – 28.7MHz	24MHz	Transistor (BJT)	27dB
Composite voltage and current feedback amplifier	18MHz – 75MHz	57MHz	Integrated circuit	50dB
Composite Bootstrap Transimpedance amplifier with voltage feedback amplifier	9.5MHz – 104MHz	94.5MHz	Transistor & Integrated circuit	12dB
Composite Dual feedback loop amplifier with voltage feedback amplifier	285kHz – 115MHz	115MHz	Transistor & Integrated circuit	15dB

- Three different technique circuit configurations with variable bandwidth (Table 2) incorporate a variable-gain transimpedance amplifier circuit.
- A signal-to noise (SNR) measurement module, which is responsible for the calculation of the SNR at the front end input. The output of the SNR measurement module controls the automatic bandwidth amplifier circuit.

This chapter has introduced an overview of optical wireless communication systems and described the motivations of this research.

Chapter 2 provides the basic background needed for the rest of the thesis. Included are an overview of photodetectors and receiver preamplifiers, and a review of previously reported solutions to the new design requirements.

Chapter 3 describes the new receiver preamplifier structures for enhanced dynamic range using passive transimpedance amplifier components. A technique is proposed using a controllable capacitor at the output of a two stage bootstrapped transimpedance amplifier. Another method using the FET as the control filter has also been studied. The challenge of circuit design using passive components is highlighted, to motivate a better solution for circuit design in Chapter 4.

Chapter 4 describes the new receiver preamplifier structures for enhanced dynamic range using active transimpedance amplifier components. A technique is proposed called the composite amplifier by combining an automatic bandwidth transimpedance amplifier with an automatic gain transimpedance amplifier.

Chapter 5 presents the outcome frequency response when the circuits in Chapter 4 are integrated with an automatic gain control (AGC). This chapter also discusses an overview basic theory of an automatic gain control (AGC).

Chapter 6 discusses the signal-to-noise ratio considerations of the receiver, which is vital in the design, and optimisation of the low noise transimpedance amplifier in Chapter 4. This chapter also discusses the design method of the SNR module, which is the feedback control system for the automatic bandwidth unit.

Chapter 7 presents the implementation details and experimental results using integrated circuits that were used to verify the proposed preamplifier designs.

Finally, in Chapter 8, the thesis is summarised and directions for future work are discussed.

References

[1.1] J. E. Padgett, C. G. Gunther and T. Hattori, "Overview of wireless personal communications," IEEE Communication Magazine., Vol. 33, No. 1, pp. 28–41, 1995.

[1.2] D. C. Cox, "Wireless personal communications : What is it?," IEEE Personal Communication Magazine, Vol. 2, No. 2, pp. 20–35, 1995.

[1.3] R. Pandya, "Emerging mobile and personal communication systems," IEEE Communication Magazine, Vol. 33, No. 6, pp. 44–52, 1995.

[1.4] R. O. LaMaire, A. Krishna, P. Bhagwat and J. Panian, "Wireless LANs and Mobile Networking : Standards and future directions," IEEE Communication Magazine, Vol. 34, No. 8, pp. 86–94, 1996.

[1.5] K. Pahlavan, A. Zahedi and P. Krishnamurthy, "Wideband Local Access : Wireless LAN and Wireless ATM," IEEE Communication Magazine, Vol. 35, No. 11, pp. 34–40, 1997.

[1.6] M. Montrose, "Printed circuit board design techniques for EMC compliance", IEEE Press, New York, 1996.

[1.7] T.K. Woodward, A. V. Krishnamoorthy, "1Gb/s Integrated optical detectors and receivers in commercial CMOS technologies", IEEE J. Selected Topics in Quantum Electronics, Vol. 5, No.2, pp. 146-156, March/April 1999.

[1.8] B.J. Thompson, "Selected papers on Free-Space Laser Communications", SPIE Optical Engineering Press, Bellingham, Vol. MS30, 1991.

[1.9] D.L. Begley, "Selected papers on Free-Space Laser Communications II", SPIE Optical Engineering Press, Bellingham, Vol. MS100, 1994.

[1.10] S.B. Alexander, "Optical Communication Receiver Design", SPIE Optical Engineering Press, London, UK Chapter 1, 1997.

[1.11] D.W. Faulkner, D.B. Payne, J.R. Stern and J.W. Balance, "Optical networks for local loop applications", IEEE J. Lightwave Tech., Vol. 7, No. 11, pp. 1741-1751, November 1989.

[1.12] T. Kwok, "A vision for residential broadband services : ATM-to-the-home",IEEE Network, Vol. 9, No.5, pp. 14-28, Sept-Oct, 1995.

[1.13] P.L. Eardley and D.R. Wisely, "1Gbit/s optical free space link operating over 40m-system and applications", IEE Proceedings on Optoelectronics, Vol. 143, No.6, pp. 330-333, December 1996.

[1.14] L. Kazovksky, M. Hickey, "Towards implementation of multi-Gb/s optical networks", IEEE LEOS Conference Proceeding, pp. 15-18, November 1993.

[1.15] D.E. Andersen, M.W. Beranek, "777 Optical LAN technology review", IEEE Electronics Computer and Technology Conference, pp. 386-390, 1998.

[1.16] T. Kibler, S. Poferl, G. Bock, H.P Huber and E. Zeeb, "Optical data buses for automotive applications", IEEE J. Lightwave Technology, Vol 22, No.9, pp. 2184-2195, September 2004.

[1.17] J.W. Kim, "An Optimized ATM-PON based FTTH access network", ICICS, pp. 1800-1804, Sept 1997.

[1.18] D.J.T. Heatley, D.R. Wisely, I.Neild and P. Cochrane, "Optical Wireless : The story so far", IEEE Communication Magazine, pp. 72-82, December 1998.

[1.19] S. Williams, "IrDA : Past, Present and Future", IEEE Personal Communications, Vol 7, No.1, pp. 11-19, February 2000.

[1.20] Infrared Data Association (IrDA), The IrDA Bulletin, http://www.irda.org, May-July 1999.

[1.21] T. Shaanan, "IrGate takes on Bluetooth and IrDA", Wireless Systems Design, pp. 43-45, February 2002.

[1.22] L. Leong, "VFIR : The roadmap for IrDA", International IC Korea Conference Proceedings, pp. 233-241, 2004.

[1.23] M. Matsumoto, "Evolution for optical wireless communications in personal area network environment", GITS, June 2004.

[1.24] P. Barker and A. C. Boucouvalas, "Performance modeling of the IrDA protocol for infrared wireless communications," IEEE Communication Magazine., Vol. 36, No.12, pp.113–117, 1998.

[1.25] Infrared Data Association, Walnut Creek, CA, "Infrared Data Association Serial Infrared Link Access Protocol (IrLAP), version 1.1," 1996.

[1.26] Infrared Data Association,Walnut Creek, CA, "Infrared Data Association Link Management Protocol (IrLMP), version 1.1," 1996.

[1.27] Infrared Data Association, Walnut Creek, CA, "Infrared Data Association Link Access Protocol Specification for 16 Mb/s Addition (VFIR), Errata to IrLAP version 1.1," 1999.

[1.28] Infrared Data Association, Walnut Creek, CA, "Infrared Data Association Serial Infrared Physical Layer Link Specification for 16 Mb/s Addition (VFIR), Errata to IrPHY version 1.3," 1999.

[1.29] A.M.Street, P.N.Stavrinou, D.C.O'Brien and D.J.Edwards, "Indoor optical wireless systems – a review" Optical and Quantum Electronics, Vol : 29, pp : 349-378, 1997.

[1.30] John R.Barry, "Wireless Infrared Communications" Kluwer Academic Publishers, Chapter 1, 1994

[1.31] R. T. Valadas, A. R. Tavares and A. M. de Oliveira Duarte, "The infrared physical layer of the IEEE 802.11 standard for wireless local area networks," IEEE Communication. Magazine, Vol. 36, No. 12, pp.107–112, 1998.

[1.32] M. Akanegawa, Y. Tanaka and M. Nakagawa, "The basic study of traffic information system with LED traffic signal," IEICE Technical Report, vol. ITS2000-8, pp. 43–48, 2000.

[1.33] M. Akanegawa, Y. Tanaka and M. Nakagawa, "Basic study on traffic information system using LED traffic lights," Proc. IASTED International Conference, Internet and Multimedia Systems and Applications (IMSA 2000), Las Vegas, USA, pp. 27–31, 2000.

[1.34] M. Akanegawa, Y. Tanaka and M. Nakagawa, "Basic study on traffic information system using LED traffic lights," IEEE Trans. Intelligent Transport Systems, Vol. 2, No. 4, pp.197–203, 2001.

[1.35] K. Phang and D. Johns, "A CMOS optical preamplifier for wireless infrared communications", IEEE Transaction Circuits and Systems II, Vol. 46, No. 7, pp. 852-859, July 1999.

[1.36] S. Goldberg," Wide dynamic range, low power dissipation optical preamplifier for wireless infrared and LAN communications", Master Thesis, University of Toronto, 2003.

Chapter 2

Background and Related Work

This chapter provides the literature review and basic foundation needed for the thesis. It begins with an overview of photodetectors, types of receiver preamplifiers and the definition of dynamic service quality. It then discusses the receiver design requirements and reviews previously reported solutions and techniques.

The development of fibre-optic communications can be traced back to the 1970's. Since that time, an extensive body of literature has developed for optical receivers and photodetectors for fibre-optic applications that can provide the interested reader with a more comprehensive treatment of these subjects [2.1-2.4]. In addition, there are two excellent references that deal specifically with optical wireless systems, their optoelectronics, and other design issues at the circuits and system level [2.5, 2.6].

2.1 Photodetector

Photodetectors are semiconductor junctions that convert the photon energy of light into an electrical signal by releasing and accelerating charge carriers, ultimately to produce a baseband voltage for regeneration [2.7]. There are various types of photodetector such as photovoltaic cells, photodiodes, and phototransistors. For high-speed optical communications, photodiodes are preferred, given their superior frequency response. Photodiodes are usually operated under reverse-bias conditions. In order to appreciate its performance in practical optical wireless systems, we have to characterise the photodiode from two points of view : the physical viewpoint and the circuit viewpoint.

<u>The physical viewpoint</u>

The presence of incident optical power, entering a semiconductor device produces thermal agitation that releases holes-electron pairs generated at various points within the diode, as illustrated in Figure 2.1 [2.8]. These carriers drift toward opposite ends of the device under

the influence of the applied field. When a carrier passes through the high-field region, it may gain sufficient energy to generate one or more new pairs of holes and electrons through collision ionisation. These new pairs will, in turn, generate additional pairs by the same mechanism. Carriers accumulate at opposite ends of the diode, thereby reducing the potential across the device until they are removed by the biasing and other circuitry in parallel with the diode, as shown in Figure 2.2. The chances that a carrier will generate a new pair when passing through the high-field region depends upon the type of carrier, the material from which the diode is constructed, and the voltage across the device. The depth and extent of the junction determines the location of the depletion region and the light wavelengths that produce an efficient response. For a given photodiode and a given wavelength, photodiode responsivity expresses the resulting efficiency through [2.8]:

$$I_p = R\Phi_e$$

where R is the diode's flux responsivity and Φ_e is the radiant flux received energy in watts

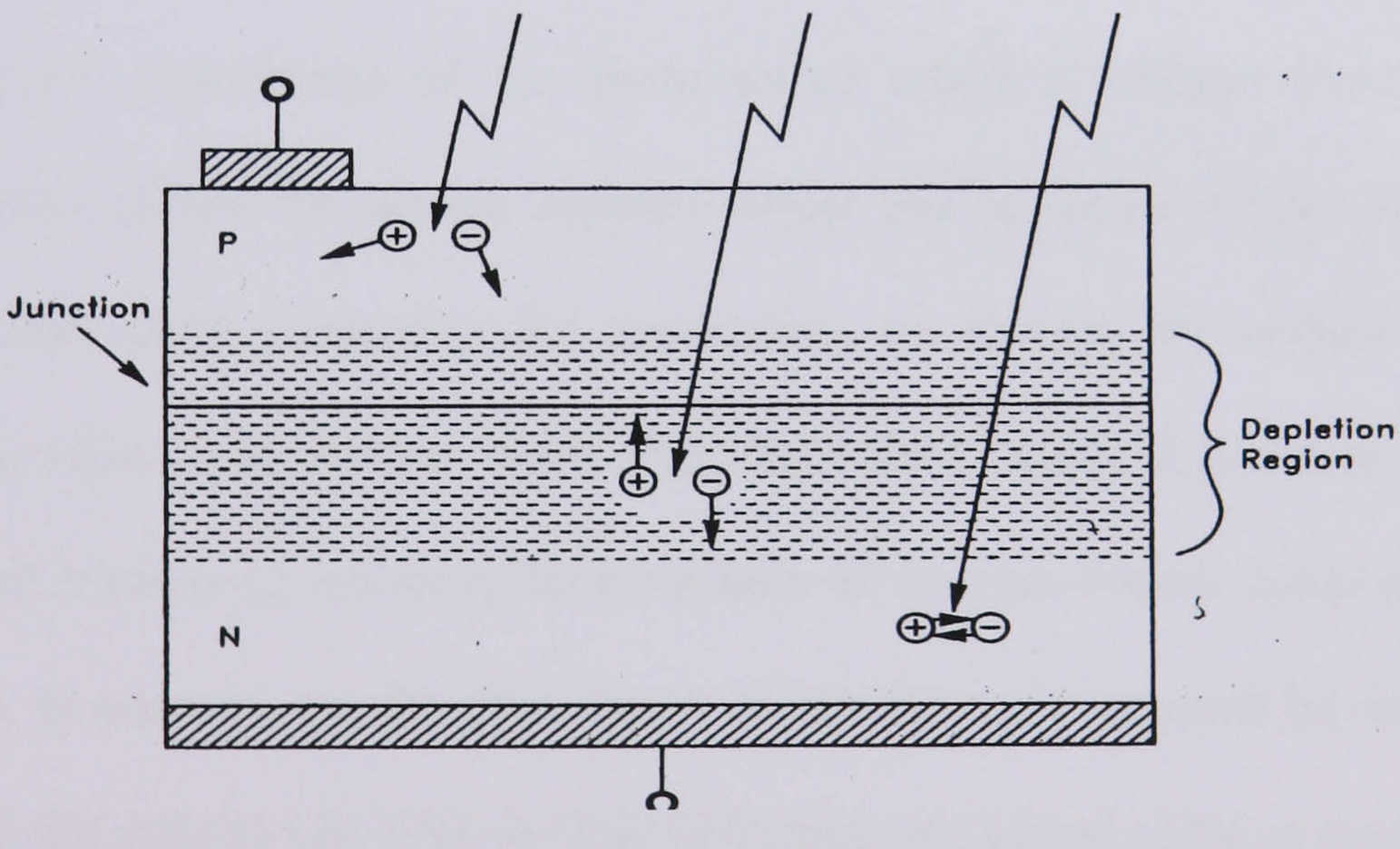

Figure 2.1 Photodetector [2.8]

The circuit viewpoint

From the discussion above and more detailed investigation, modeling the characteristics of the photodiode with discrete circuit components permits analysis of application circuits. Therefore, referring to the circuit design standpoint, however, we can suitably model the photodiode's electrical behaviour may be evaluated using the small-signal equivalent circuit model that consists of an ideal diode, a current source and parasitic elements shown in Figure 2.2.

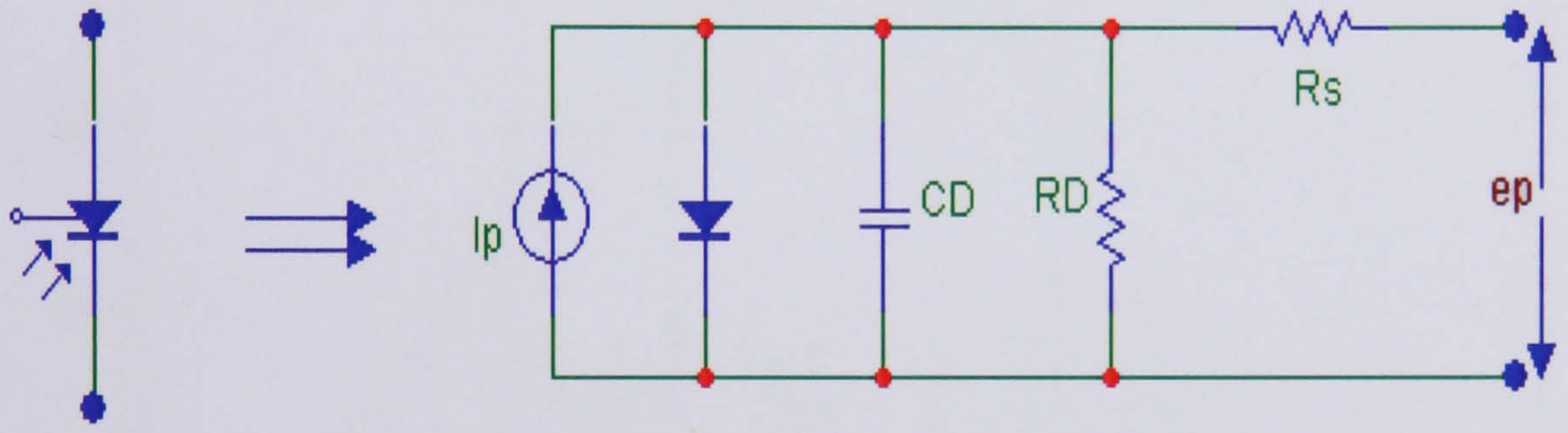

Figure 2.2 Small-signal equivalent circuit model of photodiode

C_d is the junction capacitance of the diode across which a voltage accumulates when charges produced within the device separate under the influence of the bias field. The current generator, $i_p(t)$, represents the production of charges by optical and thermal generation and collision ionisation in the diode high-field region. Resistance R_D represents the diode's dark resistance, which is the resistance of the zero-biased diode junction in the observed light. In order to use the photodiode efficiently a circuit must be designed which will respond to the current $i_p(t)$ with as little distortion and added noise as possible. In order to derive information from the circuit responding to $i_p(t)$, the statistical relationship between $i_p(t)$ (the equivalent current generator) and the incident optical power p(t) must be understood [2.7-2.8].

The sensitivity of the photodetector is a function of the wavelength, and so in order to maximise the power efficiency, the emission wavelength of the optical source should be spectrally matched to that of the photodiode. Silicon photodiodes, which are commonly used in low-cost applications, have a peak spectral efficiency in the near infrared region. Figure 2.3 shows the normalised spectral sensitivity of a typical silicon photodiode (SFH 206K), and shows how it is spectrally matched between the 780nm and 830nm wavelength of the near infrared region [2.9].

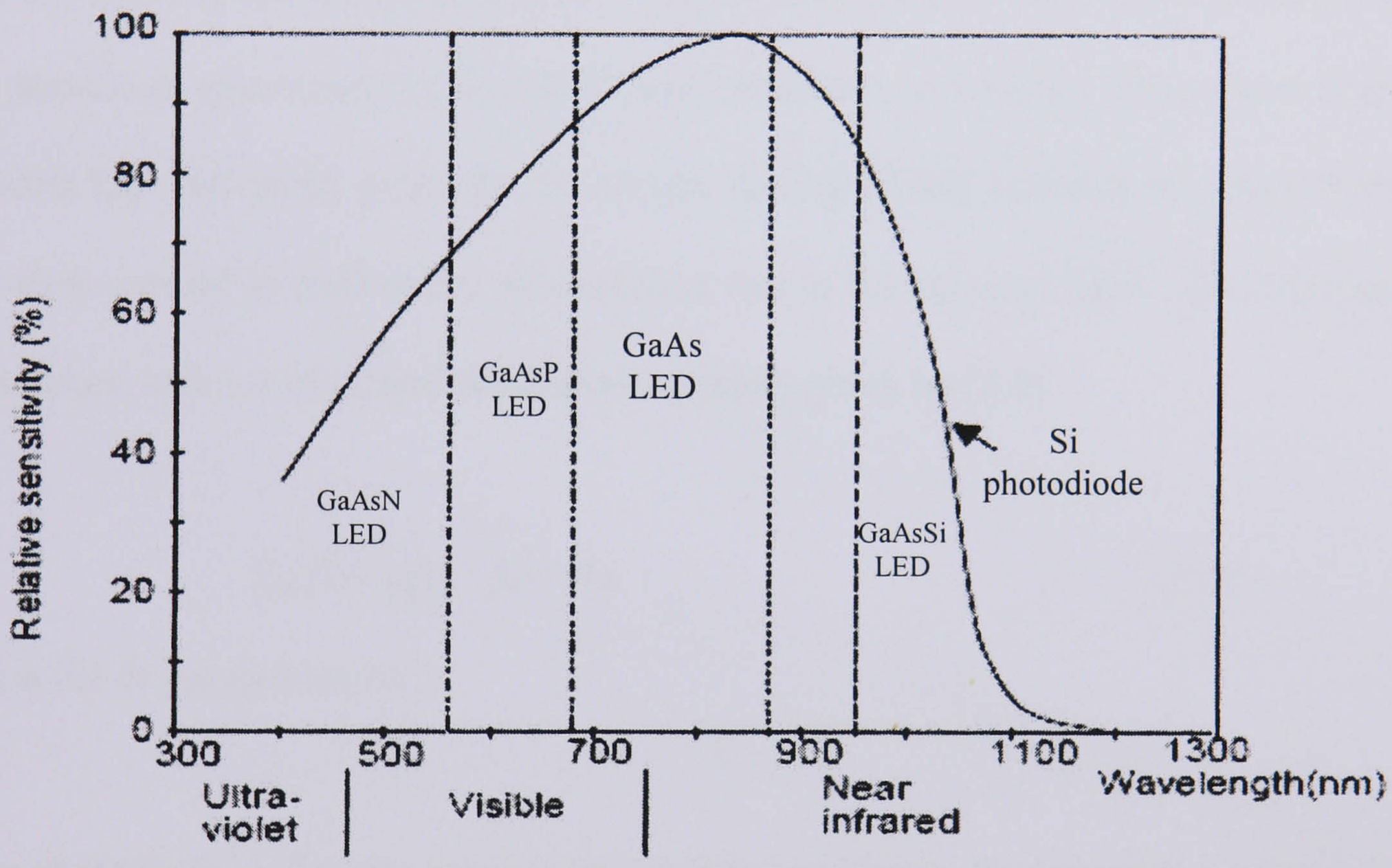

Figure 2.3 Relative spectral sensitivity of (SFH 206K) silicon photodiode [2.9]

There is a linear relationship between the photocurrent, I_p , and the irradiance, E_e, which is a measure of the intensity of the incident light, and is given in W/m^2. The photocurrent is calculated by [2.8]

$$I_p = \frac{\eta q}{h\upsilon} A_{eff} E_e = R\emptyset_e$$

where η is the quantum efficiency of device (typically in the range of 0.6 to 0.9), q is a unit electron charge (C), h is Planck's constant, υ is the frequency of the light, and A_{eff} is the effective area of the photodiode, accounting for the effect of the lens. The collective term, $R = \frac{\eta q}{h\upsilon}$, is commonly known as the responsivity of the device, and is in units of A/W. The product, $\emptyset_e$, is the received optical power in Watts. For example, the S5973 photodiode is rated to provide of photocurrent per $0.6\mu W / cm^2$ irradiance at 830 nm. The current source, I^2_n , models the shot noise generated by the dc current which includes the photodiode's intrinsic dark-current as well as the photocurrent due to background light. The noise has a white spectrum with a normalised noise power density given by [2.8]

$$I^2_n(f) = 2qI_s \quad A^2 / Hz \qquad (2.1)$$

where I_s is the dc component of I_p.

Since the photodiode is operating under reverse-bias conditions, the behaviour is dominated by the depletion capacitance across the p-n junction. As a result, it is greatly dependent on the applied bias voltage, as illustrated in Figure 2.4 for the SFH 206K, BPV22NF and S5971 silicon photodiodes. This characteristic is particularly significant when designing low-voltage receivers, where the maximum reverse bias that can be applied to the photodiode is severely limited.

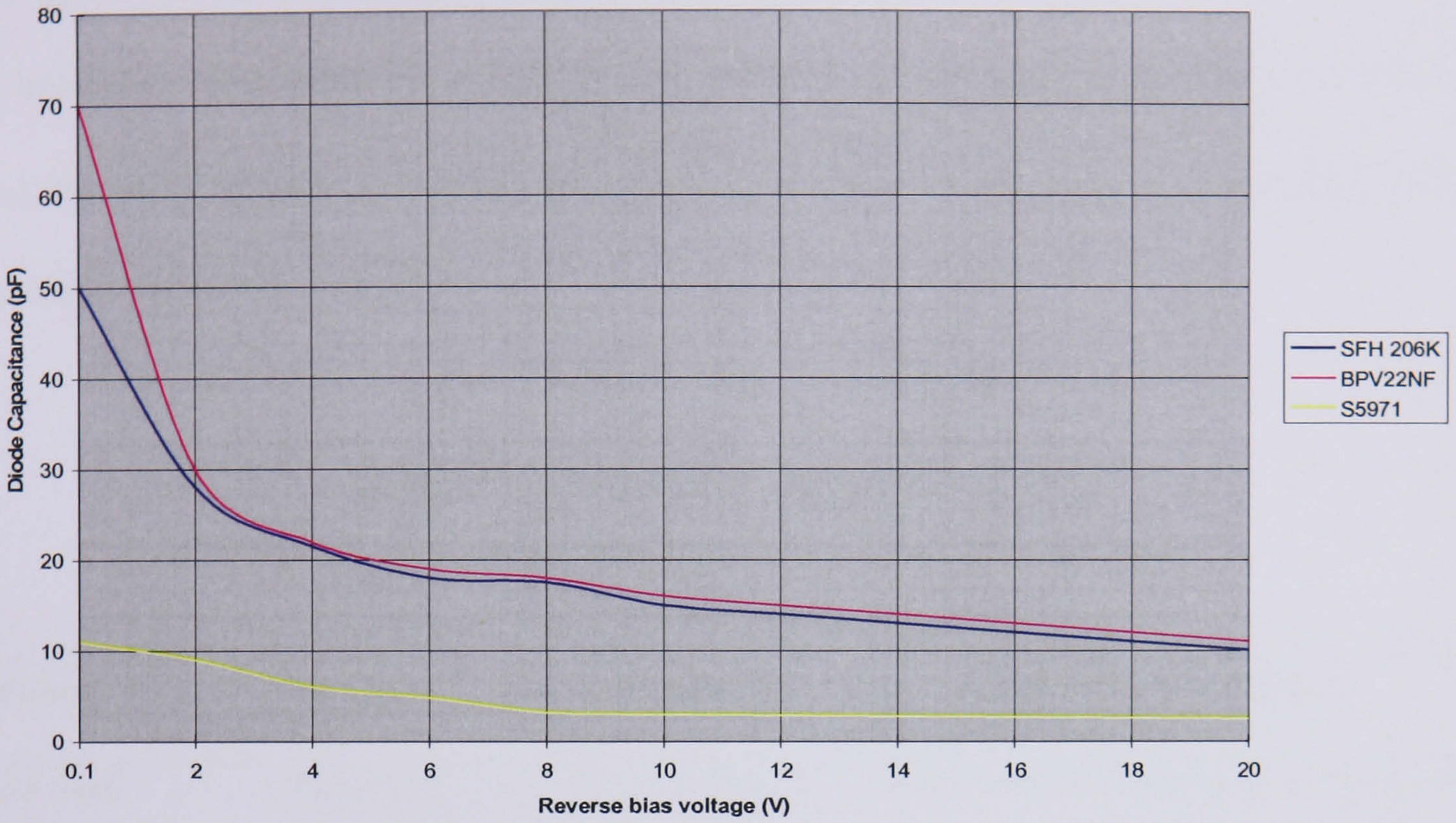

Figure 2.4 Photodiode capacitance versus Reverse bias voltage

Photodiode Variations

Two variations of the basic photodiode improve the diode's response. Physical study shows that PIN photodiodes increase the spectral bandwidth or range of optical frequencies that produce an efficient photo response. Avalanche photodiodes increase the magnitude of the output current and the response speed by permitting diode bias at the verge of breakdown. For applications of interest, PIN photodiode is preferable in optical wireless communication systems.

Noise Contributions

For a typical photodiode amplifier, the current to voltage converter exhibits a complex noise behavior. The major sources of noise in front ends are listed in Table 2.1, where e_N and i_N are rms values of random fluctuations [2.10]. The analysis of this issue will be discussed in detail in Chapter 6.

Table 2.1 Noise in Front Ends [2.10]

Source	**Type**	**Formula**	**Dominates When :**
Photocurrent	Shot noise	$i_{NSHOT} = (2eI_d)^{1/2}$	Bright ambient light, large load resistor
Load resistor	Johnson noise	$I_{Nth} = (4kT/R)^{1/2}$	Dim ambient light, small R
Amplifier	Input current noise	$i_N = \sqrt{\frac{4kT}{R}}$	Ideally, never Where R is noiseless
	Input voltage noise	$e_N = \sqrt{4kTR}$	Dim ambient light, large RC or a fast noisy amp

2.2 RECEIVER PREAMPLIFIER STRUCTURES

The receiver preamplifier performs the critical function of interfacing the photodiode to the rest of the receiver. Typically, the preamplifier converts the received photocurrent into a voltage signal. The preamplifier plays a crucial role in determining many aspects of the overall performance of the receiver including speed, sensitivity, and dynamic range.

Receiver preamplifiers are typically classified in categories as either a termination resistor (High-impedance and low-impedance) amplifier or a transimpedance amplifier.

2.2.1 High impedance amplifier

In the first approach, the photodiode is attached to a load resistor, R_L as shown in Figure 2.5. For a low-impedance receiver [2.5], R_L is chosen to be small (typically 50Ω), so that the receiver bandwidth $\frac{1}{(2\pi R_L C_T)}$ is sufficient for the signal bandwidth. A high-impedance receiver [2.4][2.11-2.12] uses the same configuration but with a large R_L, thus diminishing the effects of its thermal noise. However, the receiver bandwidth $\frac{1}{(2\pi R_L C_T)}$ is then usually smaller than the signal bandwidth, requiring an equalization stage in the form of high-pass filtering immediately following the preamplifier as shown in Figure 2.6. This is necessary to achieve the required bandwidth, because the detector output is effectively integrated due to the large time constant, and must be restored by differentiation [2.12]. Therefore, the high impedance front end gives a better improvement in sensitivity over the low impedance front end design but eventually creates a heavy demand for equalisation, and the equaliser reduces the overall dynamic range of the receiver [2.7]. The limited dynamic range is because of the attenuation from the low frequency signal components by the equalization process which causes the amplifier to saturate at high signal levels. If the amplifier is saturated before equalisation has occurred, the signal will be heavily distorted, thus

reducing the dynamic range, which is dependent upon the amount of integration and subsequent equalisation employed.

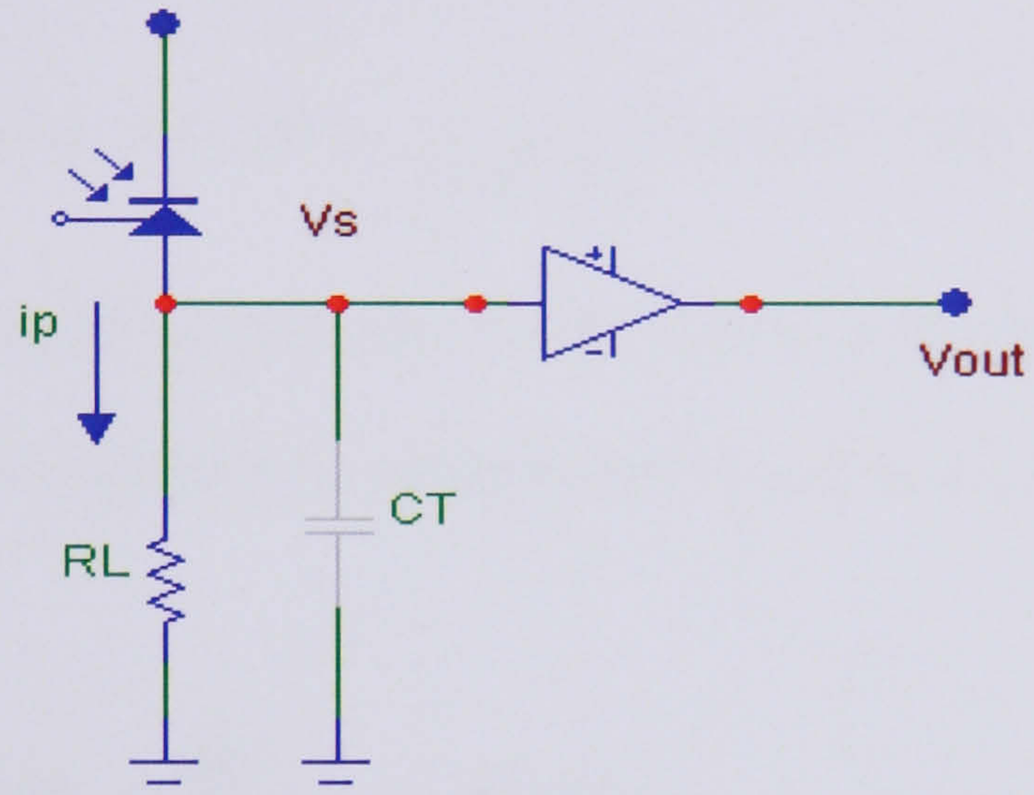

Figure 2.5 Receiver preamplifier based on a termination resistor

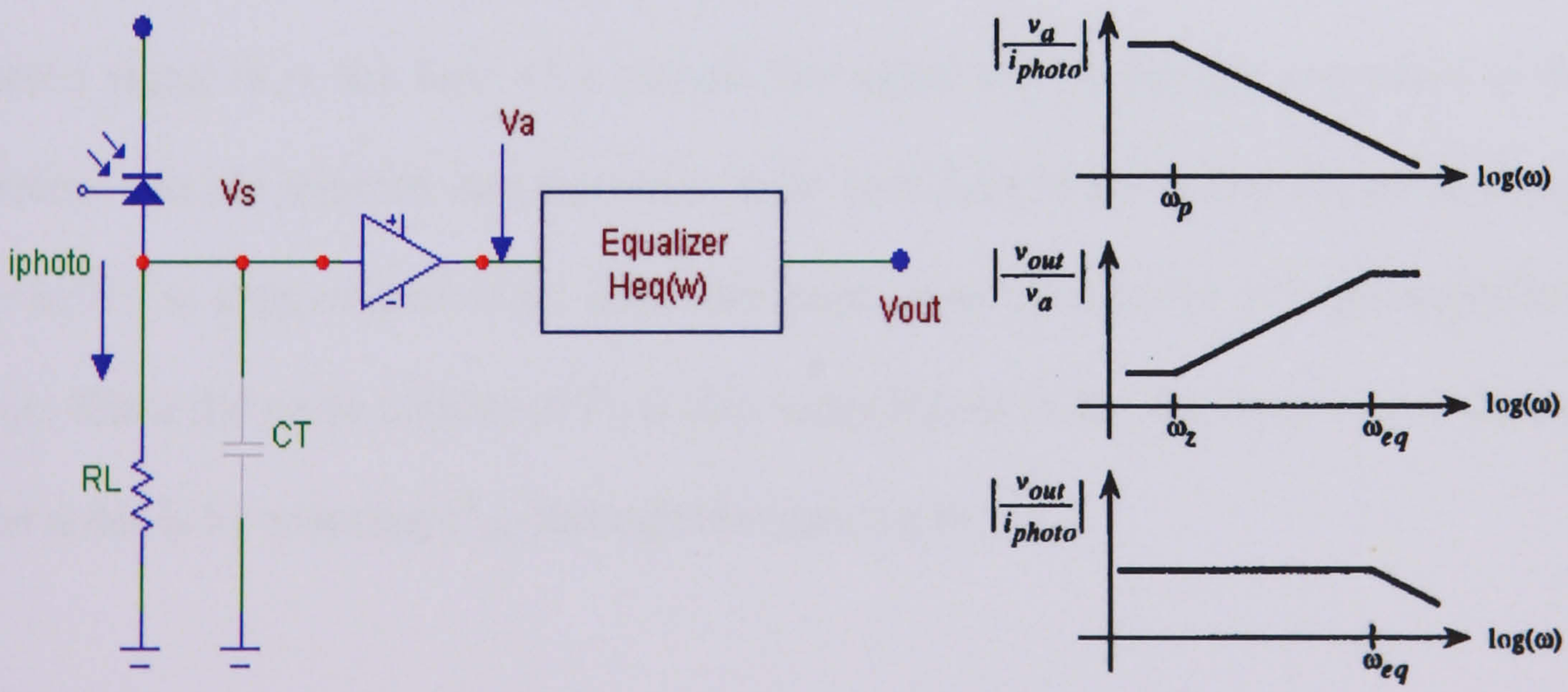

Figure 2.6 High impedance amplifier with equalisation [2.4]

The current signal, i_p , is converted into a voltage by the load resistor, and the resulting voltage signal is buffered by the voltage amplifier. C_T represents the total capacitance associated with the photodiode and the amplifier. The choice of the load resistance affects both the frequency response and the noise performance of the preamplifier. The intrinsic bandwidth of the preamplifier is equal to $\frac{1}{(2\pi R_L C_T)}$ because of the RC network. The noise can be analysed using the small-signal noise model shown in Figure 2.7. Here, the thermal noise of the load resistor is modeled by current source I^2_{nRl} with a normalised power of

$$I^2_{nRl}(f) = \frac{4kT}{R_L} \qquad A^2 / Hz \qquad (2.2)$$

where k is Boltzmann's constant and T is the absolute temperature in Kelvin. The noise of the voltage amplifier is modeled by current source I^2_n, and the voltage source V^2_n. As the desired signal is in the form of a current, the signal can be directly compared to the noise currents that are injected into the same node. It is easy to show that the noise contribution due to V_n^2 is independent of R_L when the input impedance of the voltage amplifier is very large. Since the noise current of I^2_n is also independent of R_L, the only way to minimise the total noise is by reducing I^2_{nRl} through maximising R_L.

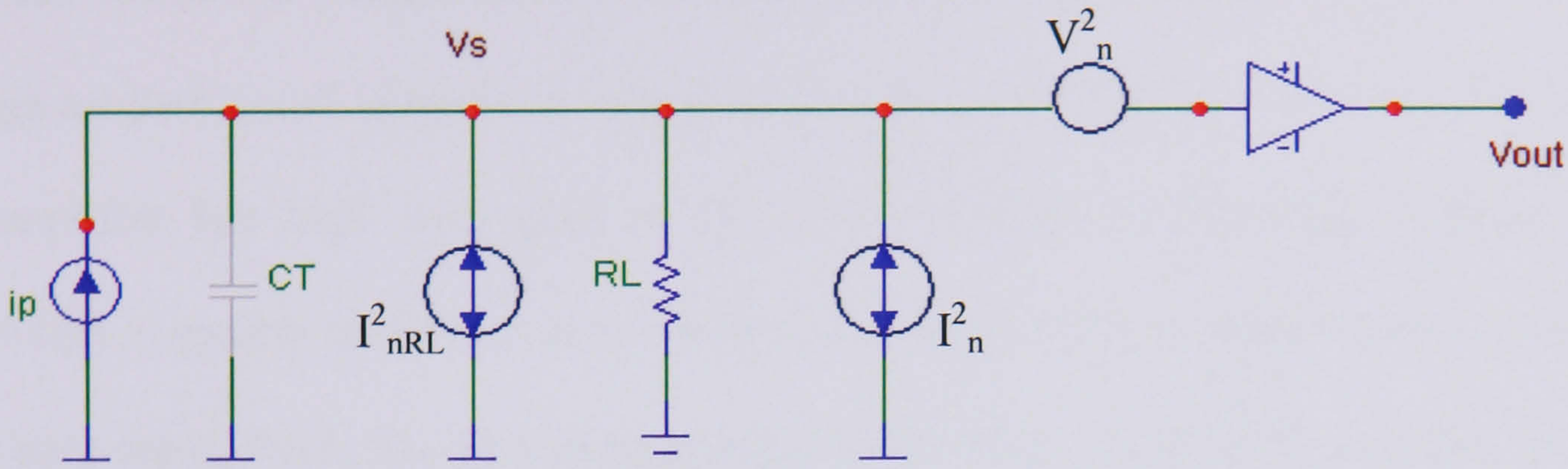

Figure 2.7 Small-signal noise model of the optical preamplifier based on a termination resistor

2.2.2 Transimpedance amplifier

Receiver preamplifiers based on the transimpedance amplifier are currently the most popular because they avoid the dynamic range problem associated with high-impedance designs, and because they provide a good compromise between the wide bandwidth of the low-impedance design and the low noise characteristics of the high-impedance design [2.12]. Given a detector (Figure 2.2) whose output is a current, the easiest way to form a voltage from it is to have a load resistor (R_L). The output full swing appears across the detector capacitance C_D, and rolls off starting at $f_{RC} = \frac{1}{2\pi R_L C_D}$. The signal voltage [2.10]

$$V_o(f) = \frac{i_p(f) R_L}{1 + j2\pi R_L C_D f}$$

Reducing R_L will reduce the RC product and speed up the system, while increasing R_L increases the bandwidth and dynamic range of the system. Another key idea is to reduce the

swing across C_D, by making the detector work into a virtual ground using a transimpedance amplifier as shown in Figure 2.8. The inverting input of amplifier draws no current, feedback forces the voltage there to be close to zero at all times. The amplifier senses the voltage across C_D and adjusts the voltage at the other end of R_F to zero it out. Provided that the amplifier has high loop gain A, the swing across C_D is greatly reduced and the bandwidth is greatly improved. Nevertheless, the amplifier input adds a significant amount of its own capacitance, C_{in}. In a transimpedance amplifier, a resistor R_f as shunt feedback is placed across the gain stage of an inverting amplifier, as shown in Figure 2.8. Here, the resistor can be made large because the negative feedback reduces the effective resistance seen by the photodiode by a factor of (1 + A) where A is the open-loop voltage gain of the amplifier. As a result, the bandwidth can be matched to that of the signal, eliminating the need for equalisation. In addition, the thermal noise contribution of the feedback resistor is minimised. For a typical transimpedance topology using active devices with load feedback resistance R_f , the transimpedance gain A_z can be approximated by :

$$A_z \approx \frac{v_{out}}{i_p} = \frac{-R_f}{1 + j\omega \dfrac{R_f (C_D + C_{in})}{A}} \tag{2.3}$$

where A is the open loop voltage gain of the amplifier and ω is the angular frequency.

so that for large open-loop gains, the transimpedance is simply equal to - R_f. Another factor which serves to reduce the amplifier bandwidth is the capacitance that is associated with the feedback resistor R_f, denote as capacitance C_f. Taking C_f into account the transfer function (2.3) becomes :

$$A_z \approx \frac{v_{out}}{i_p} = \frac{-R_f}{1 + j\omega \dfrac{R_f (C_D + C_{in})}{A} + C_f} \qquad (2.4)$$

The transimpedance rolls off dependent on the magnitude of the impedance of the feedback elements. Therefore, the transimpedance amplifier bandwidth is determined from the following equation [2.10] :

$$f_{3dB} \approx \sqrt{\frac{f_{RC} f_T}{2}} \qquad (2.5)$$

where f_T is the unity-gain crossover frequency

Equation 2.3 shows that the upper 3dB cut-off frequency of the preamplifier is a function of the capacitance of the detector, the feedback resistor and the open loop voltage gain. As a large detector means a large C_d, to achieve large bandwidths either the value of R_f is reduced or A is increased. Unfortunately, increasing A will jeopardise amplifier stability, and reducing R_f will increase the thermal noise in the system.

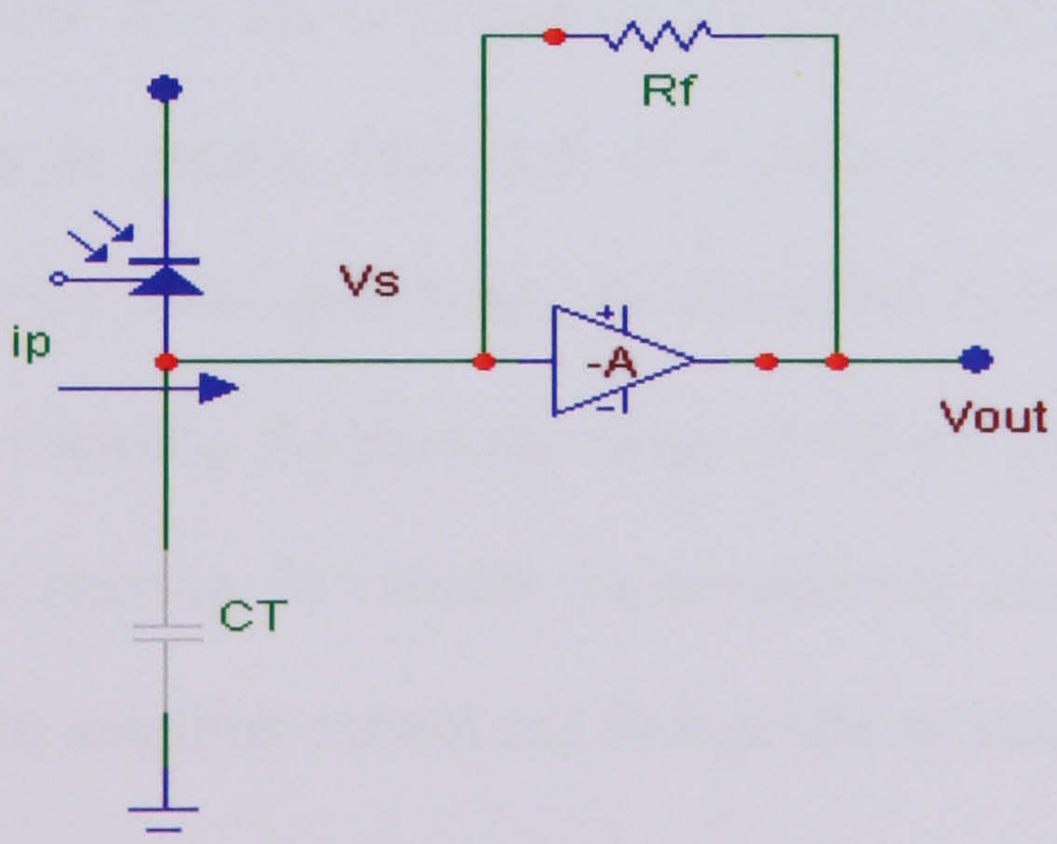

Figure 2.8 Receiver preamplifier based on a transimpedance amplifier

2.3 TRANSIMPEDANCE AMPLIFIER DESIGN REQUIREMENTS

Traditionally, the design challenge of fibre-optic preamplifiers has been in optimizing the trade-offs between sensitivity, speed, and transimpedance gain. As discussed in the previous chapter, new applications of optical communications have introduced additional receiver requirements, such as wide dynamic range, bandwidth enhancement and noise reduction. This section discusses each of these requirements in greater detail, and reviews previously reported solutions.

2.3.1 Wide Dynamic Range

A wide dynamic range is essential in order to accommodate variable link distances. Current IrDA standards, for instance, require an optical dynamic range of 51dB in order to support a link distances range from zero up to 100cm [2.13]. Although the dynamic range of a transimpedance amplifier is greater than that of a high-impedance design, it is still insufficient to handle such a wide input range. As illustrated in Figure 2.9, there are five principal techniques for extending the dynamic range of the preamplifier: 1) output signal limiting, 2) input current steering, 3) variable transimpedance gain, 4) multiple feedback impedance transimpedance amplifier control and 5) logarithmic amplifier

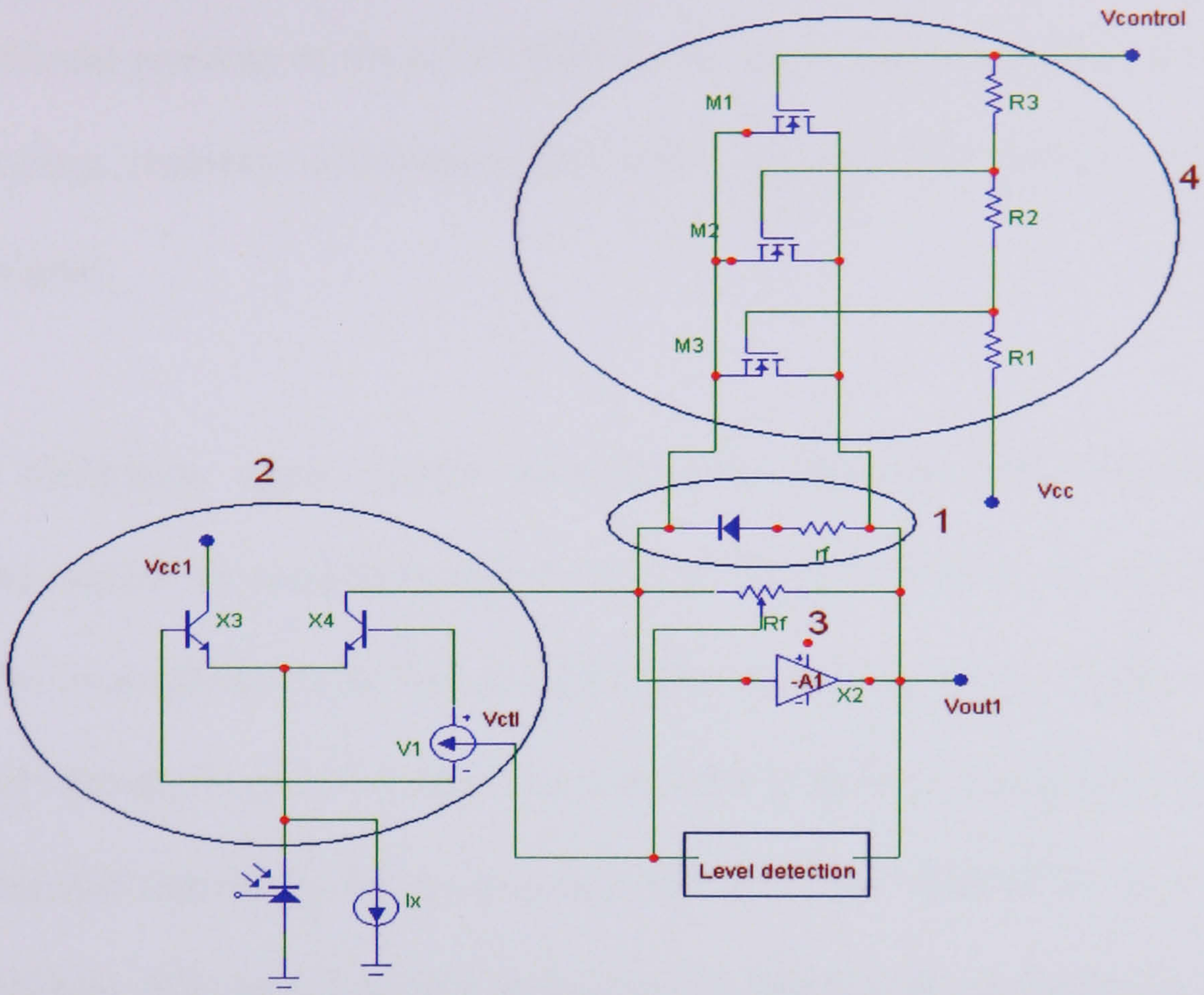

Figure 2.9 Various methods of increasing dynamic range : 1) output signal limiting, 2) input current steering, 3) variable transimpedance gain 4) multiple feedback impedance transimpedance amplifier control

The simplest technique is to limit the output swing as represented by the diode clamp in Figure 2.9. While limiting does not affect the lower limit of the dynamic range, it does increase the upper limit by allowing the receiver to accept strong signals that would have otherwise overloaded the receiver and prevented normal operation. Limiting can be performed either within the preamplifier [2.14], or in cases where the dynamic range requirements are more modest, externally by following the preamplifier with a limiter circuit [2.15-2.16]. The advantage of limiting is that it does not require level detection circuitry. However, the process of limiting destroys the amplitude information of the

received signal. As such, limiting can only be used with binary signaling schemes. In addition, limiting introduces pulse width distortions that result from the uneven gain applied to different portions of the pulse. Finally, for applications in which ambient light is an issue, limiting removes information that helps separate the ambient light from the information signal.

The second technique, input current steering, also improves the dynamic range by increasing the maximum acceptable signal level of the preamplifier. It uses a differential pair before the preamplifier to realise an adjustable attenuation of the signal current based on the control voltage, V_{ctl} [2.17-2.18]. The technique is shown conceptually in Figure 2.9. In practice, bipolar transistors are much more effective than MOSFETs for implementing the differential pair. Bipolar transistors provide much larger transconductances for the same bias current, and this is important in two respects. Firstly, the differential pair must present a low impedance to the photodiode to ensure that it does not affect the frequency response of the overall preamplifier. Secondly, a low impedance is required to help prevent fluctuations in the photodiode bias voltage when a signal is present. With bipolar transistors, a sufficiently low impedance can be achieved with much less bias current, and this reduces the noise introduced by the tail current source, I_x. The exponential voltage-to-current characteristic of bipolar transistors also helps to ensure that the photodiode bias voltage remains well regulated across a wide range of signal currents. In summary, the practical need for bipolar transistors makes the current steering technique an attractive for use in receiver preamplifier designs.

The third technique uses a transimpedance amplifier that is capable of variable gain. Recall that the feedback resistor, R_f , is one of the major sources of noise, and that its noise current contribution is inversely proportional to its resistance. Thus, for weak signals, a large R_f is desired to both minimise the noise and maximise the output signal. On the other hand, for strong signals, a small R_f is desired since the maximum input current is limited to $\frac{V_{max}}{R_f}$ where V_{max} is maximum output of the amplifier before distortion. Therefore, by adapting R_f according to the signal strength, the dynamic range may be increased without sacrificing sensitivity. Unfortunately, variable-gain transimpedance amplifiers are challenging to implement because their stability is affected by changes in the feedback resistor. The BiCMOS implementation presented in [2.19], and shown in Figure 2.10a, requires an additional dummy amplifier simply to generate a bias voltage and three *additional* variable resistors to ensure stability. Similarly, the design presented in [2.20] and shown in Figure 2.10b, requires two *additional* variable resistors. In both designs, the additional variable resistors are heuristically fine tuned with no discernible tracking relationship with the main feedback resistor, making these circuits both difficult to design, and prone to modeling errors. These problems are further complicated for fully-differential implementations, where the required number of variable resistors is doubled. The problem with these existing designs is their use of the traditional gain stage consisting of a common-emitter amplifier followed by an output buffer. The stability of the preamplifier can be greatly enhanced and preamplifier circuit significantly simplified by adopting a different topology for the gain stage. Although a constant-bandwidth circuit, variable-transimpedance amplifier was presented in [2.21], experimental results for that work have yet to be reported.

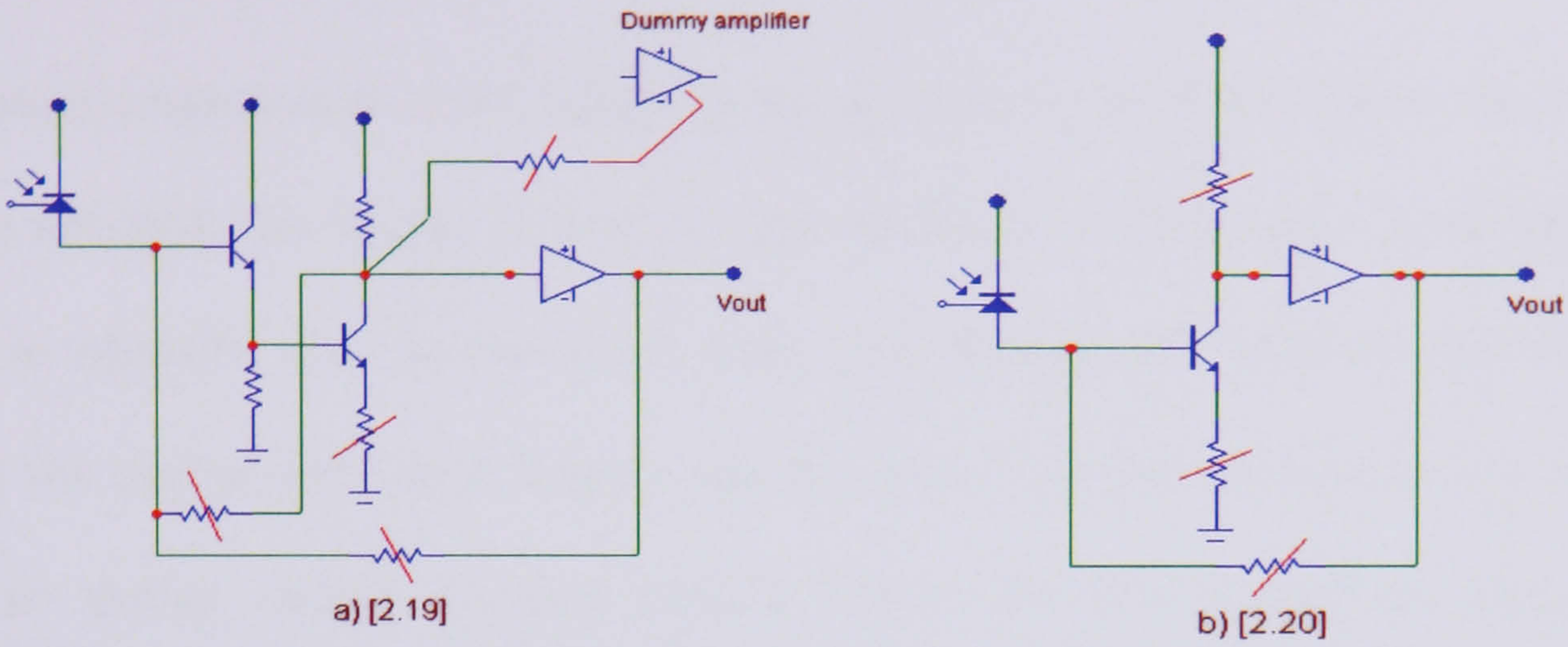

Figure 2.10 Two existing variable gain transimpedance amplifier designs [2.19-2.20]

The fourth technique uses a set of parallel NMOS transistors in the feedback path of the transimpedance amplifier [2.22]. Different gate voltages control these transistors. A common reference value sets these voltages, by simple voltage division achieved by the relative relationships of different circuit elements. The NMOS transistors and the voltage divider are jointly designed, such that the overall equivalent resistance varies approximately in an exponential ratio with the control voltage. Overall, this strategy actually implements an easily controlled automatic gain control in the front-end. In summary, this technique simply trades gain for bandwidth in a way conceptually similar to stability analysis in traditional feedback concepts.

The final technique for extending the dynamic range of the preamplifier is to use a logarithmic amplifier. The logarithmic amplifier basically compresses the amplitude range of the signal by using the log characteristic of a PN (diode, transistor) to implement the logarithmic function but can also degrade the SNR performance.

2.3.2 Bandwidth enhancement

A fundamental requirement in the design of an optical receiver is the achievement of broad bandwidth and high sensitivity, without a large sacrifice of SNR. Since a transimpedance amplifier is typically used as the input stage, this preamplifier stage is one of the key circuits in the optical link, as it largely sets the sensitivity and maximum bit rate of the receiver. Its design results are very critical due to the strong tradeoff between high bandwidth, and high sensitivity (low noise) such that a high gain is needed in order to avoid degradation of the SNR by the following stage. There are basically five principle techniques of bandwidth enhancement for front-end preamplifier designs: 1) Feedback techniques, 2) Bootstrapping, 3) Inductor peaking, 4) Capacitor peaking and 5) T network feedback configuration.

Most of the receiver preamplifier designs using transimpedance configuration incorporate a feedback resistor [2.4-2.5][2.23-2.24]. Feedback can be either negative (degenerative) or positive (regenerative). In a receiver preamplifier using a transimpedance amplifier, negative feedback is applied because of its properties, to extend the bandwidth of the amplifier.

However, because of the thermal noise of the feedback resistor, the receiver noise level is higher. There is a widespread myth that positive feedback amplifiers should be avoided because of their sensitivity to process and environmental variations that may cause them to

become unstable [2.25]. This misconception is founded in the fact that amplifiers using positive feedback do become unstable if too much positive feedback is applied. However, in practice, positive feedback will always be found to be combined with negative feedback or another configuration in which their stability is not an issue. Therefore, the benefit of using positive feedback is its ability to enhance the DC gain, and achieve higher bandwidth, without compromising the settling time, compared to negative feedback which leads to an increase in bandwidth but at the expense of gain.

Teare [2.26] introduced the positive feedback approach in his front-end preamplifier design to improve enhancement ability. The circuit is shown in Figure 2.11.

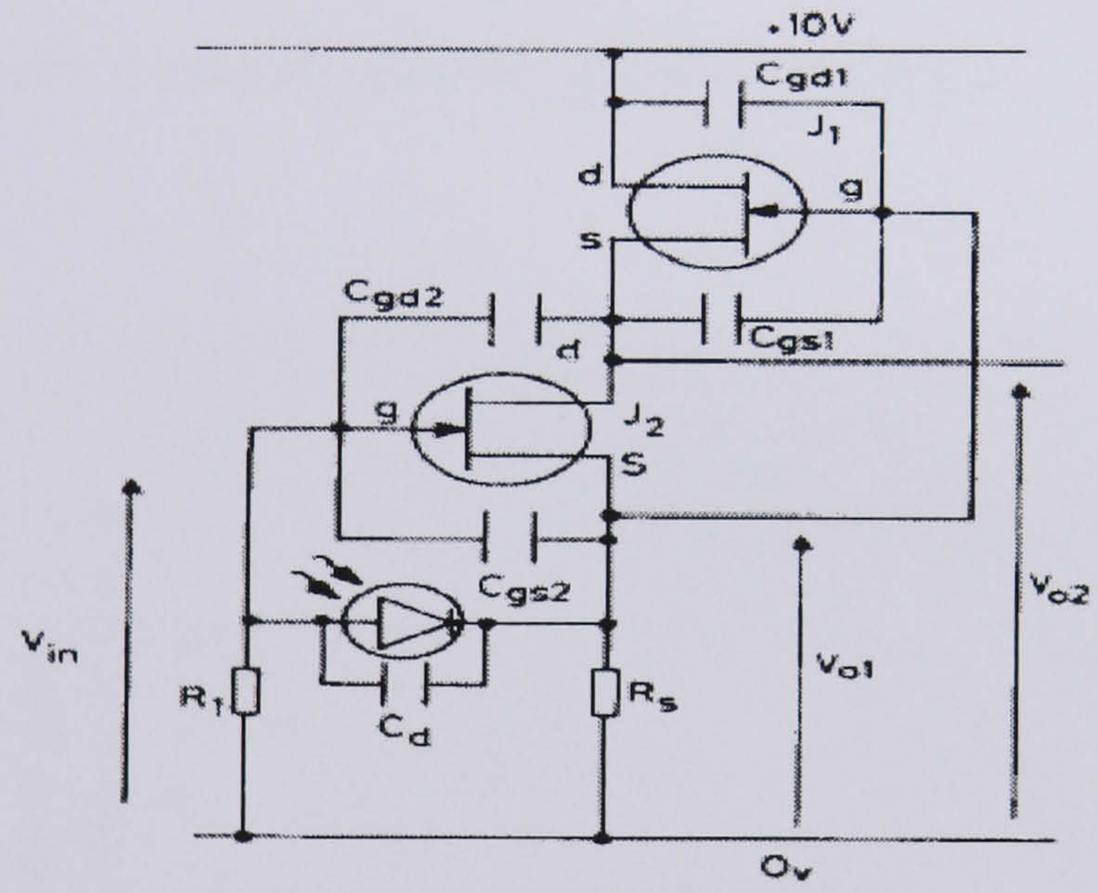

Circuit suggested by Teare

Figure 2.11 Basic receiver front-end using positive feedback [2.26]

The source resistor for J_2 can be replaced by a current source, which improves the overall enhancement ability. Since C_{gd2} is very small and is neutralised by a bootstrapping process, its effect is negligible. This also applies to C_{gs1}. The diode capacitance, C_d is bootstrapped

too, but since its value could be in terms of picofarads, it must form one of the poles. Analysis of the circuit shows that it contains a zero and two poles, from which it is deduced that it represents a positive feedback amplifier. Unfortunately, ringing can occur for this circuit.

Fjarlie [2.24] shows that the basic response is that in Figure 2.12 when responsivity or gain is traded off for an enhanced bandwidth. Positive feedback is used to compensate for the poor frequency performance. Negative feedback would yield a curve similar to the trade-off one in the Figure 2.12. In the negative feedback and trade-off cases, the amplifier must have lower input noise, since the signal levels are lower due to the poorer responsivity of the system, but with positive feedback this is not the case. The ξ curve marks the area where a better detector could be used to optimise performance.

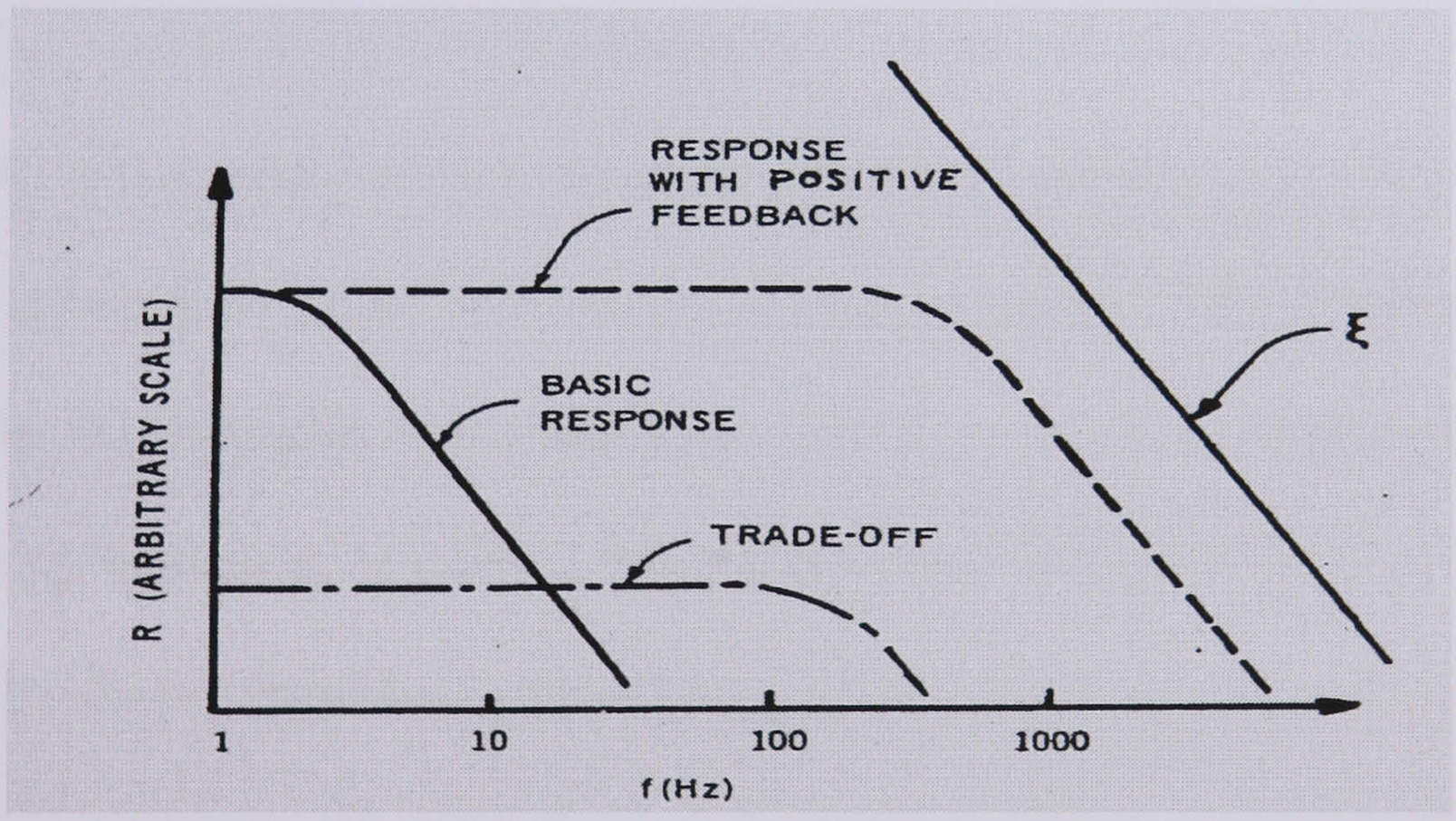

Figure 2.12 Response as a function of frequency. The basic system, the feedback system and the trade-off cases are shown. [2.24]

The second technique known as "bootstrapping" involves a positive feedback loop as described above, which causes a point in the circuit to be pulled up as if by its own bootstraps [2.27]. This principle is often used in high input impedance amplifiers, wide bandwidth designs, and in reducing the effective detector capacitance, C_D from the photodiode as discussed in section 2.1.

Figure 2.13 illustrate two types of simple bootstrap configuration. The first circuit configuration is the shunt bootstrap circuit by Hoyle [2.28-2.29]. This circuit has an additional buffer amplifier in parallel with the main transimpedance amplifier to allow the generation of a suitable forcing voltage to keep the ac voltage drop across the input capacitance at virtually zero. Frequency response plots show twice the bandwidth of the standard transimpedance amplifier. Therefore Hoyle concluded that the bootstrap method may provide a viable design option for applications with high gain and requiring a wide bandwidth. The second circuit configuration is a bootstrap buffered transimpedance by Kristein [2.30], which addresses the diode capacitance in another way. Instead of actually lowering the capacitance of the photodiode, it places a buffer (FET amplifier) in parallel with the diode. A fast buffer will respond quickly to any voltage change at its input by placing the same voltage at its output. The smaller the change in voltage across the diode capacitance, the shorter the time required to charge and discharge the capacitor. The result is a much faster response. In summary, the bootstrap buffer is an excellent alternative to reverse biasing the diode in applications where larger bandwidths and low SNR are required, but it requires a low bias current, low noise n-channel J-FET.

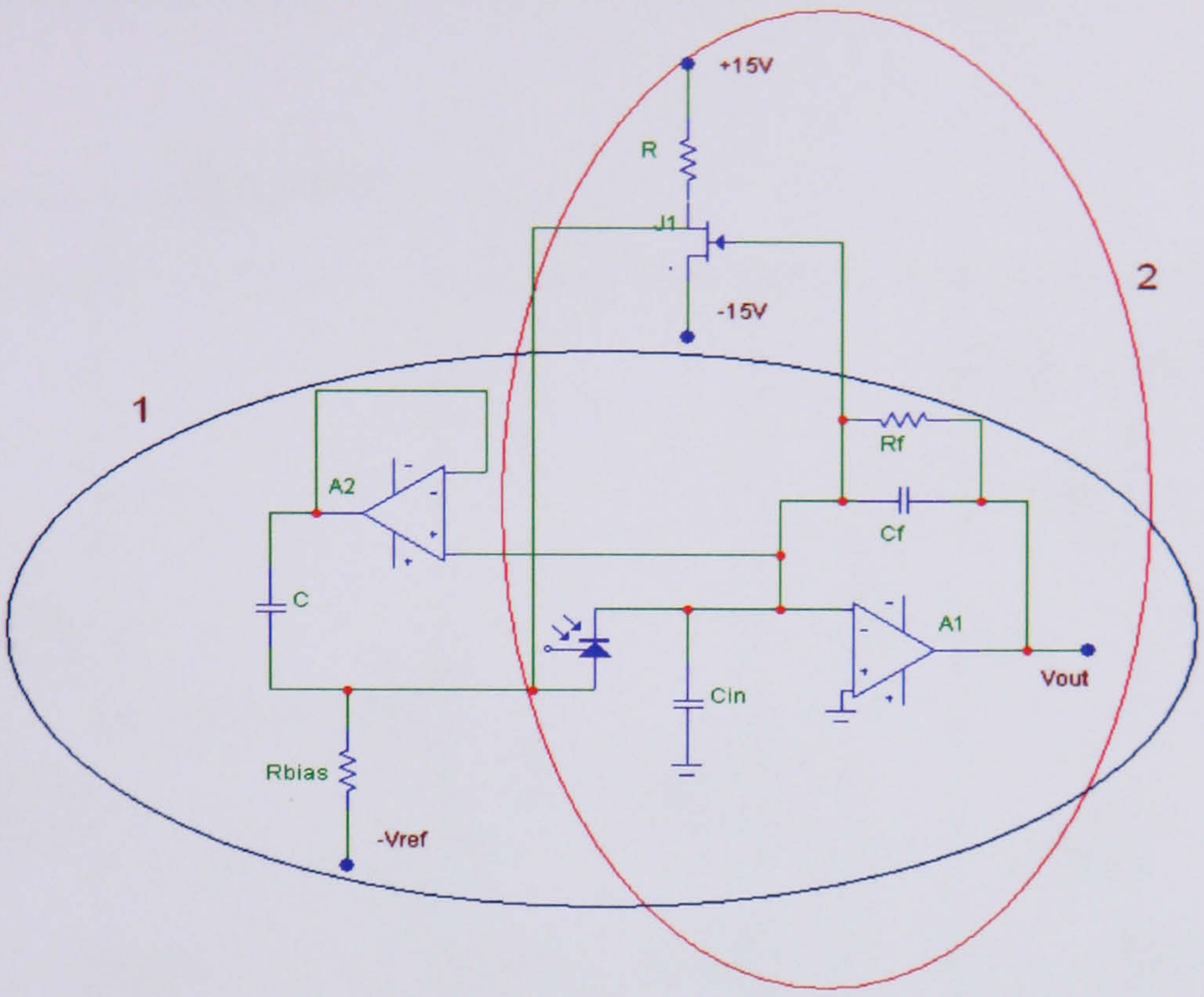

Figure 2.13 Two bootstrap transimpedance method : 1) Shunt bootstrap 2) Buffer bootstrap

The third bootstrapping transimpedance amplifier circuit by Green and McNeill [2.31] is shown in Figure 2.14. In this circuit, the gain transistor J_1 was found not necessary, as Q_1 and Q_2 provided the diode current. Q_1 itself acted as an emitter follower from the source of J_2 and Q_2 was a current source driven from the course of J_3. The diode capacitance was bootstrapped by the J_1, stage in conjunction with Q_1. Increasing R_s increased the enhancement effect to a value of 2000. An FET buffer J_3 drove a bipolar cascade circuit Q_3 and Q_4 buffered by Q_5. Overall feedback was given from the emitter of Q_5 to the gate J_1. Capacitance C_a was used to reduce the effects of stray capacitance of the feedback resistor. This element is critical in the analysis, as it is multiplied in effect by the open loop gain, and adds to the input time constant. With two modifications that R_4 and C_2 were used to bootstrap the input to J_1 to keep its input impedance high. It was concluded in [2.31] that

the bootstrap transimpedance amplifier offers the usual advantages of the transimpedance amplifier, together with an effective capacitance reduction technique.

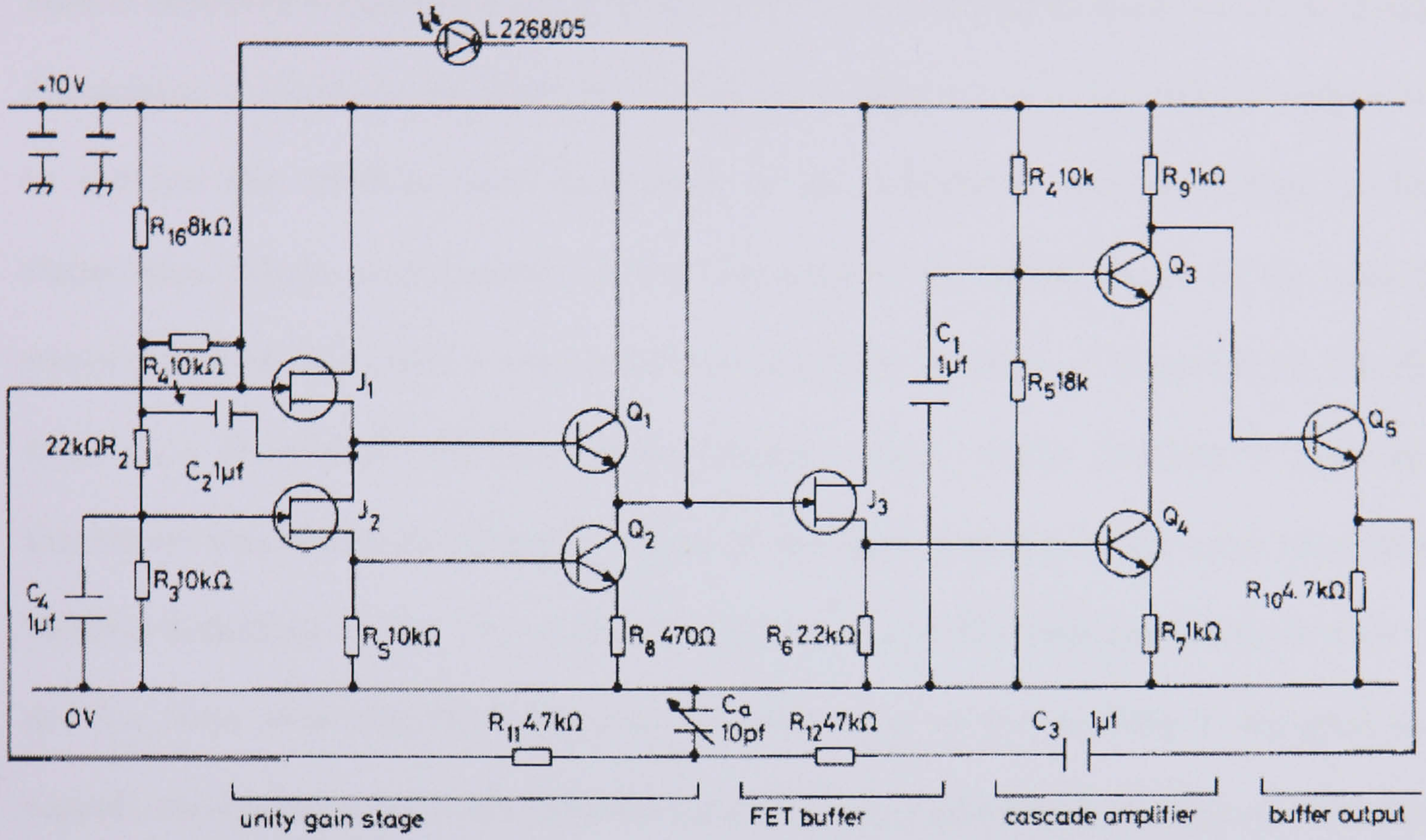

Bootstrap transimpedance amplifier

FETs = BF256A
BJTs = BSX20

Figure 2.14 Bootstrap transimpedance amplifier [2.31]

Since the inherent parasitic capacitance of devices is usually the cause of bandwidth limitation in preamplifier designs, the bootstrapping technique has been used in the preamplifier design to reduce the effective detector capacitance seen by the signal, allowing for wide bandwidth designs to be achieved [2.32-2.35].

The third technique, known as shunt peaking or inductor peaking, has historically been used to introduce a resonant peaking at the output as the amplitude starts to roll off at high frequencies. It improves the bandwidth by adding an inductor in series with the output load to increase the effective load impedance as the capacitive reactance drops at high frequencies. Analui and Hajimiri [2.36] demonstrate the effectiveness of the inductor peaking methodology, with a transimpedance amplifier as shown in Figure 2.15. The first stage is a shunt-shunt feedback transimpedance stage, which provides a low input impedance and reduce the dominant effect of the input pole due to the large photodiode junction capacitance, C_{PD}. The additional inductor, L_1, at the front-end interacts with C_{in} and $C_{PD,}$ thus enhancing the bandwidth. The next stage of the amplifier is designed as a cascade configuration with intermediate inductors. For a photodiode capacitance of 0.5pF, the circuit achieves a 2.4 times larger bandwidth than that achieved using the same circuit without the inductors. (VB is the bias voltage, C1 and C2 is the stray capacitance)

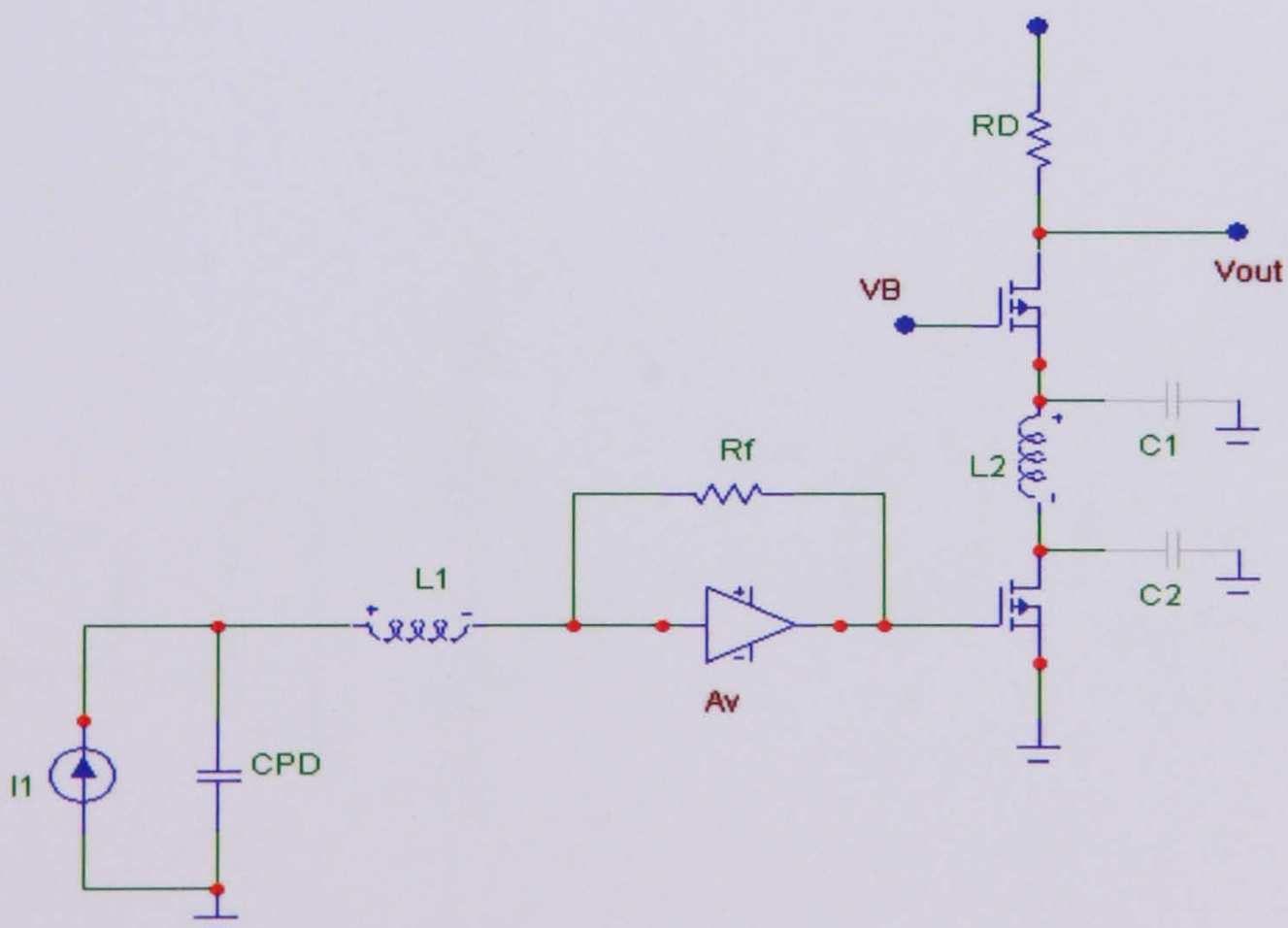

Figure 2.15 Schematic of TIA with parasitic capacitances and inductors [2.36]

Orengo et. al [2.37] suggested that the synthesis of the desired frequency response is performed by means of an integrated composite front-end amplifier. An inverting transimpedance amplifier is followed by a peaking amplifier, buffer, and further peaking amplifier, as shown in Figure 2.16. The aim of the peaking buffers is to provide a good separation between the two stages, and to introduce a high frequency peaking in the frequency response. The peaking buffers are of a source follower configuration, with an inductive load in series with the upper FET and a feedforward loop. The inverted signal drop on the inductor, ac coupled to the lower FET inverter, feeds forward and adds in phase to the signal. The effect of this peaking is to introduce a compensating zero in the frequency response. Tuning the inductance value pulls up the gain at the desired frequency but the amplitude peaking must be properly controlled to achieve gain flatness and stability. This technique based on inductive peaking to improve the high frequency performance results in a reduced bandwidth, dependence on the input photodiode parasitic capacitance.

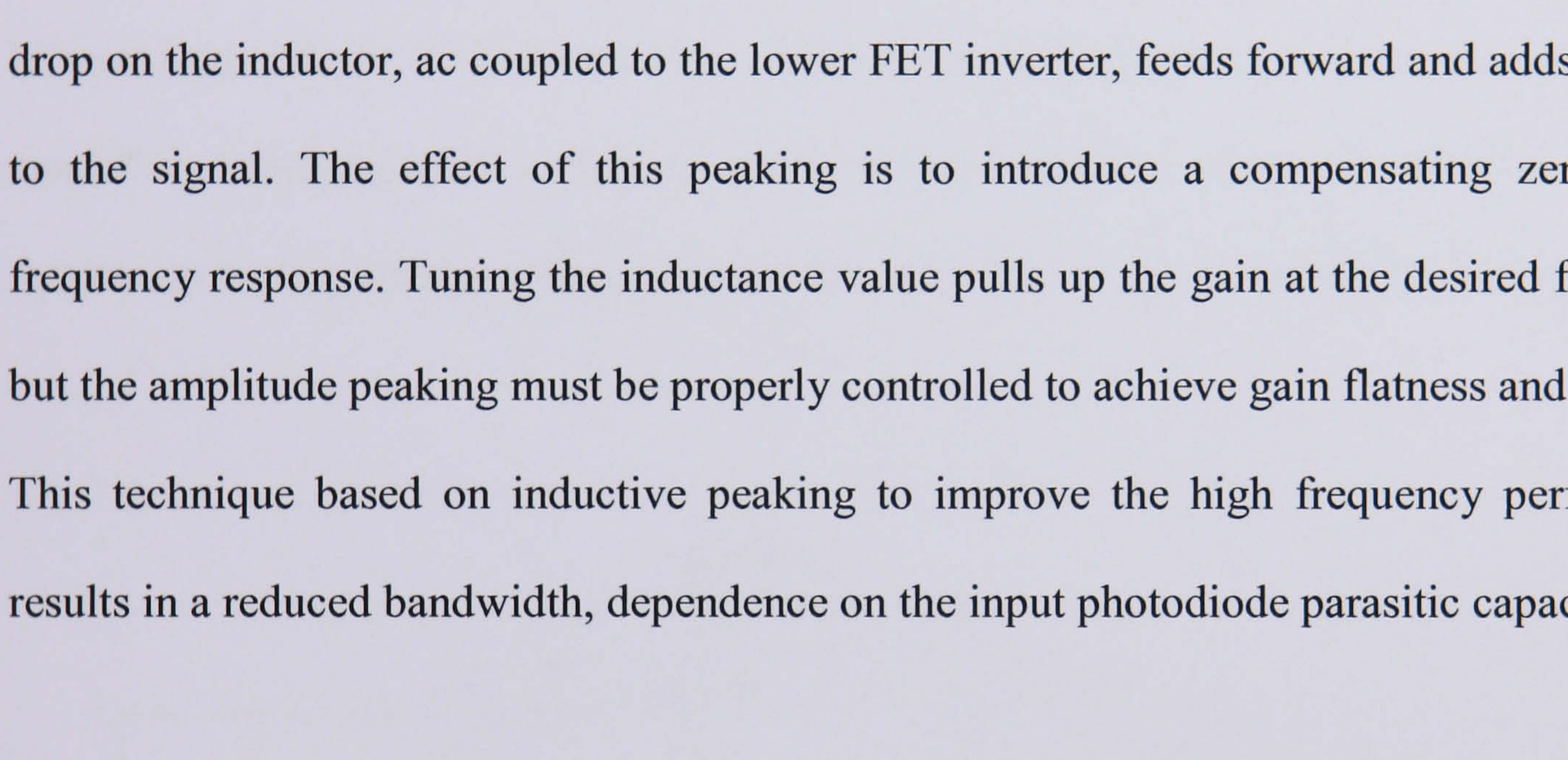

Figure 2.16 TIA with peaking buffer [2.37]

In summary, the inductor peaking technique does increase the amplifier bandwidth but the stray capacitances of the inductor often cause a bandwidth degradation rather than an improvement. To overcome this problem, the size of the inductor must be as small as possible to reduce the stray capacitance effect.

The fourth technique proposed by Chien and Chan [2.38], Vadipour[2.39] and Hamilton[2.40] to overcome the inductor peaking problem, is known as capacitive peaking (C-peaking). Figure 2.17 shows the schematic circuit of this C-peaking transimpedance amplifier represented as a shunt-shunt feedback amplifier. R_f is the effective feedback resistance, and C_p is the peaking capacitor added to the circuit for bandwidth enhancement.

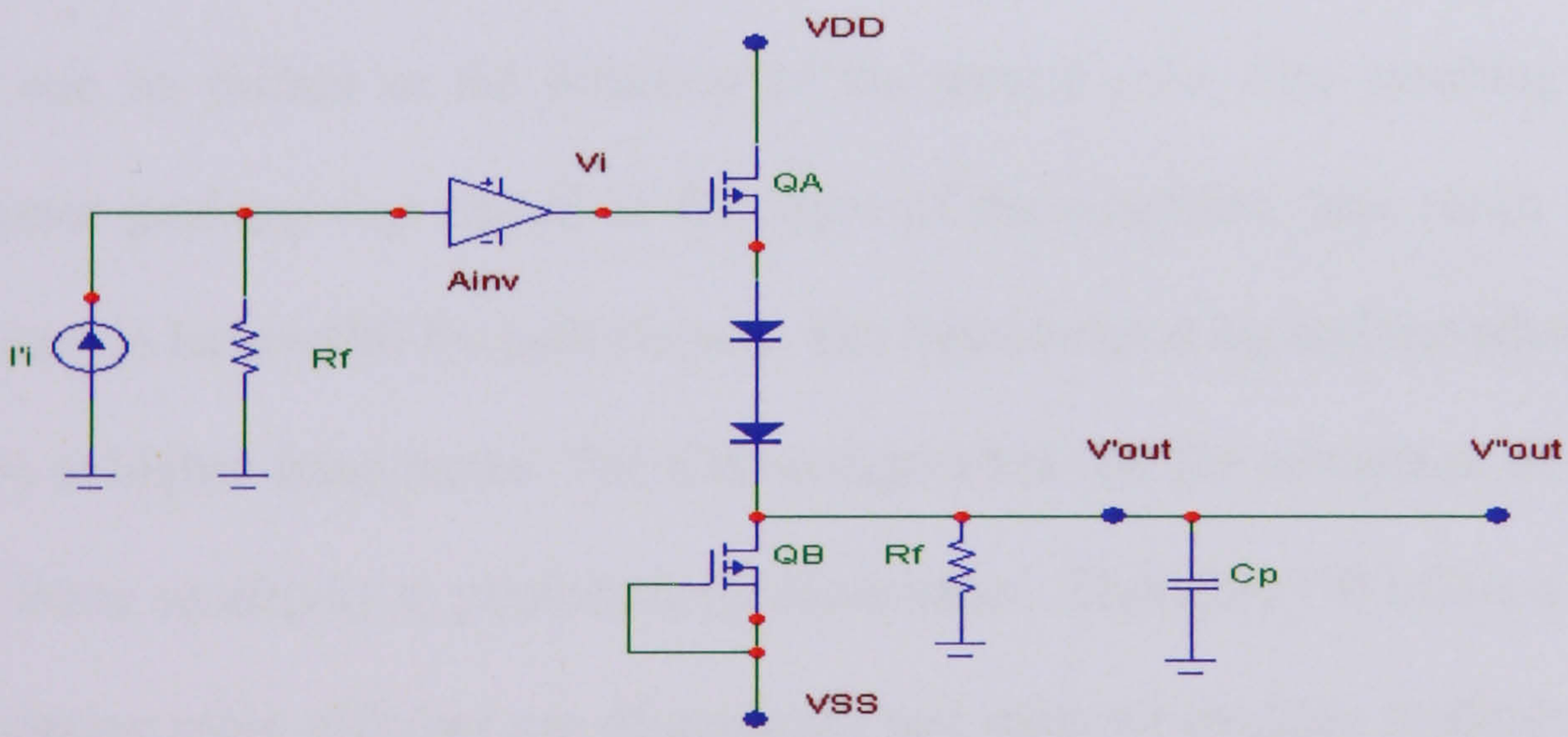

Figure 2.17 Circuit of C-peaking transimpedance amplifier with and without a peaking capacitor. [2.38]

According to the design in [2.38], adding Cp to the circuit means that the transfer functions of the circuit has an extra pole, which does not affect the input capacitance. If the quality Q factor is set more than 0.5 then the bandwidth is broadened due to the cancellation of imaginary parts. However, if Q equals 0.707, it results in a maximum in the frequency response and a peaking effect occurs. This means that the value of Q can be controlled by changing the value of Cp to adjust the bandwidth of the transimpedance amplifier. This method shows that the bandwidth of the transimpedance amplifier may be increased without sacrificing its low-frequency transimpedance gain. The factor of enhancement is around 2.0.

Yahaya [2.41], presents the effect of capacitive and inductive peaking techniques using common-base (CB) and common emitter (CE) preamplifier configurations. The peaking capacitor was connected at the output of the feedback resistor in order to create a third pole that can be shifted in the direction of the second pole, thus resulting in gain peaking. Inductor peaking was placed at the input of the amplifier. The result shows significant increase in bandwidth for both circuits. The inductor peaking had the advantage of reducing noise at higher frequencies. The CB configuration has the advantage of higher bandwidth and lower sensitivity to photodetector capacitance. Therefore CB offers a greater advantage by making more efficient use of capacitor and inductor peaking methods, compared to the CE configuration. Figure 2.18 shows an example configuration of a common base transimpedance preamplifier. Transistor Q1 act as a current buffer, while transistor Q2 and Q3 are voltage buffer with transistor Q4 as gain stage. The purpose of Q2, Q3 and Q4 is to avoid Q1 being saturated and boosting the gain. QB acts as a cascade transistor with Q1. A

topology based on a transimpedance amplifier using capacitive and inductive peaking has also been reported.[2.42] It was shown to be more robust and stable than the CB, CE or CC topology. The main drawbacks of this structure are its higher power consumption.

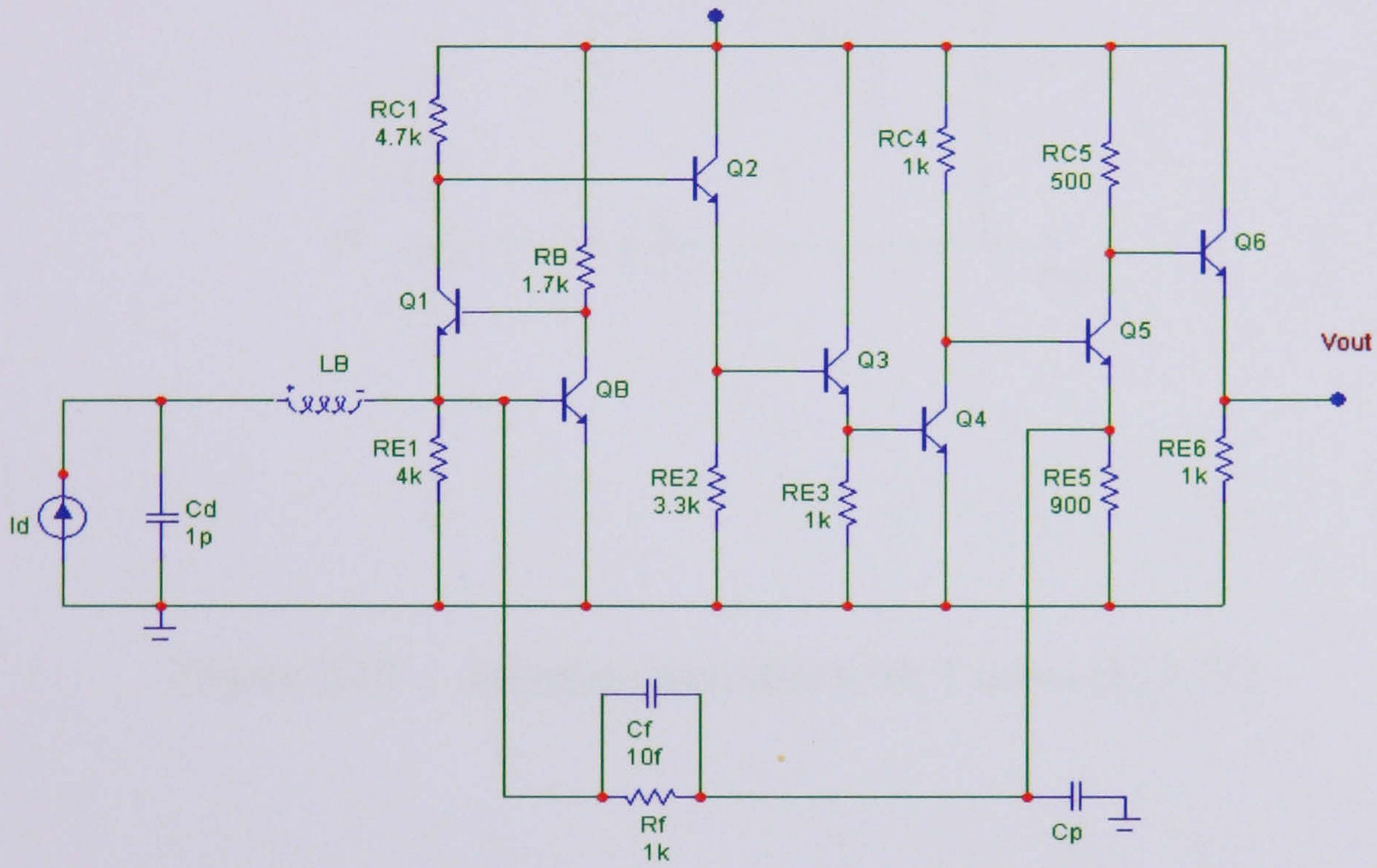

Figure 2.18 Common base transimpedance preamplifier with regulated cascade [2.41]

The fifth technique is to use a simple "T" network to replace the resistor feedback technique, as discussed earlier in the first technique.[2.43] This is due to the fact that changing resistor values can cause higher noise due to a higher valued R_F and high frequency response degradation arising from the parasitic capacitance associated with larger R_F. Using a T feedback circuit as shown in Figure 2.19, can overcome these drawbacks.[2.44] The T network consists of three feedback resistors, RF1, RF2 and RF3 and a capacitor, CF3. Without the capacitor, CF3 the T network will halve the bandwidth response. The RFs are chosen using the following equation :

$$R_F = RF1 + RF2 + \frac{RF1RF2}{RF3} \tag{2.6}$$

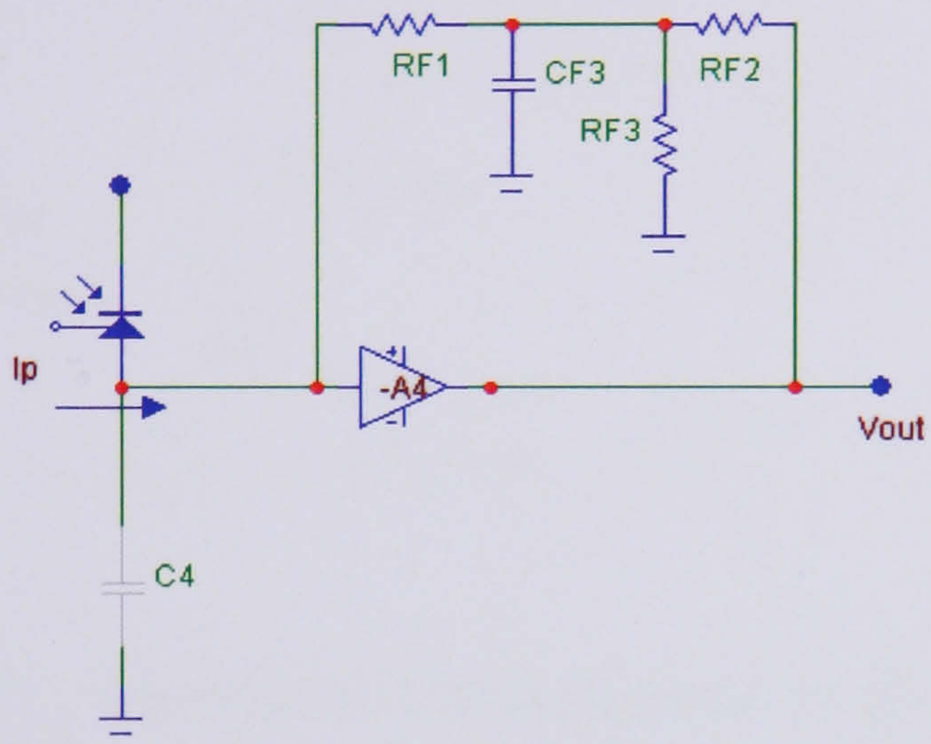

Figure 2.19 Inverting amplifier with T network.[2.44]

An additional technique is to use an external source to increase or decrease the bandwidth. The circuit in Figure 2.20 below by Centurelli,[2.45-2.46] presents a topology for a transimpedance amplifier that allows an external control over the bandwidth by applying a dc voltage to a high impedance node. The control input sinks a very low current and does not require a control voltage outside the supply range. Figure 2.20 shows the topology using ED02AH GaAs PHEMT technology for fibre optics communication. The common source-common drain cascade given by J_1 and J_2 with shunt-shunt feedback implements a typical transimpedance amplifier (TIA) and transistor J_L has been added to obtain a high impedance control input which does not interfere with the signal loop. The control voltage, V_{GG} allows modification of the bias point of transistor J_1 that adjusts the frequency

response of the TIA. The results from [2.46] show that the bandwidth change is only 2%, when the control voltage changes from 3V to 5V.

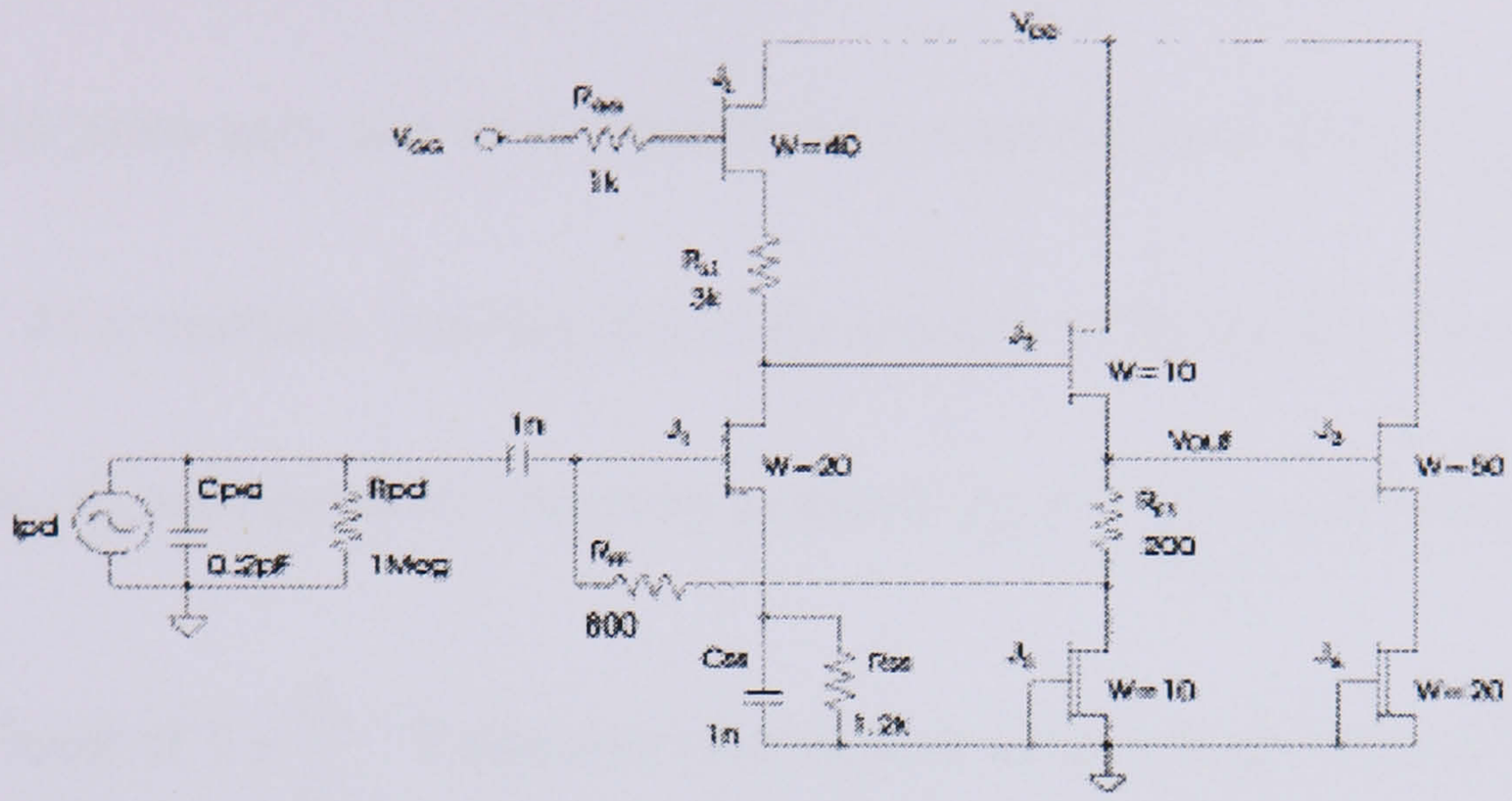

Figure 2.20 Topology of transimpedance amplifier [2.45]

2.3.3 Noise reduction

A low noise preamplifier and photodetector are crucial components of a receiver. Signal amplitude at the detector output is of very low value and in many cases is similar to the noise level value. Thus, preamplifiers should ensure adequate amplification, their own noise should be low, and their bandwidth should be broad enough to obtain non-distorted reproduction of the input signals. To minimise the amplifier noise relative to input signal, the major choices faced by a designer are in the configuration of the first stage in the amplifier because, for a device, the input noise level varies with the configuration in which it is used. Furthermore, it is the noise of the first stage that typically dominates the overall amplifier noise. Figure 2.21 illustrates the various capacitance effects through the noise

gain curve A_{noise}, plotted with amplifier gain-magnitude curve A_{OL}. Two other curves in Figure 2.21 represent the circuit's current-to-voltage gain and $\frac{1}{\beta}$ response. The A_{noise} curve begins with unity gain and then experiences a response zero at $f_{zf} = \frac{1}{2\pi R_f (C_{in} + C_s)}$. It then rises from feedback shunting due to the reaction of R_f and C_{in}. The stray capacitance shunting R_f, C_s, terminates this rise with a pole at $f_{pf} = \frac{1}{2\pi R_f C_s}$, leveling the noise gain at a plateau level of $1 + \frac{C_{in}}{C_s}$. Large-area photodiodes mean a high value of C_D will make C_{in} higher, producing a higher gain plateau.

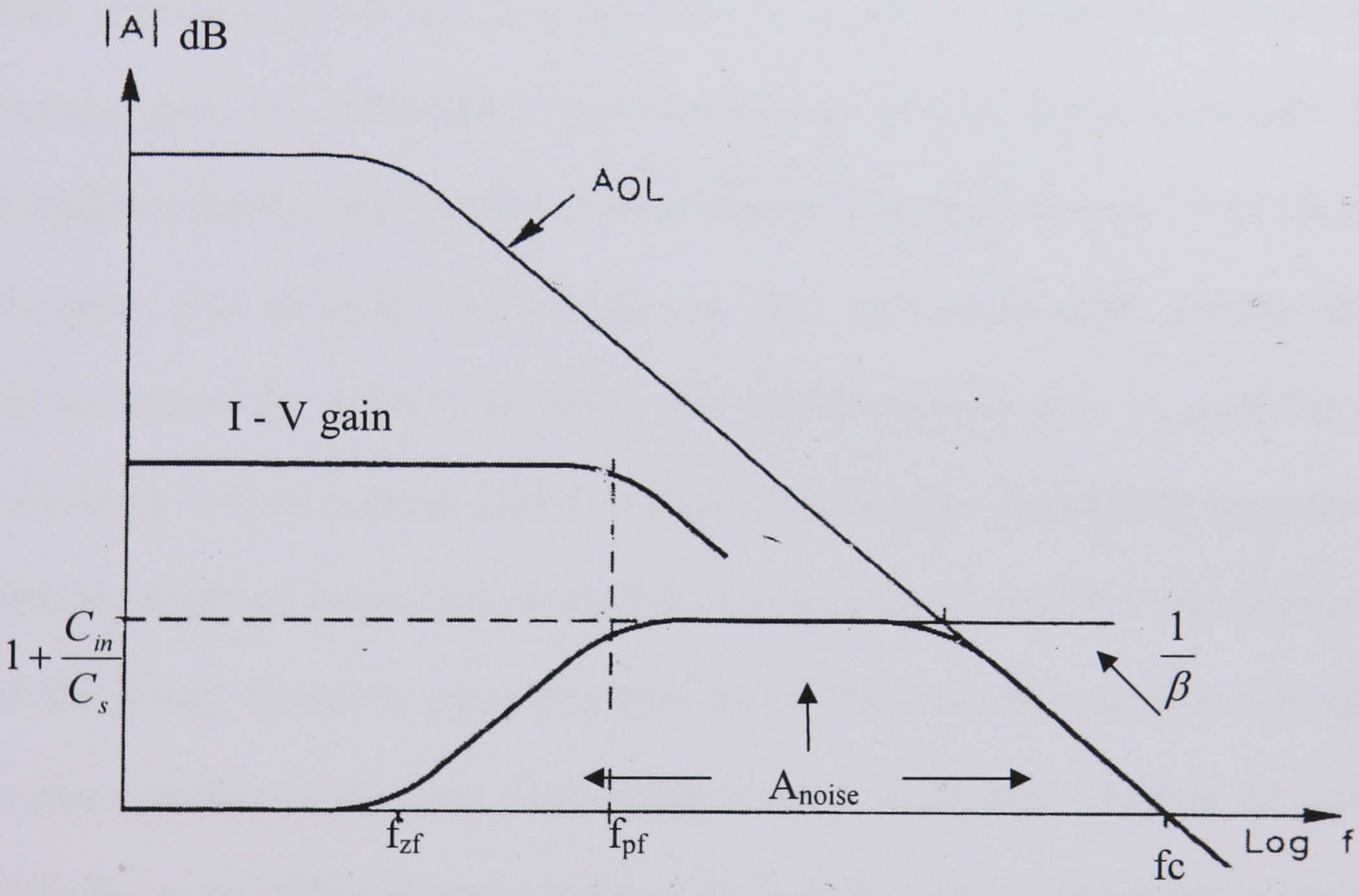

Figure 2.21 High feedback resistance and the capacitance of the input circuit causing the amplifier noise gain A_{noise} rise at the higher frequency until level by the stray capacitance and finally rolled off by the amplifier open-loop response. [2.47]

where,

A_{OL} – amplifier open loop bandwidth limit

fc- unity-gain crossover frequency of the amplifier

β – feedback factor

$C_{in} = C_D + C_a$

(C_D-photodiode capacitance, C_a – input capacitance between amplifier inputs)

Three techniques to reduce or remove the noise disadvantages have been presented by Graeme [2.48]. The first technique simply adds a feedback capacitance, C_f, in parallel with the feedback resistance, R_f of the transimpedance amplifier to reduce the circuit's high frequency noise gain, but unfortunately this method also reduces signal bandwidth. This approach reaches a point of diminishing returns, because continued increase of C_f can only reduce the noise gain to unity. The second and third techniques apply greater circuit complexity to address the noise issue better. The second method adds an amplifier and feedback elements to form a noise filtering composite amplifier. A modified integrator is added within the feedback loop of the photodiode transimpedance amplifier that permits the roll off of the higher frequency open-loop gain only. The composite amplifier structure leaves the characteristics of the current-to-voltage converter unchanged. Adding the second amplifier introduces no additional noise, because the high gain of the first amplifier isolates the composite circuit input from the second amplifier input errors. The final technique avoids the added amplifier of the composite amplifier and active filter by exploiting the filtering effects of a common phase compensation method. This method reduces the noise

gain of a photodiode transimpedance amplifier by adding a passive filter within its feedback loop. Unfortunately, this approach may either degrade or improve the noise reduction.

Howard [2.49-2.50], suggested four relative parameters to be considered when designing a low noise feedback amplifier with transimpedance characteristics as follows :-

a) The configuration of first stage in the amplifier

b) A choice between BJT, JFET or MOSFET, because the choice depends upon the amplifier frequency range and the type of amplifier.

c) Specification of component values so that the overall amplifier has the desired bandwidth and gain. It is important to choose parameter values so that the gain and bandwidth are achieved without impairing the amplifier noise performance.

d) The circuitry used to power the amplifier and the detector circuitry. These usually exhibit noise at a level much higher than the active device used at the first stage.

2.4 Voltage feedback amplifier versus Current feedback amplifier

Converting the small output current of a photodiode to a fast responding voltage is often challenging. Voltage feedback amplifiers (VFA) have the following characteristics : both inputs are high impedance, a low output impedance, high forward voltage gain and constant gain x bandwidth product. Current feedback amplifier (CFA) characteristics are high

impedance at the positive input while low impedance at the negative input, low output impedance, high forward transimpedance gain, and bandwidth independent of gain. Figure 2.22 shows the gain versus frequency plot for voltage and current feedback.

Figure 2.22 Voltage feedback amplifier and current feedback amplifier [2.51]

Comparing the two feedback amplifier characteristics above, CFAs are especially suited to implement this function. With an effective internal buffer of an inverting amplifier, the output resistance, R_o, and the photodiode capacitance, C_D, introduce a zero in the noise gain at approximately, $\frac{1}{2\pi R_o C_D}$. In comparison, the zero produced by a VFA in a similar configuration, $\frac{1}{2\pi(R_{in} // R_F)C_D}$ tends to be at a much lower frequency. This is because C_D has less effect on reduction of the photodiode bandwidth, and achieving stability is easier when using a CFA. If, C_D is sufficiently large, the open loop transimpedance gain crosses the noise gain function. As with the VFA, the closed loop amplifier can be compensated by adding a small capacitor, C_F across R_F as discussed in section 2.3.3. C_f improves stability

by counteracting the effect of the zero discussed above by introducing a low frequency pole $\frac{1}{2\pi R_f C_f}$ and inconsequential zero $\frac{1}{2\pi R_o C_f}$. In conclusion, it's more difficult to design a good current-to-voltage converter using VFA, because photodiode capacitance is often a source of instability and wide bandwidth usually comes at the expense of supply current and higher supply voltage. CFA would be an easier choice to use in the design of photodiode preamplifier, but National Semiconductor currently has developed new high speed low voltage VFA which has excellent performance in a transimpedance gain block.

2.5 Definition of Dynamic Service Quality (QoS)

Quality-of-service (QoS) can be defined as a qualitative and quantitative set of measurements used to differentiate between services in a network. These measurements may be parameters, such as response time, bandwidth requirement, jitter, signal-to-noise ratio (SNR) and etc. QoS helps in classifying services, optimising bandwidth, and in assisting service providers to better control, manage, and generate new revenue based on actual resource usage. Since reliability and service guarantee are central to QoS, its utilisation will enable networks to become more robust.[2.52] The design approach in this thesis is based on providing Quality of Service (QoS) assurance to an adaptable receiver preamplifier using IR communication. Since the received signal-to-noise ratio (SNR) determines the maximum achievable data rate and essentially determines the probability of error, it is an effective measure of the QoS. The benefit of an adaptable receiver technique is that it seeks to minimise the total transmission power subject to meeting potentially different constraints on the received SNR for the intended receiver.

2.6 Summary

The above literature review discussed the photodetector and optical preamplifier that make up the front-end of an optical receiver. The transimpedance amplifier is the most common preamplifier structure compared to the high impedance amplifier, which creates a heavy demand for equalization that reduces the overall dynamic range of the receiver. Three principal requirements for a receiver preamplifier, ie : a wide dynamic range, bandwidth enhancement and noise reduction have been described. Various techniques for achieving these three principal requirements of receiver design, have been presented from the literature.

The four techniques discussed to achieve wide dynamic range simply trade gain for bandwidth, and their configurations cause instability. Therefore, the strategy to produce a wide dynamic range receiver is to implement an easily-controlled automatic gain control in the front-end, which does not trade gain for bandwidth.

Bandwidth enhancement is a fundamental requirement in the design of optical receiver without a large sacrifice of SNR. Among the five principle techniques presented, the advantage of bootstrapping techniques is to reduce the effective photodiode capacitance in order to achieve higher bandwidth. Feedback and inductor peaking techniques also show promising increases in bandwidth but at the expense of gain, and the problem of stray capacitance. The capacitor peaking and inductor peaking techniques main drawbacks are high power consumption. The least effective bandwidth enhancement is the T resistor

network techniques. This is due to the fact that changing resistor values can cause higher noise.

A low noise preamplifier is crucial component of a receiver. It is the noise of the first stage that typically dominates the overall amplifier noise. Three techniques to reduce noise have been presented in this chapter. Unfortunately the techniques reduce signal bandwidth, and may either degrade or improve noise reduction.

Therefore, the receivers discussed in this chapter have different capabilities and characteristics, depending on the application required, mostly for the fibre optics environment. The most common receiver characteristic of the work presented is: - high bandwidth, high sensitivity and low noise, which are the trends of the future for optical wireless receivers in infrared applications.

References

[2.1] H.Kressel, "Semiconductor Devices for Optical Communications", 2nd edition, Spring-Verlag, Berlin, Germany, 1982.

[2.2] S.D. Personick, "Fiber Optics, Technology and Applications", Plennum Press, New York, 1985.

[2.3] S.E. Miller and I.P. Kaminow, "Optical Fibre Telecommunications II", Academic Press, San Diego, 1988.

[2.4] S.B. Alexander, "Optical Communication Receiver Design", SPIE Optical Engineering Press, London, UK, Chapter 6, pp. 173-201,1997.

[2.5] J.R. Barry, "Wireless Infrared Communications", Kluwer Academic Publication, Boston, Chapter 3, pp. 49-52, 1994.

[2.6] S. Hranilovic, " Modulation and constrained coding techniques for Wireless Infrared Communication channels", Master Thesis, Dept. Electrical and Computer Engineering, University of Toronto, 1999.

[2.7] S.D Personick, "Receiver Design for Digital Fiber Optic Communication Systems I", The Bell System Technical Journal, Vol : 52, pp : 843 – 874, 1973.

[2.8] J.G Graeme, "Photodiode amplifiers : Op amp solutions", McGraw Hill, Chapter 1, pp 1- 19, 1985.

[2.9] Datasheet Siemens SFH 206K Photodiode,

http:// www.chipdocs.com/datasheets/datasheet-pdf/Siemens/SFH206.html

[2.10] Philips C.D. Hobbs, "Building Electro-Optical Systems : Making it All Work", John Wiley & Sons Inc, pp : 620 – 666, 2000.

[2.11] R.G. Smith and S.D Personick, "Receiver design for optical fibre communication systems " in Semiconductor Devices for Optical Communication" 2nd edition, Chapter 4, pp. 89-160, Spring-Verlag, Berlin, Germany, 1982.

[2.12] T.V. Muoi, "Receiver design for High-Speed Optical Fibre Systems", IEEE Journal Lightwave Technology, Vol : LT-2(3), pp. 243-267, June 1984.

[2.13] Infrared Data Association (IrDA), Serial Infrared Physical Layer Link Specification, Version 1.2, **http://www.irda.org**, November 1997.

[2.14] D. Yamazaki, "156Mbit/s preamplifier IC with wide dynamic range for ATM-PON application", Electronic Letters, Vol :33, No. 15, pp. 1308-1309, 1997.

[2.15] K. Ohhata, T. Masuda, K. Imai, R. Takeyari and K. Washio, " A wide dynamic range High transimpedance Si bipolar preamplifier IC for 10Gb/s optical fibre links", IEEE Journal Solid-State Circuits, Vol :34, No. 1, pp. 18-24, January 1999.

[2.16] M. Nakamura and N. Ishihara," 1.2V, 35mW CMOS optical transceiver ICs for 50Mbit/s burst-mode communication", Electronic Letters, Vol :35, No. 5, pp. 294-395, March 1999.

[2.17] L.A.D. Van den Broeke, A.J. Niewkerk, "Wideband integrated optical receiver with improved dynamic range using a current switch at the input", IEEE Journal Solid-State Circuits, Vol : 28, No.7, pp. 862-864, July 1993.

[2.18] B. Owen, "PIN-GaAs FET optical receiver with a wide dynamic range", Electronic Letters, Vol. 18, No. 14, pp. 626-627, July 1982.

[2.19] R.G. Meyer and W.D. Mack, " A wideband low noise variable-gain BiCMOS transimpedance amplifier", IEEE Journal Solid-State Circuits, Vol : 29, No. 6, pp. 701-706, June 1994.

[2.20] H. Khorramabadi, L. Tzeng and M. Tarsia, "A 1.06 Gb/s -31dBm to 0dBm BiCMOS optical preamplifier featuring adaptive transimpedance", IEEE ISSCC Digest of Technical Papers, pp. 54-55, February 1995.

[2.21] B. Wilson and J.D. Drew, "Novel transimpedance amplifier formulation exhibiting gain-bandwidth independence", IEEE Proceeding, International Symposium Circuits and Systems, Vol : 1, pp. 169-172, June 1997.

[2.22] J.L. Cura and R.L Aguiar," Dynamic range boosting for wireless optical receivers", IEEE International Symposium Circuits and Systems, ISCAS, Vol: 4, pp. 686-689, 2001.

[2.23] C.D. Motchenbacker and F.C. Fitchen, "Low noise Electronic Design", Wiley, New York, 1973.

[2.24] E.J. Fairlie," Photodiode preamplifier systems- low noise positive feedback", Applied Optics, Vol : 16, pp: 385-392, 1977.

[2.25] M.E. Schlarmann, S.Q Malik and R.L Geiger, "Positive feedback gain-enhancement techniques for amplifier design", IEEE International Symposium Circuits and Systems, ISCAS, Vol: 2, pp. 26-29, 2002.

[2.26] M.J Teare, "Low noise detector amplifier", UK Patent 3801933, April 1973.

[2.27] T.K. Hemingway, " Electronic Designs Handbook", Business books, Chapter 15, pp. 283-295, 1979.

[2.28] C. Hoyle and A. Peyton, "Bootstrapping techniques to improve the bandwidth of treansimpedance amplifiers", Analog signal processing, IEE Colloquium, pp. 7/1-7/6, October 1998.

[2.29] C. Hoyle and A. Peyton, "Shunt bootstrapping technique to improve bandwidth of transimpedance amplifiers", Electonics Letters, Vol: 35, No.5, pp. 369-370, March 1999.

[2.30] T.R Kristein," Increasing photodiode transimpedance bandwidth and SNR with a bootstrap buffer", SENSORS, Vol: 13, Part 3, pp. 35-38, 1996.

[2.31] R.J.Green and M.G McNeill, "bootstrap transimpedance amplifier : a new configuration", IEE Proceedings, Vol: 136, No. 2, pp. 57-61, April 1989.

[2.32] R.J Green, " Experimental performance of a bandwidth enhancement technique for photodetectors", Electonics Letters, Vol : 22, No. 3, pp. 153-155, January 1985.

[2.33] M.J McCullagh and D.R Wisely," 155Mbit/s optical wireless link using a bootstrapped silicon APD receiver", Electronics Letters, Vol : 30, No. 5, pp. 430-432, March 1994.

[2.34] A.M Street, P.N. Stavrinou, D.J Edwards and G. Parry, " Optical preamplifier designs for IR-Lan applications", Optical Free Space Communication Links, IEE Colloquium, pp. 8/1-8/6, February, 1996.

[2.35] A.M Street, P.N Stavrinou, D.C O'Brien and D.J Edwards," Indoor optical wireless systems – a review", Optical and Quantum Electronics, No. 29, pp. 349-378, 1997.

[2.36] B. Analui and A. Hajimiri," Bandwidth enhancement for transimpedance amplifiers", IEEE Journal of Solid-State Circuits, Vol: 39, No. 8, pp. 1263-1270, August 2004.

[2.37] G. Orengo, E. Limiti, G. Acciari and F. Giannini," Gain enhancement and input parasitic compensation in MMIC transimpedance amplifiers for optical receivers", Microwave and optical technology letters, Vol: 17, No. 6, pp. 377-383, April 1998.

[2.38] F.T Chien and Y.J Chan," Bandwidth enhancement of transimpedance amplifier by a capacitive peaking design", IEEE Journal of Solid-State Circuits, Vol: 34, No. 8, pp. 1167-1170, August 1999.

[2.39] M. Vadipour," Capacitive feedback technique for wide-band amplifiers", IEEE Journal of Solid-State, Vol: 28, Issue 1, pp. 90-92, January 1993.

[2.40] D.K Hamilton," Performance of transfer resistance amplifiers with capacitive source in optical applications", IEE Proceedings, Vol: 138, No.1, pp. 45-51, February 1991.

[2.41] C.B Yahya, "Design of wideband low noise transimpedance amplifiers for optical communication", Proceeding 43rd IEEE Midwest Symposium on Circuits and Systems, pp. 804-807, August 2000.

[2.42] Y. Lu and M. N. El-Gamal," A 2.3V low noise, low power, 10GHz bandwidth Si-bipolar transimpedance preamplifier for optical receiver front-ends", IEEE International Symposium Circuits and Systems, ISCAS, Vol: 4, pp. 834-837, May 2001.

[2.43] C. Seidl, J. Knorr and H. Zimmermann," Simple feedback network for bandwidth enhancement of transimpedance amplifiers", Electronics Letters, Vol: 39, No. 25, December 2003.

[2.44] R. Wu, F.J Lidgey and K. Hayatleh," Frequency performance compensation of operational amplifiers with the "T" feedback network", Analog Integrated Circuits and Signal Processing, Vol: 41, pp. 79-83, 2004.

[2.45] F. Centurelli, L. Germani, R. Luzzi, P. Tommasino and A. Trifiletti," A new topology for a transimpedance amplifier with postfabrication bandwidth adjustment", Microwave and Optical Technology Letters, Vol: 25, No. 1, pp.47-51, April 2000.

[2.46] F. Centurelli, R. Luzzi, G. Scotti and A. Trifiletti," A bandwidth-compensated transimpedance amplifier for multigigabit optical receivers", Microwave and Optical Technology Letters, Vol: 30, No. 2, pp.79-81, July 2001

[2.47] J.G Graeme, "Photodiode amplifiers : Op amp solutions", McGraw Hill, Chapter 5, pp 87-106, 1985.

[2.48] J.G Graeme, "Photodiode amplifiers : Op amp solutions", McGraw Hill, Chapter 6, pp 107-128, 1985.

[2.49] R.M Howard," Low noise amplifier design and low noise amplifiers for characterizing the low frequency noise of infrared detectors", Proceedings 1998 Conference on Optoelectronic and Microelectronic materials Devices, pp. 179-182, December 1998.

[2.50] R.M Howard," Ultra low noise high gain transimpedance amplifier for characterizing the low frequency noise of infrared detectors", Review of Scientific Instruments, Vol: 70, No. 3, pp. 1860-1867, March 1999.

[2.51] W. Bacharowski, "National Semiconductor: Amplifier applications", **www.fulcrum.ru/Read/Seminars/03_10_28_seminar_NS/A...**

[2.52] M. Mirhakkak, N. Schult and D. Thomson," Dynamic bandwidth management and adaptive applications for a variable bandwidth wireless environment", IEEE Journal on Selected Areas in Communications, Vol : 19, No. 10, pp. 1984-1996, October 2001.

Chapter 3

New Transimpedance Amplifier Structures

In this chapter, three transimpedance amplifier structures to address the principal design requirements as outlined in Chapter 2 are developed: bandwidth adjustment with enhancement and wide dynamic range. This begins by demonstrating the limitation effect of the photodiode capacitance in relation to a preamplifier design. Graphical frequency plots, showing the photodiode junction capacitance effects on bandwidth, are given. Next, the developed preamplifier topology is presented, focusing on the bandwidth adjustment with enhancement parameter capabilities for a transimpedance amplifier with a FET voltage control filter. This is followed by a transimpedance amplifier with external voltage control and a bootstrap transimpedance amplifier with an adjustable capacitor. The idea

proposed in this thesis for bandwidth adjustment is to incorporate a variable filter block at the input or output of a transimpedance amplifier. The variable filter block component consisted of either: 1) a variable capacitor or 2) a variable voltage applied to the gate FET or the base of a BJT. Throughout this chapter, mathematical derivations and simulation results of the proposed designs are presented.

As mentioned in the previous chapter, junction capacitance restricts bandwidth in photodiodes. Any signal voltage developed across the diode reacts with this capacitance, shunting the diode's output current. For comparison, Figure 3.1 illustrates a simple circuit for the connection of the photodiode to an input sinusoidal signal and a load resistor. The circuit produces the ideal response $e_o = i_p R_L$ until capacitive shunting diverts i_p from R_L at higher frequencies. There, the junction capacitance of the input circuit, C_D, produces a response roll-off with a pole at a frequency of, $f_p = \frac{1}{2\pi R_L C_D}$. For most photodiode applications, large values of R_L and C_D would severely restrict performance because of bandwidth limitation. Increasing R_L produces greater gain but reduces the bandwidth set by f_p in direct proportion. Therefore Figure 3.1 is used as an analogy for an infrared optical wireless link front-end, for all, the proposed designed receivers described in Chapter 1.

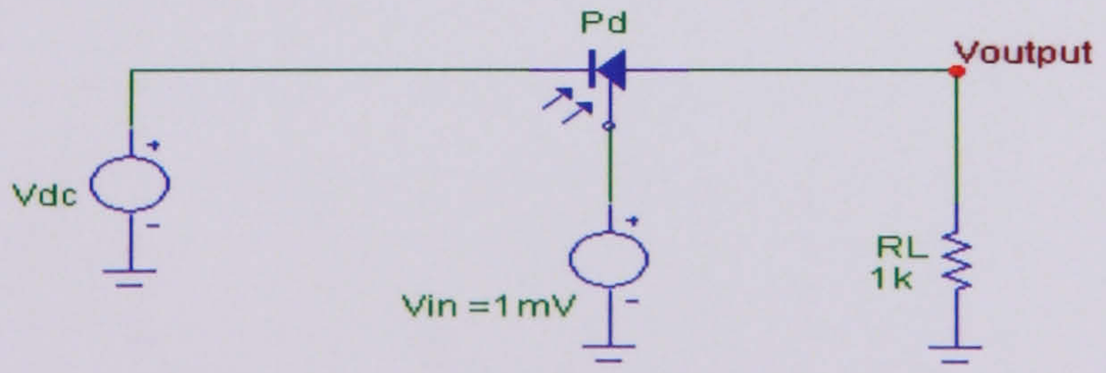

Figure 3.1 Circuit stimulation of a photodiode

By varying the junction capacitance of the photodiode, $P_{d,}$ from 13pF to 1.5pF, the frequency response of the photodiode sets the bandwidth as shown in Figure 3.2 and Figure 3.3.

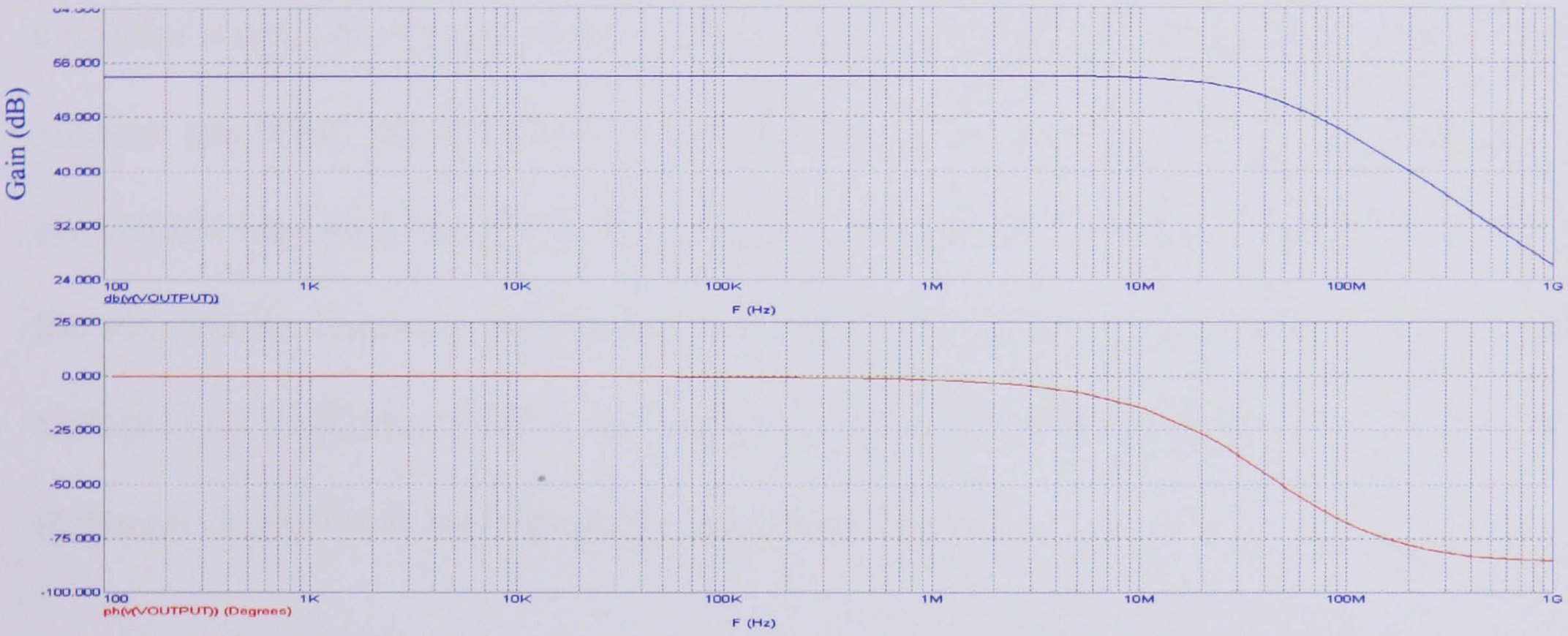

Figure 3.2 Frequency response plot when the photodiode junction capacitance is 13pF

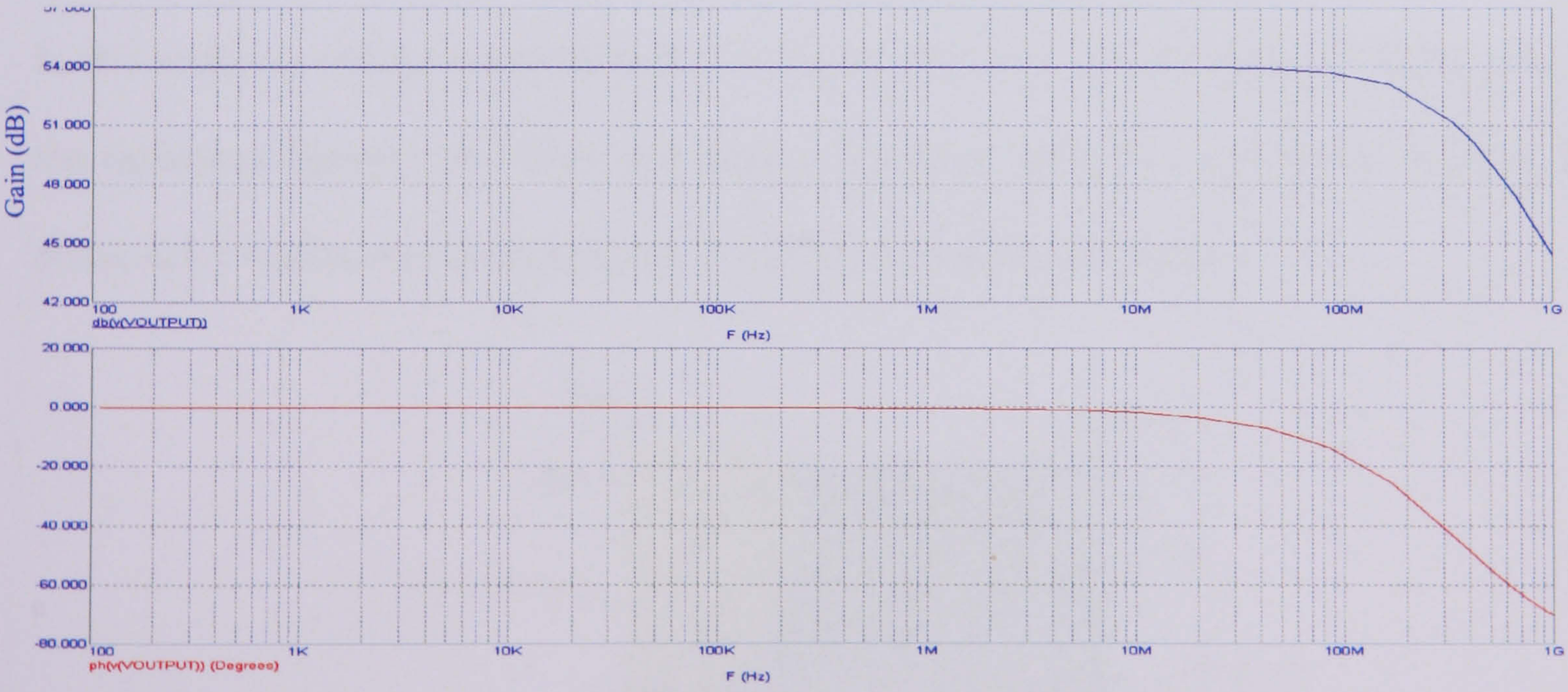

Figure 3.3 Frequency response plot when the photodiode junction capacitance is 1.5pF

Three amplifier circuit methods greatly ease this restriction through signal isolation, photodiode bias and photodiode bootstrap as discussed briefly in Chapter 2. Signal isolation removes the signal voltage from the photodiode, while supplying the signal voltage to the amplifier output. For better improvement, biasing or bootstrapping the photodiode further reduces the effect of the diode's capacitance. A reverse bias voltage applied to the photodiode improves bandwidth by reducing the diode junction's capacitance. Bootstrap of the photodiode improves bandwidth by isolating the diode capacitance from the signal voltage. For small photodiodes, the bootstrap alternative achieves greater bandwidth. This technique is applied to assist in the design of the receiver.

3.1 Transimpedance Amplifier with FET voltage control filter

In this section a voltage controlled filter using an FET as a variable resistor (VCR), where the resistance between the drain and source is controlled by the gate-source voltage, is discussed. Consider the characteristics of a JFET with pinch-off voltage = V_p :

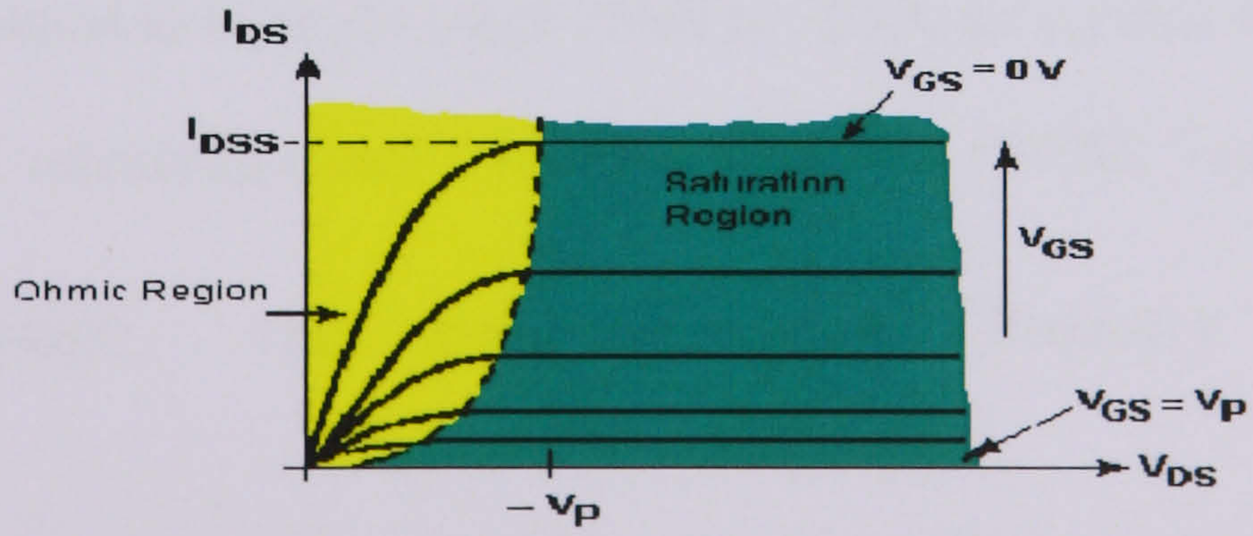

Figure 3.4 I_{DS}-V_{DS} Characteristics of a JFET [3.1]

There are two distinct regions - the saturation region and the ohmic region. In the saturation region the drain current is almost entirely independent of the drain-source voltage, whilst in the ohmic region the drain current depends on the drain-source voltage. The equation of the curve is as follows :- [3.1]

$$|V_{DS}| = |V_p| - |V_{GS}|$$

$$I_D \approx \frac{2I_{DSS}}{V_p{}^2}[V_{DS}(V_{GS} - V_p) - 0.5V_{DS}{}^2 \quad \text{.....(3.1)}$$

$$\frac{1}{r_{DS}} = \frac{I_D}{V_{DS}} \approx \frac{2I_{DSS}}{V_p{}^2}[(V_{GS} - V_p) - 0.5V_{DS}] \quad \text{.....(3.2)}$$

Making V_{GS} more negative (n-channel FET) than the transistor's threshold voltage provides additional channel electrons, reducing channel resistance and increasing the slope of the V-I curve. The result is a voltage controlled resistor. The voltage controlled filter block is, basically, a low pass filter, consisting of an FET in series with a capacitor. Figure 3.5 shows the FET in series with a capacitor simulated with a photodiode, and the simulated result is presented in Figure 3.6. The result shows that as V_{GS} increases from -0.1V to -3V, the 3dB cutoff frequency varies from 4.52 MHz to 702 kHz. This is because, as V_{GS} approaches the pinch-off value, the drain-to-source resistance increases. The R_{DS} of the FET (2N4461) is calculated to be in the range 250Ω to 750Ω, for a pinch-off value of -3V. For example, the ideal calculated cutoff frequency when R_{DS} =250Ω, $V_{GS} \sim 0V$, is $f_{3dB} = \frac{1}{2\pi(250)(100pF)} = 6.3MHz$. The simulated cutoff frequency is $f_{3dB} = \frac{1}{2\pi(R_{DS} + R_{Pd})(C_p + C_{pd})}$, assuming R_s and $R_o > R_{Pd}$, where R_s is the input resistance, R_o

is the output resistance and R_{Pd} is the photodiode resistance. The combined resistance and capacitance of the FET and photodetector has caused a variation of 1.8MHz in bandwidth compared to the ideal calculation.

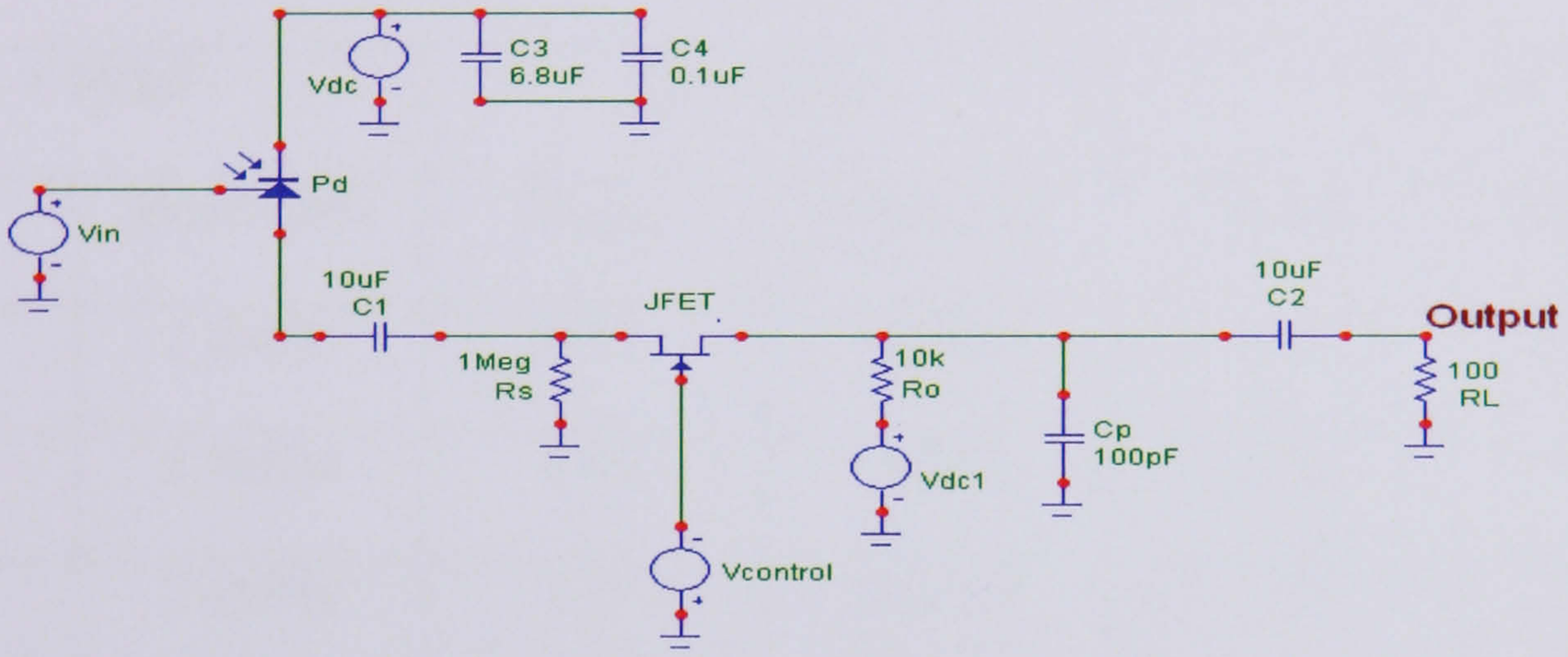

Figure 3.5 Photodiode with FET as a voltage controlled filter

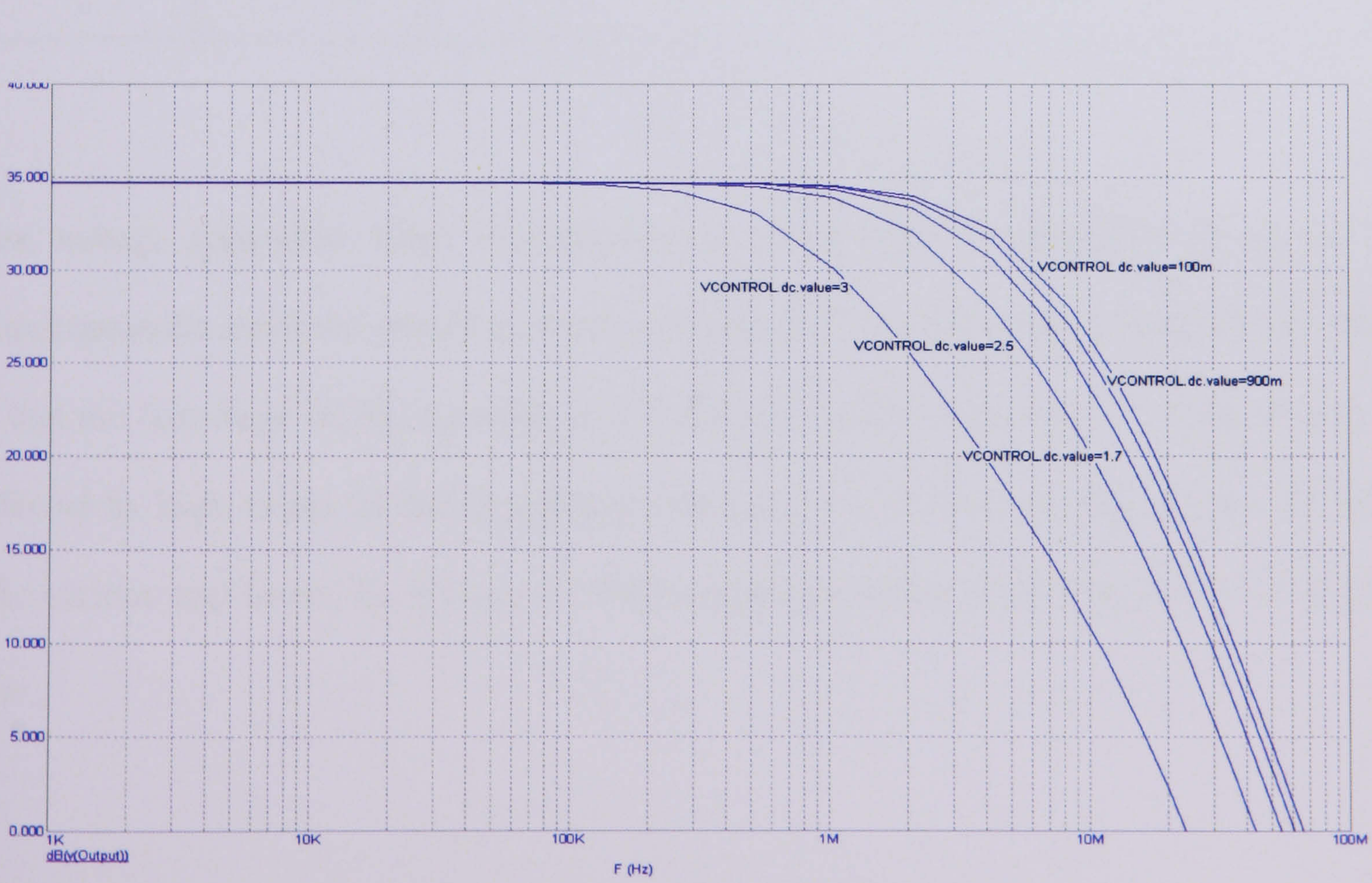

Figure 3.6 Frequency response of changing FET V_{Gs} from -0.1V to -3V

Table 3.1 shows effect of the bandwidth when C_p is being varied. As C_p increases the bandwidth of the voltage controlled filter decreases.

Table 3.1 C_p versus voltage control and bandwidth

C_p = 500pF		C_p = 100pF		C_p = 1pF	
$V_{control}$	Bandwidth	$V_{control}$	Bandwidth	$V_{control}$	Bandwidth
0.1V	2.4MHz	0.1V	4.5MHz	0.1V	4.9MHz
0.9V	2.2MHz	0.9V	4MHz	0.9V	4.3MHz
1.7V	2.1MHz	1.7V	3.2MHz	1.7V	3.2MHz
2.5V	1.6MHz	2.5V	2.2MHz	2.5V	2.2MHz
3V	675 kHz	3V	720 kHz	3V	720 kHz

The voltage controlled filter is connected in series with a common-collector (CC) transimpedance amplifier circuit as shown in Figure 3.7. The advantage of employing a CC is that the first-stage Miller capacitance is eliminated and the response is not significantly affected by high values of base spreading resistance.[3.2] Resistor R_3 ensures that the Q2 bias current, and hence $A_{2,}$ is close to 15dB, regardless of the exact values of Q1 and Q2 V_{be}.

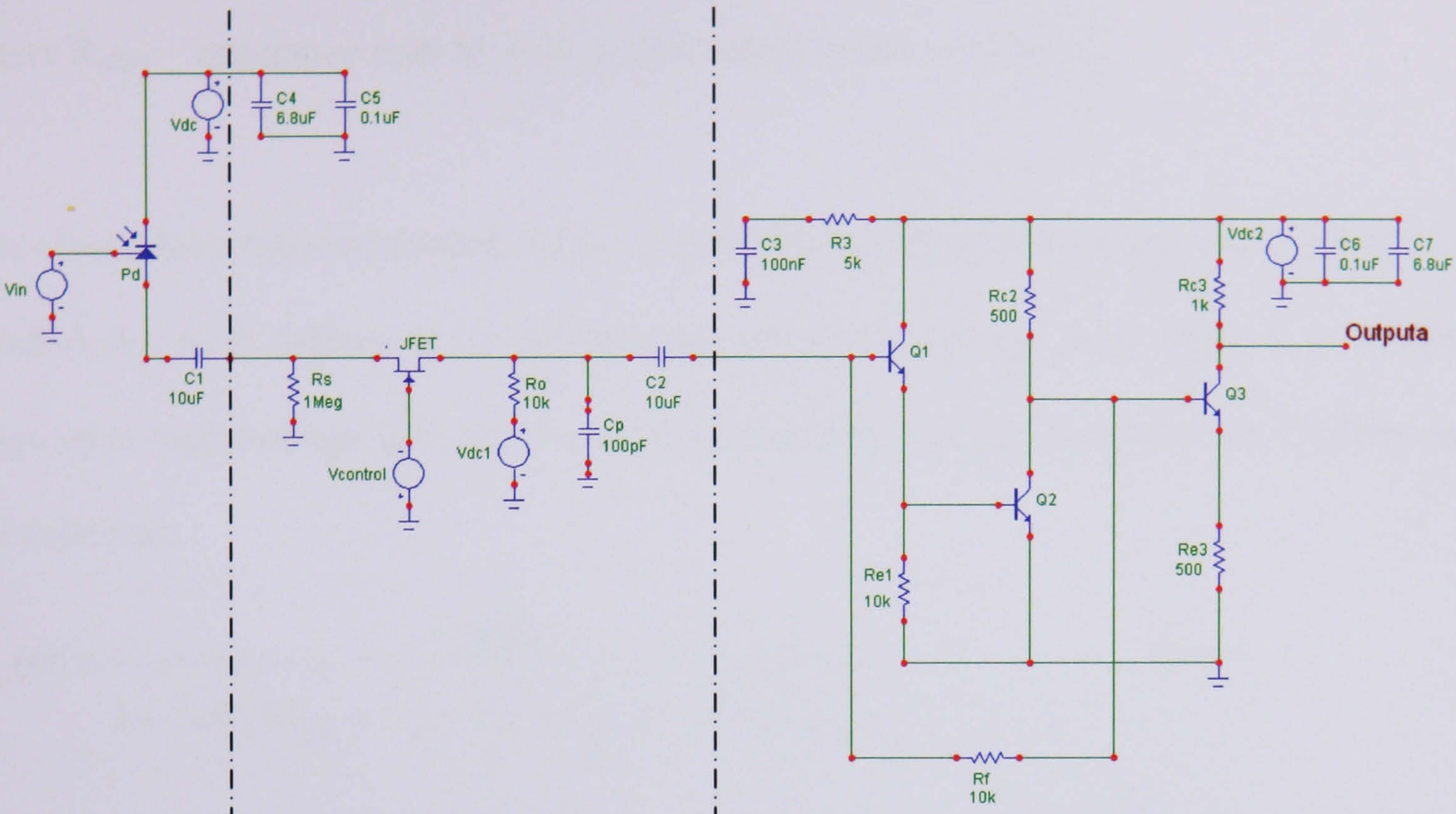

Figure 3.7 Transimpedance amplifier with voltage control filter

The closed-loop bandwidth of the transimpedance amplifier is governed by two major open-loop time constants given by equation (3.3) and (3.4) :

$$\tau_{in} = (R_{in} // R_f)C_{in} \qquad (3.3)$$

$R_{in} = R_{DS}+R_{Pd}+r_{bb1}+r_{\pi 1}+\beta_1(Re1//(r_{bb2}+r_{\pi 2}))$,

where R_{in} – open loop input resistance of the receiver

r_π – is an element in the hybrid-π transistor model

C_c - transistor capacitance between base and collector

$C_{in} = C_{Pd}+C_p+C_{c1}$

$$\tau_c = R_{c2\pi 2}(C_{\pi 2} + A_2 C_{c2}) \qquad (3.4)$$

$$R_{c2\pi 2} = [(\frac{R_f + r_{\pi 1} + r_{bb1}}{\beta} // R_{e1}) + r_{bb2}] // r_{\pi 2}$$

where $R_{c2\pi 2}$ – resistance seen by base-emitter capacitance of Q2($C_{\pi 2}$)

The closed-loop transimpedance $A_z(j\omega)$ is given by equation (3.5), where A_0 is taken to be equal A_1A_2. A_2 is defined as the second stage open loop voltage gain, while A_1 as the first stage open loop voltage gain and A_0 as the closed loop voltage gain between Q1 base and Q2 collector.

$$A_z(\omega) = \frac{-A_0 R_x}{1 + j\omega R_x (C_{pd} + C_p + C_{c1} + (\frac{\tau_c}{R_y}) - \omega^2 R_x C_{in} \tau_c} \qquad (3.5)$$

where $R_x = R_{in} // (\frac{R_f}{1 + A_0})$ and $R_y = R_{in} // R_f$

Figure 3.8 shows the simulated frequency response of the circuit. Result shows that the bandwidth of the preamplifier is determined by the voltage control filter block, via capacitor C_p. The gain of the preamplifier is 80dB, compared to the gain of the voltage control filter block Figure 3.5 without the preamplifier, is only 35dB.

The gain of the preamplifier could be further increased by adding a gain control circuit as shown in Figure 3.9. The gain control circuit uses a JFET, J1, as a variable emitter resistance in an emitter-degenerated ac amplifier, thus forming a voltage-controlled attenuator. J1 is bias from the voltage source, $V_{control}$ which also control the voltage control filter. As $V_{control}$ increases JFET will act as an ON resistance of 60Ω (max) giving an attenuation range of 0 to 40dB. R_4 and R_5 improve the linearity of the JFET. The use of a

constant dc current emitter pull-down current source looks like a very high impedance at signal frequencies, thus letting the variable-resistance FET set the gain over a wide range and at the same time provides simple biasing.[3.3-3.6] The blocking capacitor C_{dc1} was arranged, so that the FET affects only the ac signal gain. Without this capacitor, the transistor biasing would vary with FET resistance. Fig 3.10 shows the simulated results of the transimpedance amplifier with voltage filter block and gain control circuit. The bandwidth of the system has been maintained but the gain at this point is 98dB, an increase of 18dB compared to Figure 3.7 circuit without the gain control. The resistor values are calculated with the following equation:[3.3]

$$R_{c6} = \frac{V_{dc3} - V_{BE6}}{I_{ref}}, \text{ assuming } I_{ref} = 1\text{mA}$$

$$R_{e5} \cong \frac{V_T}{I_{c5}} \ln\left(\frac{I_{c5}}{I_{c6}}\right), \text{ assuming } V_T = 0.026$$

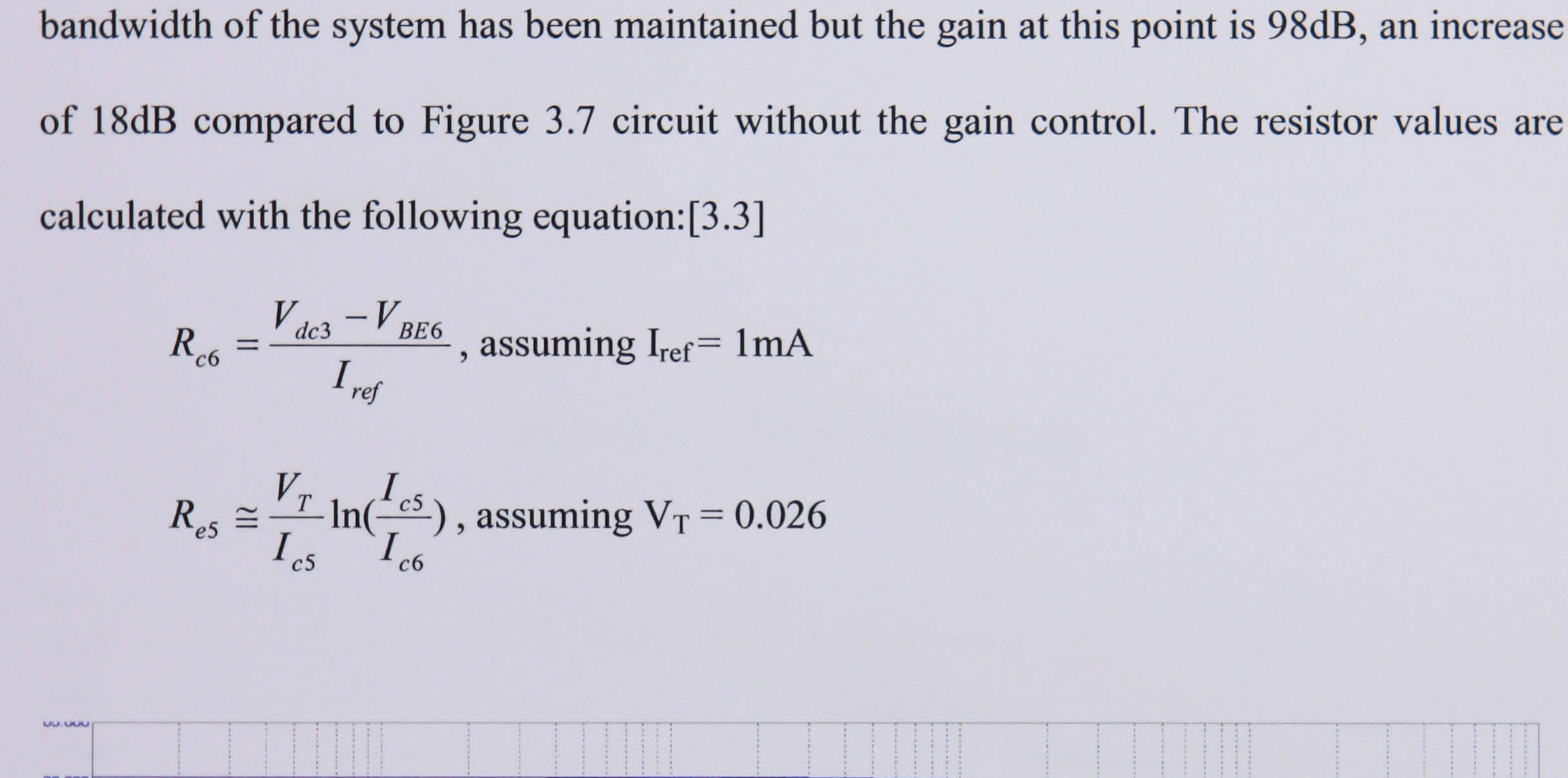

Figure 3.8 Transimpedance as a function of frequency

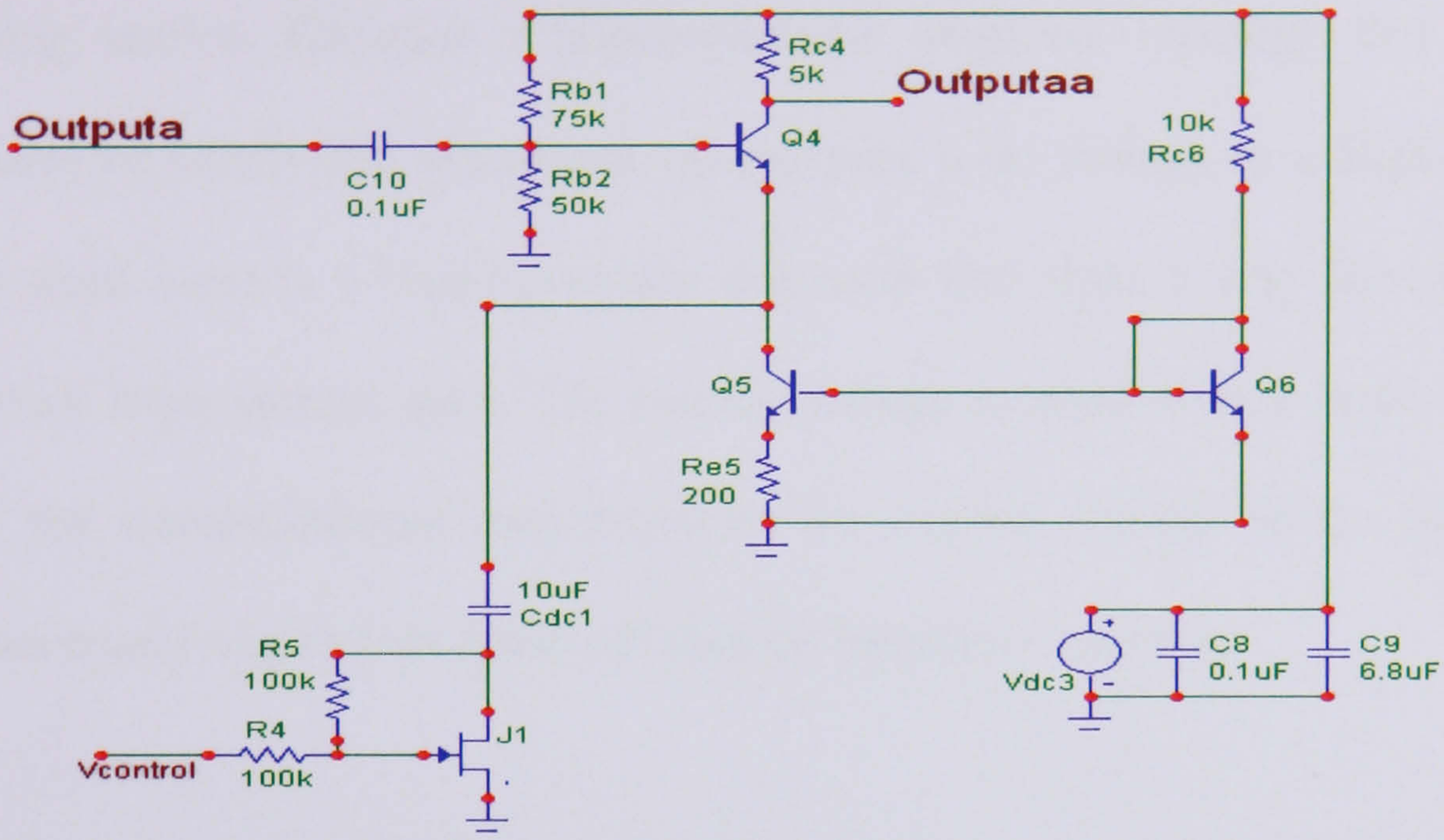

Figure 3.9 Gain control circuit

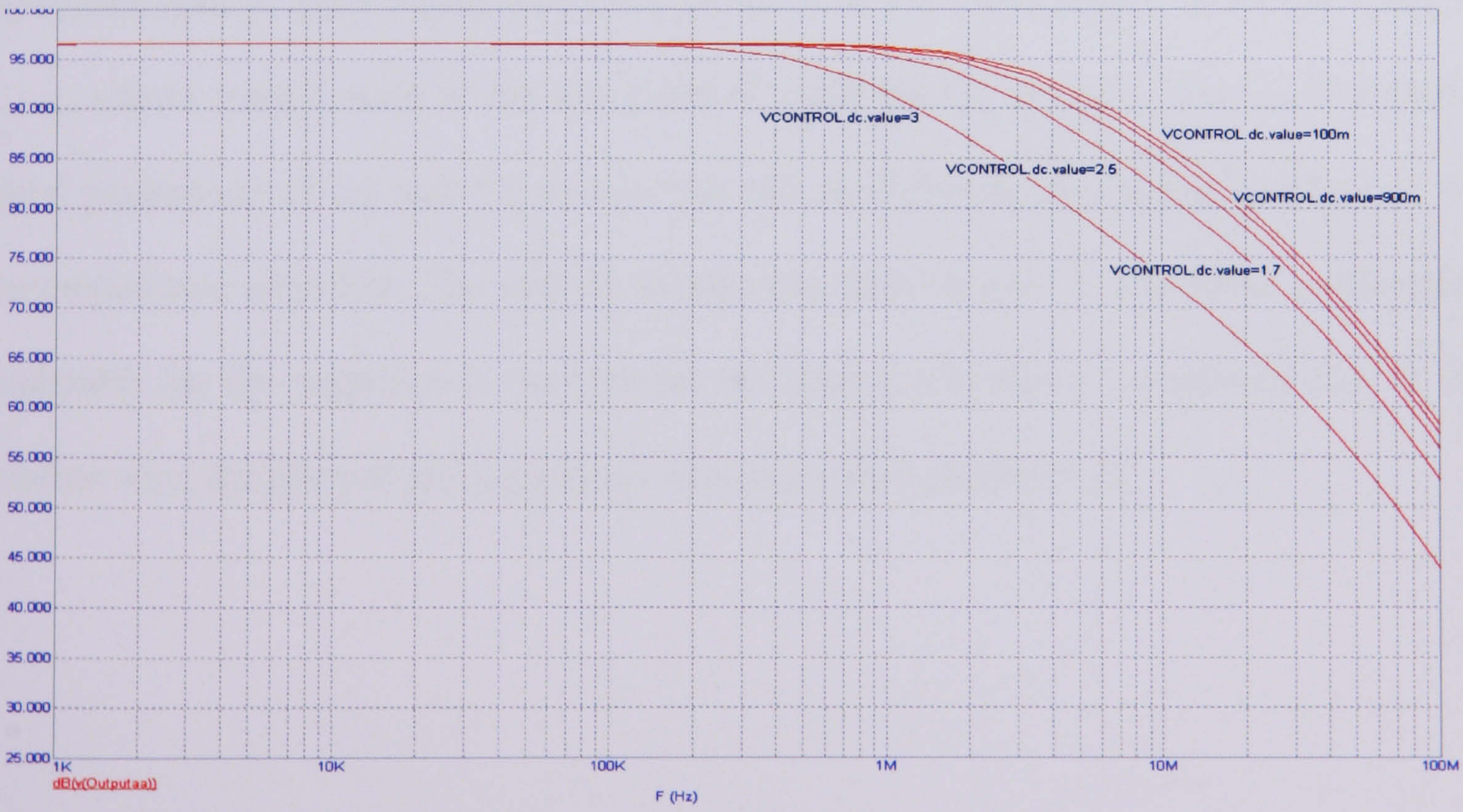

Figure 3.10 Transimpedance with gain control as a function of frequency

3.2 Transimpedance amplifier with BJT as voltage control

This following section discusses a transimpedance amplifier topology that allows an external control of bandwidth adjustment by applying a dc voltage to a high-impedance node. The control input is a Darlington pair transistor that sinks a very low current, but provides a very large current gain. The control voltage is applied to a node outside the signal path; the transimpedance loop transfers the control voltage to the input of the amplifier, thus modifying its bias point and then its frequency response.

Fig 3.11 shows the proposed topology, the common collector -common base cascade, given by Q3 and Q4 with the shunt-shunt feedback, implements a typical transimpedance amplifier, and Darlington transistors Q1 and Q2 have been added to obtain a high impedance control input which does not interfere with the signal loop. The control voltage, $V_{control}$ allows modification of the bias point of transistor Q1 and Q2; therefore the small-signal parameters of Q1 and Q2 change and this modifies the frequency response of the transimpedance amplifier. The control voltage can then be used to guarantee a minimum bandwidth for the amplifier to compensate for source impedance uncertainty due to the bonding wire, the photodiode capacitance and its ground scheme.[3.6]

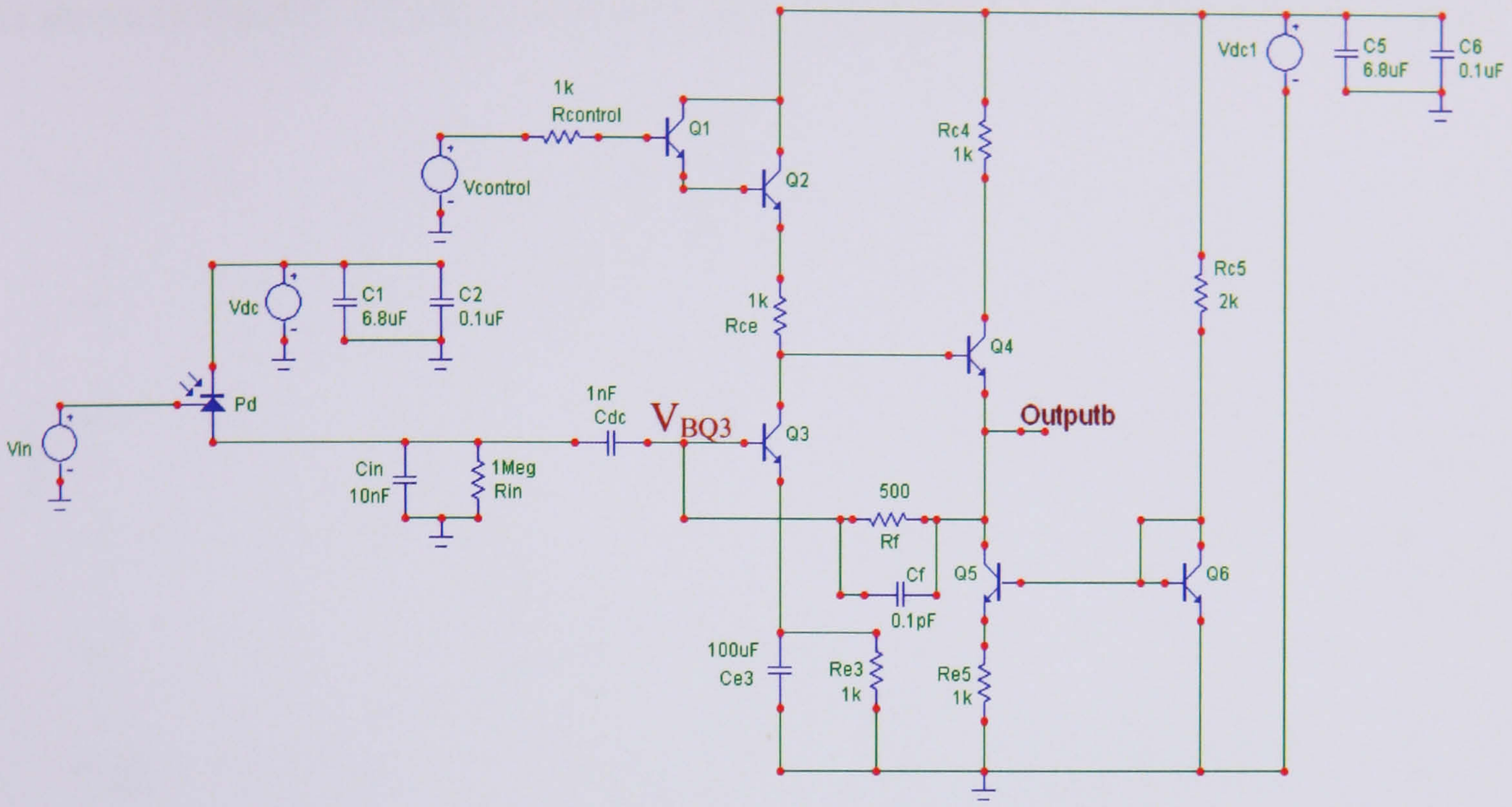

Figure 3.11 Transimpedance amplifier with external voltage control

Assuming that the bias point for Q_4 remains constant, the expression for V_{BQ3} in terms of $V_{control}$ is as follows :-

$$I_{EQ2} \approx I_{CQ3} = (\beta + 1) I_{BQ1}$$

$$I_{BQ1} = \frac{V_{control} - V_{BEQ1}}{\beta R_{CE}}$$

$$I_{BQ3} = \frac{V_B - V_{BEQ3}}{\beta R_{e3}}$$

$$I_{BQ3} = I_{CQ3} - I_{EQ3} \approx \frac{V_B - V_{BEQ3}}{\beta R_{e3}} = (\beta + 1) \frac{V_{control} - V_{BEQ1}}{\beta R_{CE}} - \frac{V_{EQ3}}{R_{e3}}$$

$$V_{BQ3} = (\beta + 1) \frac{(V_{control} - V_{BEQ1}) R_{e3}}{R_{CE}} - \beta V_{EQ3} + V_{BEQ3} \qquad (3.6)$$

As shown in Figure 3.12, equation (3.6) is almost linear, as $V_{control}$ changes from 2 – 10V.

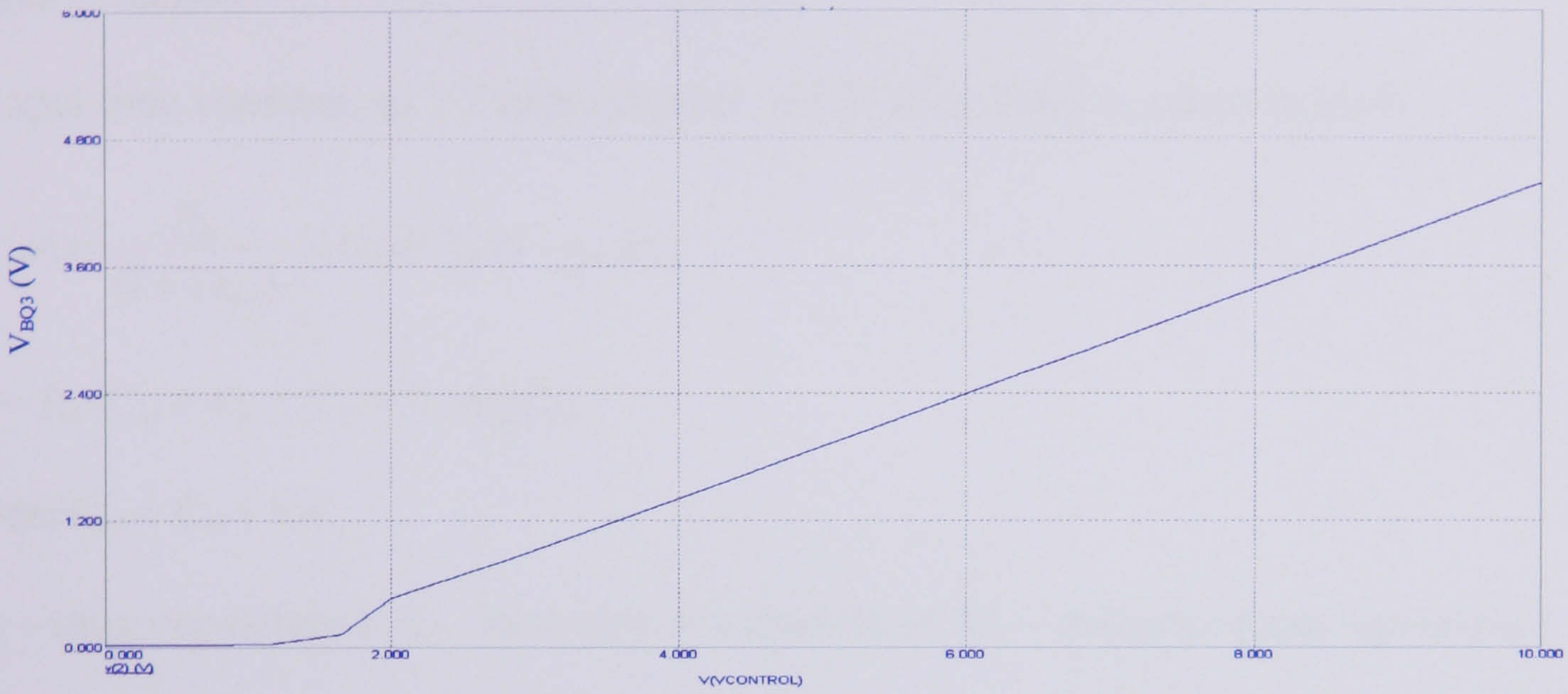

Figure 3.12 V_{BQ3} versus $V_{control}$

The transimpedance amplifier is a common-emitter, CE, shunt feedback preamplifier. A_o is assumed to be the product of the front-end gain. In most designs, A_o should be as high as possible to achieve a large bandwidth. However, a high value of voltage gain may cause instability, so most transimpedance designs have voltage gains of less than 100.[3.7-3.9] The transfer function of the transimpedance preamplifier is as follows by applying standard feedback analysis using impedances :-

$$\frac{1}{Z_{cl}(s)} = \frac{1}{Z_{ol}(s)} - \frac{1}{Z_f(s)}$$

where Z_{cl} – closed-loop transfer function

Z_{ol}- open-loop transfer function

Z_f-feedback network transfer function

The open-loop transimpedance is :

$Z_{ol}(s) = A_o(s)\dfrac{R_{in}R_f}{R_{in}+R_f}$ where $A_o(s)$ signifies that A_0 is frequency dependent

Assuming R_{in} is high.

$Z_{ol}(s) = A_o(s)R_f$

If input time constant, τ_{in} >> time constant of CE stage load, τ_{CE} then $A_o(s)$ is :-

$A_o(s) = \dfrac{A_o}{(1+s\tau_{in})}$ where A_o is $-g_{m3}R_{ce}$

$\tau_{in} = R_f(C_{in} + C_\pi + C_f + (1\text{-}A_o)C_c)$

where $C_{in} = C_d + Cs$

C_s – stray capacitance, C_π – base-emitter capacitance, C_c – collector-base capacitance

$$Z_{ol}(s) = \frac{A_o(s)R_f}{1+s\tau_{in}}$$

$Z_f(s) = \dfrac{R_f}{1+s\tau_f}$ where τ_f is the feedback time constant, R_fC_f

$$Z_{cl}(s) = \frac{A_oR_{eff}}{1+sR_{eff}(C_{in}+C_\pi+(1-A_o)(C_c+C_f))} \qquad (3.7)$$

where $R_{eff} = \dfrac{R_f}{1-A_o}$

The output of the transimpedance amplifier is connected to a current mirror dc network consisting of transistors Q_5 and Q_6. The operation of this configuration is set by a control current defined by R_{c5} which will establish the level of V_{BEQ5} and V_{BEQ6}. Assuming Q_5 and Q_6 are matched transistors, these results in the same load current. The network is also capable of ensuring that any variation in load current will be corrected by the configuration

itself. The result is sensitivity to unwanted changes that the circuit will make every effort to correct.

Fig 3.13 shows the simulated frequency response of the transimpedance stage as a function of the control voltage. The gain of this circuit changes from 27.2dB to 27.8dB, as the external control voltage changes. The overall approximated gain for this circuit is around 27dB. The control voltage is set to operate from a range of 3.5 – 9V, where at this point the transistors are operating in a linear state. Table 3.2 shows the effect of the bandwidth when R_f is being varied. As R_f increases the gain of the system increases from 27.2dB to 39.7dB, but the bandwidth decreases.

Table 3.2 R_f versus voltage control and bandwidth

$R_f = 2k\Omega$		$R_f = 1k\Omega$		$R_f = 500\Omega$	
$V_{control}$ (V)	BW (MHz)	$V_{control}$ (V)	BW (MHz)	$V_{control}$ (V)	BW (MHz)
3.5	1.7	3.5	2.9	3.5	4.7
4.5	2.7	4.5	5.2	4.5	9.1
5.5	4.4	5.5	7.9	5.5	13.6
6.5	5.7	6.5	10.1	6.5	17.9
7.5	7.3	7.5	13.3	7.5	21.8
8.5	8.5	8.5	15.3	8.5	27.8
9	9.4	9	16.4	9	28.7

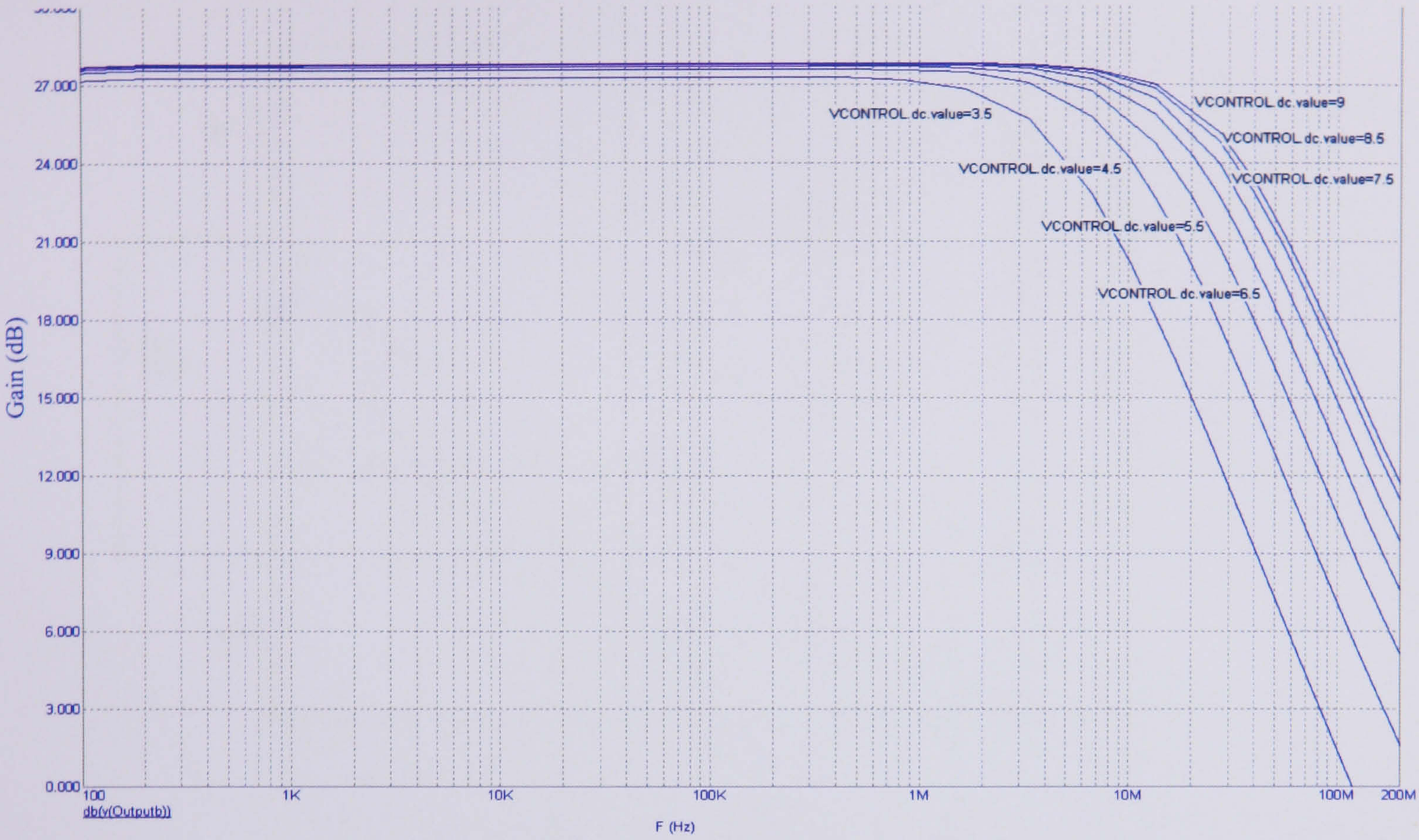

Figure 3.13 Simulated transfer function of the transimpedance amplifier

3.3 Bootstrap Transimpedance Amplifier with adjustable capacitor

A much improved version of a front-end, incorporated within a transimpedance amplifier, is shown in Figure 3.14, the topology being known as the bootstrapped transimpedance amplifier (BTA). The BTA is an attractive design, as it reduces the effective detector capacitance, C_d, seen by the signal in order to achieve relatively wide bandwidths.[3.10-3.11] The output of the emitter follower stage is feedback to the photodetector by a bootstrapping capacitor, C_b.

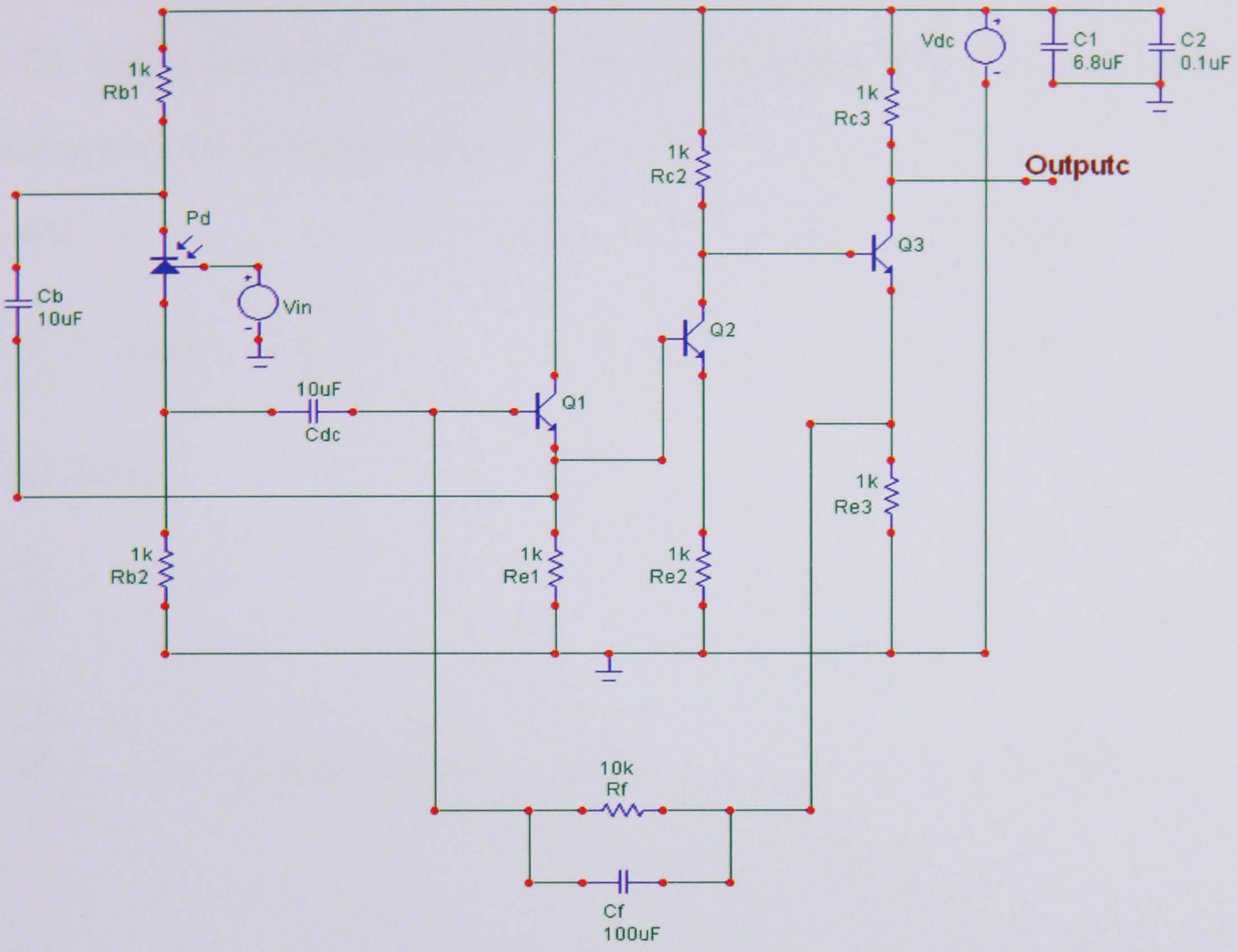

Figure 3.14 BTA Circuit [3.11]

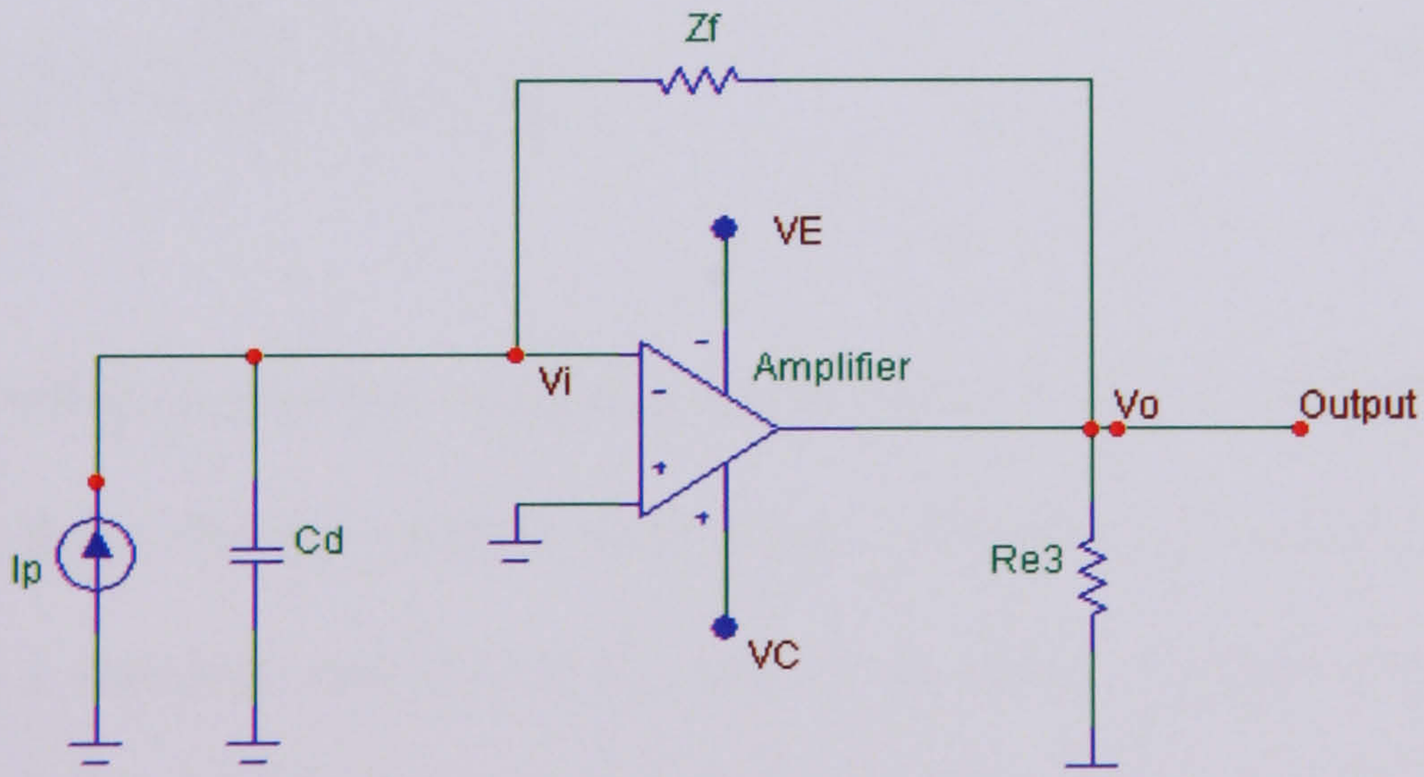

Figure 3.15 Simplified model of Figure 3.14

Assuming that the gain stages and the emitter follower can be approximated by a simplified amplifier model shown in Figure 3.15, $R_{b1}, R_{b2} >> R_{e1}$ and frequencies are considered where C_{dc} and C_b are short circuits, then the transimpedance gain, A_z, for the circuit is approximated by the following method :

$V_o = - AV_i$ .....(3.8)

$$I_p = \frac{V_i - V_o}{Z_f} + V_i j\omega C_d + \frac{V_o - 0}{R_{e3}} \quad \text{.....(3.9)}$$

From (6) into (7)

$$V_i = -\frac{V_o}{A}$$

$$I_p = \frac{\frac{-V_o}{A} - V_0}{Z_f} + (\frac{-V_o}{A}) j\omega C_d + \frac{V_o}{R_{e3}} \quad \text{.....(3.10)}$$

$$I_p AZ_f R_{e3} = [V_o(R_{e3})(A-1) + (-V_o)R_{e3}Z_f j\omega C_d + V_o AZ_f]$$

$$A_z = \frac{V_o}{I_p} = \frac{AZ_f R_{e3}}{R_{e3}(A-1) + AZ_f - j\omega C_d R_{e3} Z_f} \quad (3.11)$$

where A is the voltage gain of the amplifiers stages and Z_f is R_f // C_f in Fig 3.14.

Equation (3.11) shows that the receiver bandwidth is determined not only by the R_fC_d time constant but by a complex function of R_{e3} and C_f. In order to achieve an amplifier with bandwidth adjustment, a modification on Figure 3.14 was made, by placing a capacitor, C_p in series with the emitter resistor, R_{e3} in the second gain stage, with a feedback resistor R_f as shown in Figure 3.16.

The feedback of the circuit is taken in between resistor, R_{e3} and capacitor, C_p. By varying the capacitor, C_p the bandwidth of the circuit can be controlled. A comparison of the simulated output result for the BTA circuit and the modified BTA circuit are shown in Figure 3.17 and Figure 3.18. In each case the amplifier output is taken from the collector at Q_3. Q_3 is bias through the connection of R_{e3} and R_f to the base of Q_1. The BTA circuit has a gain of 41dB with a cut-off frequency of 1GHz, while the modified BTA circuit maintains a gain of 48.2 dB as C_p is varies until C_p is 1uF and 10uF, the gain starts to drop to 47.7dB and 44.7dB respectively. The stimulation shows that the bandwidth adjustment between each capacitor value is a ratio of 10:1 to 8:1. Table 3.3 shows the bandwidth of the modified BTA circuit as capacitor, when C_p and R_f are changed.

Table 3.3 R_f versus capacitor, C_p, bandwidth and gain

	R_f = 10 kΩ		R_f = 100 kΩ		R_f = 500 kΩ	
Capacitor value (F), C_p	Gain (dB)	Bandwidth (Hz)	Gain (dB)	Bandwidth (Hz)	Gain (dB)	Bandwidth (Hz)
1p	48.2	233M	47.7	218M	45.2	149.2M
10p	48.2	29M	47.7	27.8M	45.2	22.9M
100p	48.2	2.9M	47.7	2.8M	45.2	2.3M
1n	48.2	287k	47.7	275.4k	45.2	263.9k
10n	48.1	29k	47.5	28.2k	45.1	27.1k
100n	48.0	3.2k	47.4	2.8k	45.0	2.4k
1u	47.7	318	47.4	268	45.0	251.9
10u	44.7	52	44.0	51	41.4	45

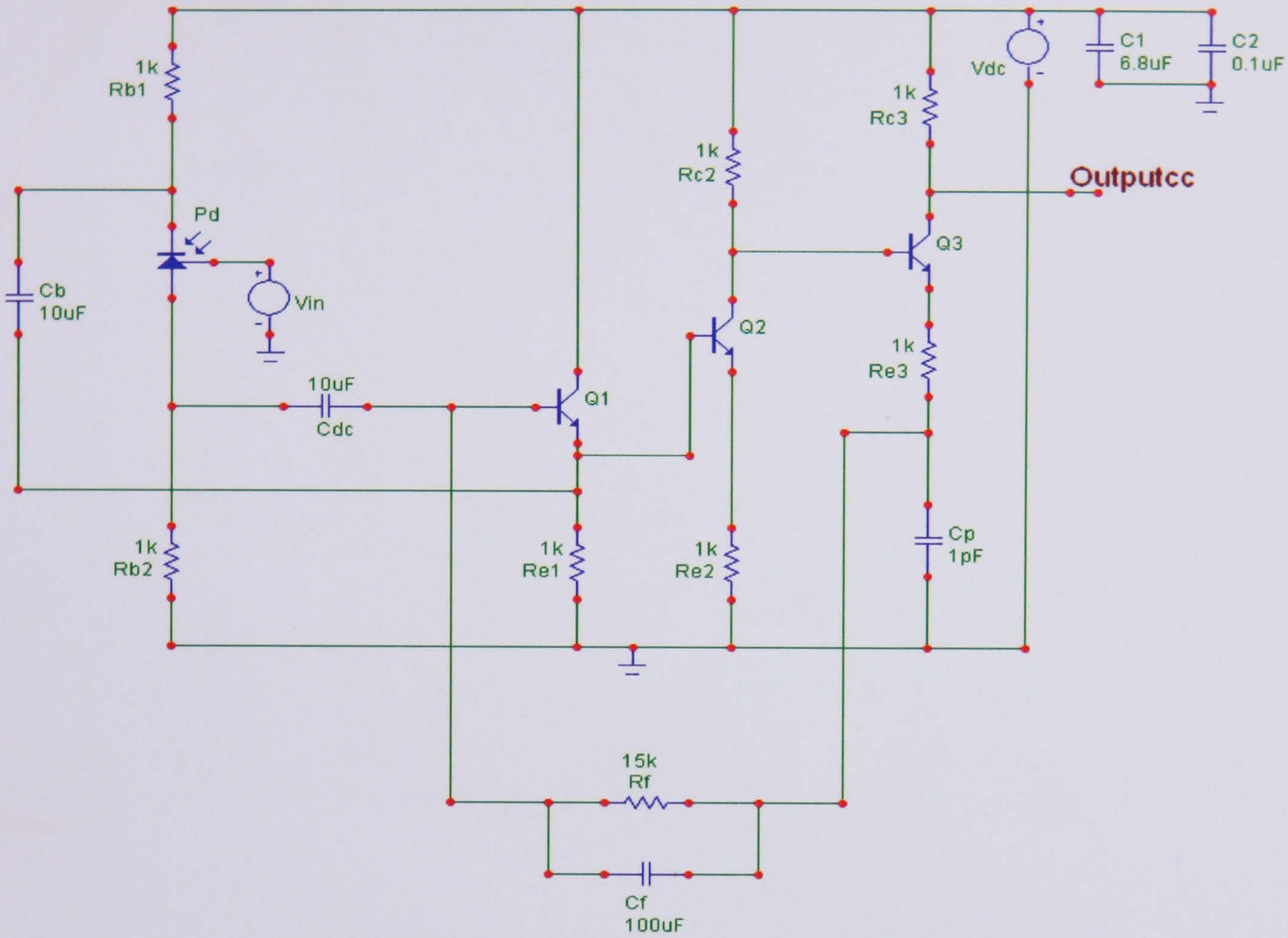

Figure 3.16 Modified BTA circuit

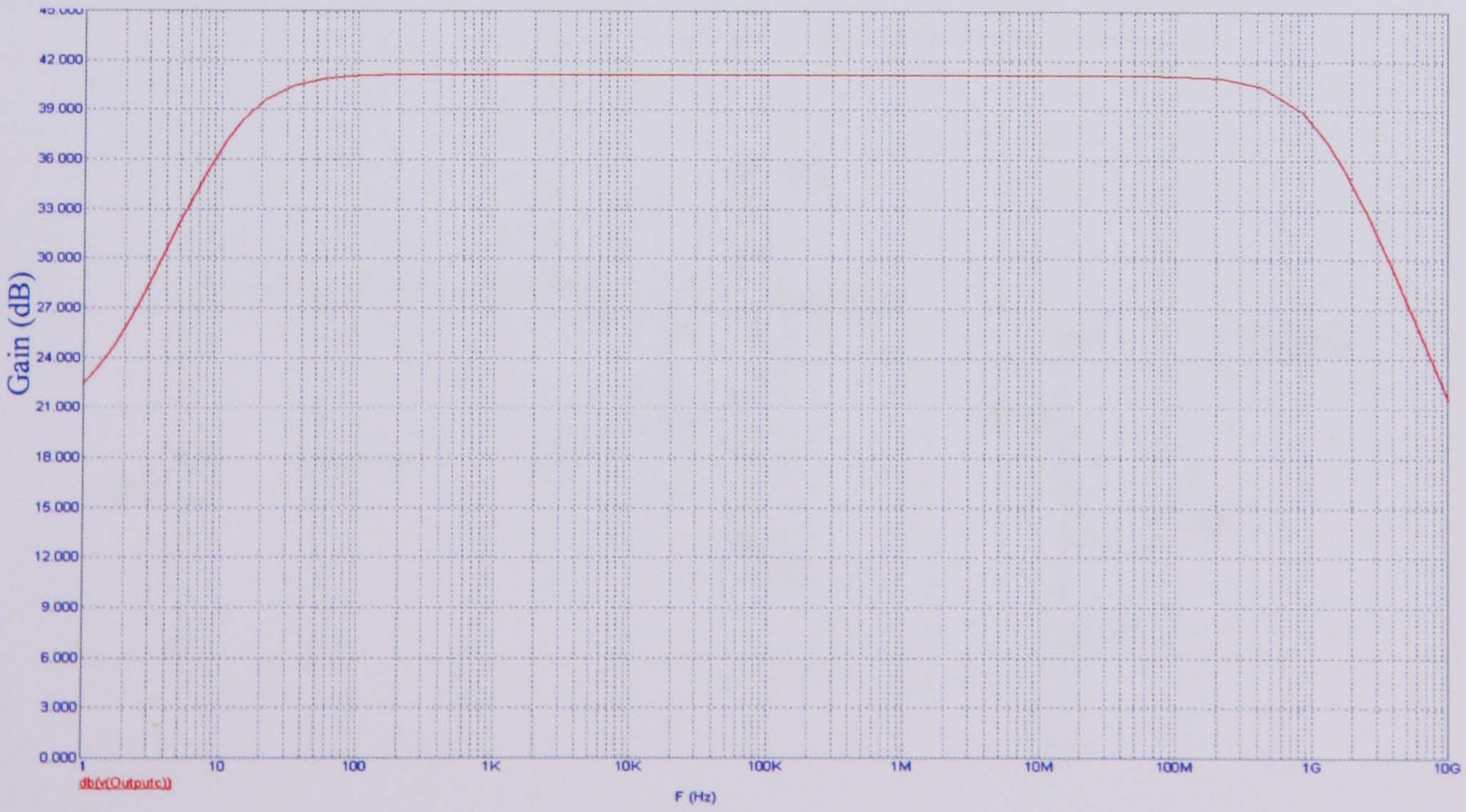

Figure 3.17 BTA Bandwidth

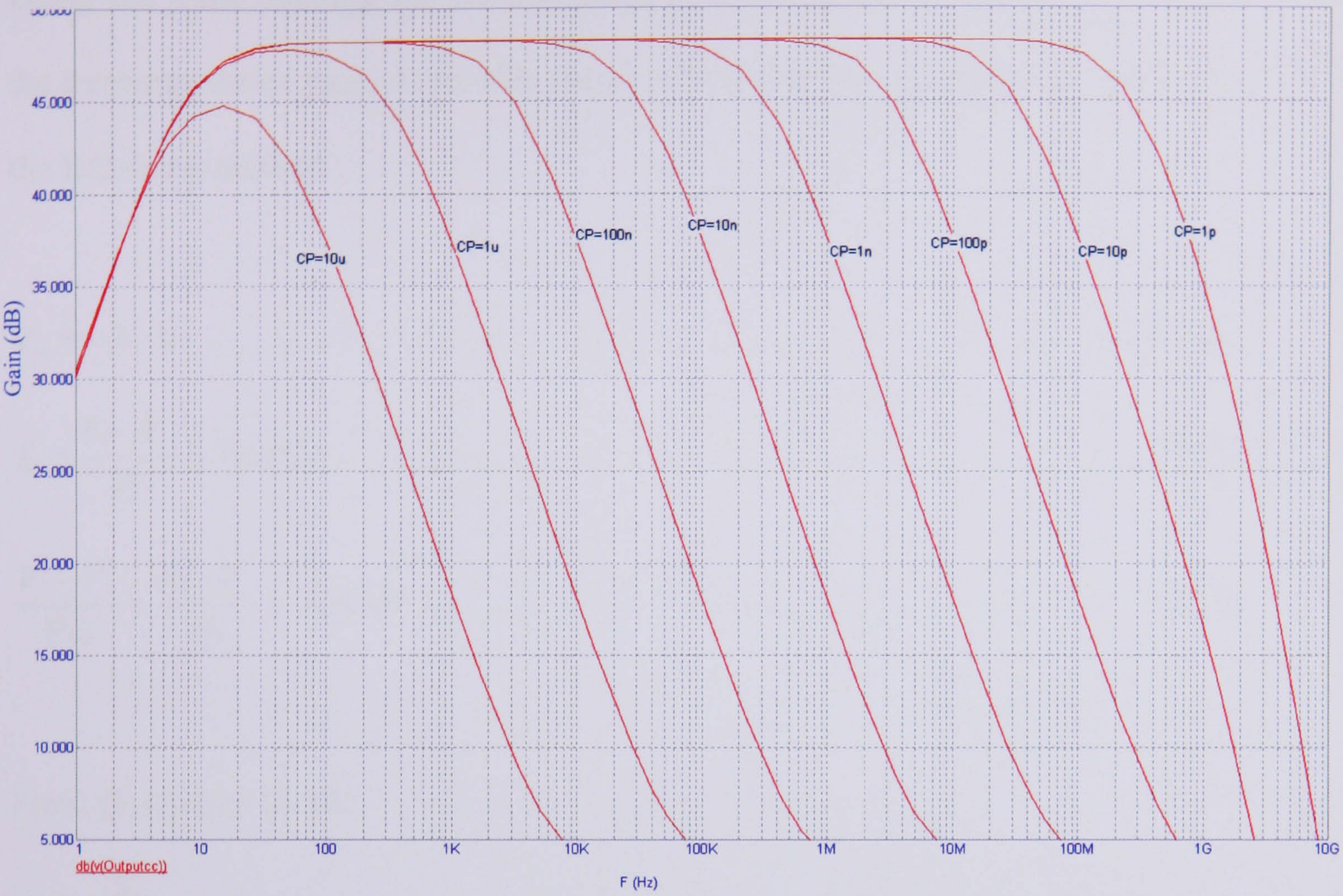

Figure 3.18 Modified BTA Bandwidth

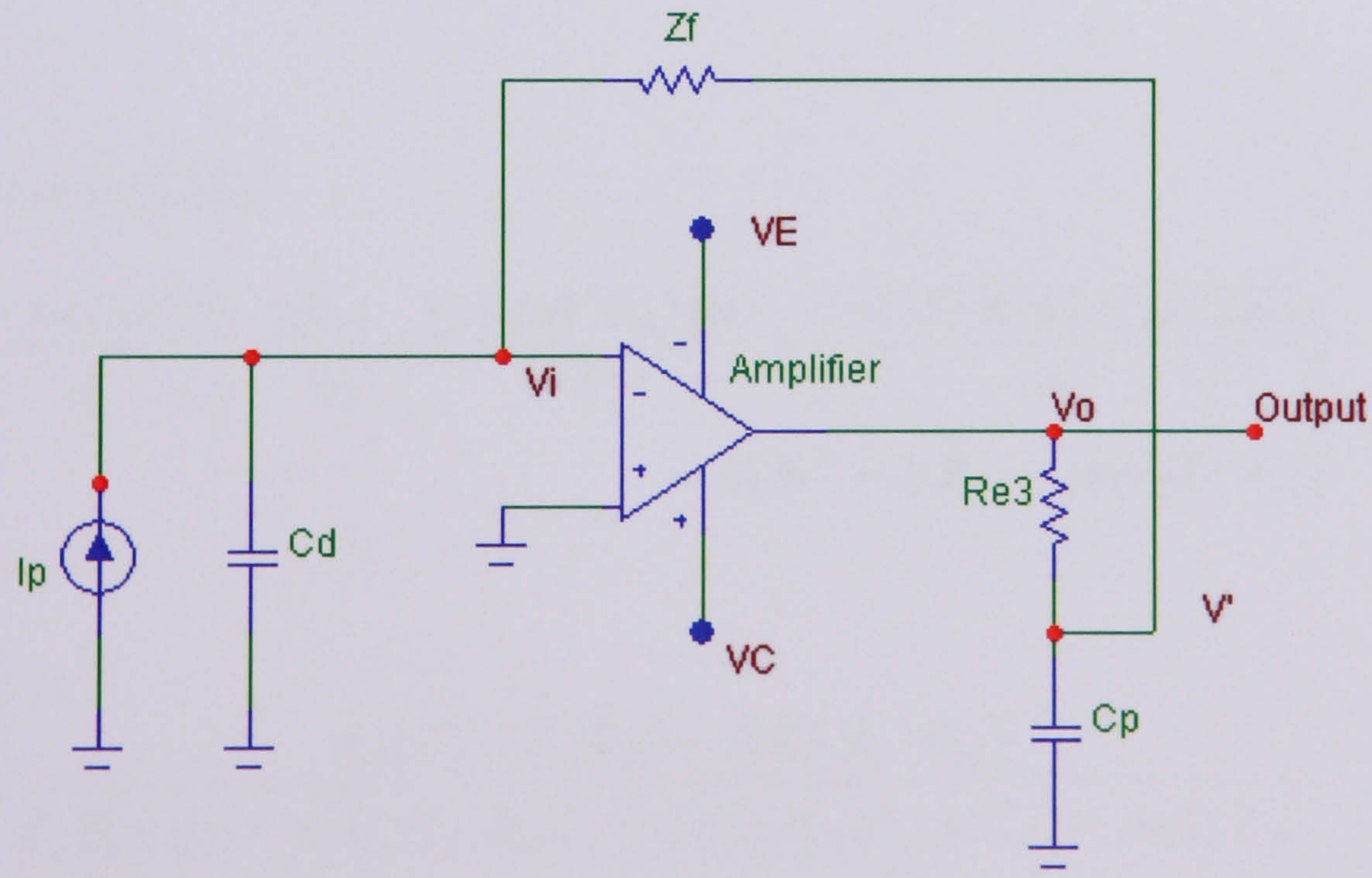

Figure 3.19 Simplified model of Figure 3.16

Using the same analogy for the bootstrapped transimpedance amplifier discussed earlier, the transimpedance gain, A_z for this circuit with adjustable capacitor, C_p is approximated by the following method :

$V_o = - A_v V_i$ ..... (3.12)

$$I_p = \frac{V_i - V'}{Z_f} + V_i j\omega C_d \quad \text{..... (3.13)}$$

$$\frac{V_o - V'}{R_{e3}} + \frac{V_i - V'}{Z_f} = j\omega C_p V' \quad \text{.....(3.14)}$$

From (3.12) into (3.13)

$$V_i = -\frac{V_o}{A_v}$$

$$V' = -\frac{V_o}{A_v}(1 + j\omega C_d Z_f) - Z_f I_p \quad \text{.....(3.15)}$$

From (3.15) into (3.14)

$$V_o[Z_f + \frac{(1 + j\omega C_d Z_f)Z_f}{A_v} - \frac{R_{e3}}{A_v} + \frac{(1 + j\omega C_d Z_f)R_{e3}}{A} + \frac{j\omega C_p Z_f R_{e3}(1 + j\omega C_d Z_f)}{A_v}]$$

$$= I_p[Z_f^2 + Z_f R_{e3} - j\omega C_p Z_f^2 R_{e3}]$$

$$A_z = \frac{V_o}{I_p} = \frac{A_v[(Z_f^2 + Z_f R_{e3}) - j\omega C_p Z_f^2 R_{e3}]}{Z_f(1 + A_v) - \omega^2 C_p Z_f^2 R_{e3} C_d + j\omega Z_f R_{e3}(C_d + C_p) + j\omega C_d Z_f^2} \quad (3.16)$$

where A_v is the voltage gain of the amplifiers stages, and Z_f is (R_f // C_f)in Fig 3.16.

Equation (3.16) shows that the receiver bandwidth is determined not only by the R_fC_d time constant but also by a complex function of R_{e3}, C_f and C_p. The modified circuit shows that the bandwidth can be varied by varying capacitor C_p, thus modifying the second stage gain.

Comparing equation (3.11) and (3.16) it shows that, with additional capacitances in a system, its bandwidth is reduced. However, in this case the extra capacitor, C_p, is the main component to achieve bandwidth adjustment.

3.4 Summary

This chapter has presented three techniques to achieve bandwidth adjustment, using passive components. Table 3.4 shows the comparison of each technique.

Table 3.4 Comparison of technique

Technique	FET voltage control filter	External voltage control	Adjustable capacitor
Gain	80dB	27.8dB	48.2dB
Cut-off Frequency	702kHz – 4.52MHz	4.7MHz – 28.7MHz	52Hz – 233MHz
Ratio	1 : 6.5	1 : 6.3	1 : 10 (between each capacitor)

Table 3.2 shows that the technique using the adjustable capacitor has a wide bandwidth of frequency range, with an average gain of 48dB. The technique using the external voltage control has a lowest gain of 27.8dB, and the bandwidth adjustment is more focused in the centre between the high frequency range (HF) to the very high frequency range (VHF). The FET voltage control filter technique has a maximum gain of 80dB, but the bandwidth adjustment is focused in the low frequency range (LF). A noise analysis of each technique will be discussed in detail in Chapter 6.

References

[3.1] R. L Boylestad and L. Nashelsky, "Electronic Devices and Circuit Theory" Prentice Hall, Chapter 4 and Chapter 12, 2002.

[3.2] M. J. N Sibley, "Optical Communications" Macmillan New Electronics, Chapter 6, 1985.

[3.3] A. S Sedra and K. C. Smith, "Microelectronics Circuits" Oxford University Press, Chapter 5 and Chapter 8, 2002.

[3.4] A. R. Hambley, "Electronics" Prentice Hall, Chapter 4, 2000.

[3.5] N. R. Malik,"Electronic Circuits – Analysis, Simulation and Design" Prentice Hall, Chapter 9, 1995.

[3.6] P. Horowitz and W. Hill,"The Art of Electronics" Cambridge University Press, Chapter 2 and Chapter 3, 2001.

[3.7] M. J. N. Sibley and R.T. Unwin,"Transimpedance optical preamplifier having a common collector front end" Electronics Letter, Vol. 18, No. 23, pp. 985-986, 1982.

[3.8] B. Wilson and I. Darwazeh, "Transimpedance optical preamplifier with a very low input resistance" Electronics Letters, Vol. 23, No. 4, pp. 138-139, 1987.

[3.9] J.L. Hullett and S. Moustakas, "Optimum transimpedance broadband optical preamplifier design" Optical and Quantum Electronics, Vol. 13, pp. 65-69, 1981.

[3.10] D. Casasent, "Electronic Circuits" Quantum Publishers, INC, Chapter 5, 1973.

[3.11] A.M. Street, P.N. Stavrinou, D.J. Edwards and G. Parry, "Optical Preamplifier designs for Ir-LAN applications" Optical Free Space Communication Links, IEE Colloquium, pp. 8/1-8/6, February, 1996.

Chapter 4

Composite transimpedance amplifier bandwidth adjustment structures

The aim of this chapter is similar to Chapter 3, in that it address the principal design requirements, outlined in Chapter 2. In this chapter, three different configurations, known as the composite transimpedance amplifier structures, were suggested. The composite amplifier technique is actually cascading two amplifiers together, where each amplifier has its own characteristics. A composite amplifier normally uses a combination of a voltage feedback amplifier and a current feedback amplifier, where the best qualities of both amplifiers can be combined to achieve a better performance. The resulting composite

amplifier can exhibit the best of each circuit and, hopefully, exhibit none of the weaknesses [4.1-4.4]. Voltage feedback operational amplifiers, such as the LMH6624, have excellent performance in applications where the gain-bandwidth product of the operational amplifier is very wide and of very low noise. Current feedback operational amplifiers, such as the LMH6732, are high speed operational amplifiers with a unique combination of high performance, low power consumption, and flexibility of application. This chapter begins by describing a combination of an integrated voltage feedback amplifier and a current feedback amplifier with adjustable bandwidth capabilities. The second configuration is a combination of the bootstrapped transimpedance amplifier, discussed in Chapter 3, with an integrated voltage feedback amplifier. The discussion which follows will be focused on the combination of the design of a dual feedback loop transimpedance amplifier using transistors with an integrated voltage feedback amplifier. The bandwidth adjustment for this system is controlled by a low pass filter. Throughout this chapter, mathematical equations will be presented and simulation results of the designs developed.

4.1 Combination of voltage feedback and current feedback amplifier

Chapter 2 has discussed briefly the characteristics and the challenges of the voltage feedback amplifier (VFA) and the current feedback amplifier (CFA), when used with a fast changing voltage. This section introduced the current-to-voltage converter using a voltage feedback amplifier even though phase shift caused by photodiode capacitance is often a source of instability [4.5]. The choice of using a VFA as a front end is because the

LMH6624 has a wide bandwidth of 1.5GHz, with very low input noise ($0.92nV/\sqrt{Hz}$), providing precise operational amplifiers with wide dynamic range [4.6]. A combination of a photodiode with the voltage feedback amplifier implements a low noise transimpedance amplifier. The transimpedance gain is set by R_f, where

$$A_v = -I_{IN} * R_f.$$

The total input current noise spectral density (i_{ni}) equation for the amplifier, configured as the basic transimpedance configuration, can be calculated with the following equation [4.6]:

$$i_{ni} = \sqrt{i_n^2 + (\frac{e_n}{R_f})^2 + \frac{4kT}{R_f}} \qquad (4.1)$$

where, i_n and e_n are the noise current and voltage respectively.

From Figure 4.1, which was obtained from equation (4.1), setting $R_f = 1k\Omega$ in the design configuration, indicates that the current noise spectral density for the configuration is around $5pA/\sqrt{Hz}$.

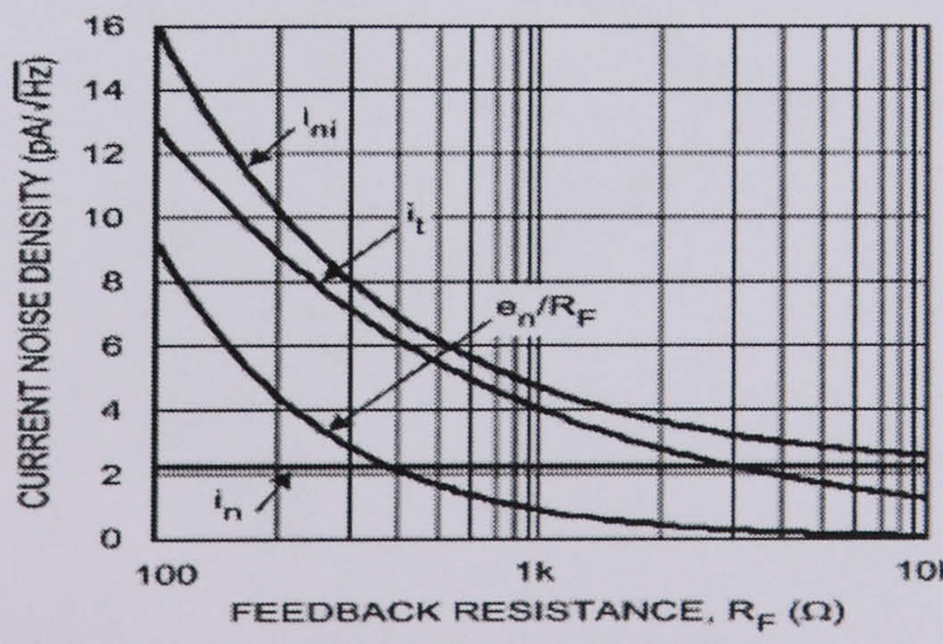

Figure 4.1 LMH6624 current noise density versus R_f [4.6]

The second stage amplifier, an LMH6732, is an adjustable supply current, current feedback operational amplifier (CFA). The supply current and, consequently the dynamic performance of the IC, can be easily adjusted by selecting the value of a single external resistor, R_p. The operating point is determined by the supply current, which, in turn, is determined by the current (I_p) flowing out of pin 8, as shown in Figure 4.2. As the supply current is increased, the following effects can be observed for the device as in Table 4.1:

Table 4.1 LMH6732 parameters related to supply current [4.7]

Specification	Effect as I_{cc} Increase
Bandwidth	Increases
Rise Time	Decreases
Output Drive	Increases
Input Bias Current	Increases
Input Impedance	Decreases

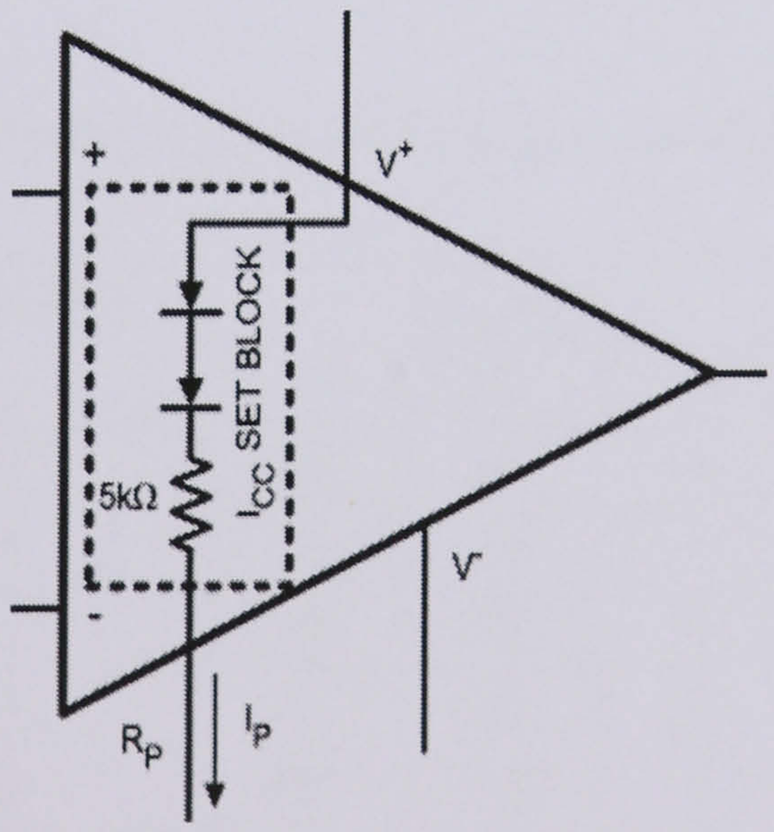

Figure 4.2 LMH6732 supply current control simplified schematic [4.7]

The terminal marked "R_p" in Figure 4.2 is tied to a potential through the resistor R_p shown in Figure 4.4. The current flowing through R_p (I_p) sets the supply current. The voltage applied to R_p and $V_{control}$ are both considered to be -5V. The relationship between I_{cc} and I_p is given by [4.7]:

$$I_p = \frac{I_{cc}}{57} \text{ (approximate ratio at } I_{cc} = 1.0\text{mA from Table 4.2)}, \qquad (4.2)$$

Knowing I_p leads to a direct calculation of R_p

$$R_p + 5k\Omega = \frac{[(V^+ - 1.6) - V^-]}{I_p} \qquad (4.3)$$

if V^+ and V^- are 5V and -5V respectively, then R_p can be determined from the following equation :

$$R_p + 5k\Omega = \frac{8.4}{I_p} \qquad (4.4)$$

In this design, I_{cc} is chosen to be 1.0mA, $A_v = 1$ and $R_{fl} = 1k\Omega$ from Table 4.2.

Therefore, from equation (4.2) and (4.3), the calculated value of $I_p = 17.54\mu A$ and $R_p = 412k\Omega$.

Table 4.2 : R_f selection for various gain settings and I_{cc} [4.7]

Gain (V/V)	I_{cc} (mA)			Unit
	9	3.4	1	
A_V = +1	700	1k	1k	Ω
A_V = +2	700	1k	1k	Ω
A_V = –1	500	750	1k	Ω
A_V = –2	400	450	1k	Ω
A_V = +6	500	500	1k	Ω
A_V = –6	200	200	1k	Ω
A_V = +21	1k	1k	1k	Ω
A_V = –20	500	500	1k	Ω

Figure 4.3 shows the graph I_p versus bandwidth for the LMH6732. As I_p increases, the bandwidth increases. From the calculation above, for $I_p = 17.54\mu A$, the bandwidth is set to approximately 55MHz.

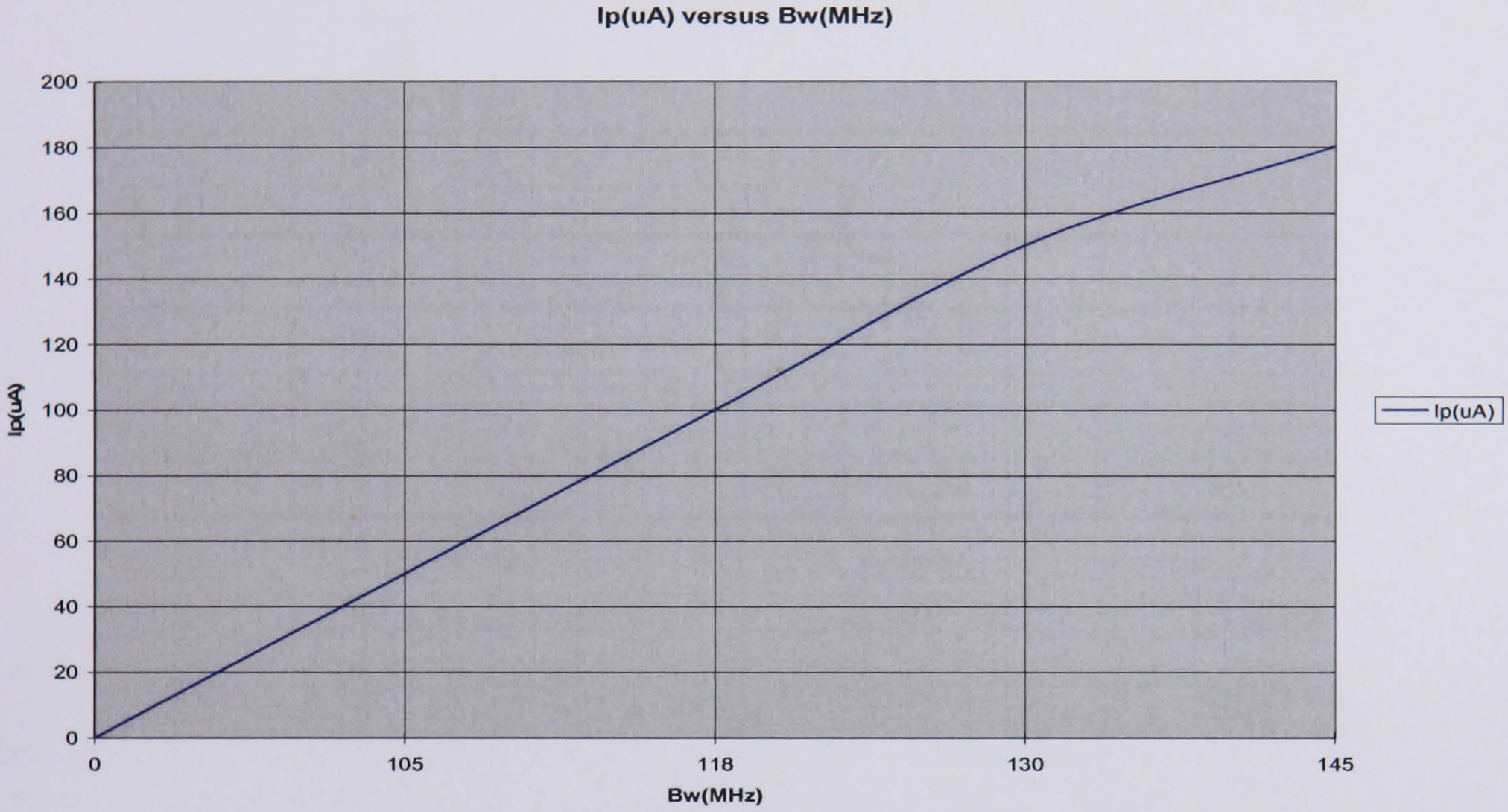

Figure 4.3 Graph Ip(μA) versus Bw(MHz)

The two stage composite amplifier configuration using the VFA and the CFA is shown in Figure 4.4. As $V_{control}$ is varied between 0V to 5V, the bandwidth of the overall composite circuit can be adjusted. Figure 4.5 shows the simulated frequency response for the first stage amplification after the LMH6624, and the frequency response for the composite amplification. The first stage gain is 44.3dB, with a 3dB cut-off frequency of 116MHz. The 3dB cut-off frequency response for the composite circuit is between 18.1MHz to 75.2MHz, producing an overall composite bandwidth adjustment of 57.1MHz. The gain at this stage is 50.1dB.

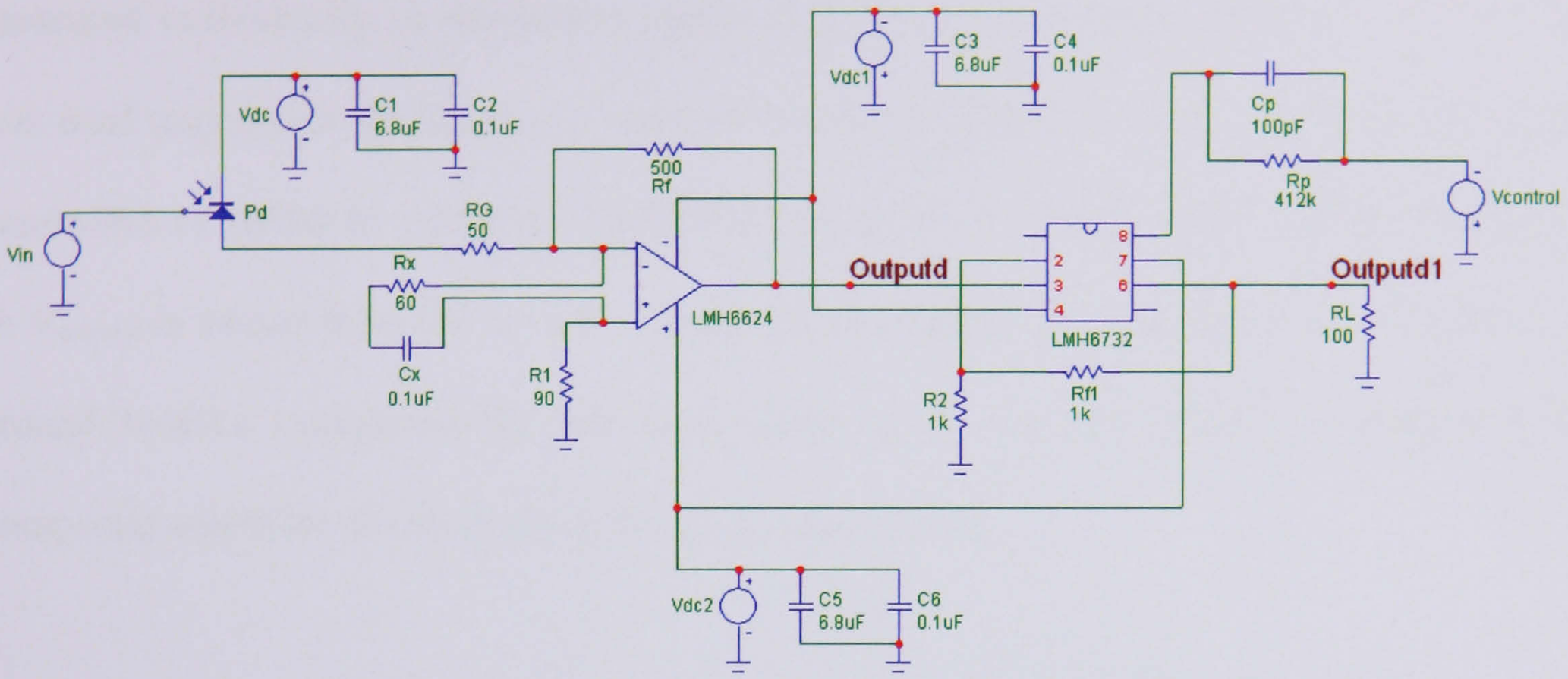

Figure 4.4 Composite Voltage and Current feedback amplifier

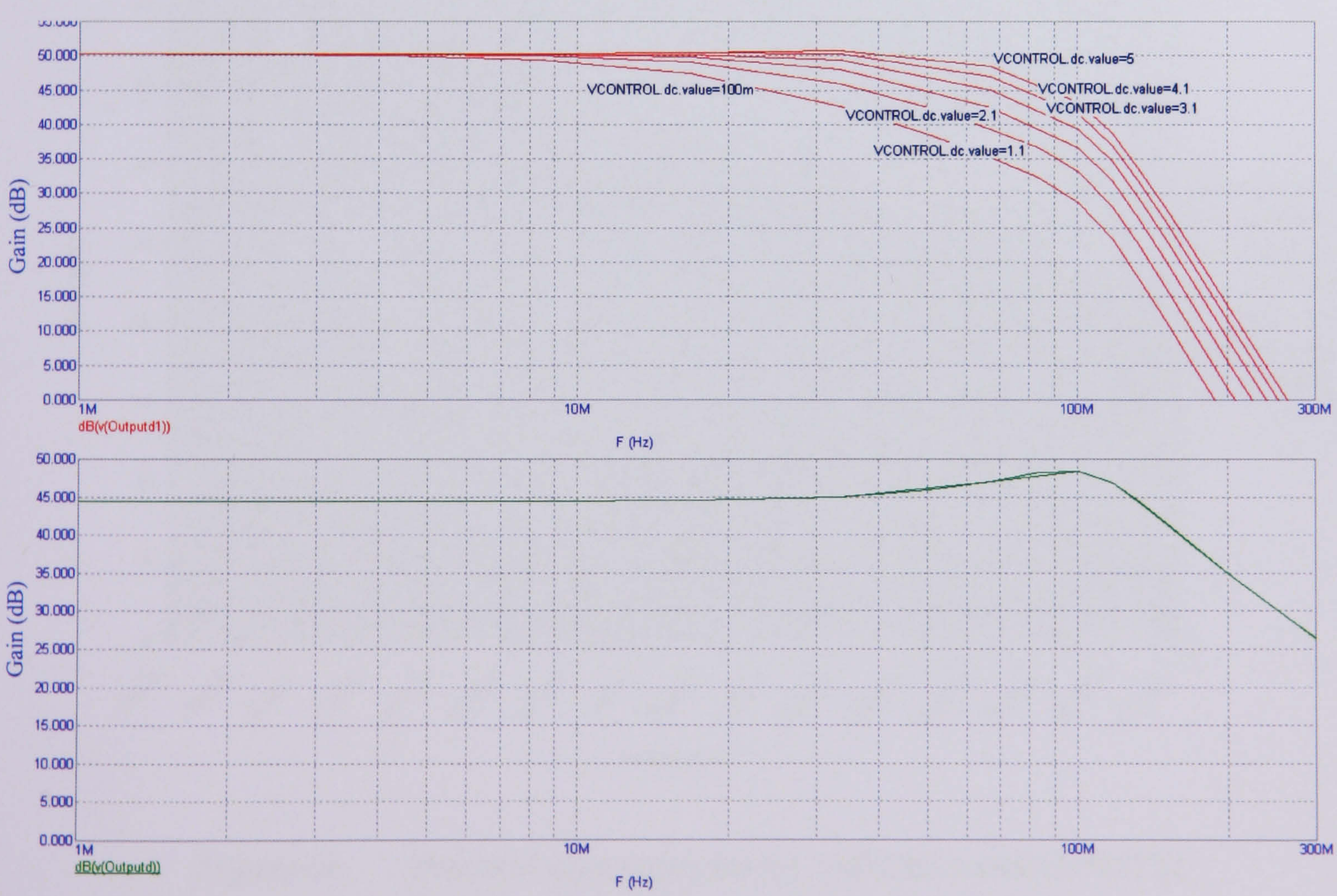

Figure 4.5 Frequency responses versus gain

The LMH6624 and LMH6732 were built on a surface mount board and each of them was measured individually. A sinusoidal signal of $5mV_{pp,}$ with a load resistance, $R_L = 100\Omega$, was used to generate the frequency response shown in Figure 4.6. The LMH6624 has a 3dB bandwidth of 105MHz, whilst the LMH6732 has a 3dB bandwidth from 35MHz to 69MHz, as $V_{control}$ is varied from 0V to -5V. Therefore, the bandwidth adjustment for LMH6732 is around 34MHz. Comparing the simulated result and the practical results in Figure 4.7, the composite amplifier circuit shows a close correspondence.

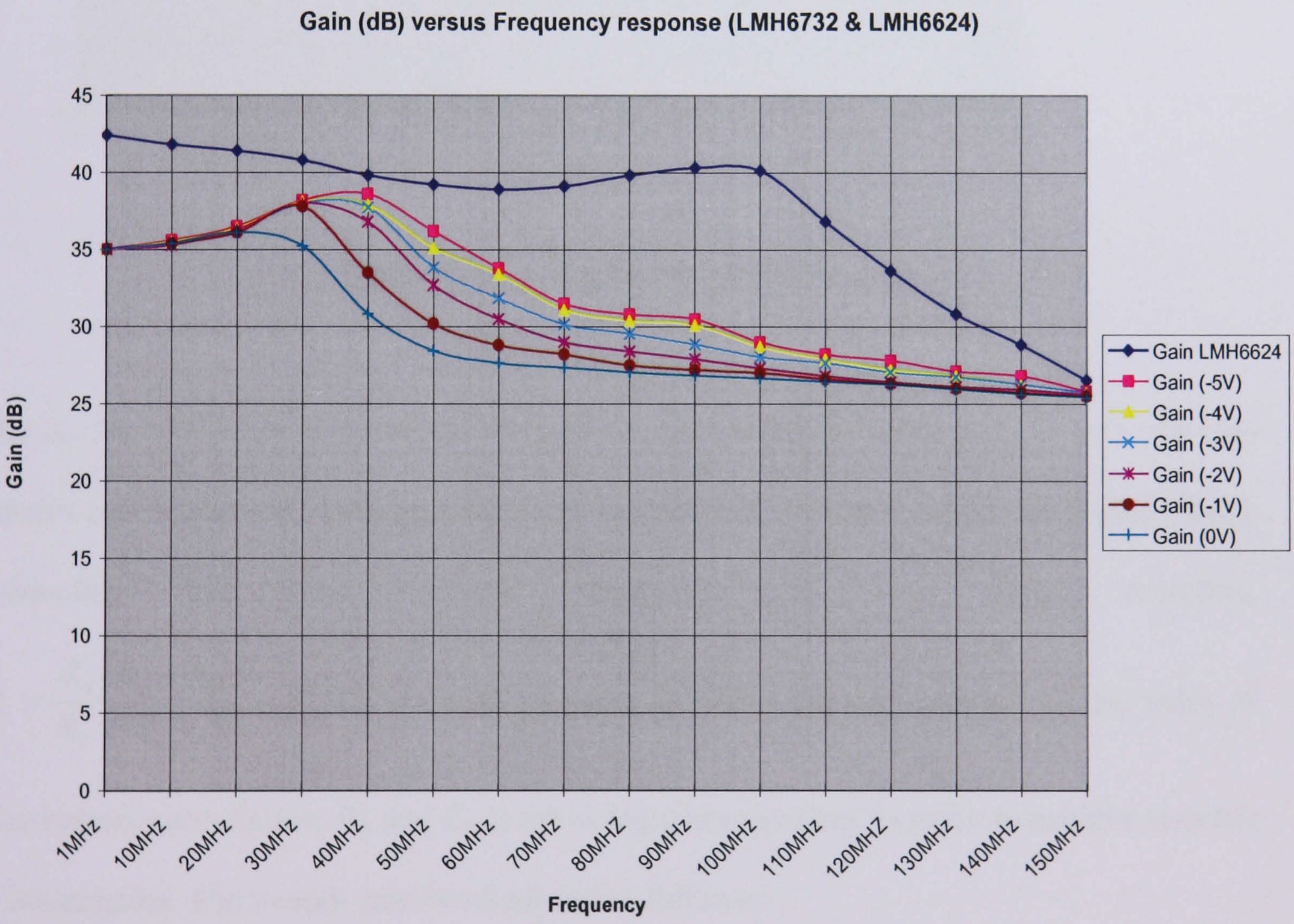

Figure 4.6 Practical measurements for LMH6624 and LMH6732

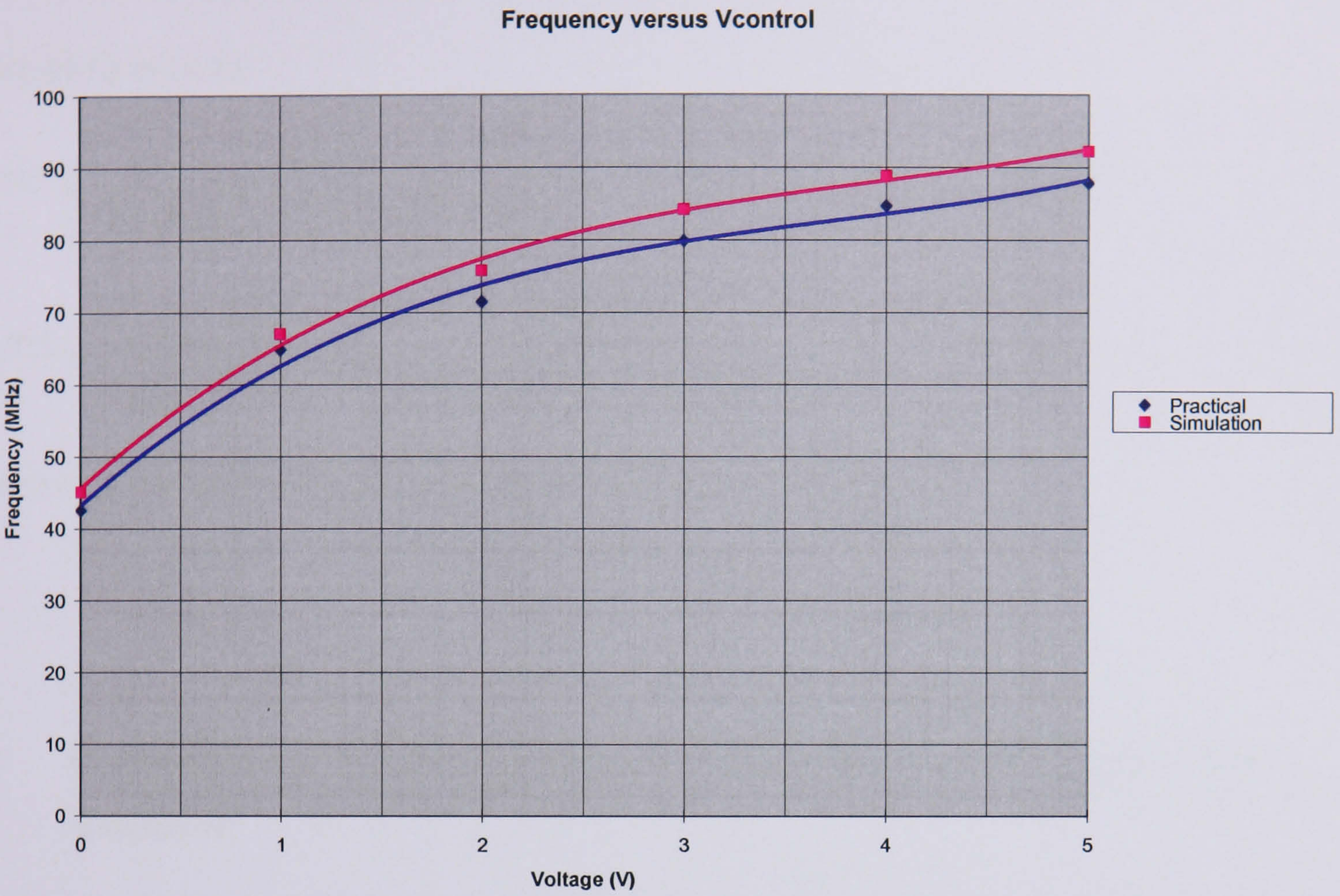

Figure 4.7 Frequency versus $V_{control}$

The A_V for LMH6624 is set to 10, whereas A_V for LMH6732 is set to 1. R_1 acts as a bias current cancellation. R_1 is calculated from the following equation : $R_1 = [R_f // (R_G + R_S)]$. Assuming that the source resistance, $R_S = 50\Omega$, therefore, $R_1 = \frac{R_f(R_G + R_S)}{R_f + R_G + R_S} = 83.333\Omega \approx 85\Omega$. A value of 90Ω is chosen to obtain a lower value of bias current cancellation. R_x and C_x is set as lag compensation, in order to achieve stability at lower gains. The overall gain is calculated as follows :

$$I_p = \frac{V_{in} - V_{output}}{R_f} + \frac{V_{in}}{R_G} + V_{in} j\omega C_d \qquad (4.5)$$

$$V_{output} = -AV_{in} \qquad (4.6)$$

$$V_{output1} = A_1 V_{in1} \approx V_{output1} = A_1 V_{output} \tag{4.7}$$

From (4.6) in (4.5)

$$\frac{V_{output}}{I_p} = \frac{-AR_f R_G}{(1+A)R_G + R_f + j\omega C_d R_f R_G} \tag{4.8}$$

$$\frac{V_{output1}}{I_p} = \frac{V_{output1}}{V_{output}} x \frac{V_{output}}{I_p} = \frac{-AA_1 R_f R_G}{(1+A)R_G + R_f + j\omega C_d R_f R_G} \tag{4.9}$$

where A is the gain of the1st stage, A_1 is the gain of the 2_{nd} stage.

4.2 Combination of bootstrap transimpedance amplifier and voltage feedback amplifier

Another proposed topology using the composite amplifier technique that provides high bandwidth is shown in Figure 4.8. The bootstrapped transimpedance amplifier which was discussed in Chapter 3 is connected in series with a voltage feedback amplifier, the LMH6624. An RC filter is used as a termination. The first stage of the BTA produces a cut-off frequency of 94.5MHz, with a gain of 51.5dB. By varying the capacitor, C_{filter}, of the RC filter between 50pF to 1nF, the bandwidth of the composite circuit can be controlled. The cut-off frequency obtained by this RC filter on the composite amplifier is from 9.5MHz to 103.5MHz, as shown on the frequency response plot of Figure 4.9. The overall gain is reduced to 12.3dB. There is a trade-off between gain and bandwidth, as the bandwidth is increased the gain of the circuit is reduced. As mentioned in Chapter 3, bootstrapping the transimpedance amplifier effectively allows for a higher transimpedance

gain, but, in this case, a composite configuration of transimpedance amplifier with adjustable bandwidth allows for a bandwidth adjustment with a trade-off of 39dB gain. Table 4.3 shows the changes in frequency response when R_f is varied.

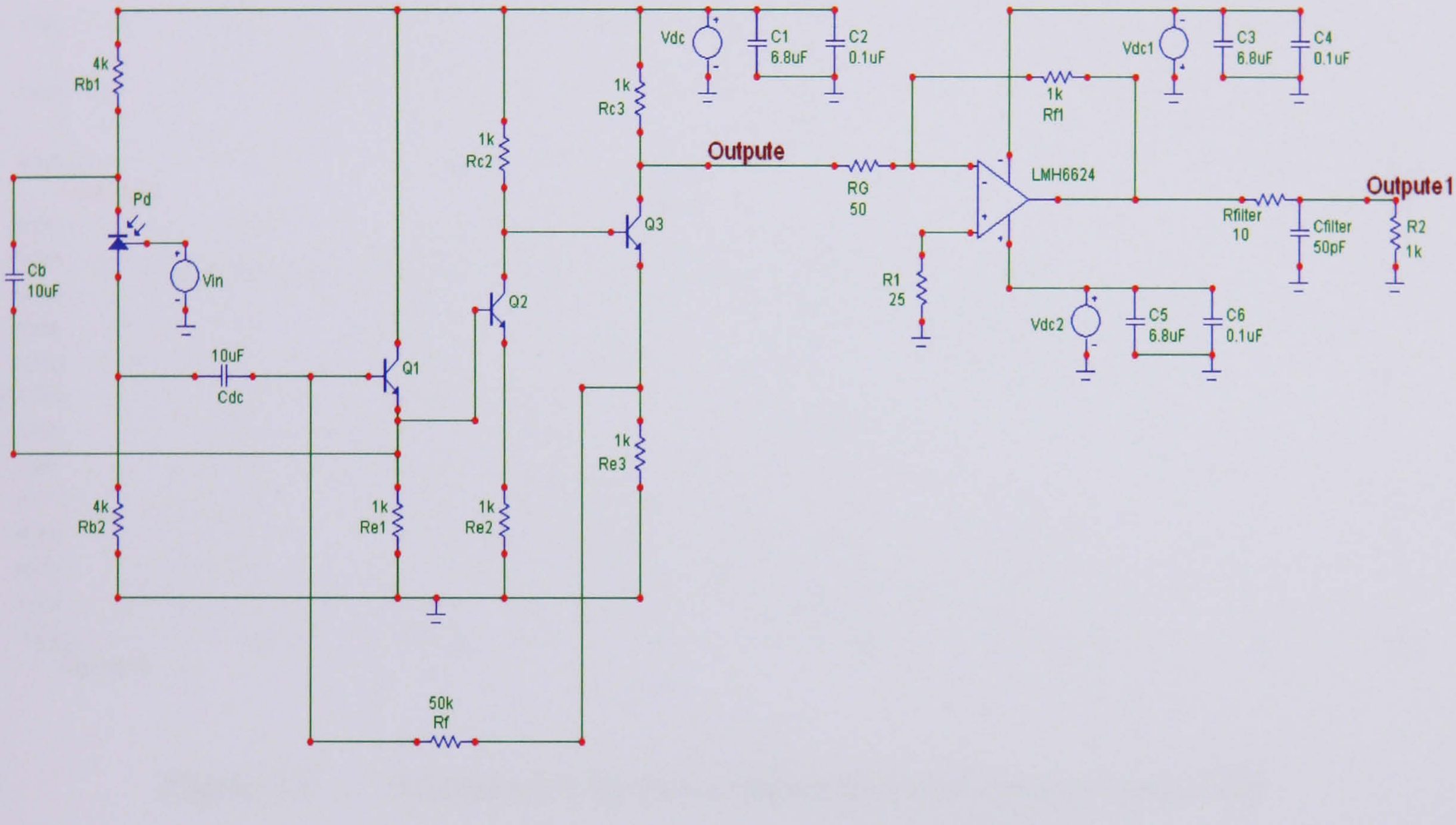

Figure 4.8 Composite bootstrap transimpedance amplifier with VFA

Table 4.3 R_f versus Frequency response

Gain (dB)	R_f (Ω)	Capacitance					
		50pF	100pF	200pF	400pF	800pF	1nF
9.36	1k	110.8MHz	72.4MHz	43.4MHz	22.9MHz	11.75MHz	9.26MHz
10.44	800	110.8MHz	72.4MHz	43.4MHz	23.4MHz	11.75MHz	9.26MHz
12.3	500	103.5MHz	71.0MHz	44.2MHz	24.3MHz	12.4MHz	9.5MHz

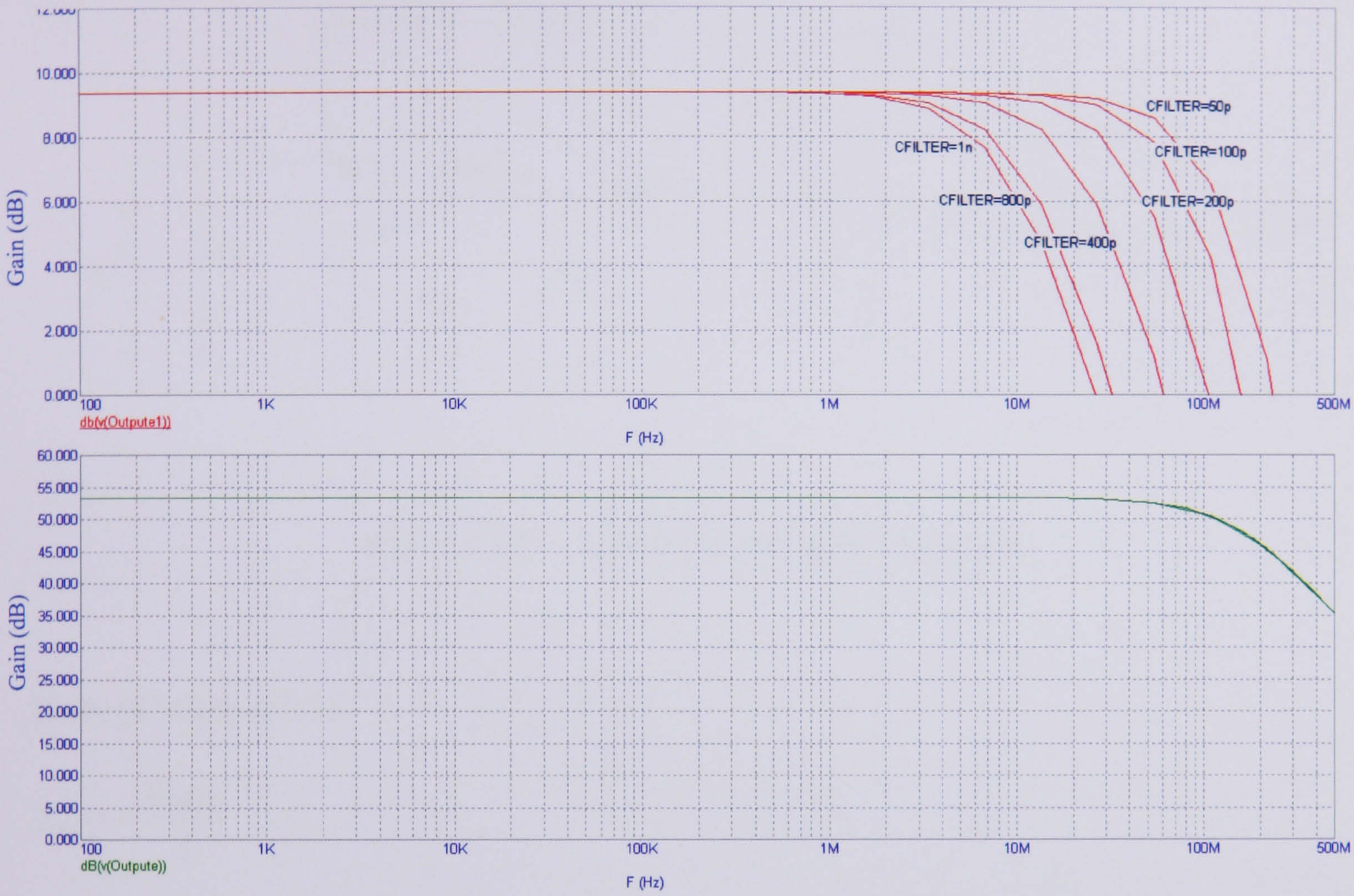

Figure 4.9 Frequency response composite transimpedance amplifier

Assuming that the gain stages and the emitter follower can be approximated by the simplified amplifier model as shown in Figure 4.10, $R_{b1}, R_{b2} >> R_{e1}$ and frequencies are considered where C_{dc} and C_b are short circuits, than the transimpedance gain, A_z, for the circuit is approximated using the following assumption, where A is the voltage gain of the first stage amplifier, and A_1 is the voltage gain of the second stage amplifier:-

$V_{output} = -AV_{in}$ .....(4.10)

$$I_p = \frac{V_{in} - V_{output}}{R_f} + V_{in} j\omega C_d + \frac{V_{output} - 0}{R_{e3}} \quad \text{.....(4.11)}$$

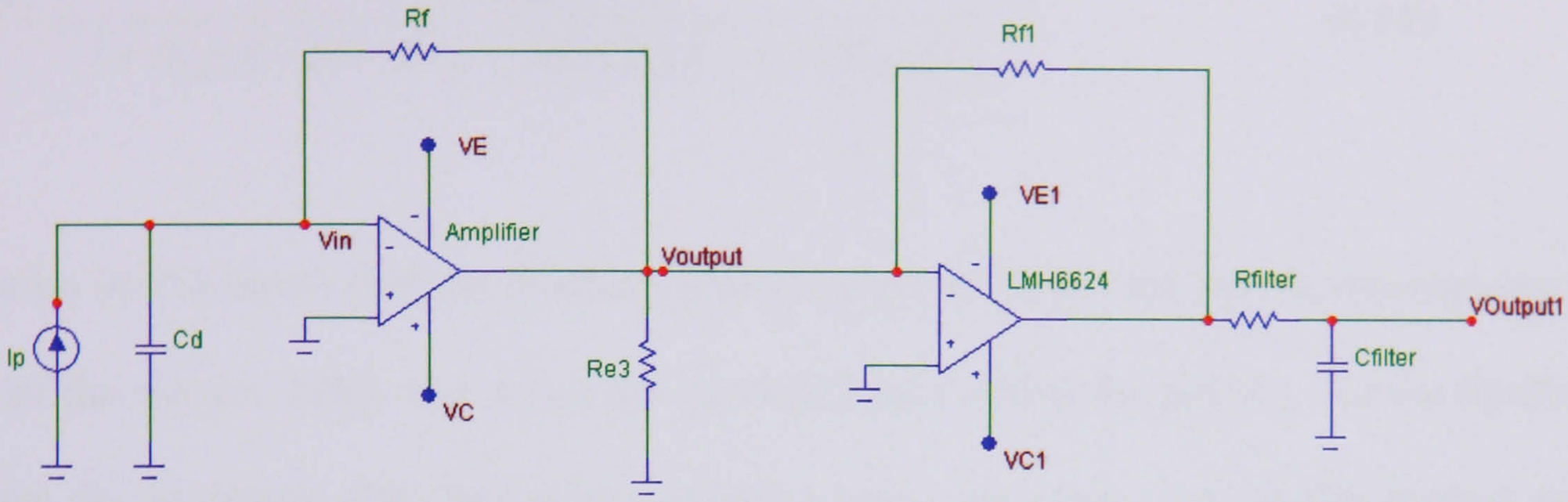

Figure 4.10 Simplified model of Figure 4.8

From (4.10) in (4.11)

$$V_{in} = -\frac{V_{output}}{A}$$

$$I_p = \frac{\frac{-V_{output}}{A} - V_{output}}{R_f} + (\frac{-V_{output}}{A}) j\omega C_d + \frac{V_{output}}{R_{e3}} \quad \text{.....(4.12)}$$

$$I_p A R_f R_{e3} = [V_{output}(R_{e3})(A-1) - (V_{output})R_{e3}R_f j\omega C_d + V_{output} A Z_f]$$

$$\mathrm{A_Z} = \frac{V_{output}}{I_p} = \frac{AR_f R_{e3}}{R_{e3}(A-1) + AR_f - j\omega C_d R_{e3} R_f} \quad (4.13)$$

$$\frac{V_{output1}}{V_{output}} = -A_1 \frac{\frac{1}{j\omega C_{filter}}}{R_{filter} + \frac{1}{j\omega C_{filter}}} \cong \frac{-A_1}{j\omega R_{filter} C_{filter} + 1} \quad (4.14)$$

From (4.13) and (4.14)

$$\frac{V_{output1}}{I_p} = \frac{-AA_1R_fR_{e3}}{1+R_{e3}(A-1)+AR_f-j\omega C_dR_{e3}R_f+j\omega R_{filter}C_{filter}} \tag{4.15}$$

Equation (4.15) shows that the feedback resistor plays an important part in determining the gain of the circuit. Table 4.4 shows the tabulated gain versus R_f and R_{f1}. As the feedback resistor, R_f, increases, the gain of the overall system increases, but, as the second stage amplification feedback resistor, R_{f1}, increases, the overall system gain reduces.

Table 4.4 Feedback resistor, R_f and R_{f1} versus gain

R_{f1} = 500Ω		R_{f1} = 800Ω		R_{f1} = 1kΩ	
R_f (Ω)	Gain (dB)	R_f (Ω)	Gain (dB)	R_f (Ω)	Gain (dB)
25k	11.51	25k	9.56	25k	8.53
50k	12.42	50k	10.44	50k	9.29
75k	12.664	75k	10.77	75k	9.73
100k	12.83	100k	10.93	100k	9.89

4.3 Combination of dual feedback loop and voltage feedback amplifier

In this section, the technique of dual feedback loops was used in a composite manner with a VFA, the LMH6624. The dual feedback loops technique was used in the amplifier for terminal impedance matching, and this is categorised as a broadband amplifier. These are used in a large variety of applications, such as wireless systems and optical communications. Amongst the variety of broadband amplifiers, the Kukeilka configuration is one of the popular circuits [4.8]. The schematic design of this type of broadband amplifier is sometimes known as the dual feedback loop amplifier, presented here. This has been improved in terms of transimpedance bandwidth by using two bipolar transistors and two peaking inductors in series with the base of the transistor, as shown in Figure 4.11. The output of the dual feedback loop amplifier is then connected in series with an inverting VFA. The output of the voltage feedback amplifier, LMH6624 is connected to resistor R_{filter} with an array of switchable capacitors, $C_{filter,}$ which control the bandwidth adjustment of the overall circuit. Each capacitor is connected to the output of a high speed dual comparator, the LM119, which compares the input voltage of $V_{control}$, as shown in Figure 4.12. The reference voltage is set between 0.1V to 5.1V. The output of each comparator is connected to an N-channel MOSFET, the SI2308DS, which acts as a switching transistor. The capacitor is linked in series with the MOSFET. When, the MOSFET switches on, the capacitor is connected to ground, when the configuration then acts as an RC filter. As the $V_{control}$ changes from 0.1V to 5.1V, each of the switchables capacitors will be activated,

where at $V_{control}$ = 5.1V, the capacitance value will be equal to C_{filter} + $C_{filter1}$ + $C_{filter2}$ + $C_{filter3}$ + $C_{filter4}$ +$C_{filter5}$.

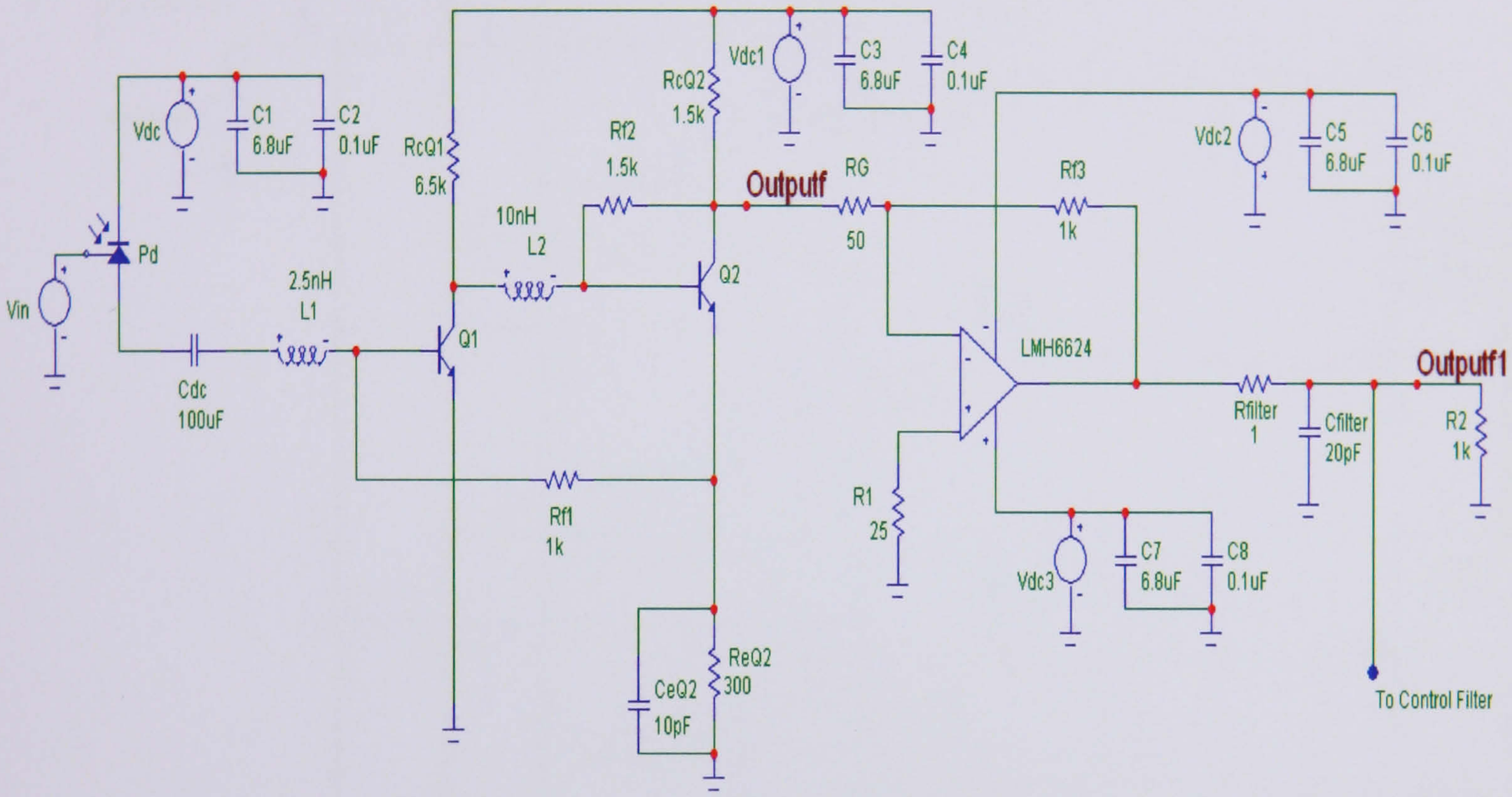

Figure 4.11 Composite dual feedback loop with VFA

This amplifier is approximated by a two-pole system with open loop poles P_1 and P_2. The local series feedback resistor, $R_{f1,}$ is used to adjust P_1 whilst the local shunt resistor, $R_{f2,}$ and series resistor, $R_{eQ2,}$ are used to adjust P_2 so that the two poles are bought to be coincident. Then, the feedback resistor, R_{f2}, is selected for a required loop gain to attain the maximally flat condition. Capacitor, C_{eQ2} is connected in parallel with R_{eQ2} to overcome the over-damped characteristics. The effect of inductors L_1 and L_2 in series with the base of the input transistor is to produce a high frequency peak, in order to broaden the bandwidth. This method is known as "series peaking" because the inductor appears in series with the source, similar to shunt peaking, but it introduces no zero in the transfer function [4.9-4.11].

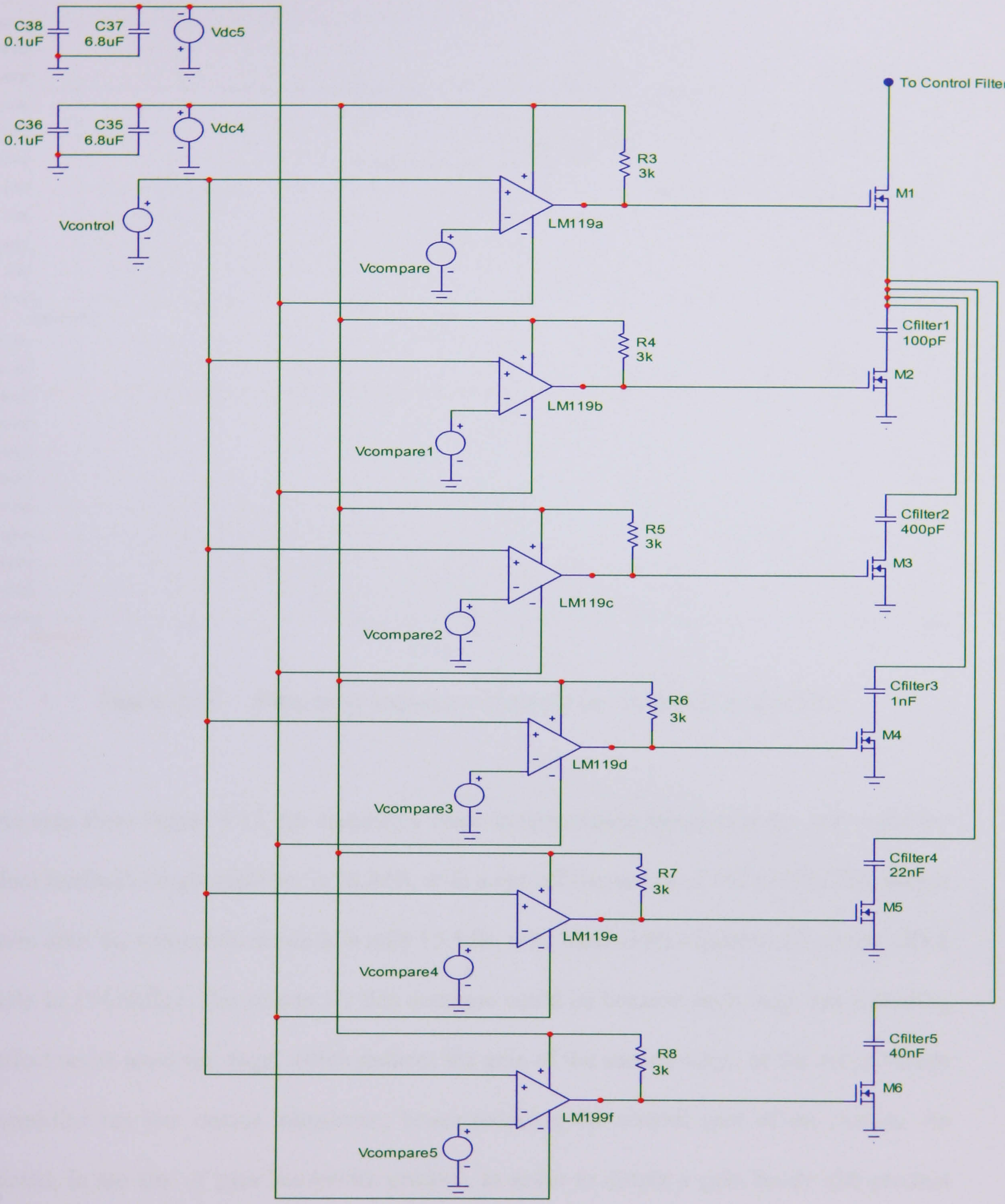

Figure 4.12 Array of RC filter with comparator

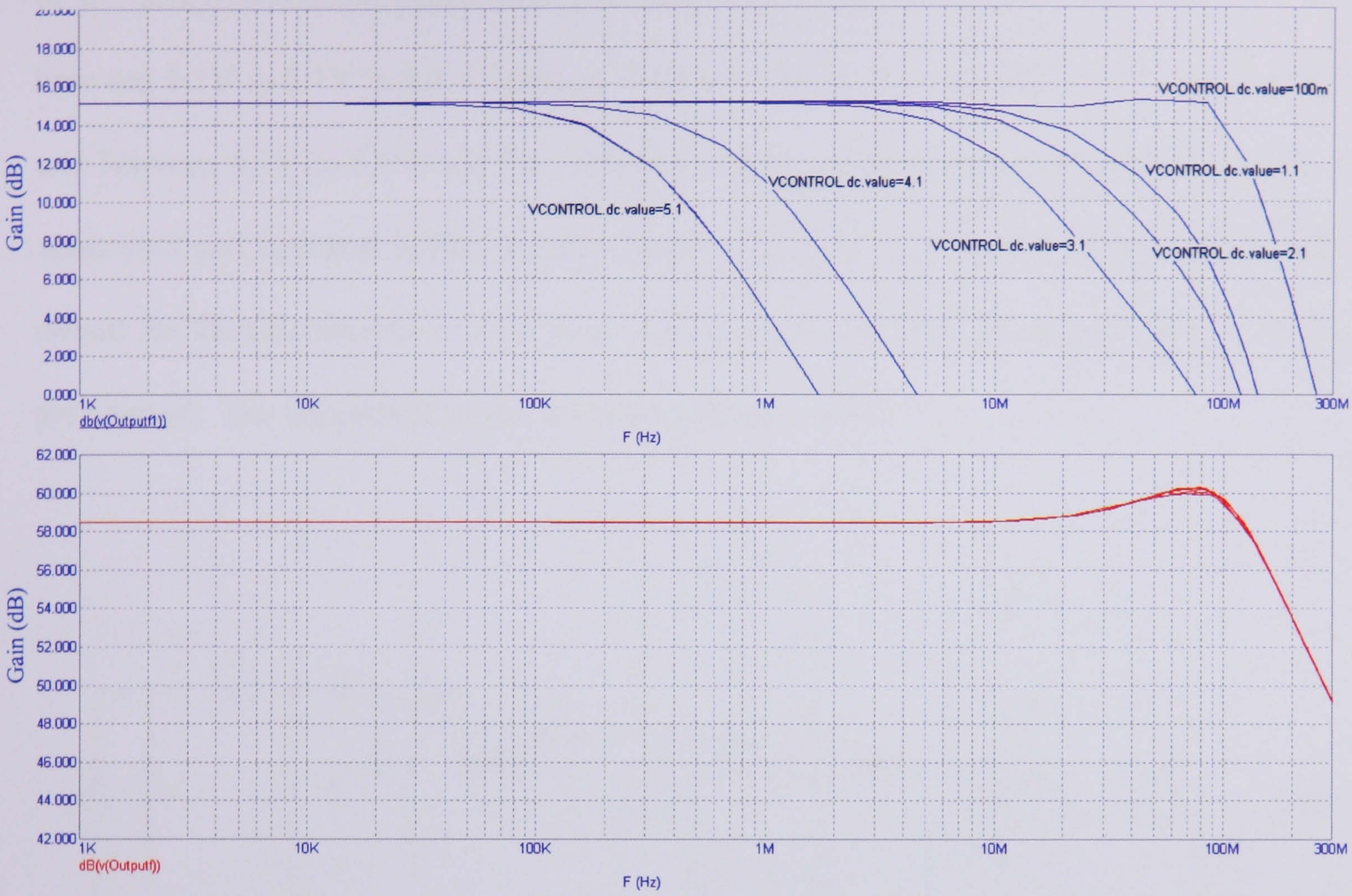

Figure 4.13 Frequency response composite transimpedance amplifier

As seen from Figure 4.13, the frequency response simulation shows that the gain from the dual feedback loops amplifier is 58.4dB, with a cut-off frequency of 167.6MHz. The output gain after the composite network is only 15.1dB, with bandwidth adjustment between 285.8 kHz to 114.8MHz. The reason for this decrease could be because each stage has a loading effect on its previous stage, which reduces the gain of the second stage, or the second stage amplifier has low output impedance, hence reducing the overall gain of the system. As stated, in the law of gain bandwidth product, in order to obtain a gain bandwidth product constant, one would have to trade gain for bandwidth or vice versa, which is equally in this case. This bandwidth adjustment is obtained by changing $V_{control}$ from 0.1V to 5.1V. The results show that the bandwidth ratio between each $V_{control}$ can be set by changing the value

of the array-switchable capacitors. The bandwidth ratio between 0.1V to 1.1V is 3.5:1, between 1.1V to 2.1V is 1.5:1, between 2.1V to 3.1V is 2:1, between 3.1V to 4.1V is 13:1, and between 4.1V to 5.1V is 2.5:1. This shows that a wide adjustable bandwidth could be controlled and operated within a given range. The open loop circuit of the dual feedback circuit for the calculations of open loop voltage gain is as follows, assuming C_{dc} and C_{eQ2} are shorted. The simplified model is shown in Figure 4.14 :

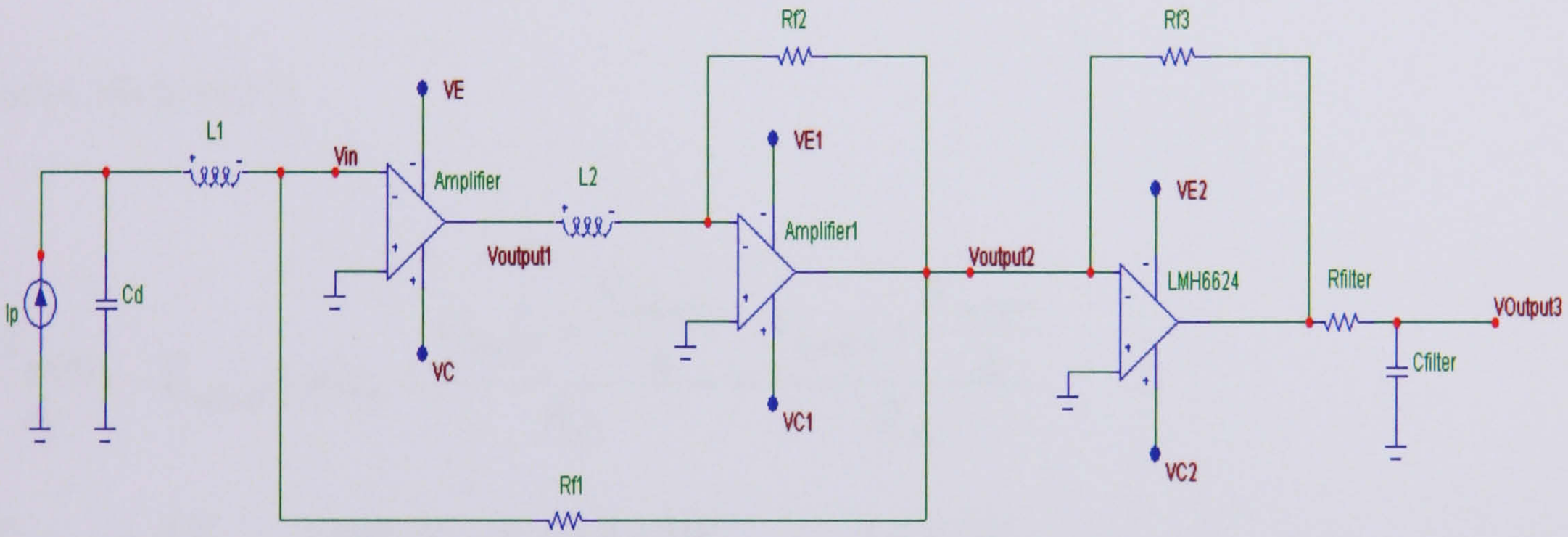

Figure 4.14 Simplified model of Figure 4.11

$$V_{output1} = -AV_{in} \tag{4.16}$$

$$[V_{in} - (V_{output1} - V_{in})j\omega L_1]j\omega C_d = I_p + \frac{V_{ouput2} - V_{in}}{R_{f1}} \tag{4.17}$$

$$V_{output2} = -A_1 V_{in2} \tag{4.18}$$

$$(V_{in2} - V_{output1})j\omega L_2 + \frac{V_{output2} - V_{in2}}{R_{f2}} = \frac{V_{output1} - V_{in}}{R_{f1}} \tag{4.19}$$

From (4.16) in (4.17)

$$[\frac{-V_{output1}}{A} - (V_{output1} + \frac{V_{output1}}{A}) j\omega L_1] j\omega C_d = I_p + \frac{V_{output2} + \frac{V_{output1}}{A}}{R_{f1}}$$

$$[-V_{output1} - (AV_{output1} + V_{output1}) j\omega L_1] j\omega C_d = AI_p + \frac{AV_{output2} + V_{output1}}{R_{f1}}$$

$$\frac{-V_{output1}[j\omega C_d R_{f1} + (A+1) j^2\omega^2 L_1 C_d R_{f1} + 1]}{A} = R_{f1} I_p + V_{output2} \qquad (4.20)$$

From (4.18) in (4.19)

$$(\frac{-V_{output2}}{A_1} - V_{output1}) j\omega L_2 + \frac{V_{output2} + \frac{V_{output2}}{A}}{R_{f2}} = \frac{V_{output1} + \frac{V_{output1}}{A}}{R_{f1}}$$

$$\frac{(-V_{output2} - A_1 V_{output1}) j\omega L_2 R_{f2} + A_1 (A+1) V_{output2}}{A_1 R_{f2}} = \frac{(A+1) V_{output1}}{R_{f1}}$$

$$[-j\omega L_2 R_{f2} R_{f1} + R_{f1} A_1 (A+1)] V_{output2} = [A_1 R_{f2} (A+1) + A_1 j\omega L_2 R_{f2} R_{f1}] V_{output1}$$

$$\frac{V_{output2}}{V_{output1}} = \frac{A_1 (A+1) R_{f2} + A_1 R_{f1} R_{f2} j\omega L_2}{A_1 (A+1) R_{f1} - R_{f1} R_{f2} j\omega L_2} \approx K \qquad (4.21)$$

Substituting (4.21) into (4.20)

$$\frac{-V_{output2}[j\omega C_d R_{f1} + (A+1) j^2\omega^2 L_1 C_d R_{f1} + 1]}{KA} = R_{f1} I_p + V_{output2}$$

$$-V_{output2}[j\omega C_d R_{f1} + (A+1) j^2\omega^2 L_1 C_d R_{f1} + 1] - V_{output2}(KA) = KAR_{f1} I_p$$

$$\frac{V_{output2}}{I_p} = \frac{-AR_{f1}K}{j\omega C_d R_{f1} - \omega^2 (A+1) L_1 C_d R_{f1} + 1 + AK} \tag{4.22}$$

$$\frac{V_{output3}}{V_{output2}} = \frac{-A_2}{j\omega R_{filter} C_{filter} + 1} \tag{4.23}$$

$$\frac{V_{output3}}{I_p} = \frac{-AA_2 R_{f1} K}{(j\omega C_d R_{f1} - \omega^2 (A+1) L_1 C_d R_{f1} + 1 + AK)(j\omega R_{filter} C_{filter} + 1)} \tag{4.24}$$

It should be pointed out that there is a limitation to input series peaking. The loss and the parasitic capacitance of the monolithic inductors makes them poor candidates for L_1 in Figure 4.11. It would be better to employ a bond wire instead but the length and shape of the wire and the capacitance of the photodiode must be tightly controlled [4.11].

4.4 Summary

This chapter has presented three techniques for achieving bandwidth adjustment, using the method of combining different characteristic amplifiers, known as the composite amplifier. Table 4.5 shows the comparison of each technique. The technique using a dual feedback loop and a VFA has a bandwidth range and variation of bandwidth adjustment, with a gain of 15.13dB. The technique using bootstrap a transimpedance amplifier with a VFA has the lowest gain, 12.3dB, and the bandwidth adjustment is more focused in the centre between the high frequency range (HF) to very high frequency range (VHF). The composite VFA

and CFA technique has the highest gain, 50.1dB, but the bandwidth adjustment ratio is very small. Noise analysis of each technique will be discussed in detail in Chapter 6.

Table 4.5 Comparison of composite amplifier technique

Technique	VFA and CFA	Bootstrap TIA and VFA	Dual Feedback Loop and VFA
Gain	50.1dB	12.3dB	15.3dB
Cut-off Frequency	18.1MHz – 75.2MHz	9.5MHz – 103.5MHz	285.8 kHz – 114.8MHz
Ratio	1 : 4	1 : 10.8	Varies depends on the capacitor value setting

References

[4.1] Tim Kalthoff, Tony Wang and R. Mark Stitt, "Classical op amp or current feedback op amp? This composite op amp gives you the best of both worlds" Application Bulletin, Burr-Brown, 1991.

[4.2] John Austin, "Current feedback amplifiers : Review, stability analysis and applications" Application Bulletin, Burr-Brown, 2000.

[4.3] Mark Sauerwald, "Composite amp provides high gain and bandwidth" EDN Access, 1994.

[4.4] Chris Toumazou, Alison Payne and John Lidgey, "Current feedback versus voltage feedback amplifier: History, Insight and relationships" IEEE International Symposium Circuits and Systems, pp. 1046-1049, 1993.

[4.5] Hooman Hashemi,"Photo-diode Current to Voltage Converters" Application Brief 104, National Semiconductor, 2002.

[4.6] Datasheet LMH6624, National Semiconductor, 2003

[4.7] Datasheet LMH6732, National Semiconductor, 2004

[4.8] Yu Chang Chen and Shey Shi Lu, "Analysis and design of CMOS broadband amplifier with dual feedback loops" IEEE Proceedings Asia-Pacific Conference, pp.245-248, 2002.

[4.9] G. Palumbo and J. Choma, "An overview of analog feedback part I: Basic theory" Analog Integrated Circuits and Signal Processing, No. 17, pp. 175-194, 1998.

[4.10] G. Palumbo and J. Choma, "An overview of analog feedback part II:Aamplifier configurations in generic device technologies" Analog Integrated Circuits and Signal Processing, No. 17, pp. 195-219, 1998.

[4.11] Behzad Razavi, "Design of integrated circuits for optical communications" McGraw-Hill, Chapter 4, 2003.

Chapter 5

Integration of bandwidth control and automatic gain control

Optical receivers may experience vastly different input currents because the transmitted optical power, ambient noise and the efficiency of the photodiode may vary from one link to another. Thus, transimpedance amplifiers must accommodate a relatively wide dynamic range, typically from a few microamperes to a few milliamperes. For example, assume a transimpedance amplifier with $R_f = 1k\Omega$ and $V_{out} = 0.8V$ when $I_{in} = 0$. If a logical one, represented by $I_{in} = 100\mu A$, is injected into a transimpedance amplifier, the voltage output of the amplifier will change by $100\mu A \times 1k\Omega = 100mV$. If I_{in} rises to 1mA, it cannot be

accommodated within V_{out}, and the circuit becomes heavily nonlinear. This overload behaviour appears at first sight benign for large input currents. Unfortunately, at high speeds, other effects arise that make overload undesirable. In bipolar transimpedance amplifiers it may drive some of the transistors into saturation, degrading the speed considerably. Therefore, it is suggested that the gain of the transimpedance amplifier must be automatically adjusted such that high input currents do not distort the output waveform. The detailed concepts are different from typical voltage amplifiers; transimpedance amplifiers sense currents with only one polarity because photodiodes injects either electrons or no charge into the transimpedance amplifier. This means that the average value of the output voltage varies in proportion to the average amplitude of the input current. This chapter begins with an introduction to automatic gain control (AGC) theory. This is then followed by a discussion concerning the designed circuit configuration using the LMH6504. The final discussion will be focused on the frequency response plotted for each of the circuits discussed in Chapter 4, linking with the AGC.

5.1 Automatic Gain Control (AGC) Theory

The most general description of an AGC system from a practical point of view is presented in Figure 5.1(a) [5.1]. The input signal is amplified by a variable gain amplifier (VGA) whose gain is controlled by an external signal V_x. The output from the VGA can be further amplified by a stage to generate an adequate level of V_o. The output signal's parameters, such as amplitude, are sensed by the detector, any undesired component being filtered out

and the remaining signal is compared with a reference signal. The result of the comparison is used to generate the control voltage V_x, and adjust the gain of the VGA.

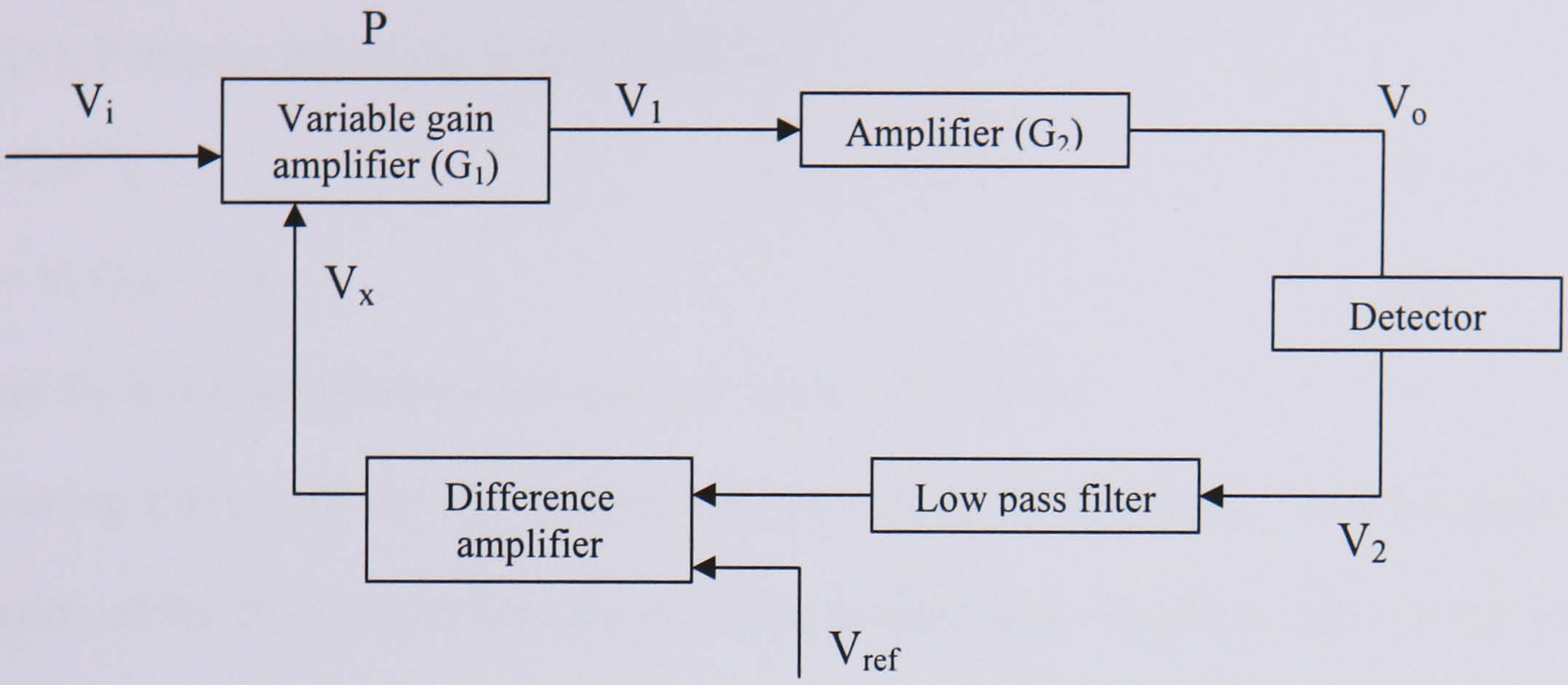

Figure 5.1(a) AGC block diagram [5.1]

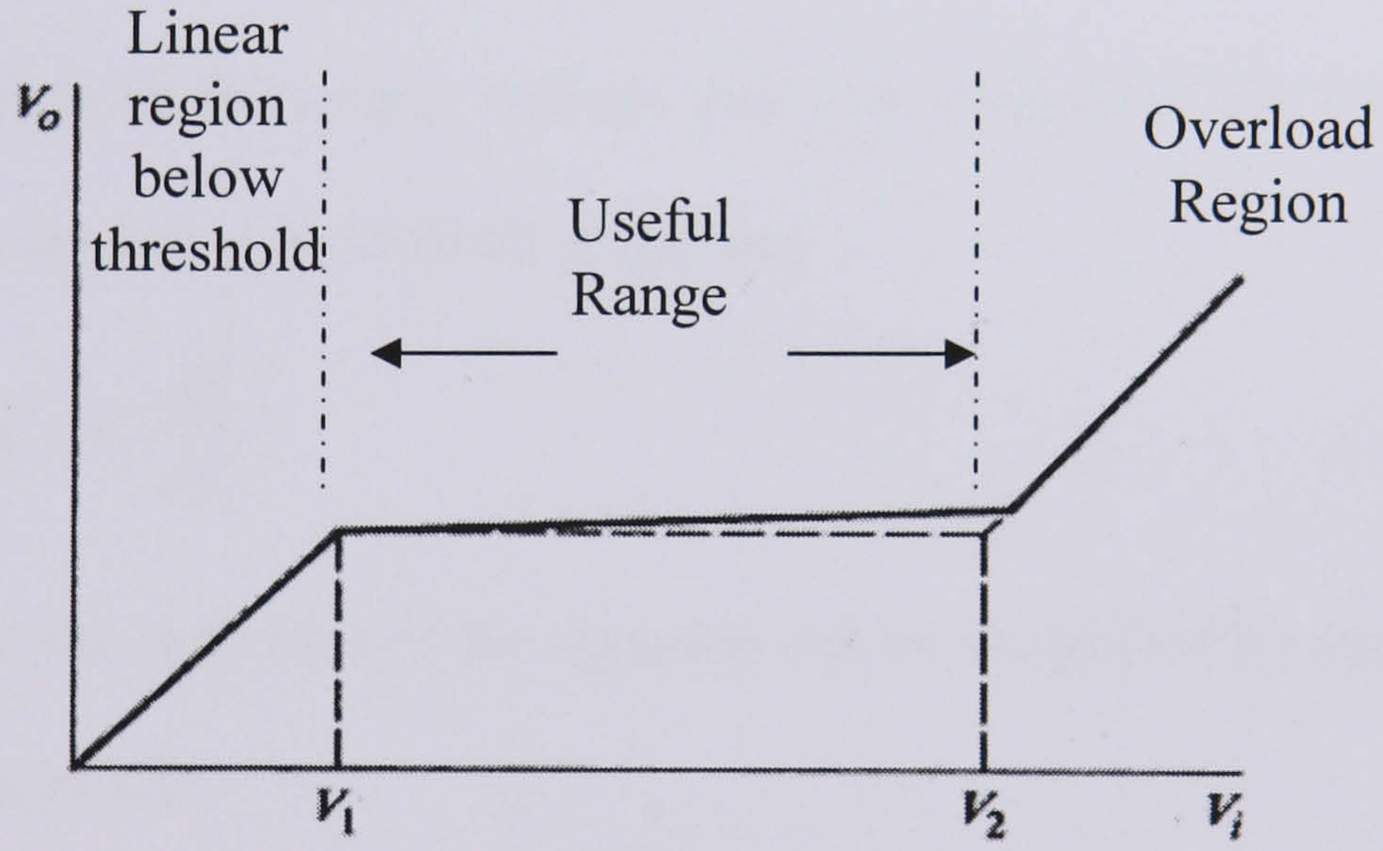

Figure 5.1(b) A typical AGC's transfer function [5.1]

An AGC is essentially a negative feedback system [5.2]. A typical transfer function for an AGC system is illustrated in Figure 5.1(b). The graph shows that, for low input signals, the AGC is disabled and the output is a linear function of the input. When the output reaches a

threshold value, V_1, the AGC becomes operative and maintains a constant output level until it reaches a second threshold value, V_2. During this state, the AGC becomes inoperative again, to prevent stability problems at high levels of gain. The variable gain amplifier (VGA), P has the following transfer function :-

$$P = G_1 e^{\alpha V}{}_x \qquad (5.1)$$

$$V_o = V_i\, G_1 e^{\alpha V}{}_x G_2 \qquad (5.2)$$

where G_1 is a constant and α is a constant factor of the VGA

Assuming unity gain for the detector and the difference amplifier, the combined transfer function of the filter and difference amplifier is label as F. Therefore the control voltage is given by :

$$V_x = (V_{ref} - V_o)F \qquad (5.3)$$

From (5.2) assuming $K = G_1 e^{\alpha V x} G_2$, then $V_o = KV_i$

To consider the change in the output voltage due to a change in the input voltage, the derivative of V_o with respect to V_i is taken as follows :-

$$\frac{dV_0}{dV_i} = \frac{d}{dV_i}(KV_i) = K + V_i \frac{dK}{dV_i} \qquad (5.4)$$

The last derivative on the right side of the equation can be simplified by applying the chain rule and using equation (5.3)

$$\frac{dK}{dV_i} = \frac{dK}{dV_x}\frac{dV_x}{dV_i} = \frac{dK}{dV_x}\frac{dV_x}{dV_o}\frac{dV_o}{dV_i} = \frac{dK}{dV_x}(-F)\frac{dV_o}{dV_i} \qquad (5.5)$$

$$\frac{dV_o}{dV_i}(1 + FV_i \frac{dK}{dV_x}) = K \qquad (5.6)$$

Equation (5.6) shows that the loop gain is a function of the input signal which translates into a relative degree of non-linearity and complicates the analysis of the transient response of the system.

5.2 Automatic gain control circuit configuration

There are many component and circuit configurations that can be used as a variable gain amplifier (VGA), which is the main component of an AGC system. The main factors that must be taken into consideration while selecting a suitable circuit are :

a) Frequency response

b) Available control voltage

c) Desired control range of the VGA

d) System configuration

Figure 5.2 illustrates a suggested automatic gain control circuit that employs two, LMH6504 integrated circuits. The LMH6504 is a wideband dc-coupled voltage-controlled gain stage followed by a high-speed current feedback operational amplifier which can directly drive a low impedance load. Looking into its internal chip configuration, the device combines a closed loop input buffer, a voltage controlled variable gain cell and an output CFA amplifier [5.3]. The input buffer is a transconductance stage whose gain is set by the gain setting resistor, R_G. The output amplifier is a current feedback operational amplifier and is configured as a transimpedance stage whose gain is set by and is equal to the feedback resistor, R_F. The maximum gain, $A_{VMAX,}$ of the device is defined by the ratio :

$\beta\frac{R_F}{R_G}$, where β is the gain multiplier with a nominal value of 0.965 [5.3]. It has a gain control bandwidth of 150MHz, where its maximum gain is set by external components, and the gain can be reduced all the way to cut-off. In AGC applications, the control loop forces the LMH6504 to have a fixed output amplitude. The input amplitude will vary over a wide range, and this can be an issue that limits dynamic range. The way to avoid this problem is to have a high value of R_G, which increases the load resistance and therefore decreases the load current demanded. With an increased R_G, R_F will also have to increase to keep the same A_{VMAX}, and this will decrease the overall bandwidth. Therefore an RC combination is placed across R_F to counteract the negative effect on BW when a large value of R_F is used.

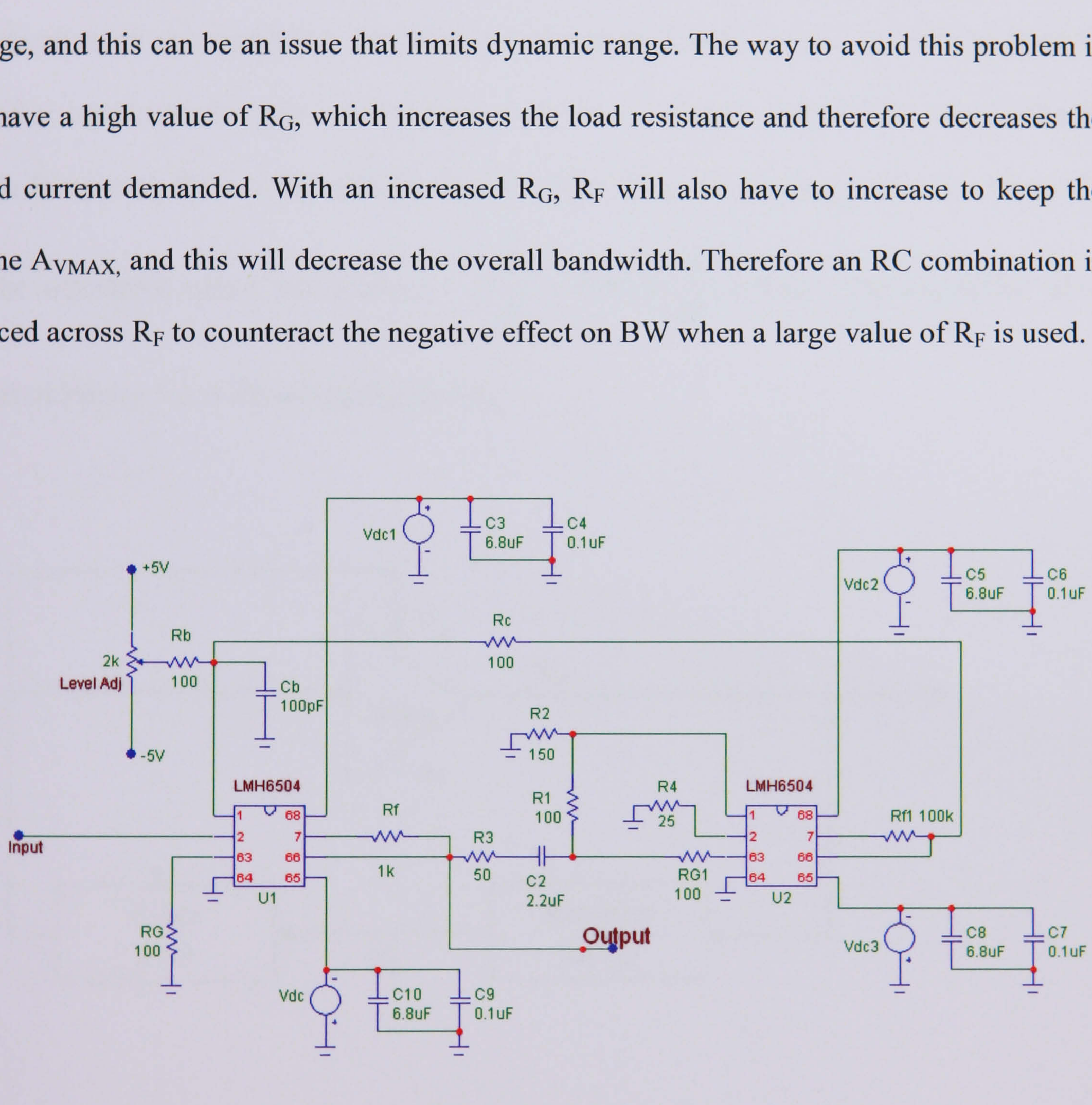

Figure 5.2 Proposed AGC circuit

In Figure 5.2, U1 receives the input signal and produces an output signal of constant amplitude. U2 is configured to provide negative feedback. Therefore, U2 generates a rectified gain control signal that works against an adjustable bias level, which may be set by the potentiometer, and R_b. C_b integrates the bias and negative feedback. The resultant gain control signal is applied to the U1 gain control input, V_g via pin 1. The bias adjustment allows the U1 output to be set at an arbitrary level less than the maximum output specification of the amplifier. Rectification is accomplished in U2 by driving both the amplifier input and the gain control input with the U1 output signal. The voltage divider that is formed by R1 and R2 sets the rectifier gain. The maximum gain set for Figure 5.2 can be calculated using the formula : $\beta \frac{R_f}{R_G} \approx 0.965(\frac{1k}{100}) = 9.65$. The simplified block model of Figure 5.2 is shown in Figure 5.3.

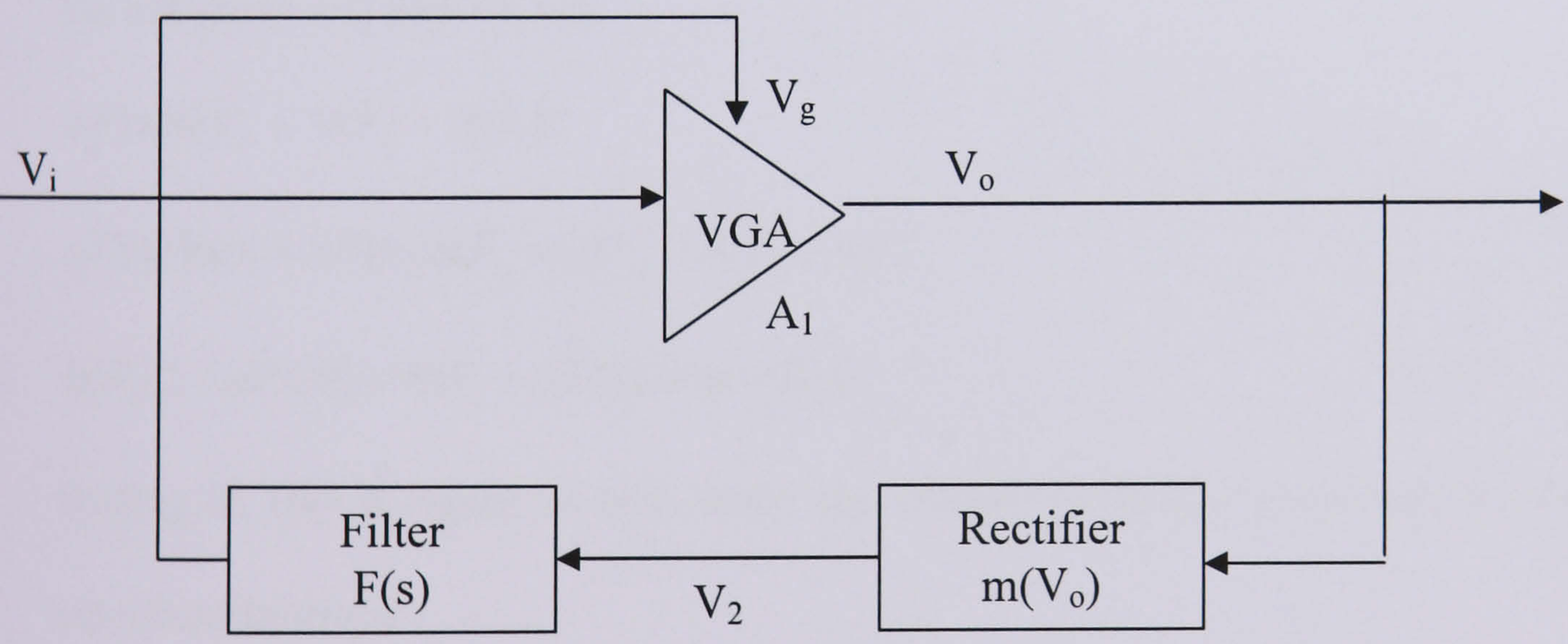

Figure 5.3 Simplified model of Figure 5.2

Assume the VGA has the following transfer function :

$$A_1 = Ke^{aV_g} \tag{5.7}$$

$$V_o = V_i A_1 \approx V_i Ke^{aV_g} \tag{5.8}$$

where K is a constant and a is a constant factor of VGA.

$$V_2 = m \mid V_o \mid \tag{5.9}$$

$$V_g = F(s)V_2 \approx F(s)m \mid V_o \mid \tag{5.10}$$

where F(s) represents the filter transfer function, and m is a constant

Applying the logarithm function on both side of equation (5.8)

$$\ln V_o = aV_g + \ln V_i K \tag{5.11}$$

The control voltage can be expressed as :

$$aV_g = \ln V_o - \ln V_i K \tag{5.12}$$

Substitute (5.10) into (5.12)

$$aF(s)mV_o = \ln V_o - \ln V_i K$$

$$aF(s)\ln m + aF(s)\ln V_o = \ln V_o - \ln V_i + \ln K$$

$$\ln V_o[1 - aF(s)] = \ln V_i + aF(s)\ln m - \ln K \tag{5.13}$$

Setting m and K equal to one, since the interest is in the output-input relationship, the equation becomes :

$$\ln V_o[1 - aF(s)] = \ln V_i \tag{5.14}$$

Expressing V_o and V_i in decibels, the following equivalence is :

$$\ln V_o = 2.3\log V_o \approx \frac{2.3}{20} V_{odB} = 0.115 V_{odB}$$

Therefore, equation (5.14) becomes :

$$V_{odB} = \frac{V_{idB}}{1 - aF(s)} \tag{5.15}$$

Equation (5.15) shows that the behaviour of the system is determined by the *a* factor of the VGA and the filter F(s). F(s) is usually a low pass filter, since the bandwidth of the loop must be limited to avoid stability problems.

The important parameter in any control system is the steady-state error that is defined as [5.4]:

$$e_{ss} = \lim_{t \to \infty} e(t) = \lim_{s \to o} sE(s)$$

where E(s) is the error signal in the feedback path.

Applying the definition to the above AGC system, the position error constant is given by :

$$e_{ss} = \frac{1}{1 - aF(0)}$$

where F(0) is the DC gain of the F(s) block, and a is the constant factor of the exponential law VGA. Thus, in order to maintain the steady state error as small as possible, the DC gain of the F(s) block must be as small as possible. The simplest F(s) block that can be used is a first order low pass filter. The transfer function is as follows [5.5]:

$$F(s) = \frac{P}{\frac{s}{B} + 1}$$

where P is the DC gain of the filter, and B is the bandwidth. Using this expression in the equation of the steady state error :

$$e_{ss} = \frac{1}{1 - aP}$$

The total DC output of the AGC system is given by :

$$V_{oDC} = \frac{V_{iDC}}{1 - aP}$$

It can be seen from the equation that the loop gain, K, must be less than 1.

The transient response of the AGC is simulated for small signal sinusoid, 1mV and large signal sinusoid, 200mV as shown in Figure 5.4. The result shows that the amplitude of the AGC remains constant.

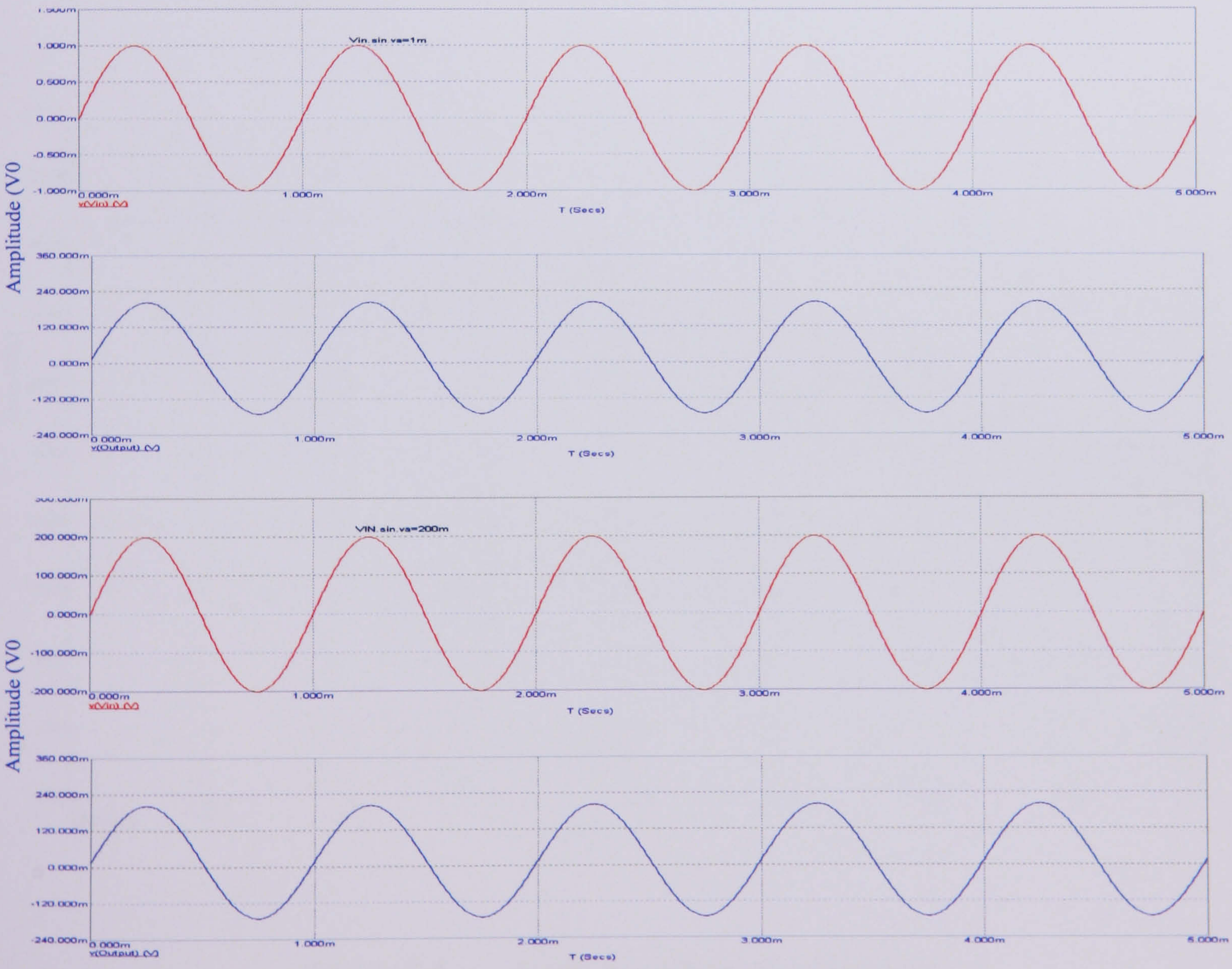

Figure 5.4 Variation of input signal, V_{in} amplitude with time

Figure 5.5 shows the frequency response of the AGC. The result shows that the output gains maintain at 25dB with a cut-off frequency of around 102MHz. If R_f is set to 2.2kΩ, the gain will increase 6dB, but the cut-off frequency reduces to 99.8MHz. This means that, as R_f increases the gain increase at the expense of bandwidth. Table 5.1 shows the gain and bandwidth variation as R_f is varied. It shows that a 2dB increase in gain gives a large reduction in bandwidth. In addition the simulation also shows that, by varying the amplitude of the input signal does not have any affect to the gain of the circuit in the frequency response plot.

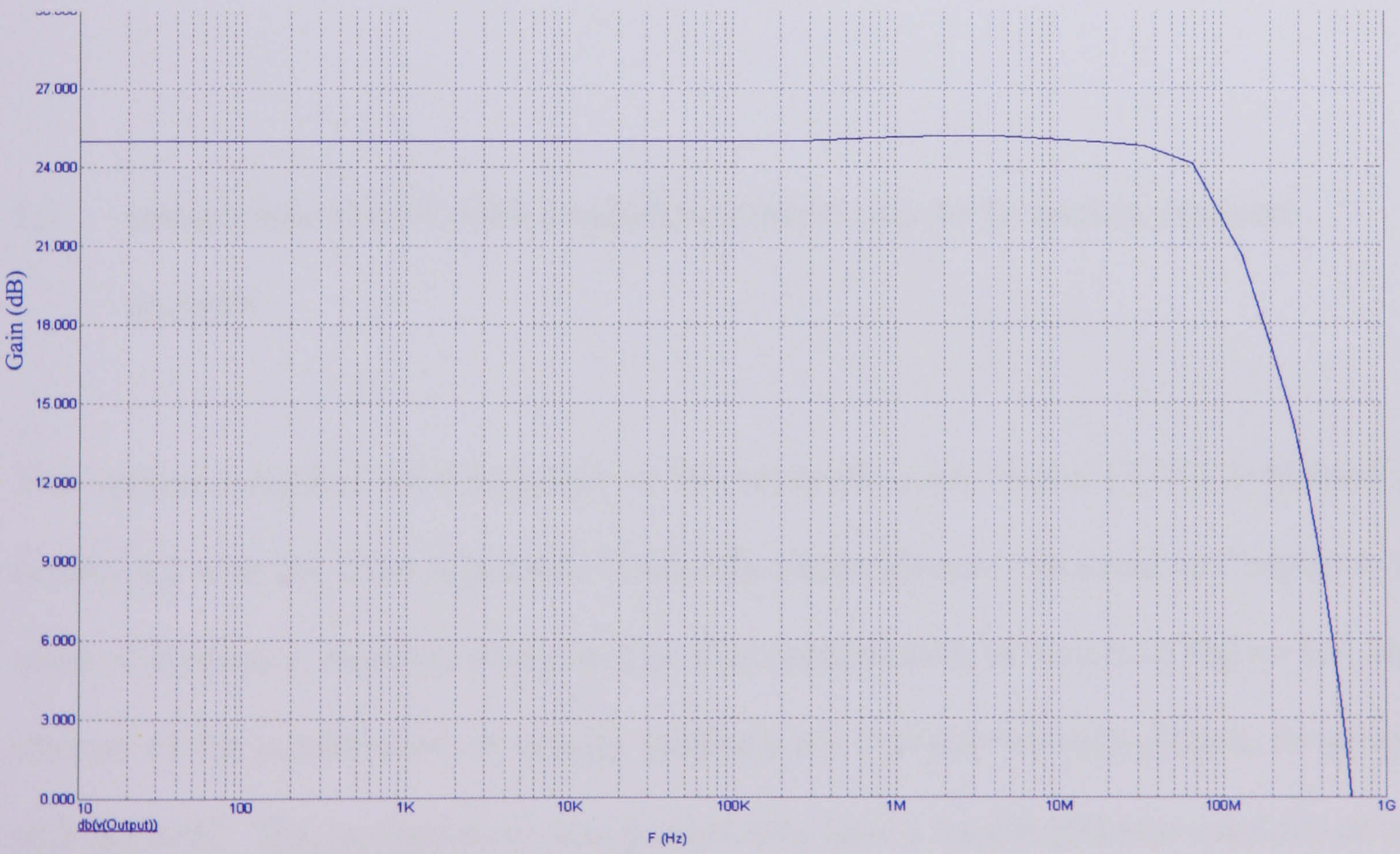

Figure 5.5 AGC circuit frequency responses

Table 5.1 R_f versus gain and bandwidth

R_f (Ω)	Gain (dB)	Bandwidth (MHz)
1k	18.9	260.3
1.6k	23	140.2
2.2k	25.8	88.1
2.8k	27.9	66.7
3.4k	29.6	43.9
4k	31	33.2

5.3 Integration of AGC with bandwidth control circuits frequency response analysis

This section considers the integration of the automatic gain control (AGC) explained in section 5.2 with the three adjustable bandwidth design circuits discussed in Chapter 4, in terms of frequency response analysis. The first configuration is shown in Figure 5.6, and consists of the combination of voltage feedback and current feedback circuits integrated with the AGC. The configuration arrangement is to have a transimpedance amplifier at the front -end, then the converter input current is fed into the adjustable bandwidth amplifier and the AGC amplifier. The aim of this configuration is have the adjustable bandwidth

amplifier set the required bandwidth of the front-end, and then to have an AGC amplifier to regain any signal level losses occur during the transition from the transimpedance amplifier stage and the second stage, adjustable-bandwidth amplifier.

The frequency plot for Figure 5.6 is shown in Figure 5.7. The first graph is the output response taken at point Output2. The overall gain after AGC stage is 54.2dB with an adjustment of bandwidth from 44.3MHz to 90.4MHz. The control voltage is between 0.1V to 5V. The second graph is taken at point Output1, which is the frequency response after the bandwidth adjustment amplifier. The gain at this stage is 50.1dB with an adjustment of bandwidth between 47.1MHz to 93.2MHz, for the same control voltage. Finally the third graph shows the response at point Output, which is the frequency response after the transimpedance amplifier. The gain at this stage is 44.3dB, with a cut-off frequency of 116.3MHz. The simulated results show that automatically adjusting the gain will have an impact on the scope of bandwidth adjustment. In this case an increase of 4.5 dB gain results in the maximum adjustable bandwidth range decreasing from 93.2MHz to 90.4MHz, whilst the minimum adjustable bandwidth range decreases from 47.1MHz to 44.3MHz.

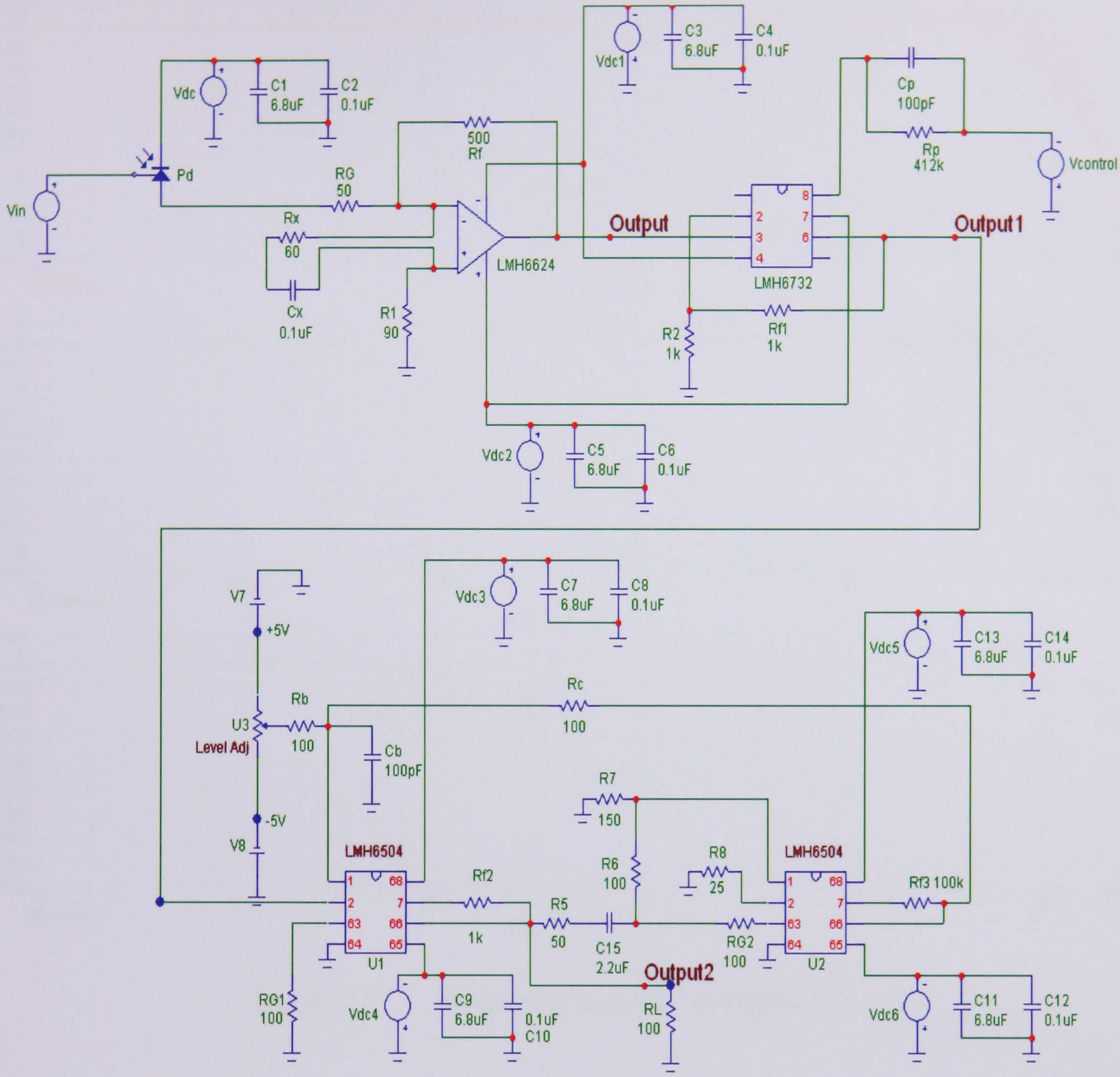

Figure 5.6 Integration of AGC with voltage feedback and current feedback amplifier

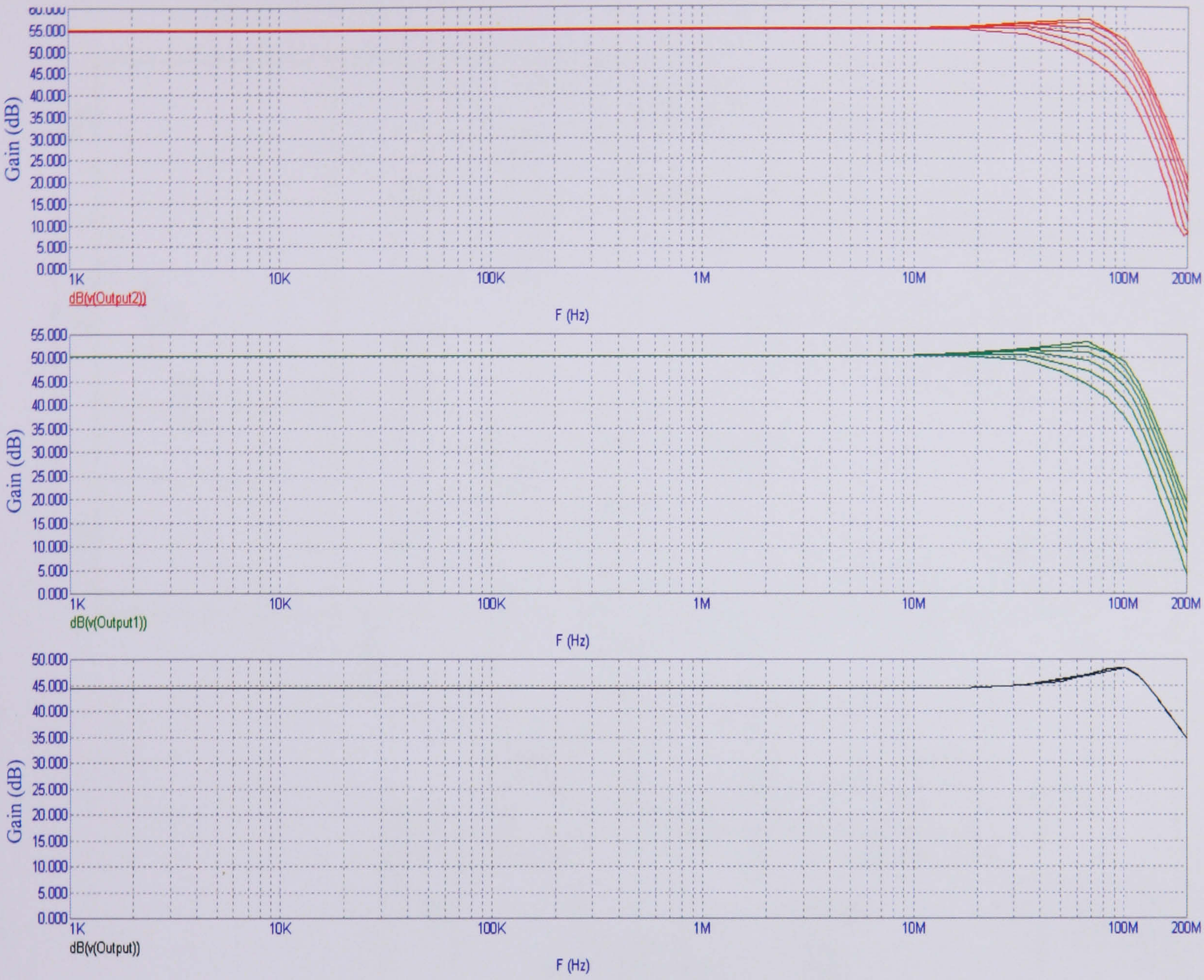

Figure 5.7 Frequency response of Figure 5.6

The second configuration as shown in Figure 5.8, is the combination of bootstrap transimpedance amplifier and voltage feedback amplifier integrated with the AGC. The frequency response is shown in Figure 5.9. The gain after the bootstrap transimpedance amplifier is 53.3dB with a cut-off frequency of 109.7MHz.Varying C_{filter} from 50pF to 1nF, produces a bandwidth adjustment range of 7.5MHz to 104.1MHz. The gain at stage two is only 10.4dB. The integration of the AGC with this configuration increases the overall gain to 31.1dB, but the adjustable bandwidth range is only from 9.4MHz to 60.7MHz.

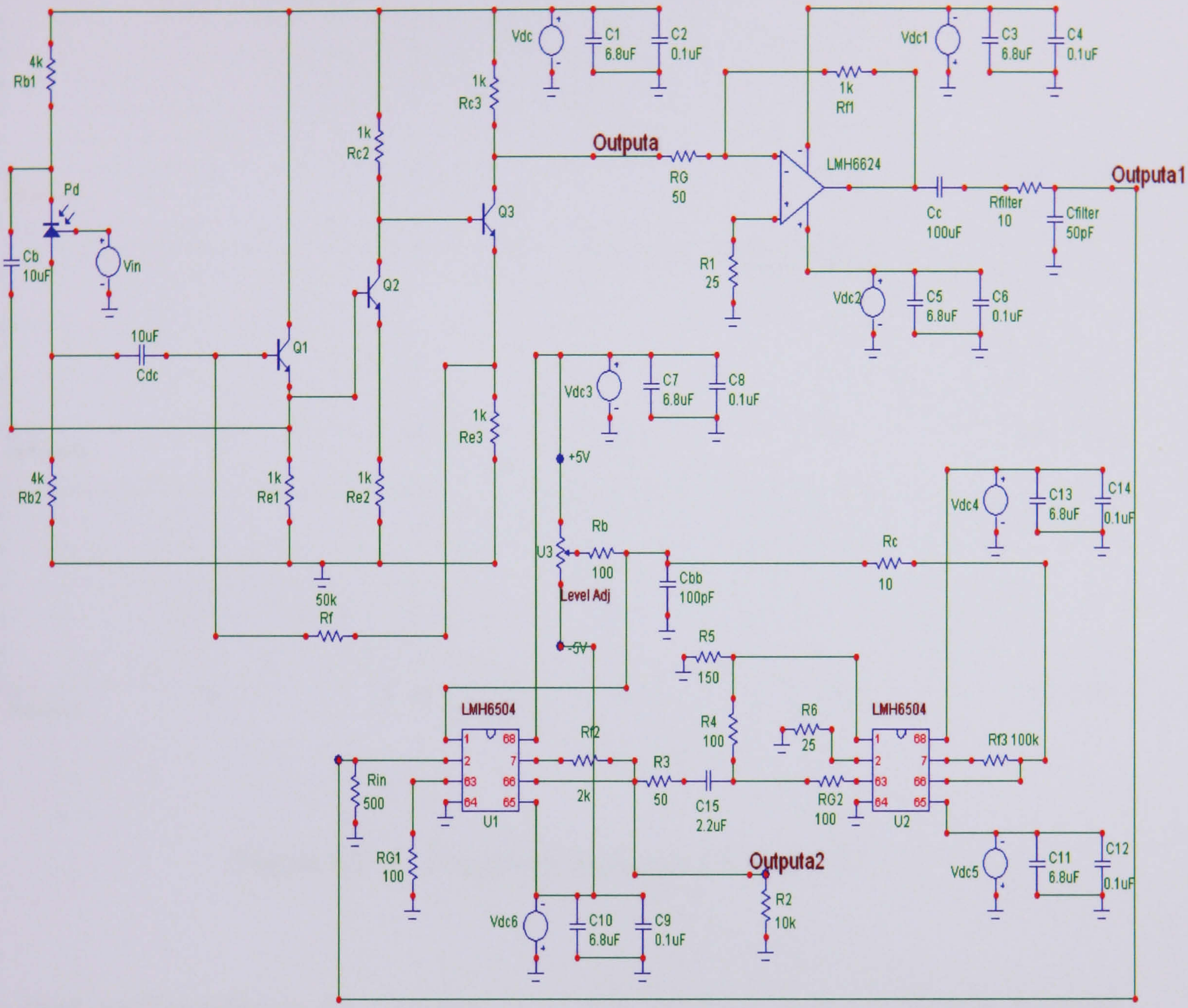

Figure 5.8 Integration of AGC with bootstrap transimpedance amplifier and voltage feedback amplifier

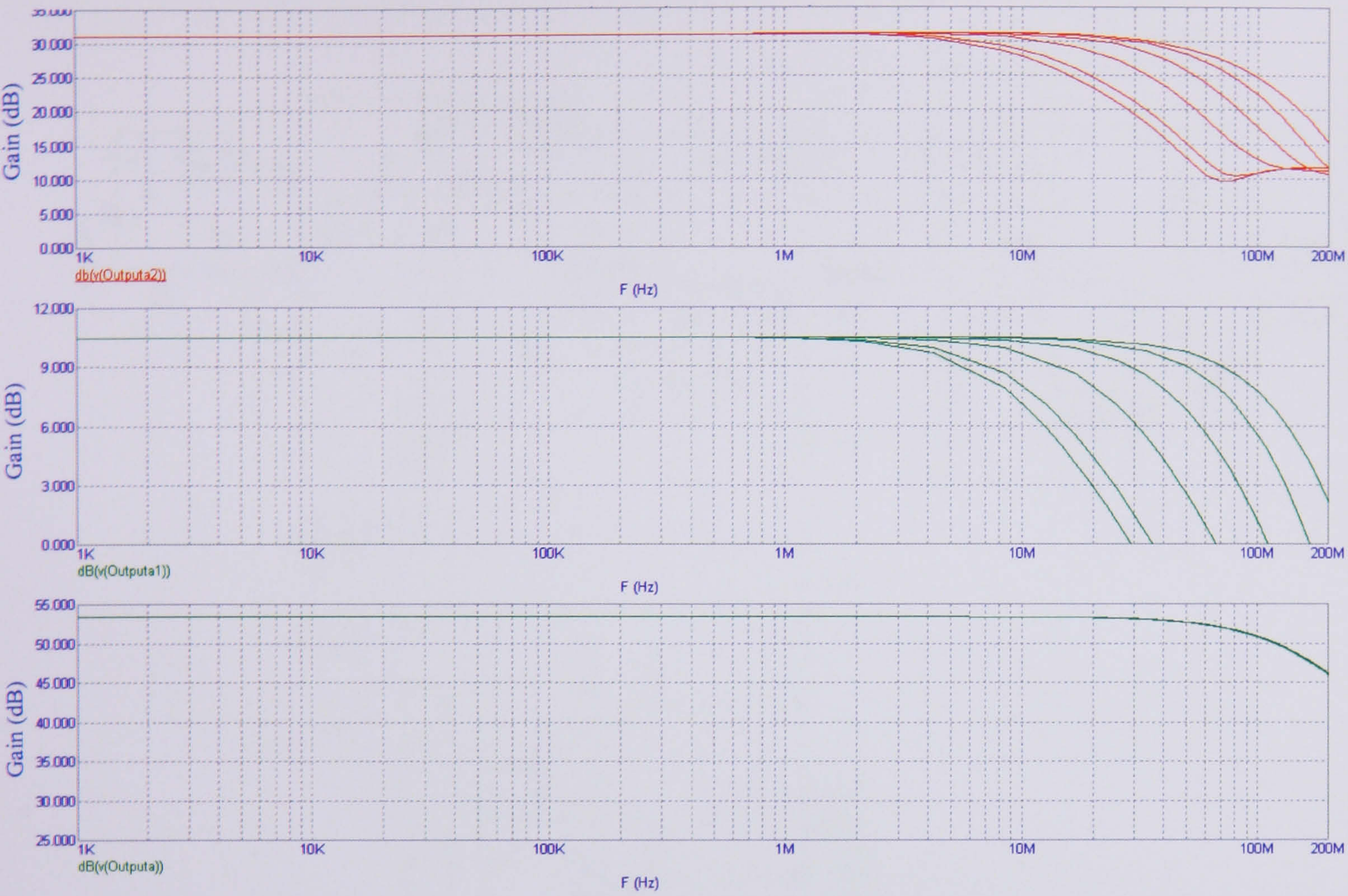

Figure 5.9 Frequency response of Figure 5.8

The third configuration is the combination of dual feedback loop and voltage feedback amplifier integrated with the AGC illustrated in Figure 5.10. The overall gain after AGC, as shown in Figure 5.11, is 35dB. As the control voltage is varied between 0.1V to 5V, the bandwidth adjustment is from 243.5 kHz to 106.1MHz. The first stage dual feedback loop amplifier produces a gain of 58dB with a cut-off frequency of 158MHz. The second stage amplifier with low pass filter shows a great decrease in gain, 16.6dB. The bandwidth adjustment varies between 246.0 kHz to 117.5MHz, for the same control voltage. This result also shows that as gain increases, the bandwidth will reduce for the system.

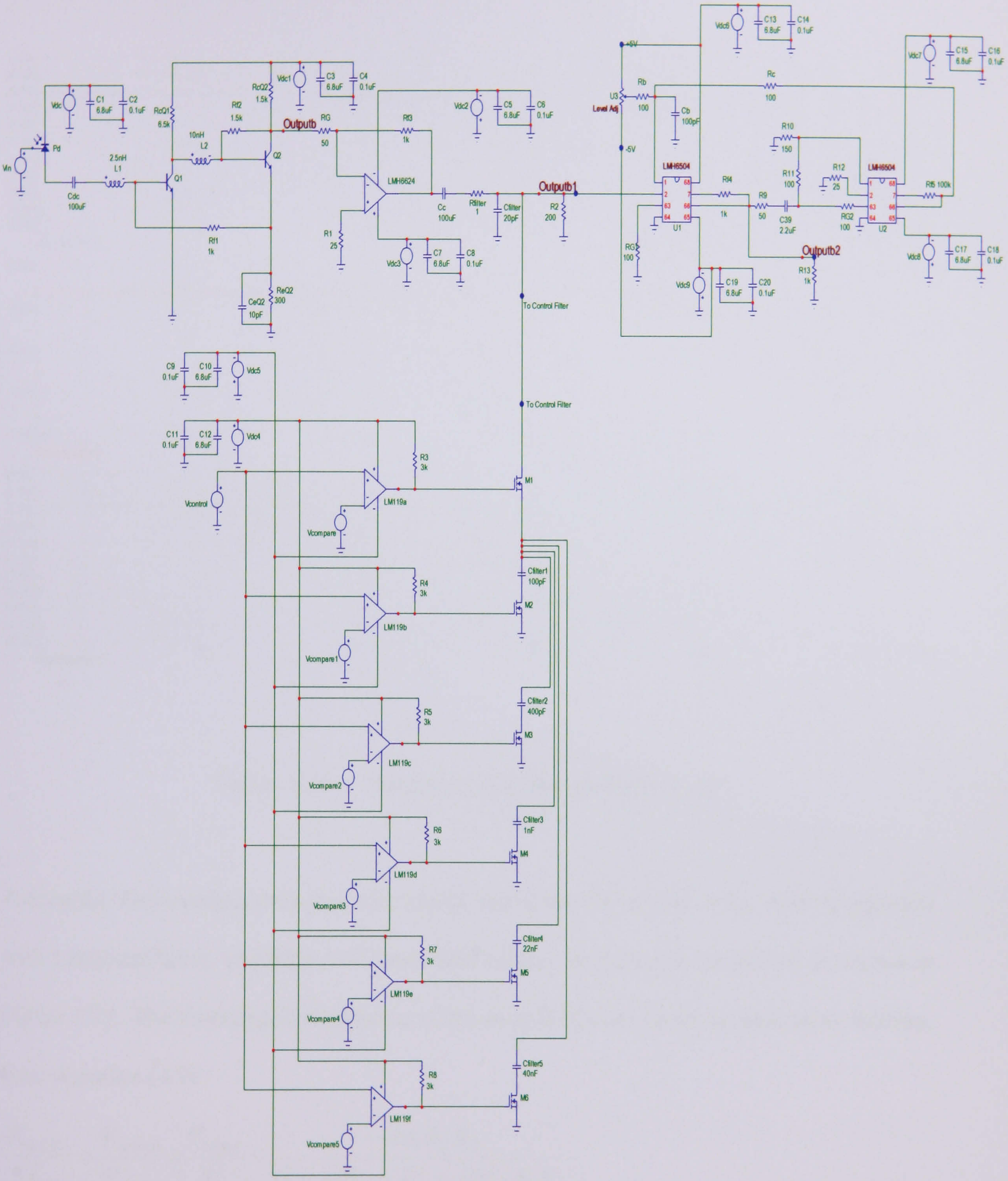

Figure 5.10 Integration of AGC with dual feedback loop and voltage feedback amplifier

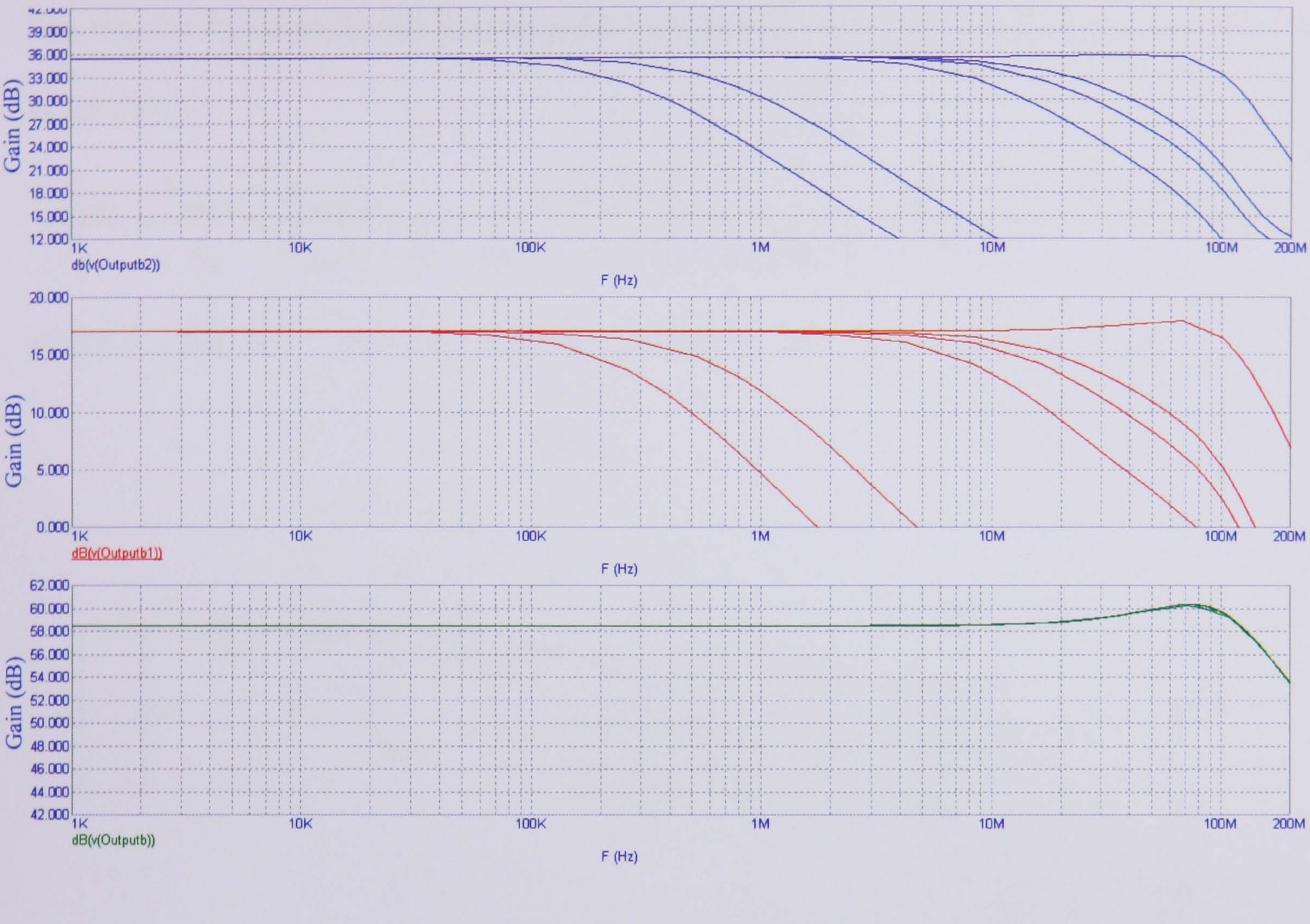

Figure 5.11 Frequency response of Figure 5.10

Taking the first configuration as a role model, the schematic model of the AGC integration with transimpedance amplifier and bandwidth control amplifier is simplified, as shown in Figure 5.12. The mathematical equation of the overall system could be derived as follows, from equation (4.9) :

$$\frac{V_{output1}}{I_p} = \frac{V_{output1}}{V_{output}} x \frac{V_{output}}{I_p} = \frac{-AA_1R_fR_G}{(1+A)R_G + R_f + j\omega C_d R_f R_G}$$

From equation (5.15),

$$V_{odB} = \frac{V_{idB}}{1-aF(s)} \approx \frac{V_{output2}}{V_{output1}} = \frac{1}{1-aF(s)}, \text{ s} = \text{j}\omega$$

The transfer function for the transimpedance amplifier with bandwidth control and AGC is as follows :-

$$\frac{V_{output2}}{I_p} = \frac{V_{output1}}{I_p} x \frac{V_{output2}}{V_{output1}} = \frac{-AA_1R_fR_G}{(1+A)R_G + R_f + j\omega C_d R_f R_G}\left(\frac{1}{1-aF(j\omega)}\right) \qquad (5.16)$$

where A - gain of 1st stage, A_1 – gain of 2nd stage, a – factor of VGA, F(s) - filter

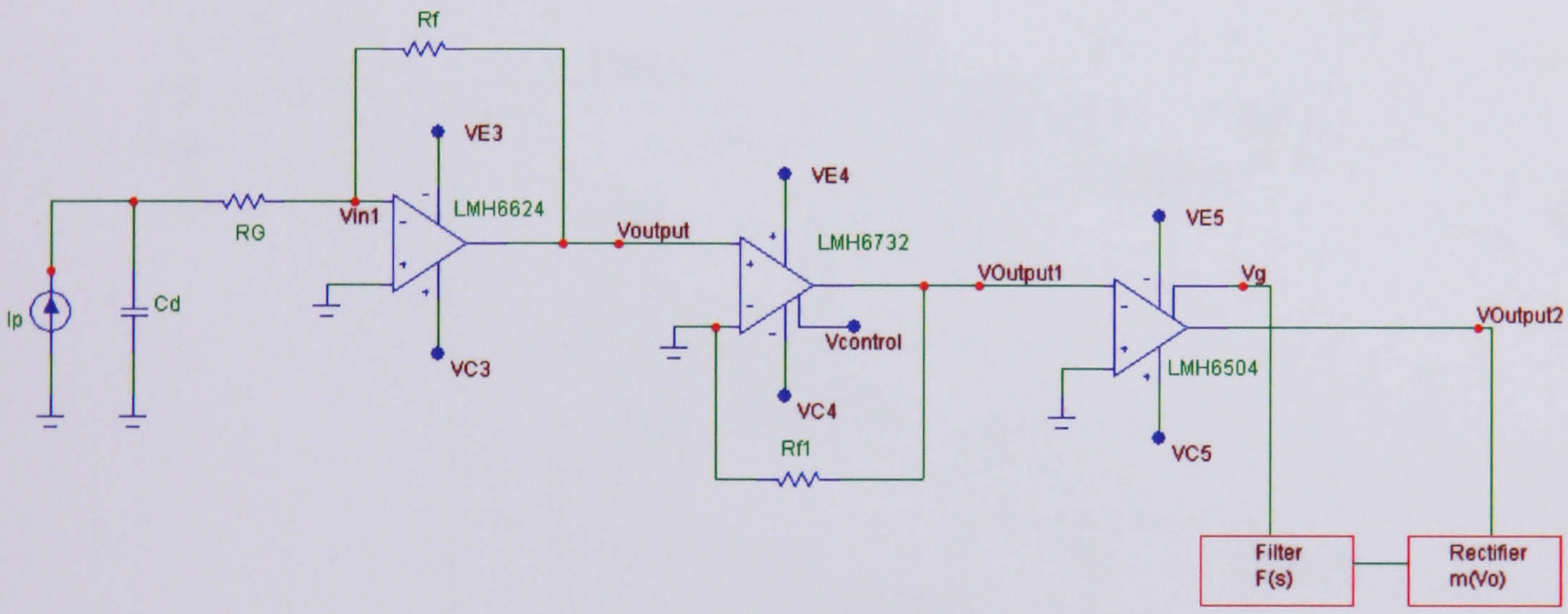

Figure 5.12 Simplified model of VBA before VGA configuration

5.4 Bandwidth control and AGC or AGC and bandwidth control?

In this section the discussion is focused on the circuit configuration for best performance, whether the bandwidth control should be before the AGC, or vice versa. To further illustrate this matter, the combination of voltage feedback amplifier and current feedback amplifier with AGC is chosen as an example. The circuit configuration where the AGC is

placed in series with the transimpedance amplifier and the output from AGC is connected to the bandwidth control circuit is shown in Figure 5.13.

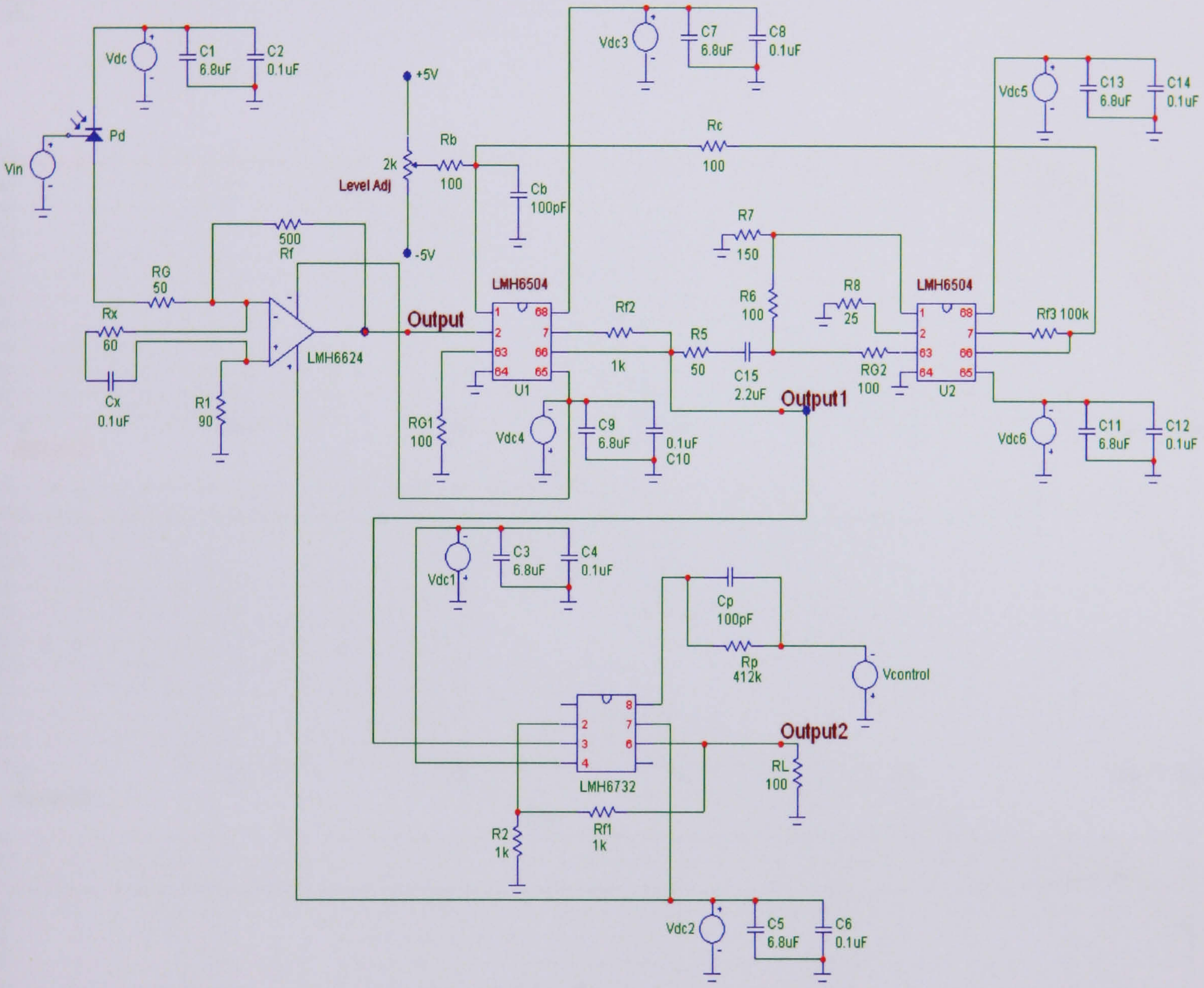

Figure 5.13 AGC before bandwidth control configuration

The simulated output frequency response of Figure 5.14 shows a difference in the range of bandwidth adjustment compared to Figure 5.6. The frequency response at stage one after the transimpedance amplifier remains unchanged, with a 44.3dB gain and cut-off frequency off 116.3MHz. The gain after the AGC circuit increases to 48.7dB, with a slight reduction in bandwidth to 112.3MHz. At point Output2, the frequency response shows that the gain

after bandwidth control circuit is 54.2dB. The bandwidth adjustment at this point is between 18.1MHz to 72.2MHz. This shows that the range of bandwidth adjustment has shifted to a lower frequency range compared to the variable bandwidth amplifier before AGC.

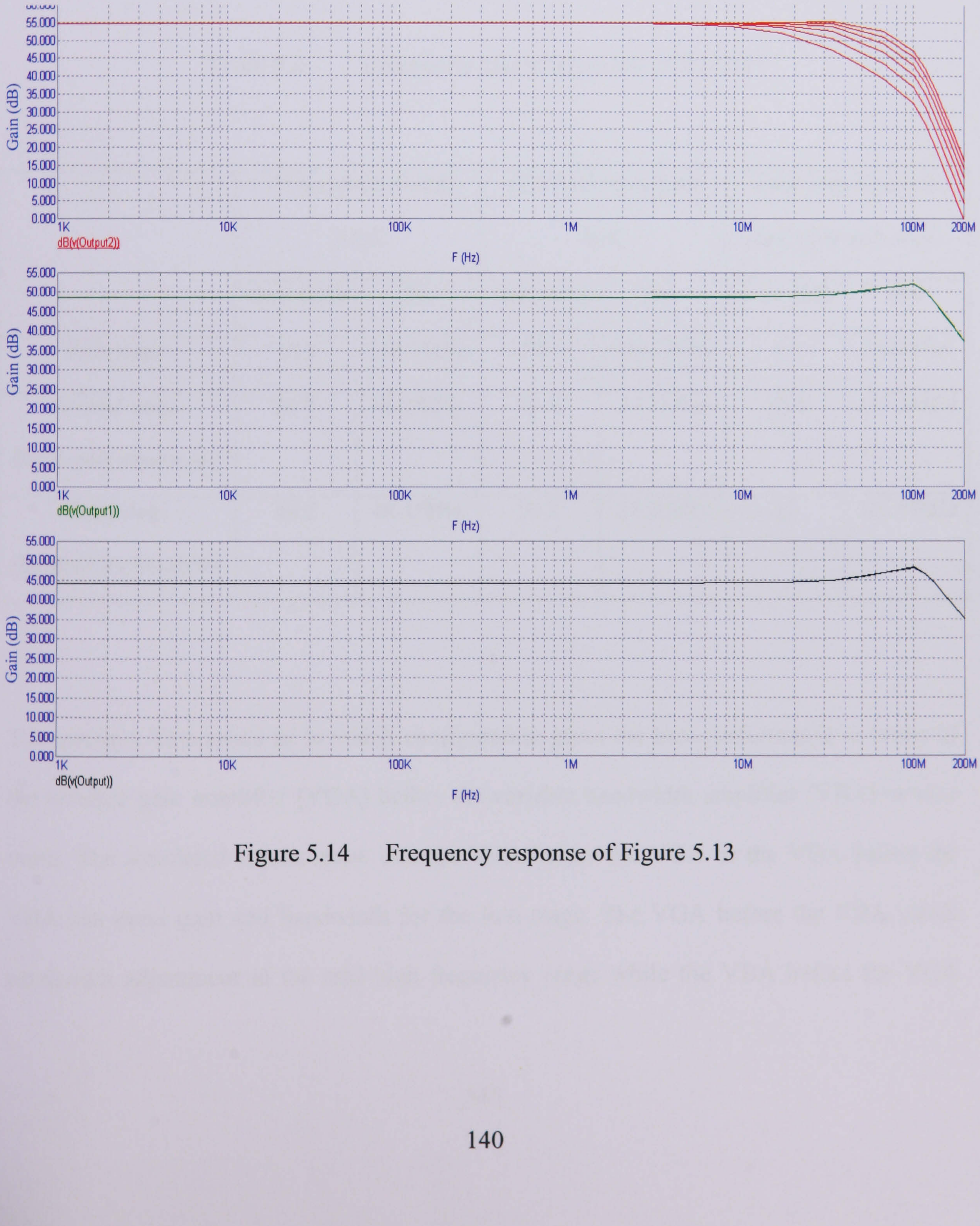

Figure 5.14 Frequency response of Figure 5.13

5.5 Summary

This chapter presents the outcome of the frequency response when the composite amplifier techniques discussed in Chapter 4 are integrated with an AGC. The results show that each configuration has its own advantages and disadvantages in terms of gain and bandwidth, as shown in Table 5.2. The noise analysis comparison will be further issued in a later chapter.

Table 5.2 Composite amplifier circuit with AGC

	VFA and CFA with AGC		BTA and VFA with AGC		Dual loop feedback and VFA with AGC	
	Gain (dB)	Bw	Gain (dB)	Bw	Gain (dB)	Bw
First stage	44.3	116.3MHz	53.3	109.7MHz	58	158MHz
Second stage (Bandwidth adjustment)	50.1	46.1MHz	10.4	96.6MHz	16.6	117.2MHz
Third stage (Bandwidth adjustment)	54.2	46.1MHz	31.1	51.3MHz	31	105.8MHz

The question then arises as to which configuration gives the best performance in terms of the variable gain amplifier (VGA) before the variable bandwidth amplifier (VBA) or vice versa. The simulated results show that the VBA before the VGA or the VGA before the VBA has same gain and bandwidth for the first stage. The VGA before the VBA yields bandwidth adjustment in the mid high frequency range while the VBA before the VGA

exhibits a much higher frequency range of bandwidth adjustments. Table 5.3 shows the comparison result between them. In terms of noise analysis comparison, it will be discussed in detail in chapter 6.

Table 5.3 Comparison between VBA-VGA or VGA-VBA

	VBA – VGA		VGA - VBA	
	Gain (dB)	Bw	Gain (dB)	Bw
First stage	44.3	116.3MHz	44.3	116.3MHz
Second stage	50.1	47.1MHz – 93.2MHz	48.7	112.3MHz
Third stage	54.2	44.3MHz – 90.4MHz	54.2	18.1MHz – 72.2MHz

References

[5.1] J. R Smith, "Modern Communication Circuits" McGraw Hill Electrical and Computer Engineering Series, 2nd edition, 1998.

[5.2] U.L. Rohde, T. T. N. Bucher, "Communication receivers : Principles and design" McGraw Hill, 1998.

[5.3] Datasheet LMH6504, National Semiconductor 2004.

[5.4] F. D. Waldhauer, "Feedback" John Wiley & Sons, New York, 1982.

[5.5] C. W. Sayre, "Complete Wireless Design" McGraw Hill, New York, 1982.

Chapter 6

Signal to Noise Ratio (SNR) – Optical Wireless Systems

An understanding of the noise is required for a receiver's performance to be precisely characterised. The amount of noise present in a receiver will be the primary factor that determines the receiver's sensitivity. In this chapter, a review of the definition of noise in infrared communication is presented to demonstrate the effects of receiver noise on performance. The noise sources that are commonly found in an optical wireless receiver are then discussed, including noises that are of optical as well as of electrical origin. Then, an equivalent circuit model that will describe the noise performance of the circuits designed in

Chapter 3, Chapter 4 and Chapter 5 will be presented. The final part of this chapter is the discussion of the developed signal to noise ratio module using multipliers.

6.1 Definition of noise in infrared communication

Noise, defined in the broadest practical terms, is any signal present in the receiver other than the desired signal or any unwanted disturbance that masks, corrupts, reduces the information content of or interferes with the desired signal. In the optical wireless communication environment, it is known as "ambient noise". The sources of noise available in a receiver circuit are divided into two classes [6.1]:

i) Intrinsic noise sources arising from fundamental physical effects in optoelectronic and electronic devices used to construct the receiver.

ii) Coupled noise sources arising from interactions between receiver circuitry and the surrounding environment.

In addition, noise in a receiver can be described as either additive or signal-dependent. Additive noise is a source of noise that is present whether there is a signal at the receiver or not, while a signal-dependent noise is one that is observed only when there is a signal present at the receiver. Figure 6.1 illustrates a simple model for an optical receiver, and the major contributors to the noise present in the receiver. The received signal, and any optical

background that may be present, are photodetected and then amplified in a linear signal path.

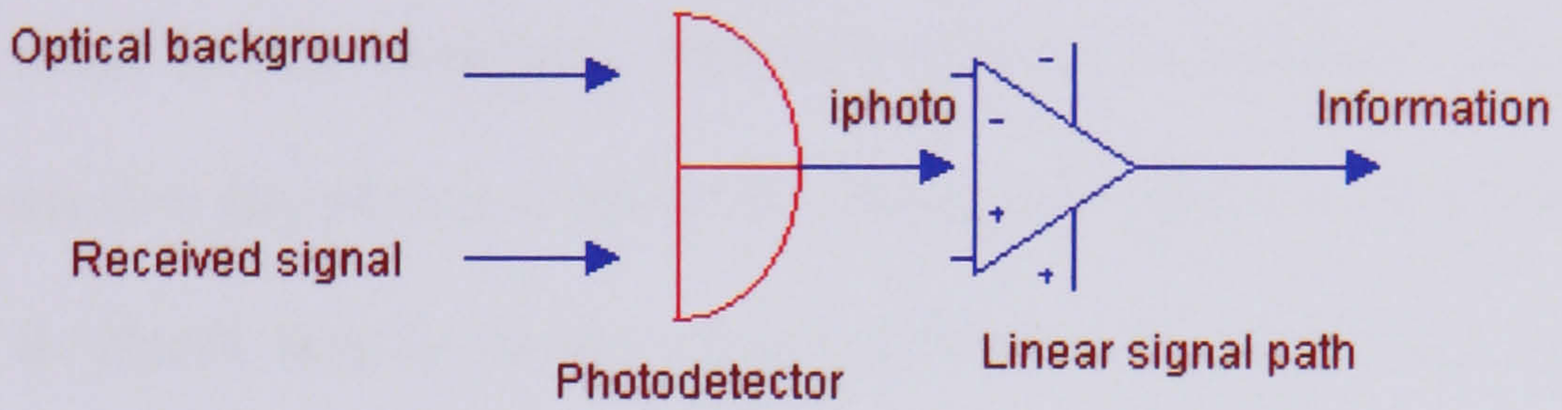

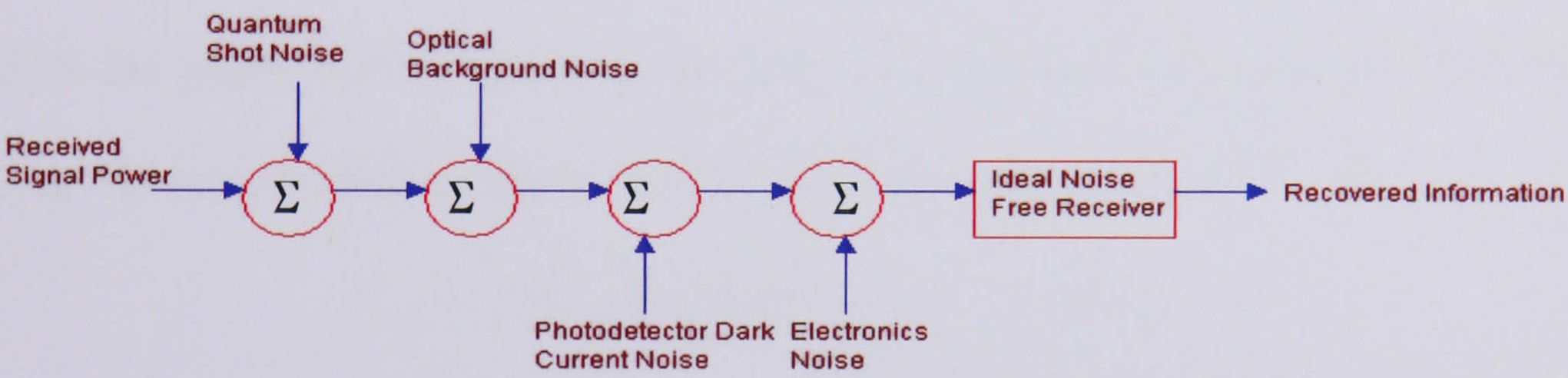

Figure 6.1 Simple receiver model and noise sources in the receiver [6.1]

The implications of each noise source will be addressed, shown right to left in Figure 6.1. Receiver electronic noise consists of three primary components: thermal noise, electronic shot-noise, and $\frac{1}{f}$ noise. Thermal noise is the type most often associated with receivers. Also known as Johnson noise, it is a result of thermally-induced random fluctuations in the charge carriers in a resistance. The power spectral-density for thermal noise is white for all frequencies within a defined bandwidth and, since thermal noise inherently results from the accumulated effect of large quantity of individual charge motions, it exhibits Gaussian statistics. Nyquist showed that the open circuit RMS voltage produced by a resistance R is as follows [6.2-6.3]:

$$V_n = \sqrt{4kTBR} \quad \text{(volt rms)} \qquad (6.0)$$

where k is Boltzmann's constant, T is absolute temperature in Kelvin and B is the observation bandwidth in Hz.

Electronic shot noise is that associated with the passage of carriers across a potential barrier. This means that any photocurrent in the photodiode will have electronic shot-noise associated with it. Based strictly on the characteristics of the noise, it is impossible to distinguish between the quantum shot noise arising from photons being detected with a photodiode, and the electronic shot noise arising from the photocurrent flowing through the junction in the photodiode. Therefore, the total electronic shot noise associated with a current, $I_{DC,}$ flowing through a potential barrier is given as follows [6.3]:

$$I_{shot} = \sqrt{2qI_{DC}B} \ \text{(amps)} \qquad (6.1)$$

where q is the electronic charge, and B is the bandwidth

$\frac{1}{f}$ noise has been observed as low frequency fluctuations in the resistance of a semiconductor. In resistors it is called "excess noise" and has been a concern in optical receiver design when the receiver is required to have a low frequency cut-off that is less than a few tens of MHz. The amount of $\frac{1}{f}$ noise present depends on the choice of transistors used in the first stages of the receiver. A Si bipolar transistor's $\frac{1}{f}$ noise is noticeable in the tens of kHz region.

Dark current flows whether the photodetector is illuminated or not, and results from the presence of current leakage paths in the photodetector. Since the dark-current in a photodiode flows through a p-n junction just as the signal photocurrent does, the dark current will also have a shot-noise term associated with it.

In addition, photodetector thermal noise exists, due to the present of resistance, R_d. The impact of photodetector thermal noise will be influenced by the method of termination of the photodetector. In a photodiode, the parallel resistance is the junction leakage resistance and is typically so large that it and any associated current-noise can be ignored. Then there is the generation and recombination noise that results from statistical fluctuation in the rate of generation and recombination of charged particles within the detector material. The current noise expression for generation-recombination noise is :

$$I_{G-R} = 4q^2\eta(\Phi_s + \Phi_b)Ag^2B + 4q^2G_{th}g^2B \qquad (6.2)$$

where Φ_s is the radiant incident power from the signal, and Φ_b is the radiant incident power from the background, A is detector area, g is photoconductive gain, B is frequency bandwidth, and G_{th} is thermal conductance.

It is sometimes known as the "twice shot-noise" because it is proportional to $4qI_{DC}$.

The noise in an optical wireless receiver can be influenced by additional non-signal related sources of optical energy that fall on the photodetector, namely quantum shot noise and optical background noise. Quantum shot noise is the result of the discreteness of photon arrivals. It is due to background light sources, such as sunlight, fluorescent lamp light, and incandescent lamp light, as well as the signal-dependent source. Since the background light

striking the photodetector is normally much stronger than the signal light, the dependency of noise on the input signal may be neglected and the photon noise can be considered to be additive white Gaussian noise [6.4]. The amount of background radiation collected by a free-space optical receiver is dependent on the receiver's field-of-view, as well as its optical bandwidth.

6.2 Noise model of a receiver

Noise model of a Transimpedance Amplifier

Amplification of low-level signals is a critical function of any receiver, due to the noise sources describe in section 6.1. The overall noise performance of an amplifier is related to the noise characteristics of the individual devices and components that form the amplifier circuit. Two established techniques have been used as indicators of the noise performance of an amplifier. The first, known as the noise figure, NF, is simply the noise factor, F, expressed in terms of dB ;

$$\text{where, } F = \frac{SNR_{input}}{SNR_{output}} \text{ and } NF = 10\log_{10}(F)\,(\text{dB}) \qquad (6.3)$$

The Friis formula for the overall noise factor for a three stage amplifier combination is given by :

$$F_{Total} = F_1 + \frac{F_2 - 1}{G_1} + \frac{F_3 - 1}{G_1 G_2} \qquad (6.4)$$

where F_1 and G_1 are noise factor and power gain of first stage amplifier

F_2 and G_2 are noise factor and power gain of second stage amplifier etc, and all amplifiers are assumed to have the same bandwidth.

Equation (6.4) shows that if the gain of the first stage is large, the noise performance of a cascade of subsystems will be dominated by the noise performance of the first-stage. In an optical wireless receiver, the photodetector and the first stages of the amplifier are known as the receiver front-end. This will generally be the principal factor in determining the overall noise performance and sensitivity of the receiver. Unfortunately, noise figure has some drawbacks when used to describe noise performance of amplifiers intended for an optical wireless receiver. It is defined using a resistive source, but a photodiode is dominated by capacitance, so the magnitude of the source impedance varies with frequency in the first stage amplifier in the receiver. Therefore the second technique that overcomes the noise figure drawbacks is to model an amplifier using equivalent noise sources, $V_n(\omega)$ and $I_n(\omega)$, as illustrated in Figure 6.2 for a receiver consisting of a signal source such as a photodetector and an amplifier.

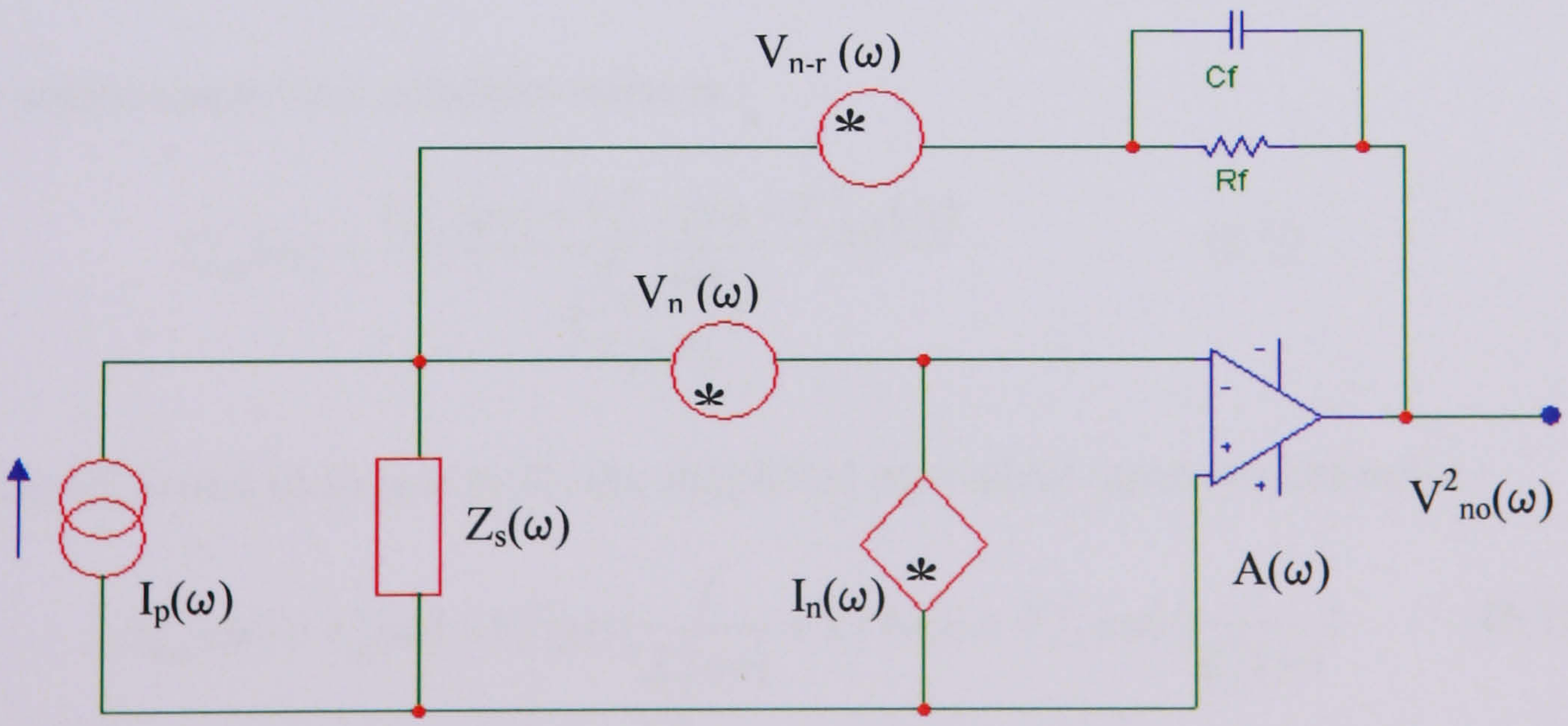

Figure 6.2 Noise model of amplifier

Assuming only amplifier noise, using the noise analysis principles approach discussed by Motchenbacher [6.5] and the principle of superposition in linear circuits, the noise power at the amplifier output is given by :

$$V_{no-1}^2(\omega) = I_n^2(\omega)\frac{Z_f(\omega)^2}{[1+\frac{1}{A(\omega)}+\frac{Z_f(\omega)Z_s(\omega)}{A(\omega)}\}]^2} \qquad (6.5)$$

(Replacing $V_n(\omega)$ and $V_{n\text{-}r}(\omega)$ as short circuits, where $Z_f = R_f//C_f$)

Then, the output noise for voltage noise is given by :

$$V_{no-2}^2(\omega) = V_n^2(\omega)\frac{[1+Z_f^2(\omega)Z_s^2(\omega)]}{[1+\frac{1}{A(\omega)}+\frac{Z_f(\omega)Z_s(\omega)}{A(\omega)}]^2} \qquad (6.6)$$

(Replacing $I_n(\omega)$ as an open circuit and $V_{n\text{-}r}(\omega)$ as a short circuit)

$$V_{no-3}^2(\omega) = V_{n-r}^2(\omega)\frac{1}{[1+\frac{1}{A(\omega)}+\frac{Z_f(\omega)Z_s(\omega)}{A(\omega)}]^2} \qquad (6.7)$$

(Replacing $I_n(\omega)$ as an open circuit and $V_n(\omega)$ as a short circuit)

The transfer function : $\frac{V_{no}(\omega)}{I_p(\omega)} = \frac{-Z_f(\omega)}{1+\frac{1}{A(\omega)}+\frac{Z_f(\omega)Z_s(\omega)}{A(\omega)}]}$ (6.8)

The total output source and amplifier noise is :

$$I_{neq}^2(\omega) = \frac{V_{no-1}^2(\omega)+V_{no-2}^2(\omega)+V_{n0-3}^2(\omega)}{[\frac{V_{no}(\omega)}{I_p(\omega)}]^2} \qquad (6.9)$$

Substituting (6.5) and (6.6) into (6.8), the simplified equivalent input current-noise :

$$I_{neq}^2(\omega) = I_n^2(\omega)+V_n^2(\omega)\{\frac{1}{Z_f^2(\omega)}+Z_s^2(\omega)\}+V_{n-r}^2(\omega)\{\frac{1}{Z_f^2(\omega)}\} \qquad (6.10)$$

Since a photodetector is a capacitive current source, $Z_s(\omega) = j\omega C_d$, setting $Z_f(\omega) = R_f$

$$I_{neq}^2(\omega) = I_n^2(\omega) + V_n^2(\omega)((\frac{1}{R_f^2} + (j\omega C_d R_f)^2) + V_{n-r}^2(\omega)(\frac{1}{R_f^2}) \qquad (6.11)$$

Equation (6.11) shows that the influence of voltage-noise increases with frequency. The detector capacitance acts as high pass filter to the voltage noise sources of the amplifier. At low frequencies the contribution of voltage noise to the overall current flowing is small, due to the large impedance of the capacitor. At high frequencies, the amounts of circulating current due to voltage noise increase because the capacitor's impedance decreases. The implications of noises for the front-end of an optical wireless receiver can be summarised in Figure 6.3.

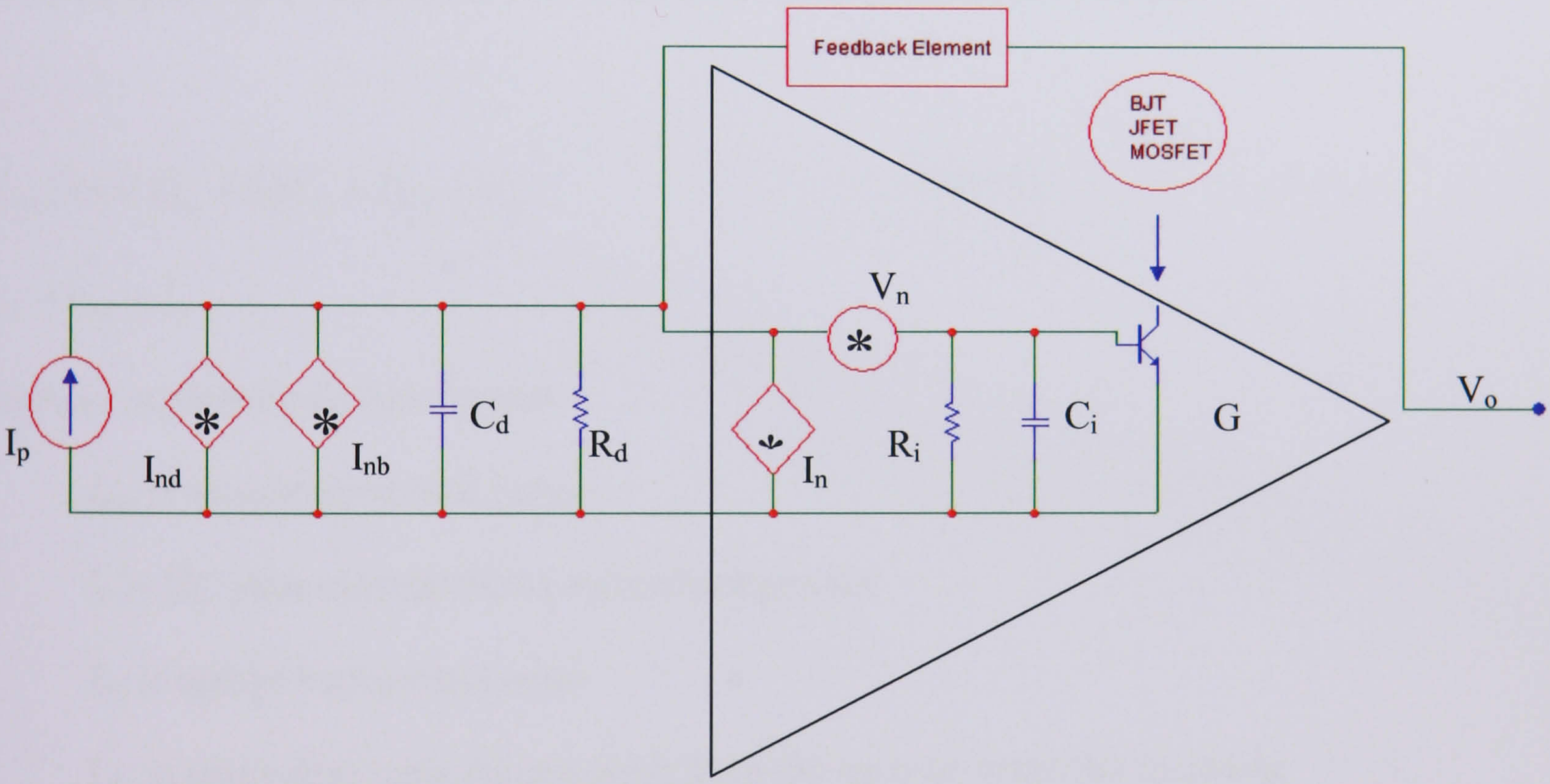

Figure 6.3 An equivalent noise model of input stage of preamplifier, where I_p is the photocurrent, I_{nd} is the detector noise, I_{nb} is the background noise, C_d, R_d are capacitance and resistance of a detector, I_n, V_n are current noise and voltage noise of a preamplifier, R_i, C_i are input resistance and input capacitance of a preamplifier, G is the voltage gain of a preamplifier [6.6].

Assume an optical signal and background noise impinge on the photodetector inducing a current in the external load resistor. If P_t is the average optical power, then I_p the photocurrent, is given by :

$$I_p(\omega) = \frac{\eta q P_t(\omega)}{h\nu} \qquad (6.12)$$

where q is the electron charge, η is the quantum efficiency, h is Planck's constant, and ν is the optical frequency of the light.

Therefore, the expressions for the current sources in the models illustrated in Figure 6.2, assuming that a PIN photodetector is being used in the receiver, are as follows :

$$I^2_{Total}(\omega) = I^2_{neq} + 2qI_{dk} + I^2_{shot} + I^2_{nb} \qquad (6.13)$$

$$I_{dk} = I_{dm} + I_b$$

where I_{dk} is photodiode dark current

I_{dm} is unmultiplied dark current

I_b is DC photocurrent due to optical background

I_{nb} is optical background noise

I_{neq} is equivalent input current-noise from the receiver amplifier including photodiode thermal noise

If the general expression for $I_{Total}(\omega)$ is converted to frequency f in Hz, the equivalent input current-noise can be expressed as a power series :

$$I^2_{Total}(f) = I^2_{shot} + \sum_{j=-b}^{a} x_j f^j \qquad (6.14)$$

where I_{shot} is the spectral density of the unmultiplied quantum shot-noise associated with the signal, and the coefficients x_j may, depending on the details of the receiver and system implementation, be proportional to received signal power, optical background, etc. The $\frac{1}{f}$ noise has been excluded in the above expression, since the receivers are used at high frequencies [6.7-6.8]. In practical cases, equation (6.14) can be limited to [6.9]

$$I^2_{Total}(f) = I^2_{shot} + x + x_1 f + x_2 f^2 \qquad (6.15)$$

From equation (6.15), a figure of merit for an optical wireless receiver can be defined and used to describe the noise performance of the system, by assuming the amount of signal related quantum shot noise is essentially constant,

$$I^2_{Total}(f) = I^2_{shot} + I^2_{rcvr}(f) \qquad (6.16)$$

I^2_{shot} is unmultiplied quantum shot-noise associated with the signal, and $I^2_{rcvr}(f)$ is the equivalent input current noise due to all other noise sources present in the receiver.

Parameter $\kappa(f)$ is indicative of the difference between the receiver's total equivalent input current noise density, and the noise-density due to the quantum shot noise of the signal as :

$$\kappa(f) = \frac{I^2_{Total}(f)}{I^2_{shot}} = \frac{I^2_{shot} + I^2_{rcvr}(f)}{I^2_{shot}} \qquad (6.17)$$

Using equation (6.10) to describe the amplifier noise, and equation (6.13) to describe photodetector noise, the signal photocurrent and dark current, then the equivalent input current-noise at the receiver's input is given by :-

$$I_{Total}^2(\omega) = I_n^2(\omega) + V_n^2(\omega)\{[\frac{1}{Z_f^2} + Z_s^2(\omega)]\} +$$

$$V_{n-r}^2(\omega)\{\frac{1}{Z_f^2}\} + I_{th-Rd}^2 + 2qI_{dk} + I_{shot}^2 + I_{nb}^2 \qquad (6.18)$$

where $Z_s(\omega) = j\omega C_d$, $Z_f(\omega) = R_f$, neglecting C_f, $I_{th-Rd}^2 = \frac{4kT}{R_d}$, $V_{n-r}^2(\omega) = 4kTR_f$

Assuming that the receiver is illuminated by a signal with a constant power level P_t, and ignoring any optical background, the equivalent input current noise density is :

$$I_{Total}^2(\omega) = I_n^2 + V_n^2\{\frac{1}{R_f^2} + [j\omega C_d R_f]^2\} + \frac{4kT}{R_f} + \frac{4kT}{R_d} + 2qI_{dk} + I_{shot}^2 \qquad (6.19)$$

$$I_{Total}^2(f) = I_{shot}^2 + x_0 + x_2 f^2$$

where $x_0 = I_n^2 + \frac{V_n^2}{R_f^2} + \frac{4kT}{R_f} + \frac{4kT}{R_d} + 2qI_{dk}$

$$x_2 = V_n^2\{4\pi^2 C_d^2 R_f^2\}$$

From equation (6.16), the degradation from the quantum shot-noise limited current density is then given by :

$$\kappa = 10\log\frac{I_{shot}^2 + x_0 + x_2 f^2}{I_{shot}^2}\,\text{dB} \qquad (6.20)$$

The total equivalent input current noise is :

$$I_{Total}^2 = I_{shot}^2\int_0^\infty |H_t(f)|^2\,df + x_0\int_0^\infty |H_t(f)|^2\,df + x_2\int_0^\infty |H_t(f)|^2\,f^2 df \qquad (6.21)$$

where $H_t(f)$ is the amplitude normalized frequency dependent portion of the overall receiver transimpedance, given by $H_t(f) = 1$ for $0 < f < B$

0 for $f > B$

The signal-to-noise ratio for a quantum shot-noise generated by the ambient environment with a transimpedance amplifier is as follows :

$$SNR = \frac{I_p^2}{\int_0^\infty I_{Total}^2(f)df} = \frac{(\frac{\eta q P_t}{h\nu})^2}{2q\frac{\eta q}{h\nu}\int_0^\infty |H_t(f)|^2\, df + x_0\int_0^\infty |H_t(f)|^2\, df + x_2\int_0^\infty |H_t(f)|^2\, f^2 df} \quad (6.22)$$

and the signal-to-noise ratio for a quantum shot-noise generated under constant illumination with a transimpedance amplifier is given by :

$$SNR = \frac{I_p^2}{\int_0^\infty I_{Total}^2(f)df} = \frac{(\frac{\eta q P_t}{h\nu})^2}{2q\frac{\eta q}{h\nu}P_t\int_0^\infty |H_t(f)|^2\, df + x_0\int_0^\infty |H_t(f)|^2\, df + x_2\int_0^\infty |H_t(f)|^2\, f^2 df} \quad (6.23)$$

$$SNR = \frac{(\frac{\eta q P_t}{h\nu})^2}{2q\frac{\eta q}{h\nu}P_t B + x_0 B + \frac{x_2 B^3}{3}} \text{ for noise bandwidth, B.}$$

$$SNR = \frac{(RP_t)^2}{2qRP_t B + (I_n^2 + \frac{V_n^2}{R_f^2} + \frac{4kT}{R_f} + \frac{4kT}{R_d} + 2qI_{dk})B + \frac{V_n^2(4\pi^2 C_d^2 R_f^2)B^3}{3}} \quad (6.24)$$

6.2.1 Noise current of shot noise and thermal noise

The shot noise current, I_{shot}, of a photodiode, and the thermal noise current, I_{th}, of a resistor, as discussed in section 6.1, are compared in the plot shown in Figure 6.4 and Figure 6.5 for a bandwidth of, B=100Hz using equation (6.0), $I_{th} = \sqrt{\frac{4kTB}{R}}$ and equation 6.1, $I_{shot} = \sqrt{2qI_pB}$. Assuming q is $1.6\text{x}10^{-19}$, k is $1.38\text{x}10^{-23}$and T is 273K.

The plot concludes that, as photodiode current, I_p, increases, shot noise increases while thermal noise decreases with an increase in resistance.

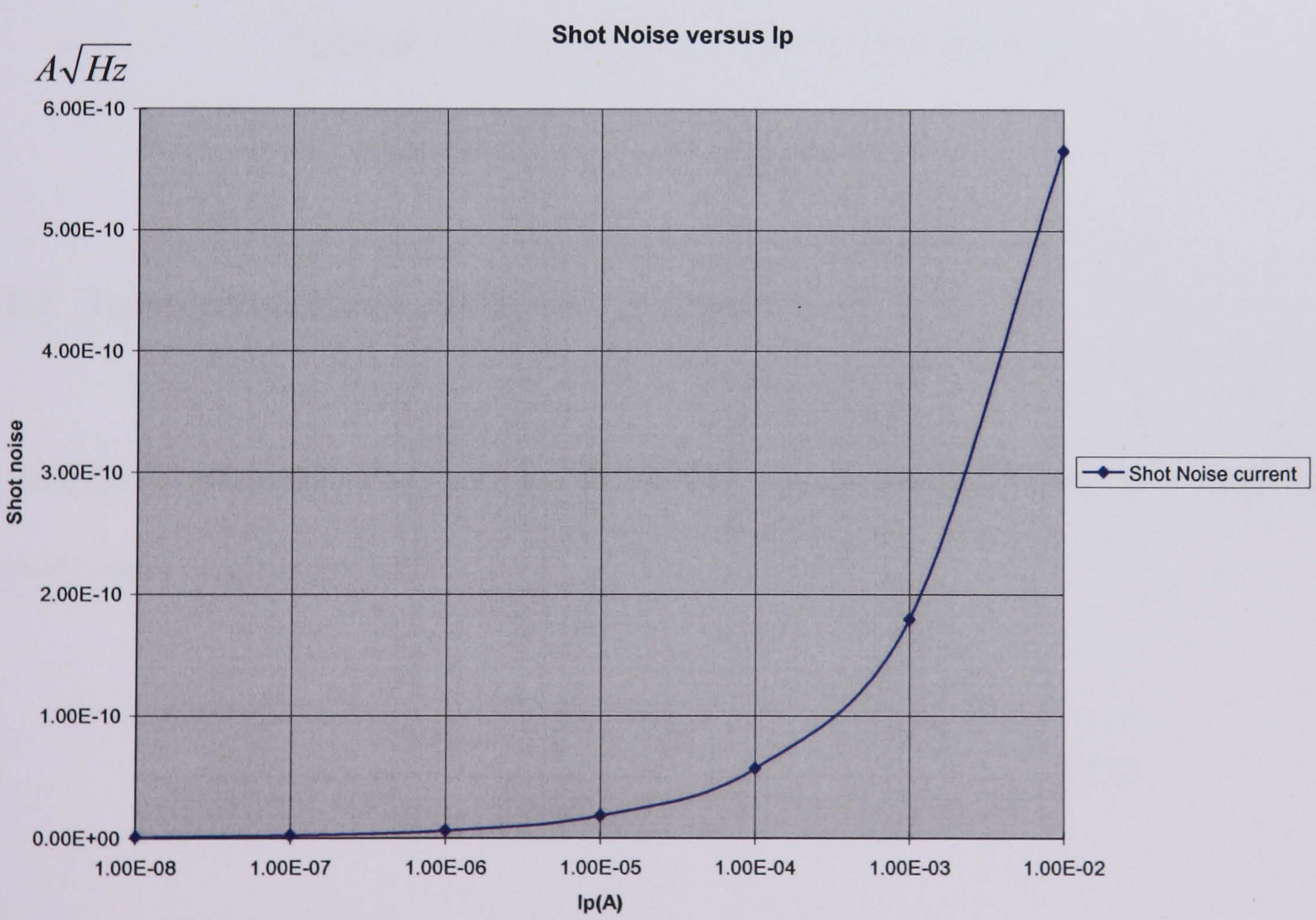

Figure 6.4 Plot of Noise current for shot noise

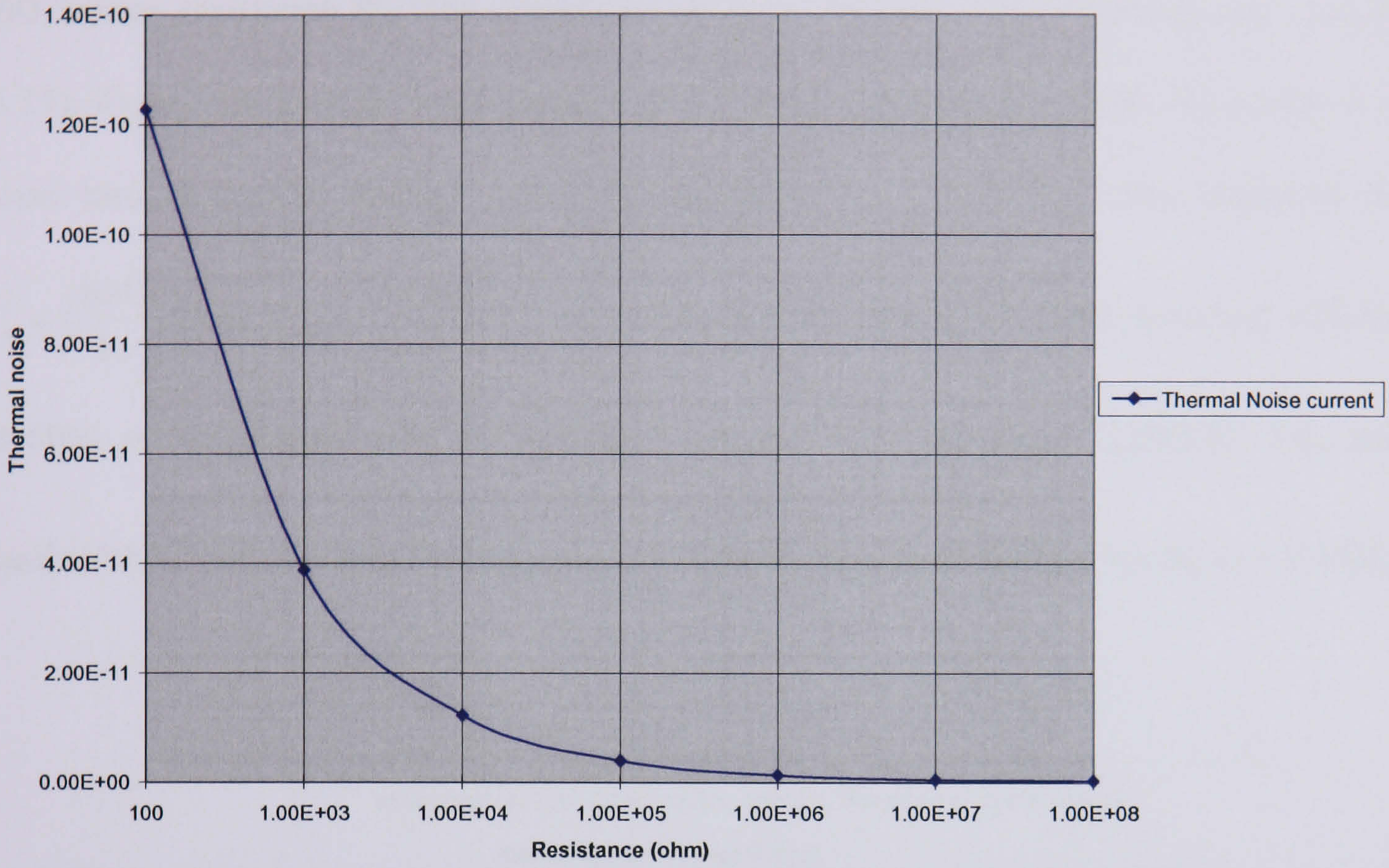

Figure 6.5 Plot of Noise current for thermal noise

6.2.2 Relationship between SNR and bandwidth

A simplified relationship between the noise figure for an amplifier and the voltage-noise current noise model is [6.10] :

$$NF = 10\log\frac{4kTR_s + V_n^2 + I_n^2 R_s^2}{4kTR_s} \qquad (6.25)$$

For the case of $V_n = 0$ and a 1.0dB amplifier noise figure at room temperature 273°K with a 50Ω source resistance R_s, the current-noise, I_n is $8.83\text{pA}/\sqrt{Hz}$ calculated from equation (6.25). Figure 6.6 illustrates the signal current and the degradation from the quantum shot noise limited current density during illumination, for a receiver using equation 6.12, $I_p^2 = (\frac{\eta q P_t}{h\nu})^2$ and $I_{shot}^2 = 2q\frac{\eta q}{h\nu}P_t B$, assuming a p-i-n photodiode with quantum efficiency of 80% at wavelength 1.55 microns, the receiver rolls off above 100MHz. The noise-bandwidth of this single-pole response is $\frac{\pi}{2}$ greater than the 3dB bandwidth, or 157MHz.

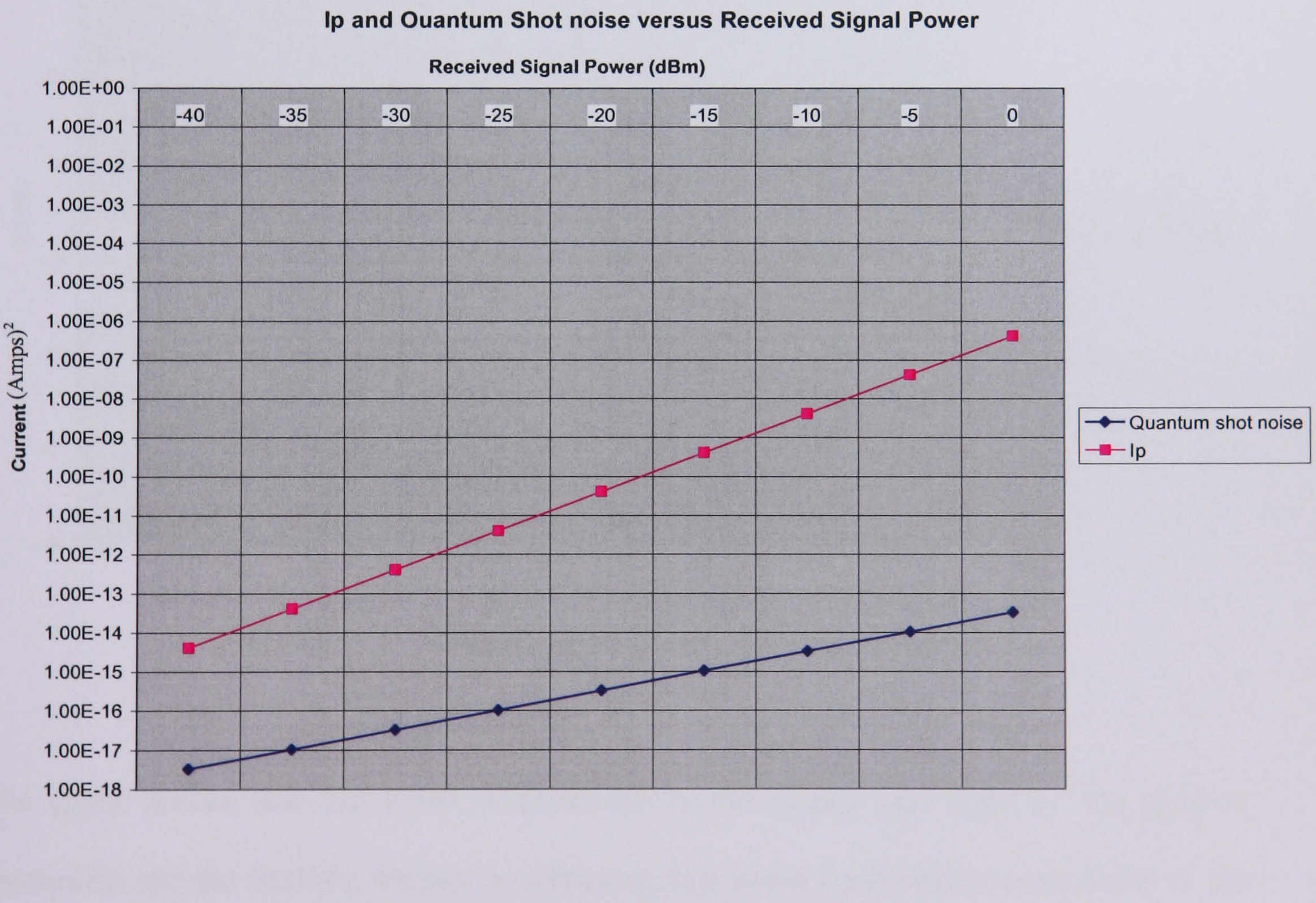

Figure 6.6 I_p and Quantum shot noise versus P_t

The graph shows that the detected signal power varies as the square of the optical signal power and quantum shot noise is evident for received signal powers approaching 0dBm.

Figure 6.7 illustrates the relationship between SNR and bandwidth from equation 6.23, assuming $P_t = 5mW$, $I_{dk} = 1nA$, $R_f = 1k\Omega$ and $R_d = 1M\Omega$ for two cases, when $V_n = 0$, $I_n = 8.83pA/\sqrt{Hz}$ and $V_n = 31.6\mu V/\sqrt{Hz}$ and $I_n = 8.83pA/\sqrt{Hz}$.

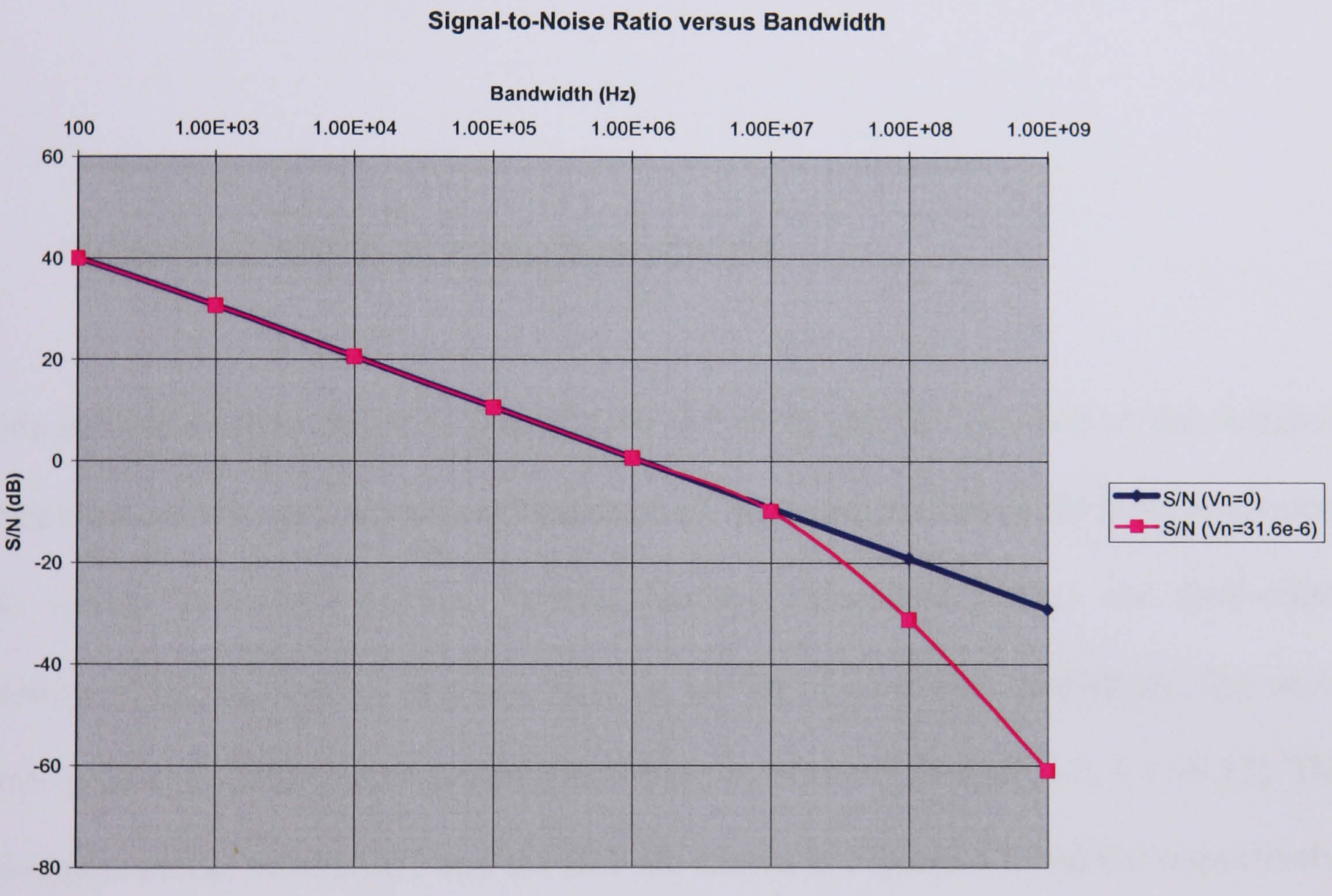

Figure 6.7 Relationship between SNR and bandwidth

The graph shows that the terms proportional to the square and cube of the receiver bandwidth are the limiting factors in achieving low-noise performance, especially at the high frequency range. Thus, during the design of low noise optical wireless receiver, every effort centres on making the coefficients x_2 as small as possible.

In real cases the signal-to-noise ratio, including optical background noise, from equation (6.23), is defined as :

$$SNR = \frac{(RP_t)^2}{2qRP_tB + (I_n^2 + \frac{V_n^2}{R_f^2} + \frac{4kT}{R_f} + \frac{4kT}{R_d} + 2qI_{dk} + I_{nb}^2)B + \frac{V_n^2(4\pi^2 C_d^2 R_f^2)B^3}{3}} \qquad (6.26)$$

and if an input signal contains noise, the signal-to-noise ratio could be defined as follows :

$$SNR = \frac{S+N}{N} \approx \frac{S}{N} + 1 \qquad (6.27)$$

6.3 Output noise density of the designed circuits

In this section, the discussion is focussed on the noise analysis on each of the designed preamplifier circuits. The analysis is facilitated by the consideration of the input equivalent noise voltage and noise current. Bipolar junction transistors (BJTs) and field-effect transistors (FET) are one of the key building blocks of electronic amplifiers. The noise sources present in both the components have been extensively studied [6.5, 6.11-6.13]. The small-signal model for the FET and the BJT are shown in Figures 6.8 and 6.9 respectively. To simplify the analysis of the FET, direct effects from the gate-drain feedback capacitor will be ignored. This is usually valid, since in most devices the gate source capacitance is approximately ten times the gate drain capacitance [6.10].

For the BJT, the base spreading resistance, r_x, accounts for any resistance between the base terminal contact and the actual active base region of the device. The base current and

collector current shot noises are accounted for by two noise current generators i_{bBJT} and i_{cBJT}. The resistances r_π, r_μ and r_0 are dynamic resistances, they do not dissipate energy and do not contribute thermal noise. In this analysis, secondary effects that are introduced by the internal feedback r_μ and C_μ will be ignored for simplicity. C_π is composed of two contributions from the space charge in the emitter junction and the diffusion capacitance of the emitter junction that increases with emitter current.

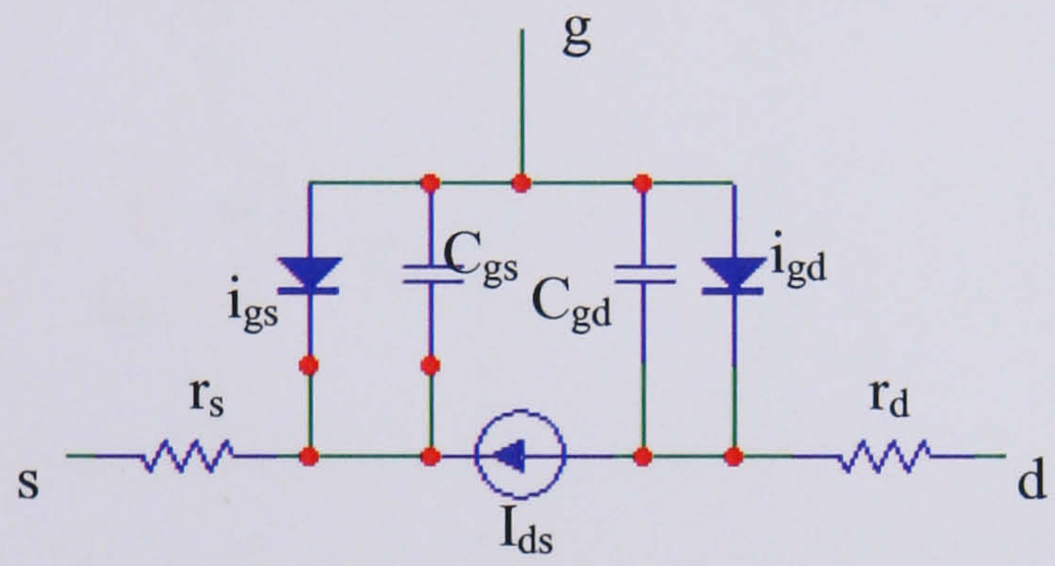

Figure 6.8 FET small-signal model

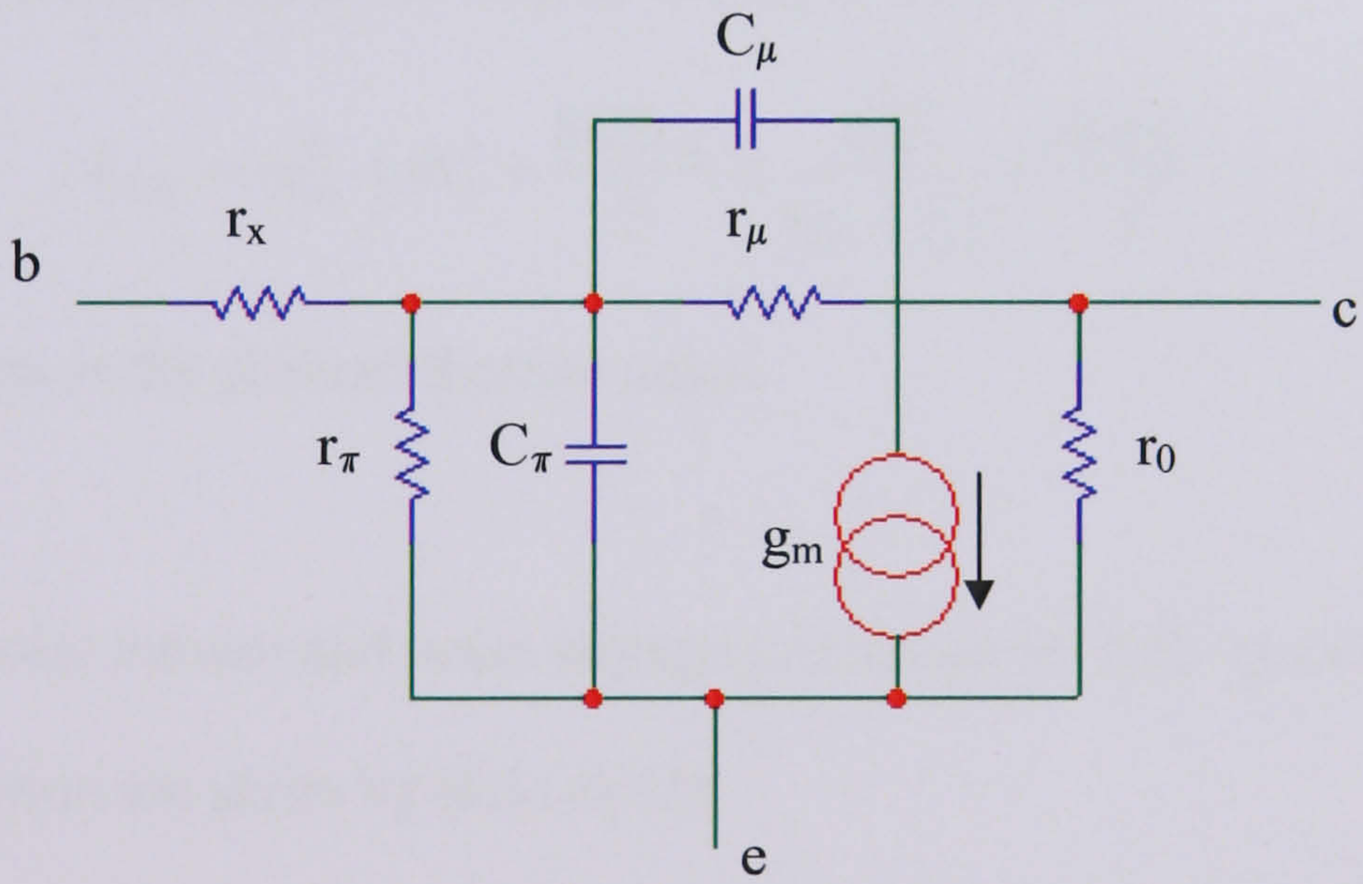

Figure 6.9 BJT small-signal hybrid-π model

Case (a): Transimpedance amplifier with FET voltage control filter

In this case, the FET is used as a voltage control resistor in parallel with capacitor, C_p connected to a transimpedance amplifier using a BJT as shown in Figure 6.10.

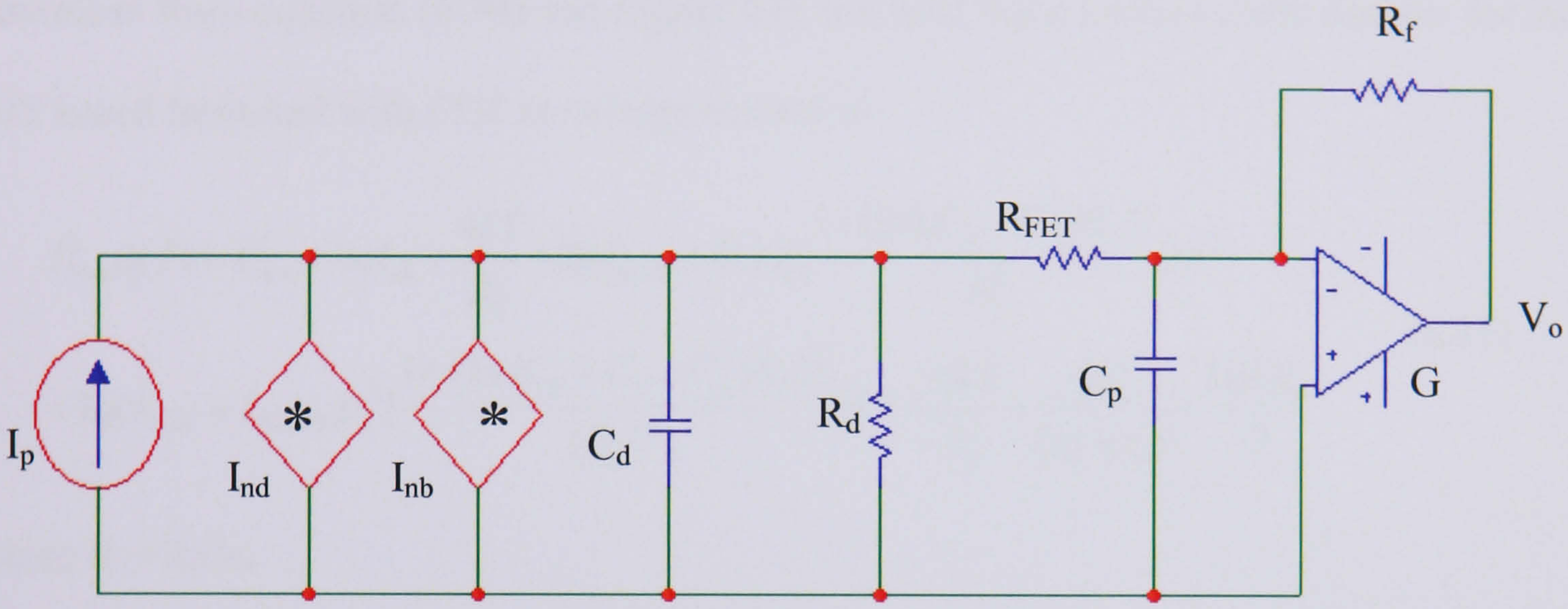

Figure 6.10 Circuit Noise Model for case (a)

Therefore in this analysis the noise related to R_{FET} is defined as,

$$I_{FET} = in_{rd}^2 + in_{rs}^2 + \frac{8kTg_m}{3} \cong \frac{4kT}{(r_d + r_s)} + \frac{8kTg_m}{3} \qquad (6.28)$$

where the last term is the channel thermal noise.

The equivalent noise current and noise voltage generators for BJT operating in the common emitter configuration are given by [6.11-6.12]

$$V_n^2(f) \cong \frac{1}{2} r_x q I_{bBJT} (\frac{f_c}{f}) + 4kTr_x + 2qI_{cBJT} r_e^2 \qquad (6.29)$$

$$I_n^2(f) \cong 2qI_{bBJT} (\frac{f_c}{f}) + 2qI_{bBJT} + 2qI_{cBJT} (\frac{f}{f_t})^2 \qquad (6.30)$$

where I_{cBJT} is DC collector current, I_{bBJT} is DC base current, r_e is dynamic resistance of the emitter =$(1/g_m)$, f_c is 1/f corner frequency, f_t is transition frequency $\approx \frac{1}{2\pi r_e C_\pi}$

Therefore from equation (6.30) and Figure 6.9, the total input current noise density for the BJT based front-end with FET as voltage control is :

$$I_{Total}^2 a(f) = I_{shot}^2 + 2qI_{dk} + \frac{4kT}{R_d} + 2qI_{bBJT} + 4kTr_x[\frac{1+(2\pi(C_d+C_p)R_f)^2}{R_f^2}]f^2$$
$$+2q(I_{cBJT}+I_{B2BJT})r_e^2[\frac{1+(2\pi(C_\pi+C_d+C_p)R_T)^2}{(R_T)^2}]f^2 + \frac{4kT}{R_f} + \frac{4kT}{(r_d+r_s)} + \frac{8kTg_m}{3} \quad (6.31)$$

where $R_T=R_f//r_\pi$

Figure 6.11 shows the simulated input and output noise density for case (a).

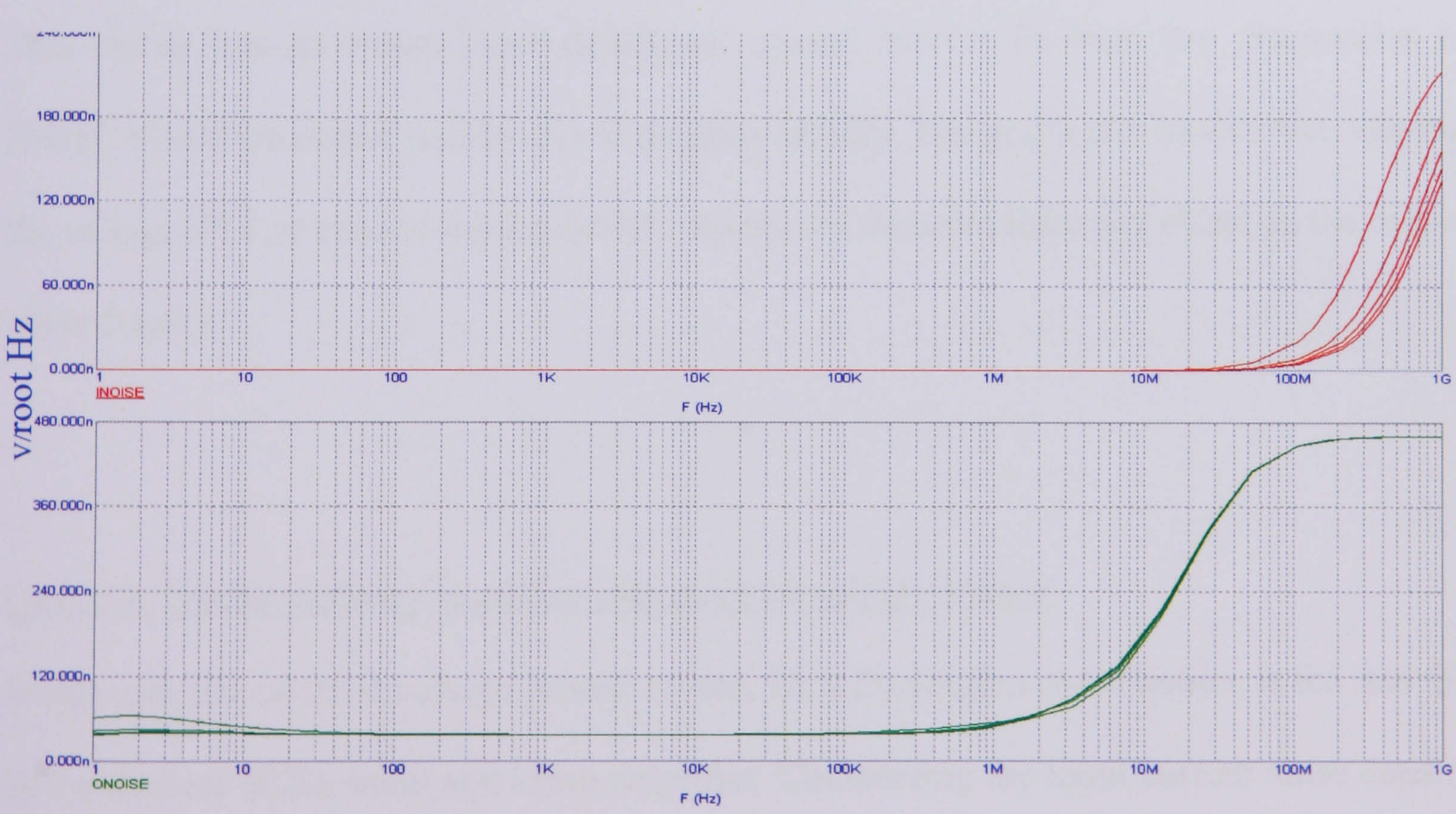

Figure 6.11 Input and Output noise density for FET Voltage control filter and transimpedance amplifier

Since collector current is related to base current by the DC current gain, β as $I_{cBJT}=\beta I_{bBJT}$

and dynamic resistance is $r_e = \frac{1}{g_m} = \frac{1}{\frac{q}{kT} I_{cBJT}} = \frac{V_T}{I_{cBJT}}$, where $V_t = \frac{kT}{q}$

Equation (6.31) can be rewritten as follows :

$$I_{Total}^2 a(f) = I_{shot}^2 + 2qI_{dk} + \frac{4kT}{R_d} + \frac{2q}{\beta} I_{cBJT} + 4kTr_x [\frac{1+(2\pi(C_d + C_p)R_f)^2}{R_f^2}]f^2$$
$$+2q\frac{V_t^2}{I_{cBJT}}[\frac{1+(2\pi(C_\pi + C_d + C_p)R_T)^2}{(R_T)^2}]f^2 + \frac{4kT}{R_f} + \frac{4kT}{(r_d + r_s)} + \frac{8kTg_m}{3} \quad (6.32)$$

where $R_T=R_f//r_\pi$ and shot noise current from I_{b2BJT} is negligible

The input noise density graph shows high noise distortion in the high frequency region, indicating that this circuit would be seriously affected by noise if operated at that region. This circuit has an output noise density of around 50nV/$\sqrt{Hz}$ from low frequencies to 2MHz, where the output noise starts to increase rapidly. The graph also shows that, varying the voltage FET to control the bandwidth adjustment does not have any effect on the output noise density.

Case (b): Transimpedance amplifier with external voltage control

In this case the external voltage control source, via a Darlington combination, is fed into Q3 BJT transistor of the transimpedance amplifier. Considering the input current noise density from the external voltage,:

$$I^2_{n(external)}(f) = \frac{4kT}{R_{control} + R_s + r_x} + 2qI_{bBJT} + 2qI_{cBJT} r_e^2 (2\pi C_\pi)^2 f^2 \qquad (6.33)$$

Then considering the input current noise density from the BJT transimpedance amplifier :

$$I^2_{BJT}(f) = I^2_{shot} + 2qI_{dk} + \frac{4kT}{R_d} + \frac{2q}{\beta} I_{cBJT} + 4kTr_x[\frac{1+(2\pi(C_d + C_f)R_f)^2}{R_f^2}]f^2$$
$$+2q\frac{V_t^2}{I_{cBJT}}[\frac{1+(2\pi(C_\pi + C_d + C_f)R_T)^2}{(R_T)^2}]f^2 \qquad (6.34)$$

where $R_T = R_f // r_\pi$

Therefore from equation (6.33) and (6.34), the total input current noise density is :

$$I^2_{nTotal}b(f) = I^2_{n(external)} + I^2_{BJT}$$

$$I^2_{nTotal}b = I^2_{shot} + 2qI_{dk} + \frac{4kT}{R_d} + \frac{2q}{\beta} I_{cBJT} + 4kTr_x[\frac{1+(2\pi(C_d + C_f)R_f)^2}{R_f^2}]f^2 \qquad (6.35)$$
$$+2q\frac{V_t^2}{I_{cBJT}}[\frac{1+(2\pi(C_\pi + C_d + C_f)R_T)^2}{(R_T)^2}]f^2 + \frac{4kT}{R_{control} + R_s + r_\pi} + \frac{2q}{\beta} I_{cBJT} + 2q\frac{V_t^2}{I_{cBJT}}(2\pi C_\pi)^2 f^2$$

Figure 6.12 shows the simulated input and output noise density of case (b). The input noise density graph shows noise distortion at low frequencies from 10nV/$\sqrt{Hz}$ to 1nV/$\sqrt{Hz}$, due to 1/f noise and high frequency as the external voltage is varies. This circuit has an output noise density at around 7nV/$\sqrt{Hz}$ at low frequencies until after 3MHz, when the output noise increases according to the external control voltage. The bandwidth adjustment taken at frequency 10MHz has an output noise density which varies from 11nV/$\sqrt{Hz}$ to 8nV/$\sqrt{Hz}$ as the external voltage varies from 3.5V to 9V. As the frequency range goes

higher the effect of the noise becomes larger. The bandwidth adjustment taken at frequency 30MHz shows that the output noise density varies from $12nV/\sqrt{Hz}$ to $21nV/\sqrt{Hz}$ for voltages from 3.5V to 9V.

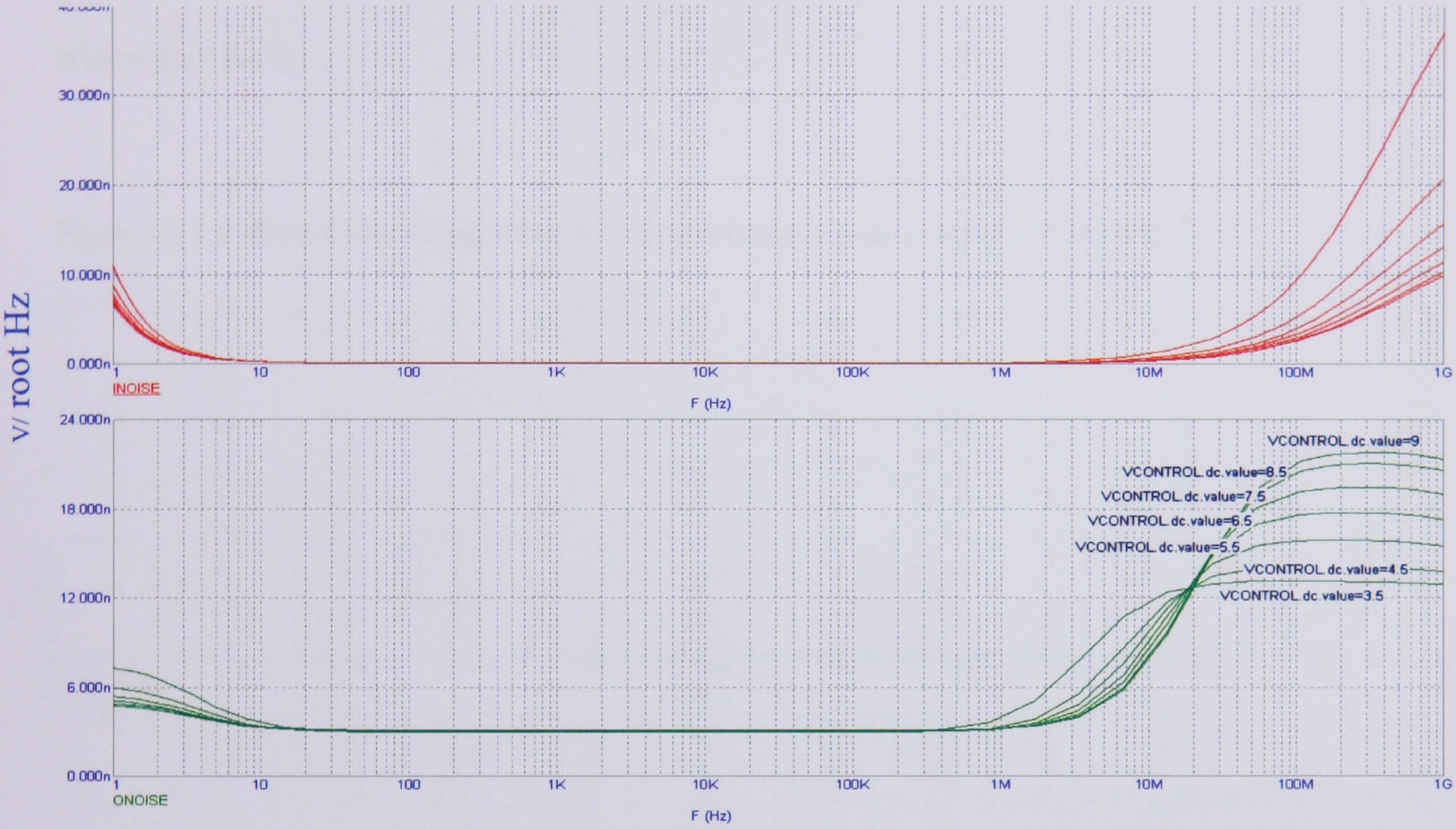

Figure 6.12 Input and Output noise density for transimpedance amplifier with external voltage control

Case (c): Bootstrap transimpedance amplifier with adjusting capacitor

In case (c), the feedback of the transimpedance amplifier is taken in between capacitor, C_p and resistor R_{e3}. The feedback impedance (R_f in parallel with the parasitic C_f) has been referred back to the input, as such that the input impedance is equal to $R_f//C_d//C_f//C_p$. Therefore the input equivalent noise current density based on equation (6.30) is :

$$I_{nTotal}^2 c(f) = I_{shot}^2 + 2qI_{dk} + \frac{4kT}{R_d} + \frac{2q}{\beta} I_{cBJT} + 4kTr_x[\frac{1+(2\pi(C_d + C_f + C_p)R_f)^2}{R_f^2}]f^2$$
$$+2q\frac{V_t^2}{I_{cBJT}}[\frac{1+(2\pi(C_\pi + C_d + C_f + C_p)R_T)^2}{(R_T)^2}]f^2 \quad (6.36)$$

where $R_T = R_f // r_\pi$

Figure 6.13 shows the simulating input and output noise density for case (c).

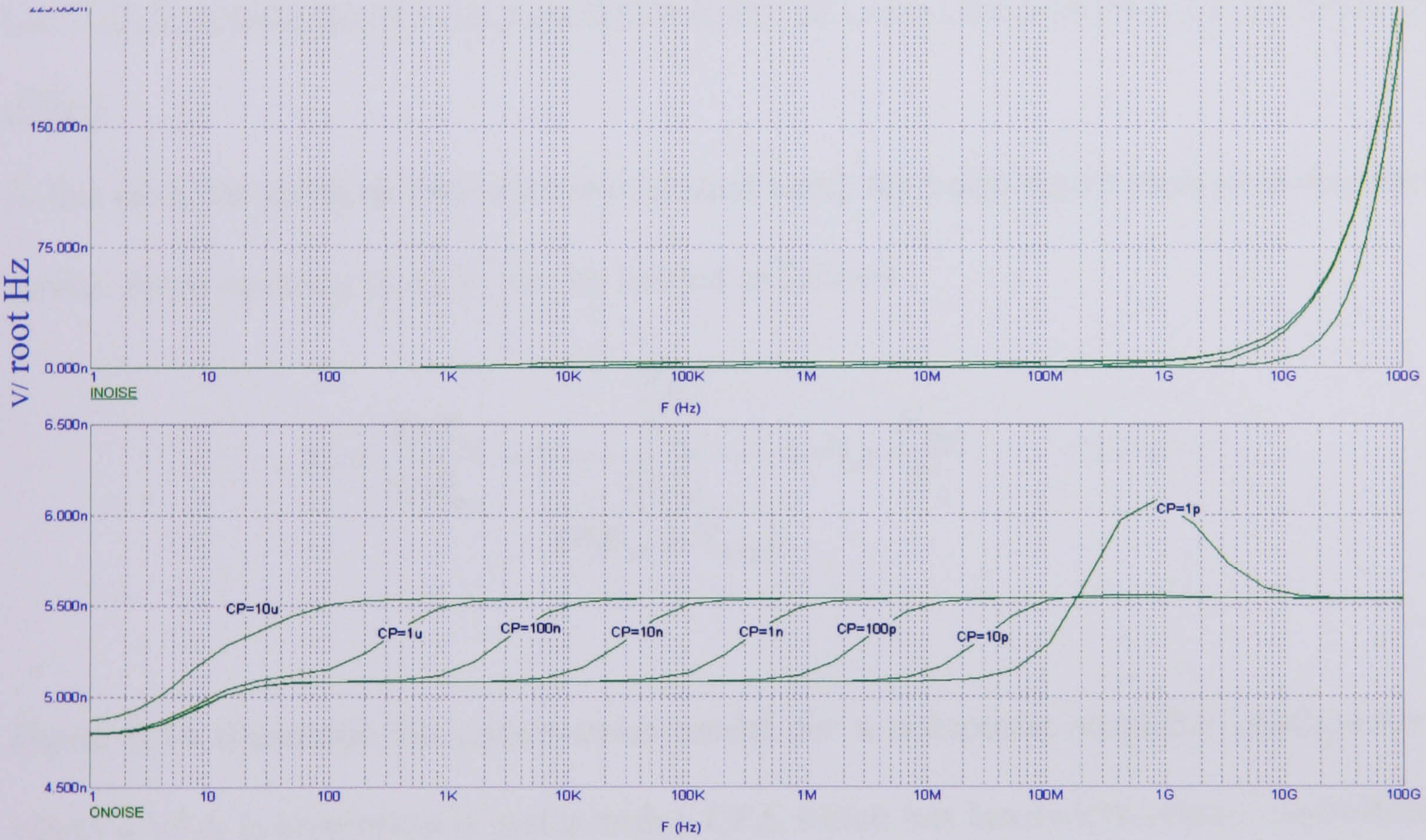

Figure 6.13 Input and Output noise density for bootstrap transimpedance amplifier with adjusting capacitor

With the bootstrapping technique the input noise density is almost $3nV/\sqrt{Hz}$ until, after 2GHz, the noise increases to $29nV/\sqrt{Hz}$. The bandwidth adjustment range output noise density is between $5nV/\sqrt{Hz}$ to $5.5nV/\sqrt{Hz}$, for values between 10pF to 10uF for C_p. The highest output noise density is $6nV/\sqrt{Hz}$ at a frequency of 1GHz, using a capacitance of

1pF. The 3dB bandwidth for a capacitance of 1pF is only 233MHz which means that the output noise density at that point is only $5.7\text{nV}/\sqrt{Hz}$.

Comparing the three methods of cases (a), (b) and (c), the bootstrapping technique is the method that exhibits the lowest output noise density.

Case (d): Combination of voltage feedback amplifier (VFA) and current feedback amplifier (CFA)

In this case, the noise performance is evaluated using the noise figure method as discussed earlier. From equation (6.4), F_1 can be written as follows :

$$F_1 = \frac{SNR_{in}}{SNR_{out}} = \left[\frac{\frac{S_{in}}{N_{in}}}{\frac{GxS_{in}}{G(N_{in}+N_{amp})}}\right] = 1 + \frac{N_{amp}}{N_{in}} \qquad (6.37)$$

Figure 6.14 illustrates the circuit noise model for a composite amplifier configuration, where a VFA is connected in series with a CFA which has bandwidth control capabilities. The gain set for the LMH6624 as in Chapter 4, G, is $\frac{-R_f}{R_G} = \frac{-500}{50} = -10$ and for the LMH6732, G_1 is $[1+\frac{R_f}{R_G}] = [1+\frac{1k}{1k}] = 2$.

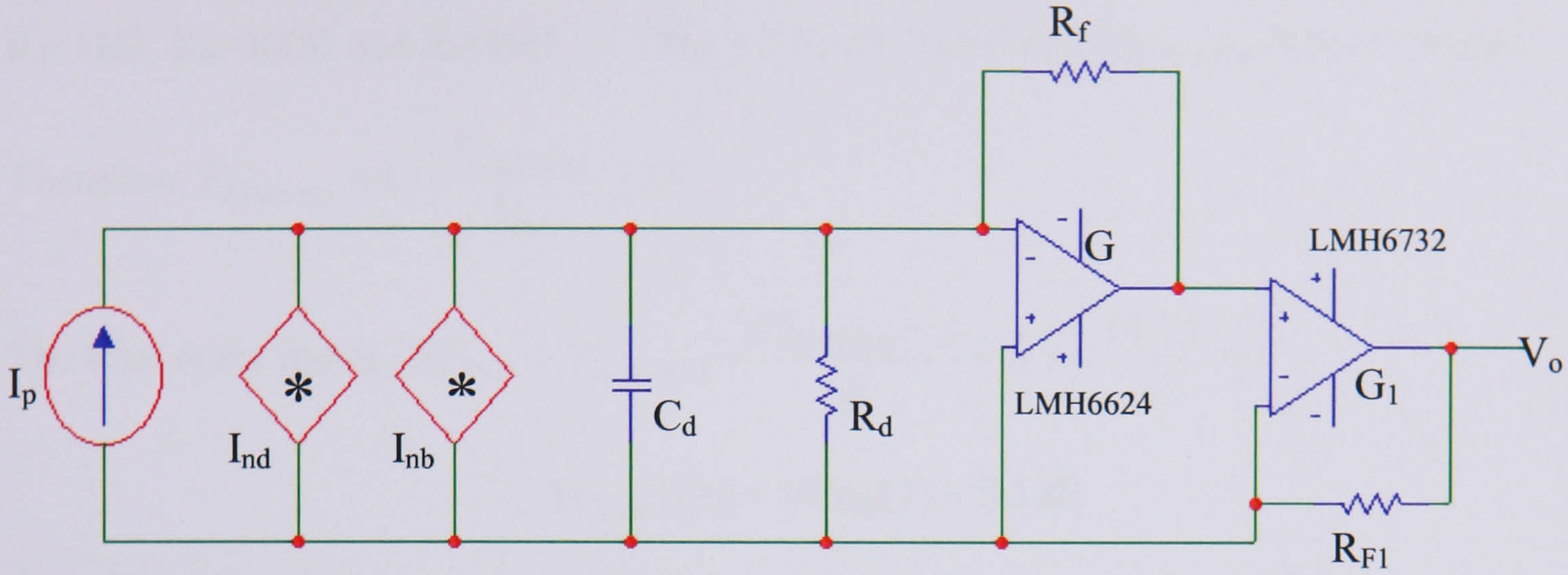

Figure 6.14 Circuit noise model for case (d)

The calculated LMH6624 noise figure is as follows:

$N_{in} = 4kTR_G$ Volts^2

$$N_{LMH6624} = V_n^2(1+\frac{R_G}{R_F})^2 + I_n^2(R_1 + \frac{R_1R_G}{R_F})^2 + 4kTR_1(1+\frac{R_G}{R_F})^2 + 4kTR_G + 4kTR_F(\frac{R_G}{R_F})^2 \text{ Volts}^2$$

From the data sheet [6.14]: $V_n^2 = 8.46e-19V/\sqrt{Hz}$ and $I_n^2 = 5.29e-24A/\sqrt{Hz}$,

R_1=90Ω, R_G=50Ω and R_f=500Ω : N_{in} = 7.53e-19 Volts^2 and $N_{LMH6624}$=3.54e-18 Volts^2

Therefore $F_{LMH6624} = 1 + \frac{N_{LMH6624}}{N_{in}} = 5.7$

The calculated LMH6732 noise figure is as follows :

$N_{in} = 4kTR_o$ Volts^2 ,where R_0 is the output impedance of the LMH6624

$$N_{LMH6732} = V_n^2 + I_n^2 + I_n^2(\frac{R_FR_2}{R_F+R_2})^2 + 4kTR_2(\frac{R_F}{R_F+R_2})^2 + 4kTR_F(\frac{R_2}{R_F+R_2})^2 \text{ Volts}^2$$

From the data sheet [6.15]: $V_n^2 = 7.05e-17V/\sqrt{Hz}$ and $I_n^2 = 8.1e-23A/\sqrt{Hz}$,

R_2=1kΩ, R_0=500Ω and R_f=1kΩ : N_{in} = 7.5e-18 Volts^2 and $N_{LMH6732}$=9.8e-17 Volts^2

Therefore $F_{LMH6732} = 1 + \frac{N_{LMH6732}}{N_{in}} = 14$

The total noise figure, $NF_{Total} = F_{LMH6624} + \frac{F_{LMH6732} - 1}{G} = 5.7 + \frac{14-1}{10} = 7$

$$NF_{Total}(dB) = 10\log(7) = 8.5dB$$

Therefore the input equivalent noise current density is :

$$I_{Total}^2 d(f) = \frac{4kT}{R_d} 10^{\frac{NF_{Total}}{10}} f + V_n^2 \{\frac{1}{R_f^2} + [j\omega C_d R_f]^2\} f^2 + \frac{4kT}{R_f} + \frac{4kT}{R_d} + 2qI_{dk} + I_{shot}^2 \qquad (6.38)$$

Figure 6.15 shows the simulating input and output noise density for case (d).

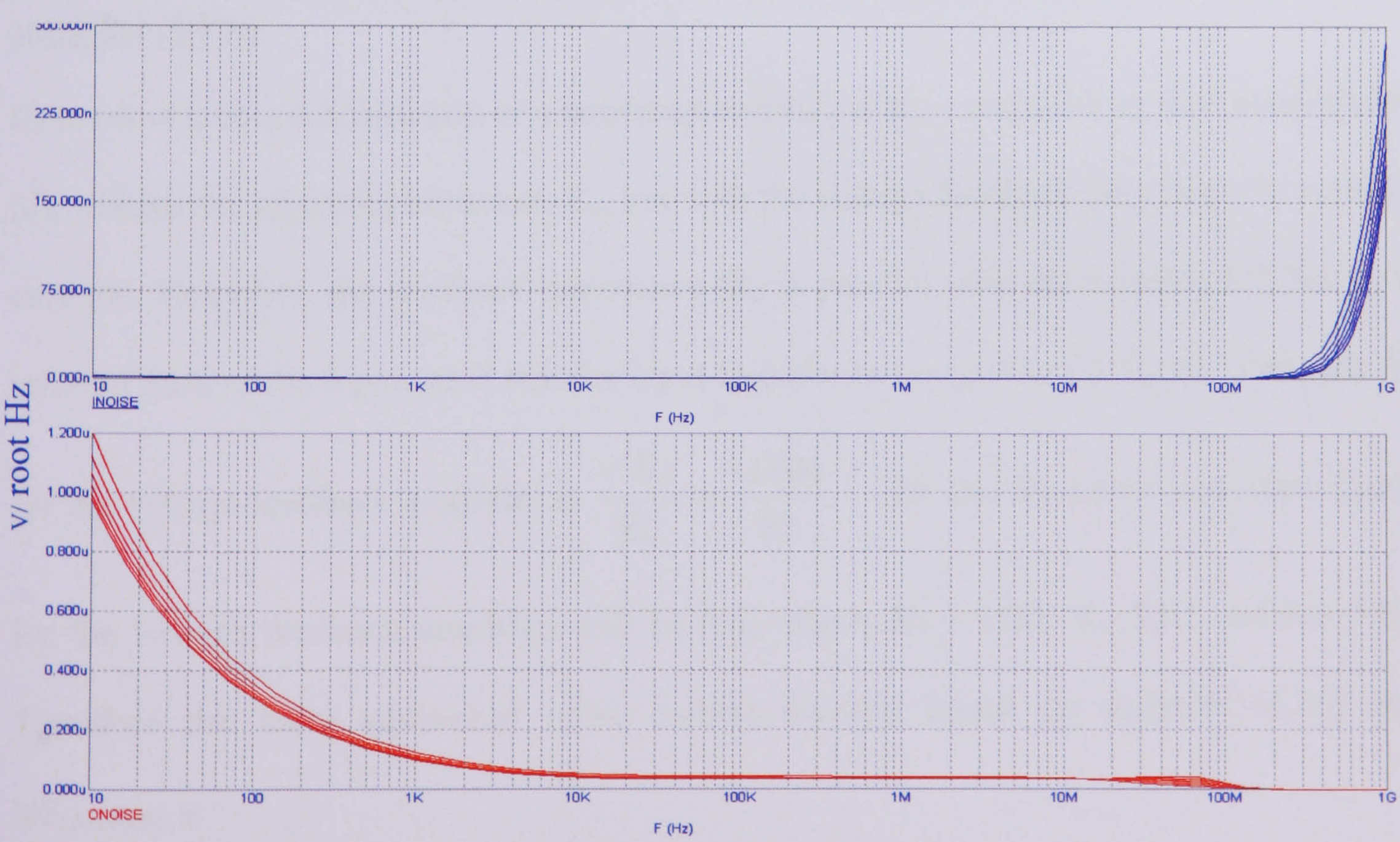

Figure 6.15 Input and Output noise density for voltage feedback amplifier and current feedback amplifier

The composite amplifier configuration shows a low input noise density from low frequencies to 200MHz, after which it increases from 5nV/$\sqrt{Hz}$. The output noise density is 1.2μV/$\sqrt{Hz}$ at low frequencies for a bandwidth control voltage of 0.1V. It decreases to 1μV/$\sqrt{Hz}$ for a bandwidth control voltage 5V. The high noise results probably due to the effect of 1/f noise. The overall output noise density decreases until 35nV/$\sqrt{Hz}$ throughout the mid and high frequency ranges. At frequency between 20MHz to 70MHz, the output noise density varies between 10nV/$\sqrt{Hz}$ to 30nV/$\sqrt{Hz}$,due to the bandwidth adjustment function.

Case (e): Combination of boostrap transimpedance amplifier and voltage feedback amplifier (VFA)

Case (e) will be a combination of a bootstrap transimpedance amplifier as discussed in case (c), without the adjusting capacitor, C_p, but with the voltage feedback amplifier discussed in case (d). Therefore, the feedback impedance (R_f in parallel with the parasitic C_f) has been referred back to the input, such that the input impedance is equal to $R_f//C_d//C_f$. The gain set for the voltage feedback amplifier is $\frac{-R_f}{R_G} = \frac{-1000}{50} = -20$ and the calculated noise figure for the voltage feedback amplifier will be 2.6, where, R_f = 1kΩ, R_1=25Ω and R_G=50Ω. Therefore the input equivalent noise current density, based on equation (6.36) and $NF_{LMH6624}$ is :

$$I_{nTotal}^2 c(f) = I_{shot}^2 + 2qI_{dk} + \frac{4kT}{R_d} 10^{\frac{NF_{LMH6624}}{10}} f + \frac{2q}{\beta} I_{cBJT} + 4kTr_x [\frac{1+(2\pi(C_d + C_f)R_f)^2}{R_f^2}] f^2$$
$$+ 2q \frac{V_t^2}{I_{cBJT}} [\frac{1+(2\pi(C_\pi + C_d + C_f)R_T)^2}{(R_T)^2}] f^2 \quad (6.39)$$

where $R_T = R_f // r_\pi$

Figure 6.16 shows the simulated input and output noise density for case (e).

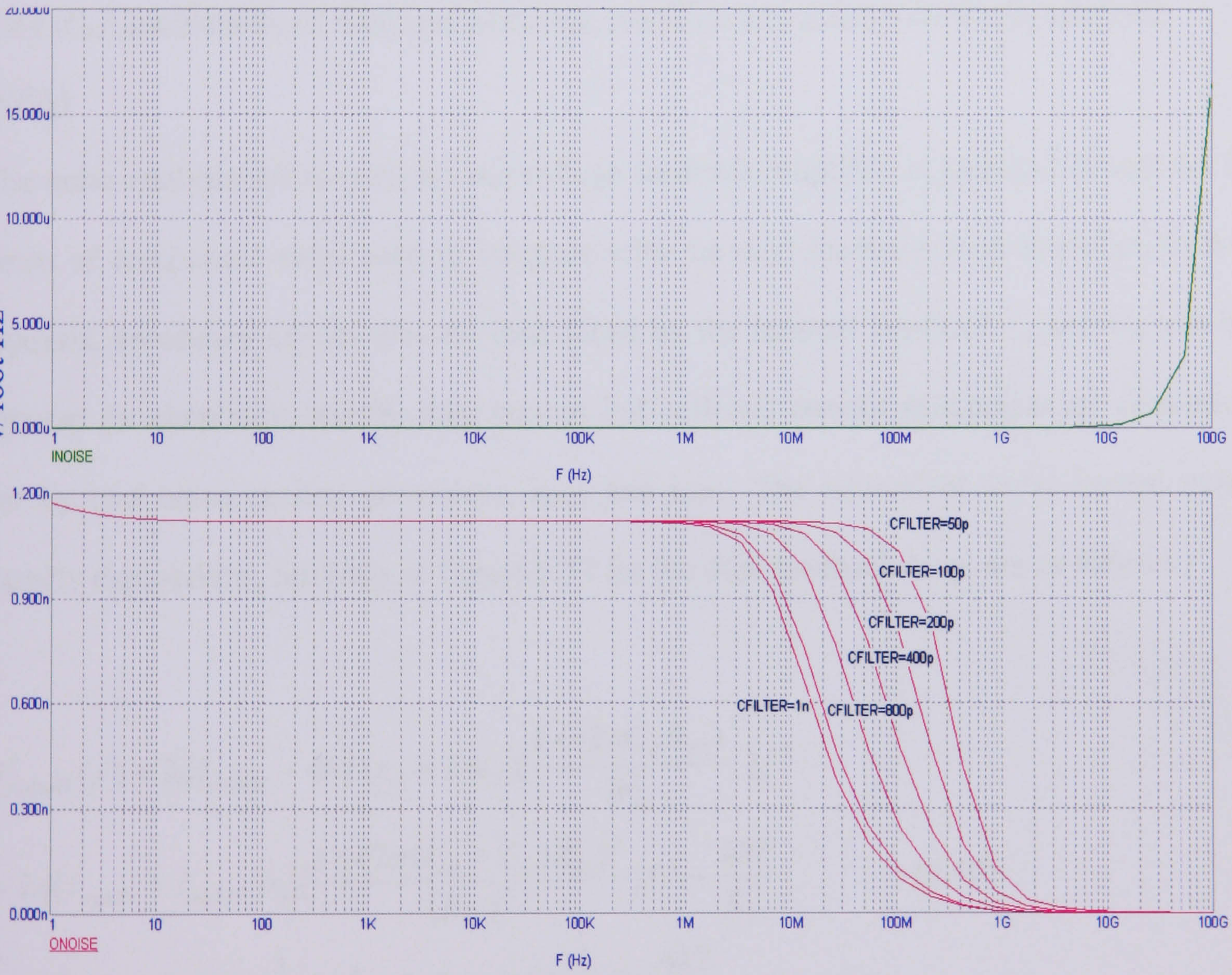

Figure 6.16 Input and Output noise density for bootstrap transimpedance amplifier with voltage feedback amplifier

The input noise current density shows a flat 380pV/$\sqrt{Hz}$ from 1Hz to 10GHz and starts to increase. In simulation the output noise density, shows a flatness of 1.1nV/$\sqrt{Hz}$ from 1Hz to 80MHz, when it starts descending according to the capacitor value which adjust the bandwidth. The simulated results also showed that the output noise density remains constant during the bandwidth adjustment process.

Case (f): Combination of dual feedback loop amplifier and voltage feedback amplifier (VFA)

The noise analysis for case (f) for the voltage feedback amplifier is identical to case (e) in terms of component value used to integrate with the dual feedback loop amplifier. In this analysis, secondary effects that are introduced by the internal feedback r_μ and C_μ will be ignored for simplicity, and the base current and collector current shot noises are accounted for by two noise current generators, i_{bBJT} and i_{cBJT}. The equivalent input current noise density expressions, referring to Figure 6.17 for the dual feedback loop, are as follows ;

$$I_{n(dual)}^2(f) = 2qI_{b1BJT} + 4kT(r_{x1} + 2\pi L_1)[\frac{1+(2\pi C_d R_{f1})^2}{R_{f1}^2}]f^2$$
$$+ 2q(I_{c1BJT} + I_{b2BJT})r_{e1}^2[\frac{1+(2\pi(C_\pi + C_d)R_{T1})^2}{(R_{T1})^2}]f^2 + \frac{4kT}{R_{f1}} \qquad (6.40)$$
$$+ 4kT(r_{x2} + 2\pi L_2)[\frac{1}{R_{f2}^2}]f^2 + 2qI_{c2BJT}r_{e2}^2[\frac{1}{R_{T2}^2}] + \frac{4kT}{R_{f2}}$$

where $R_{T1}=R_{f1}//r_{\pi 1}$, $R_{T2} = R_{f2}//r_{\pi 2}$

The total input current noise density is :

$$I_{nTotal}^2 f(f) = I_{n(dual)}^2 + I_{n(LMH6624)}^2$$

$$I_{nTotal}^2 f(f) = I_{shot}^2 + 2qI_{dk} + \frac{4kT}{R_d} 10^{\frac{NF_{LMH6624}}{10}} f + \frac{2q}{\beta} I_{c1BJT}$$
$$+ 4kT(r_{x1} + 2\pi L_1)[\frac{1+(2\pi C_d R_{f1})^2}{R_{f1}^2}]f^2$$
$$+ 2q\frac{V_{t1}^2}{I_{c1BJT}}[\frac{1+(2\pi(C_\pi + C_d)R_{T1})^2}{(R_{T1})^2}]f^2 + \frac{4kT}{R_{f1}} \qquad (6.41)$$
$$+ 4kT(r_{x2} + 2\pi L_2)[\frac{1}{R_{f2}^2}]f^2 + 2q\frac{V_{t2}^2}{I_{c2BJT}}[\frac{1}{R_{T2}^2}] + \frac{4kT}{R_{f2}}$$

where shot noise current from I_{b2BJT} is negligible

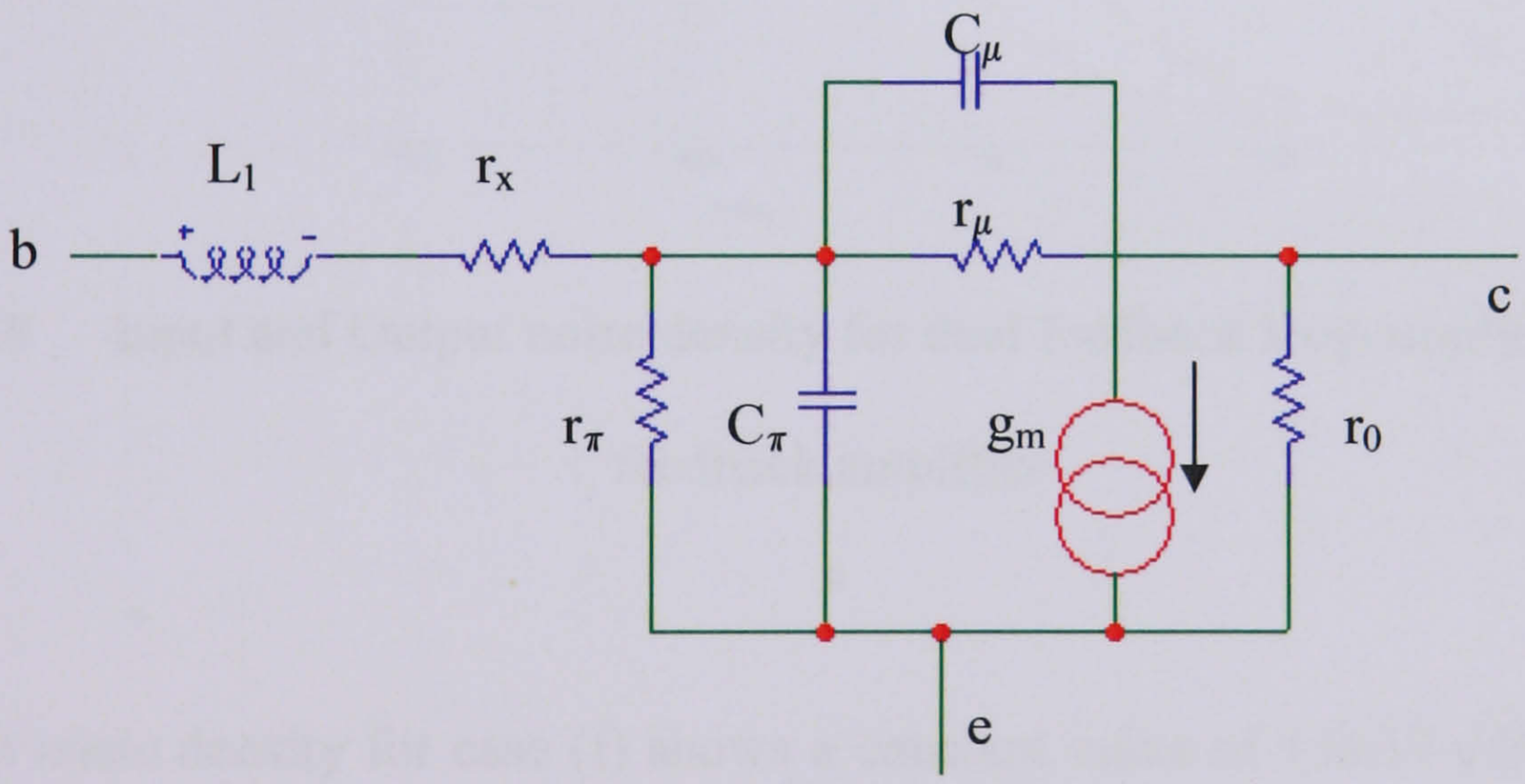

Figure 6.17 BJT small-signal hybrid-π model with series inductor

Figure 6.18 shows the simulated input and output noise density for case (f). The input noise density shows distortion, due to the voltage control that sets the array of capacitors. The

input noise density is around 225pV/$\sqrt{Hz}$ from low frequency until 10MHz, the fluctuation of noise density between 184pV/$\sqrt{Hz}$ to 385pV/$\sqrt{Hz}$ starts to occur throughout the high frequency range..

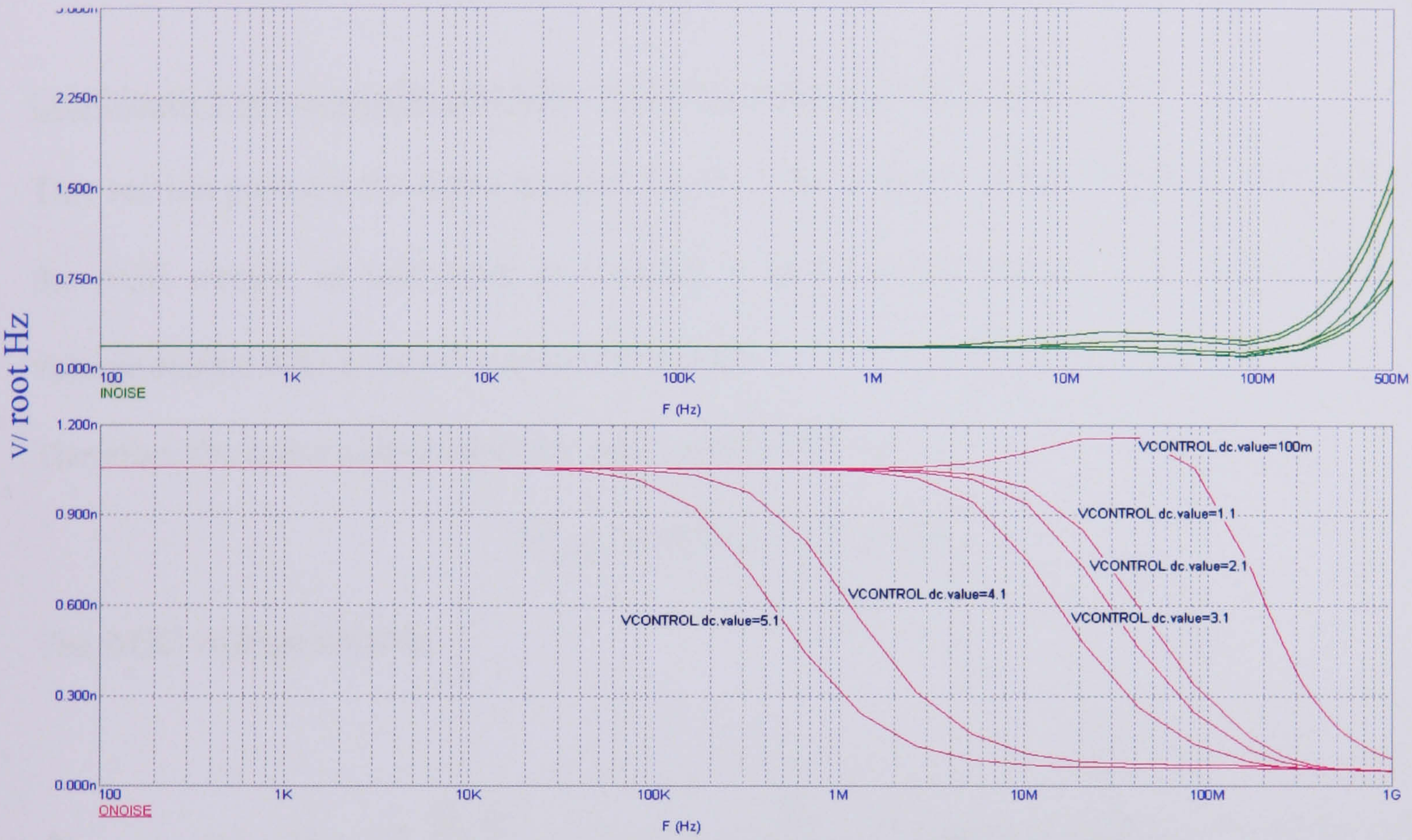

Figure 6.18 Input and Output noise density for dual feedback loop amplifier with voltage feedback amplifier

The output noise density for case (f) shows a constant value of 1.0nV/$\sqrt{Hz}$, with a slight peak to 1.1nV/$\sqrt{Hz}$ at frequency between 20MHz to 50MHz. These simulated results predict that there is no change in output noise density, during the bandwidth adjustment process.

Comparing the three composite methods of cases (d), (e) and (f), bootstrapping and the dual feedback loop technique exhibit the lowest output noise density. Another observation is that in case (e) and case (f), the output noise density, tends to decrease as the frequency increases, possibly due to the low pass filter configuration which was set to implement the bandwidth adjustment function.

Combination of composite amplifier technique with automatic gain control

This section presents the noise analysis for the circuits discussed in Chapter 5. The gain for the AGC circuit, as calculated in Chapter 5, is 10. Assuming the AGC is driven by a voltage source with a source resistance of 50Ω.

Therefore the noise delivered to the input of the AGC is

$$N_{inAGC} = 4kTR_s = 7.53e-19 .$$

The AGC voltage noise is

$$N_{ampAGC} = V_n^2 + I_n^2 + I_n^2(\frac{R_F R_G}{R_F + R_G})^2 + 4kTR_G(\frac{R_F}{R_F + R_G})^2 + 4kTR_F(\frac{R_G}{R_F + R_G})^2 = 1.97e-17 .$$

where from the data sheet [6.16]: $V_n^2 = 1.9e-17V/\sqrt{Hz}$ and $I_n^2 = 6.76e-24A/\sqrt{Hz}$,

R_G=100Ω and R_f=1kΩ

$$F_{AGC} = 1 + \frac{N_{ampAGC}}{N_{inAGC}} = 27$$

Figure 6.19 shows the input and output noise density for the AGC circuit. The simulated input noise density is around $6\mu V/\sqrt{Hz}$, whereas the output noise density is almost

$114\mu V/\sqrt{Hz}$. The results show that the main contribution of noise for the AGC is mainly from the low frequency range or flicker noise.

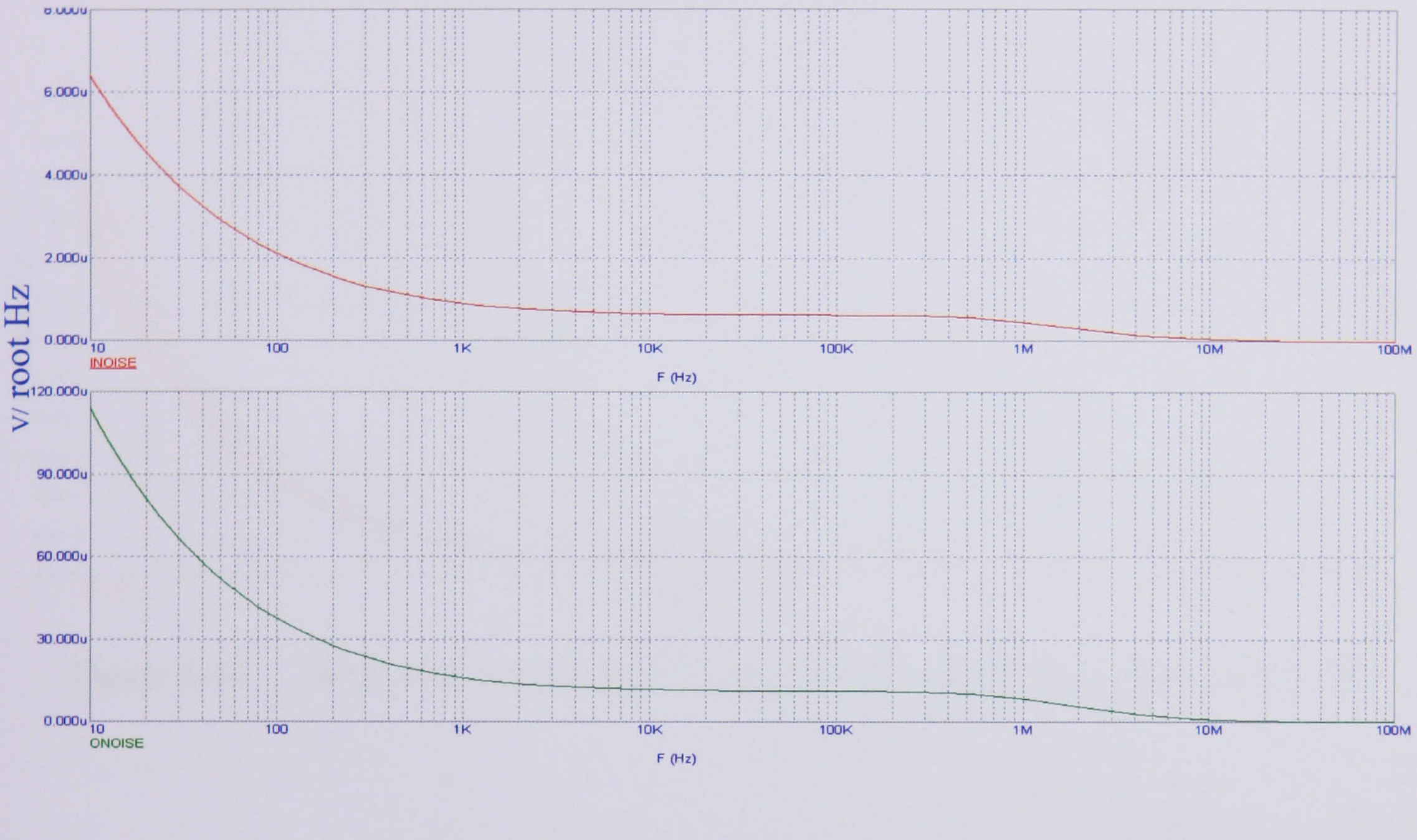

Figure 6.19 Input and Output Noise density for AGC circuit

The following figures, 6.20 to 6.22, show the simulated output noise density versus frequency for the three configurations discussed in Chapter 5. The simulated output noise density is taken at the output of the AGC system. All the three figures show high output noise between 10Hz to 1 kHz. The output noise for the combination of VFA and CFA amplifiers as shown in Figure 6.20 is around $0.97\mu V/\sqrt{Hz}$, decreasing to $0.15\mu V/\sqrt{Hz}$ at 2k Hz, and the value is maintained until a peak at the cut-off frequency. The combination of BTA and VFA amplifier exhibits the highest output noise density, $13.3\mu V/\sqrt{Hz}$, decreasing to $1.6\mu V/\sqrt{Hz}$ at 2k Hz, and it further reduces after 10MHz, as illustrated in

Figure 6.21. The dual loop feedback and VFA combination, shows an output noise density of $3.7\mu V/\sqrt{Hz}$. At 2kHz, the output noise density is $0.5\mu V/\sqrt{Hz}$ decreasing to $0.09\mu V/\sqrt{Hz}$ after 10MHz as illustrated in Figure 6.22

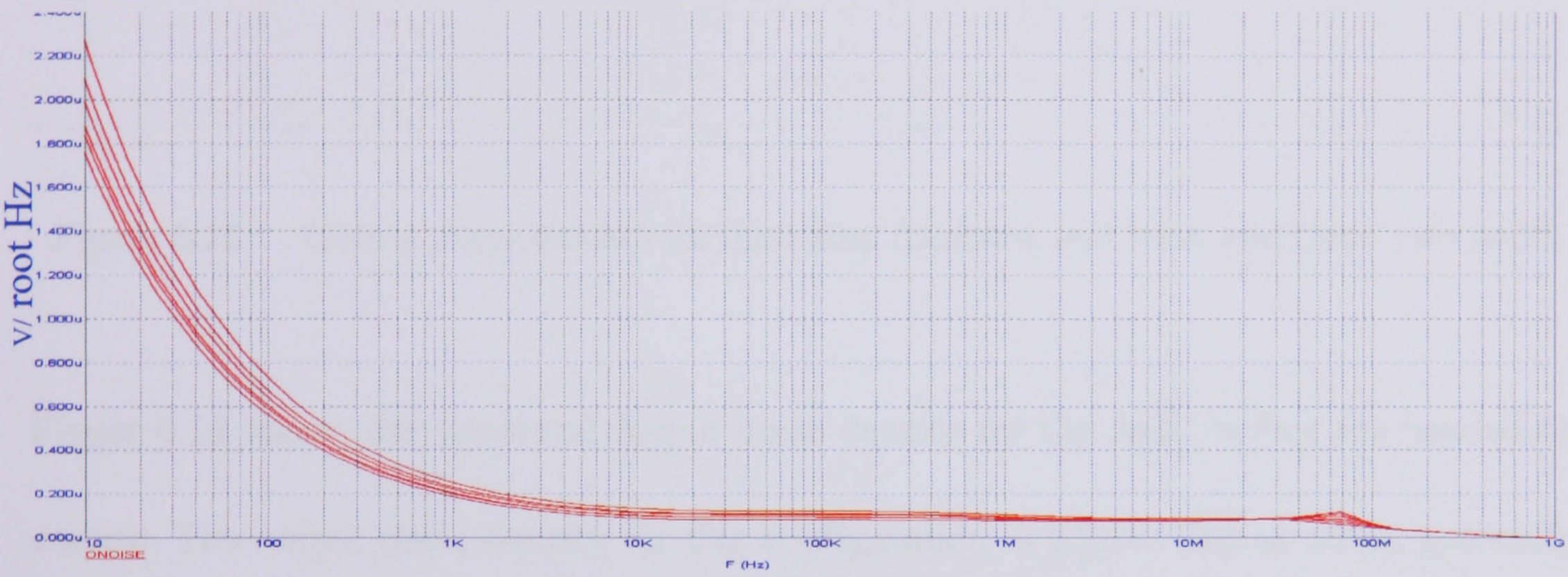

Figure 6.20 Output noise density for composite VFA and CFA amplifier with AGC

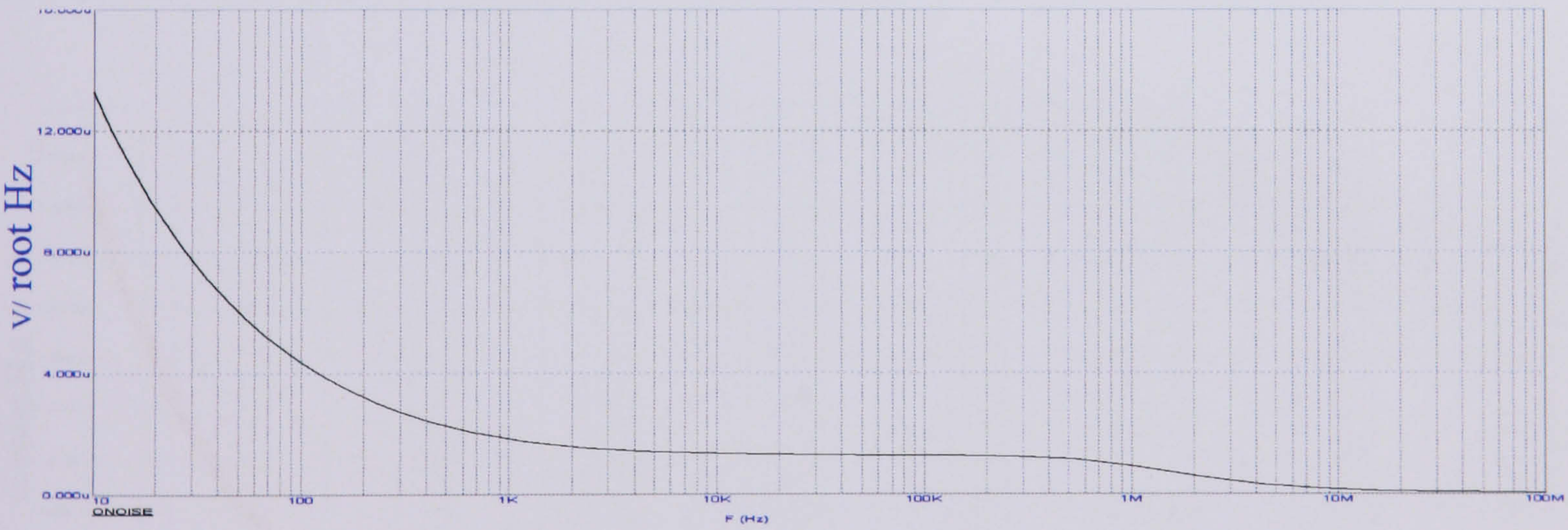

Figure 6.21 Output noise density for BTA and VFA amplifier with AGC

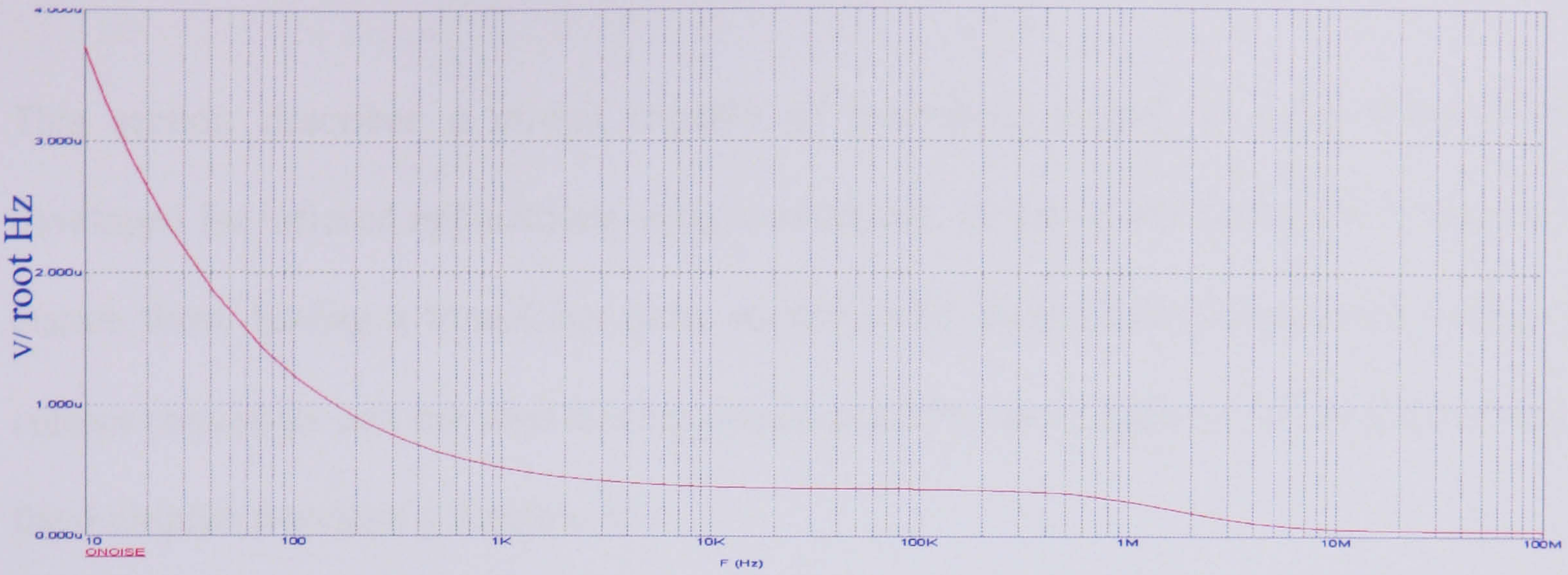

Figure 6.22 Output noise density for dual loop feedback and VFA amplifier with AGC

Figure 6.23 shows the simulated output noise density for the AGC before the bandwidth control. The output noise density for this configuration is $2.0\mu V/\sqrt{Hz}$ at 10Hz, gradually dropping to $0.2\mu V/\sqrt{Hz}$ at 2kHz. Compared to Figure 6.20, the AGC before bandwidth control exhibits higher noise.

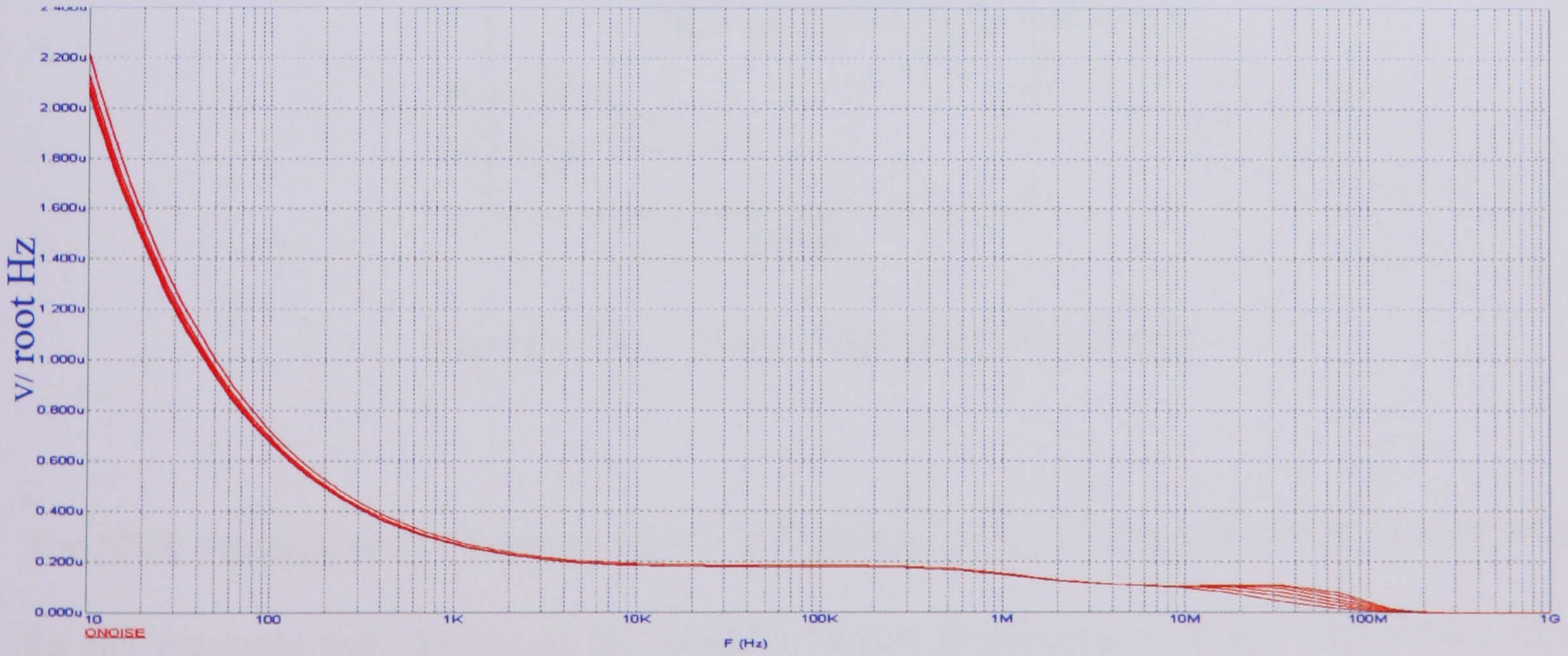

Figure 6.23 Output noise density for AGC before bandwidth control

6.4 Signal to Noise Ratio module design configuration

This section describes a circuit capable of measuring signal to noise ratios (SNR) developed for infrared applications using a multiplier. In theory the multiplier is based on a classic form, having a translinear core, supported by three (X,Y,Z) linearised voltage to current converters and the load driving output amplifier as in Figure 6.24. In general terms the multiplier provides a function of :

$$W = \frac{(X1 - X2)(Y1 - Y2)}{U} + Z \qquad (6.42)$$

where the variables W, U, X, Y and Z are all voltages. When connected as a simple multiplier, with X = X1-X2, Y = Y1-Y2 and Z=0, U= 1V, the output expression will be as follows :

$$W = XY \qquad (6.43)$$

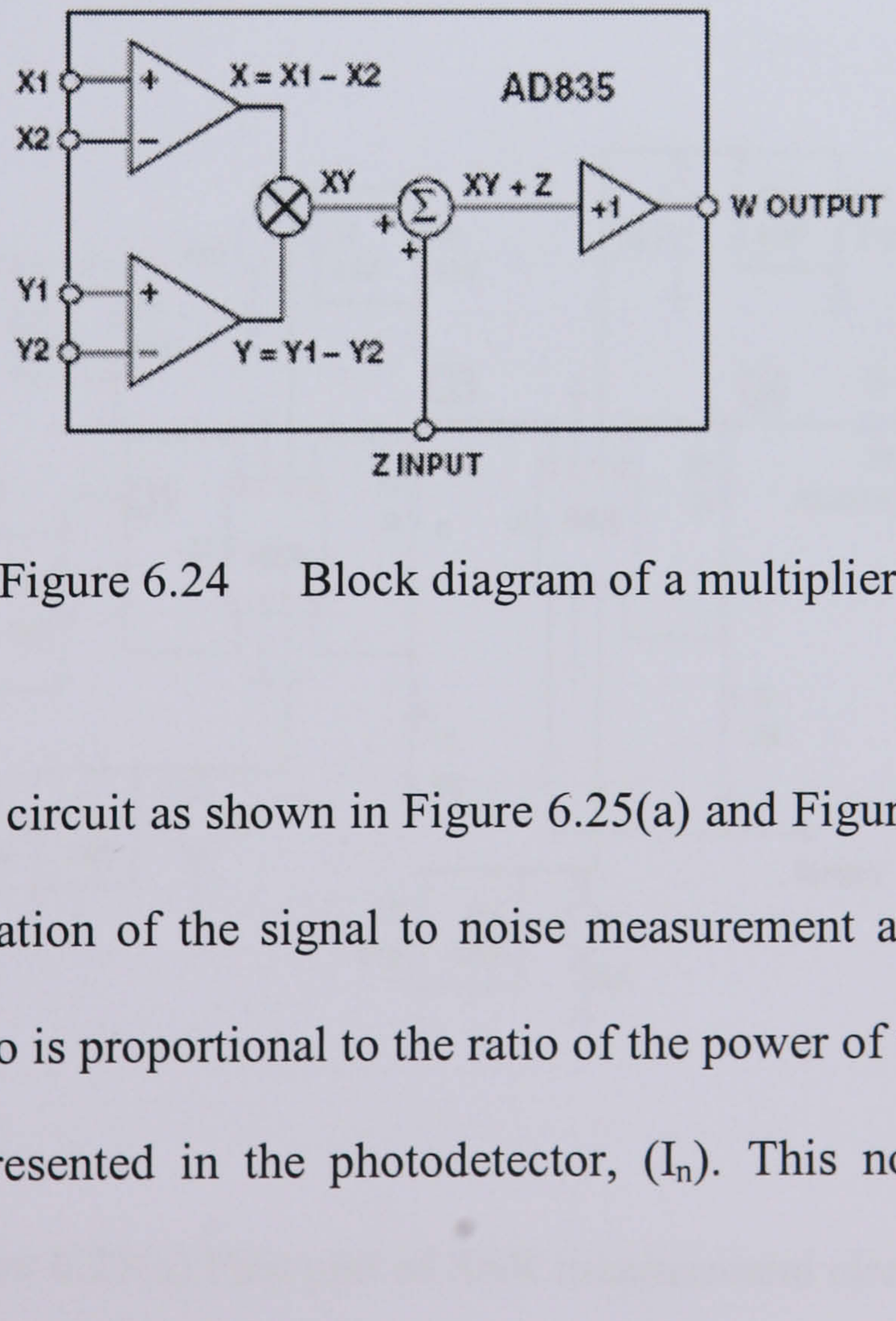

Figure 6.24 Block diagram of a multiplier

The SNR measurement circuit as shown in Figure 6.25(a) and Figure 6.25(b) is responsible for the dynamic calculation of the signal to noise measurement at the front-end's input. This signal to noise ratio is proportional to the ratio of the power of the input signal (I_p) and optical noise power presented in the photodetector, (I_n). This noise current is roughly

proportional to the photodiode current. The circuit implementation is the ratio of the signal after the transimpedance amplifier squared amplitude to the squared noise, $\frac{V_o^2}{I_n^2}$, where V_o is proportional to I_p and $I_n^2 = 2qI_xB$ (q is the charge of the electron, I_x is the noise current in the photodetector and B the bandwidth).

The SNR circuit measurement presented consists of three multipliers and one divider, implemented with a multiplier in a feedback loop. The divider is used to execute the necessary division $(\frac{1}{I_n})$ and the three multipliers are used to achieve the squared SNR result. The front end of the SNR circuit consists of two bandpass filter to implement the desired "average" measure of the SNR.

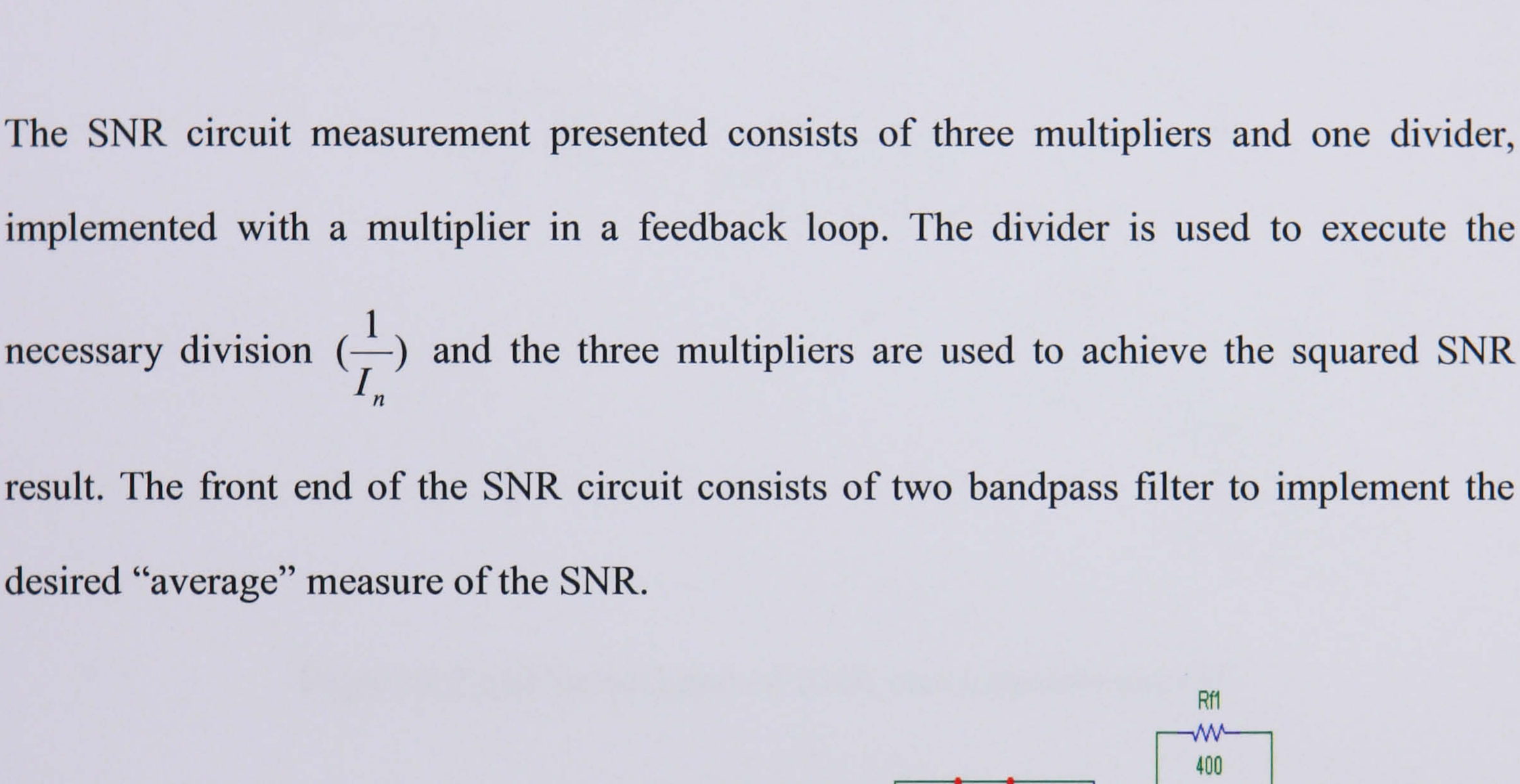

Figure 6.25(a) First part of SNR measurement circuit

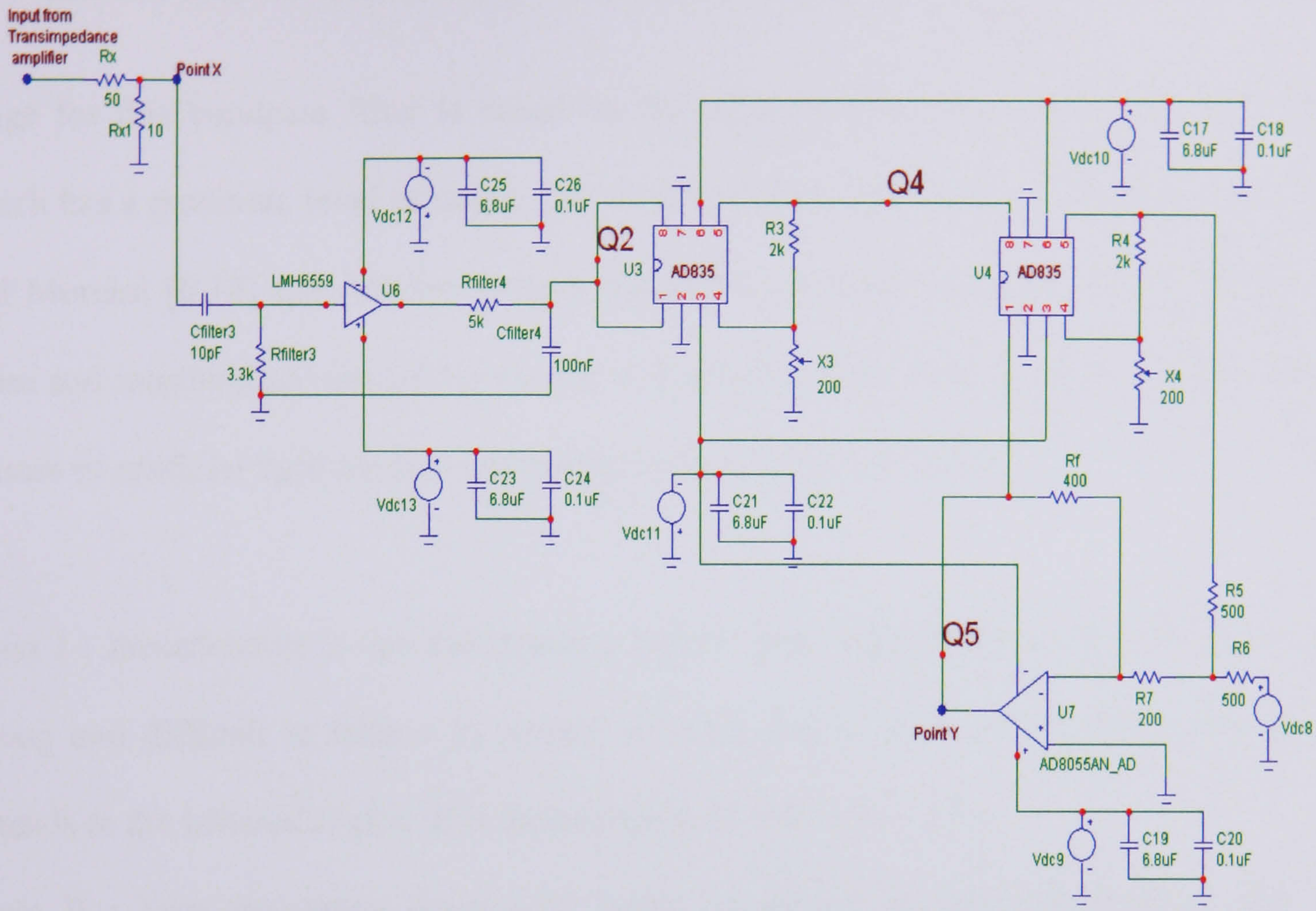

Figure 6.25(b) Second part of SNR measurement circuit

As seen in Figure 6.25(a), the circuit consists of a bandpass filter where its cutoff frequency is between 10MHz to 60MHz. There is a multiplier, U1 which squares the input signal, I_p, which has been converted to V_o by the front-end transimpedance amplifier. Multiplier, U2 multiplies the input signal, V_0^2 with the noise signal, $\frac{1}{I_n^2}$ from multiplier, U4. The output result of U2 is amplified by an amplifier U8, where its gain has been set to 2. The output of U8 is connected to an AC to DC converter, as in Figure 6.26.

Figure 6.25(b) also consists of a bandpass filter, but with a cutoff frequency between 200Hz to 5MHz. Multiplier, U3, performs the noise square function, I_n^2. Reference voltage, V_{dc8},

is set to 1V has been connected to the output of the multiplier, U4. An amplifier, U7 is used as a feedback loop for multiplier, U4 to perform the function, $\frac{1}{I_n^2}$. The cutoff frequency range for this bandpass filter is based on the assumption of taking the frequency range which has a moderate level of noise. Referring to the research work by Boucouvalas [6.17] and Moreira [6.18] that wireless indoor infrared communication systems are affected by noise and interference induced by natural and artificial light sources, there are four distinct classes of artificial light sources interfering devices being identified. :

Class I : Incandescent lamps that produce narrow band interfering signals which are very strong and difficult to reduce by optical filtering due to their broad optical spectra and extends to the infrared region. It is in the region of 100Hz to 2 kHz.

Class II : Low frequency fluorescent lamps driven by conventional ballasts that also produce very strong interference with spectra extending up to several kHz (500kHz).

Class III : High frequency fluorescent lamps geared by electronic ballasts that produce lower amplitude interference but whose spectra is very broad, extending to more than 1MHz.

Class IV : Tungsten lights, TV remote controls and IR headphones are additional sources of noise affecting low frequencies up to 100kHz, 6MHz and 15MHz. Therefore knowledge of the environment in which wireless infrared links operate is paramount for setting the specification for optimum link performance.

Figure 6.26 shows a fast AC to DC converter, which converts the output voltage from amplifier, U7. The output positive rectifier DC voltage is then inverted into negative DC

voltage by amplifier, X3, set to have a gain of 1, since the amplifier bandwidth adjustment voltage control accepts negative DC input only.

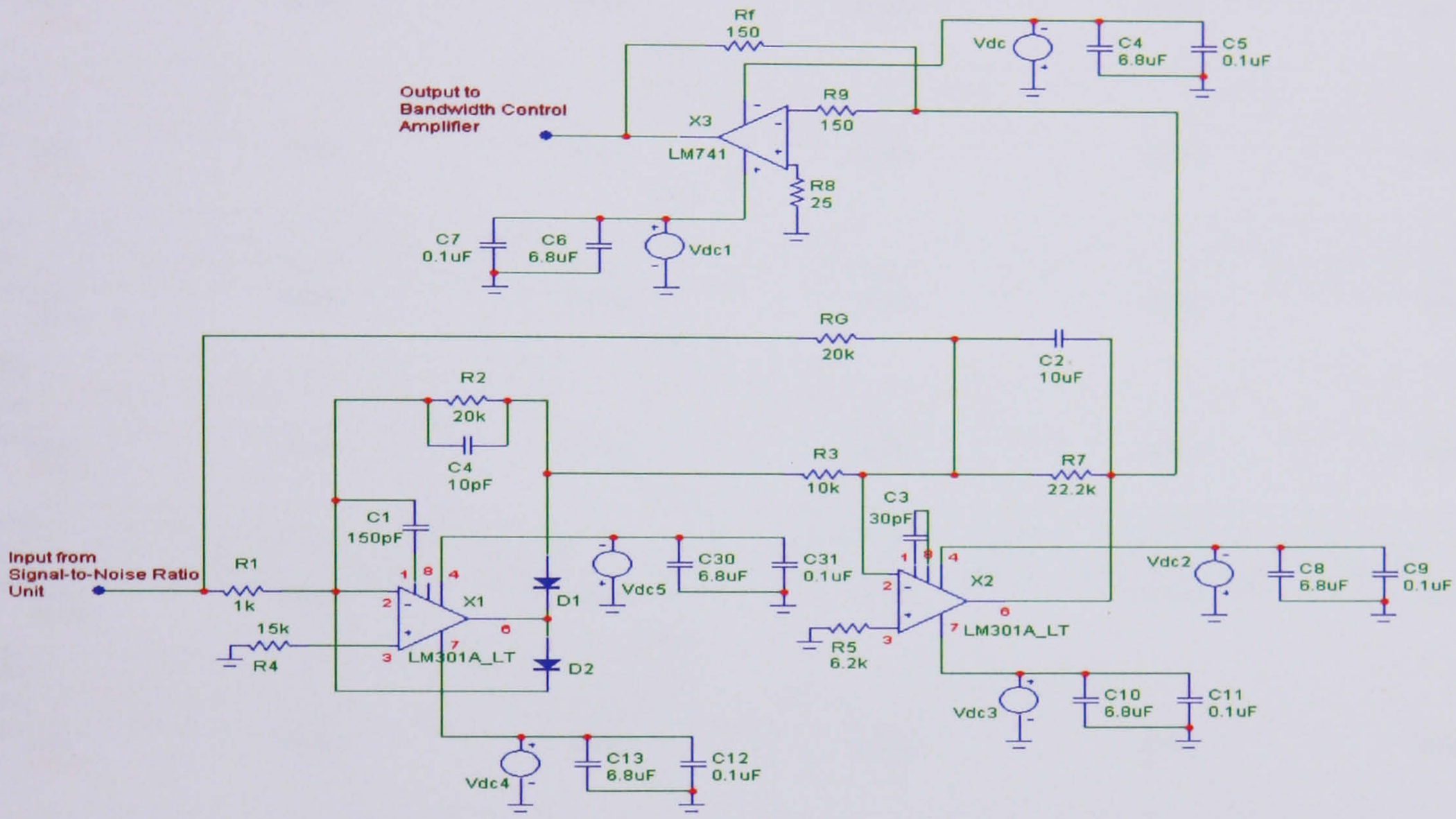

Figure 6.26 AC-DC converters with inverting amplifier.

Figure 6.27 illustrates an example behavior of the SNR measurement circuit with a sinusoidal input signal at 10 kHz. The transient responses shows the multiply and divider signal of each section of the SNR circuit. As seen from the transient response Q3 and Q4 output is the square of the input frequency Q1 and Q2. Q6 is the inverse of the input frequency of the division.

Figure 6.28 illustrates an example behavior of the input signal of the SNR measurement circuit versus the output of the SNR measurement circuit after the AC-DC converters with inverting amplifier. The transient responses show a very small output variations from -2.937V to -2.925V.

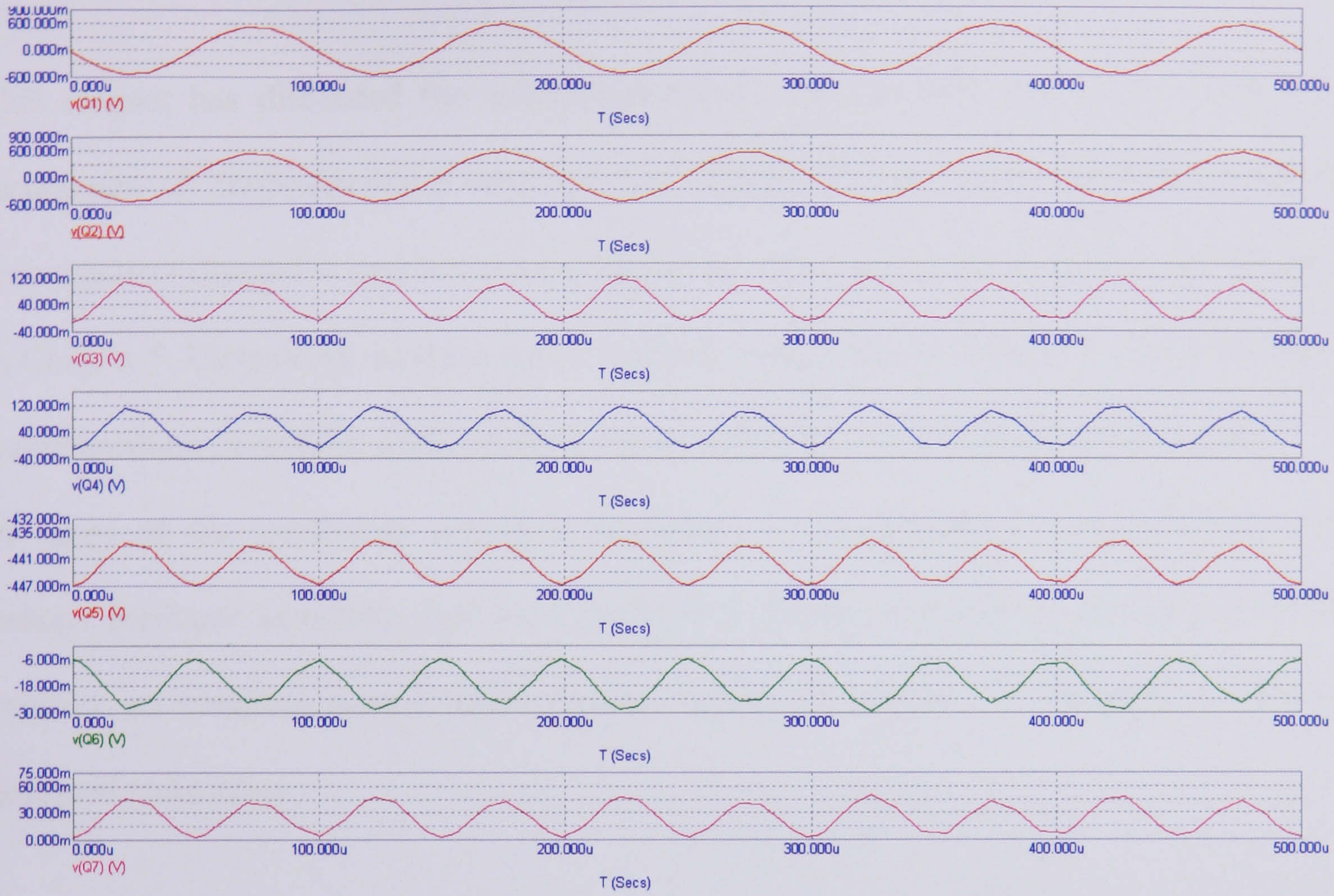

Figure 6.27 Simulated transient responses for the SNR circuit

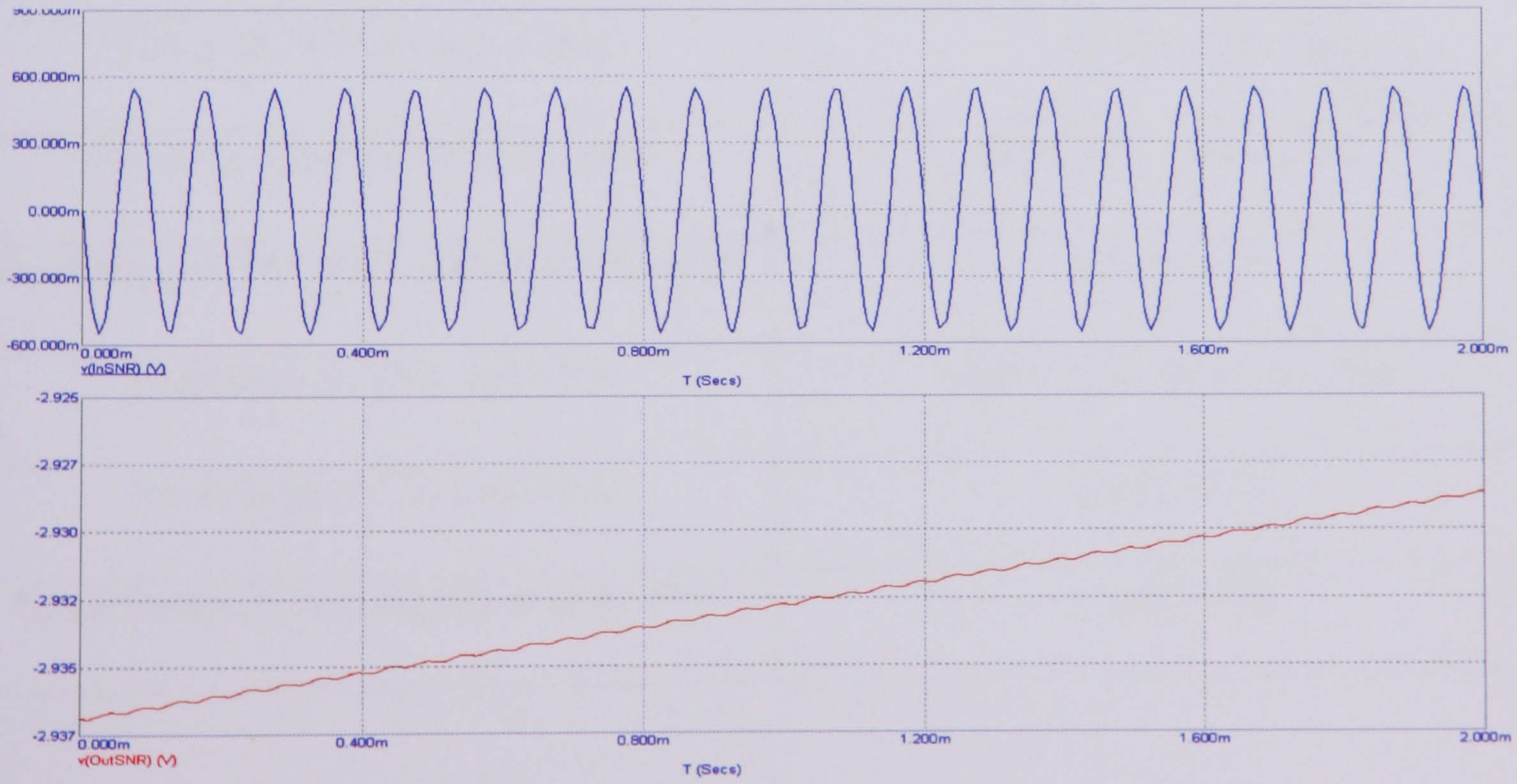

Figure 6.28 Simulated transient responses for the input SNR versus output SNR

6.5 Summary

This chapter has discussed the noise performance analysis and simulation of the three techniques of transimpedance amplifier in Chapter 3, the three composite amplifier techniques in Chapter 4, and the three integrations of the composite amplifier with the AGC in Chapter 5. Comparing the three transimpedance amplifiers in Chapter 3, the bootstrapped transimpedance amplifier with adjusting capacitor has the lowest output noise density.

In terms of the composite amplifier technique, the bootstrapped transimpedance with voltage feedback amplifier, dual loop feedback amplifier, and voltage feedback amplifier exhibits an identical output noise density. Table 6.1 tabulates a summary of the six designed techniques.

Table 6.1 Summary of the output noise density for the six designed techniques

Designed circuits	Output noise density
TIA with FET voltage control	$50\text{nV}/\sqrt{Hz}$
TIA with external voltage control	$8\text{nV}/\sqrt{Hz}$ -$11\text{nV}/\sqrt{Hz}$
Bootstrapped TIA with adjustable capacitor	$5.5\text{nV}/\sqrt{Hz}$
Combination VFA and CFA	$10\text{nV}/\sqrt{Hz}$ to $30\text{nV}/\sqrt{Hz}$
Bootstrapped TIA and VFA	$1.1\text{nV}/\sqrt{Hz}$
Dual feedback loop amplifier with VFA	$1.1\text{nV}/\sqrt{Hz}$

Table 6.2 summarises the output noise density for the circuits discussed in Chapter 5. The results show that, after AGC integration, the output noise increases, compared to the situation before integration.

Table 6.2 Summary of the output noise density for composite amplifier with AGC

Designed circuits	Output noise density
VFA and CFA with AGC	$0.97\mu V/\sqrt{Hz}$
BTA and VFA with AGC	$13.3\mu V/\sqrt{Hz}$
Dual loop feedback and VFA with AGC	$3.7\mu V/\sqrt{Hz}$

The simulated results show that VBA before VGA yields a better noise output density as shown in Table 6.3. Therefore in terms of noise comparison, the VBA before VGA is the better configuration.

Table 6.3 Comparison of output noise density between VBA-VGA or VGA-VBA

Method configuration	Output noise density
VBA – VGA	$0.97\mu V/\sqrt{Hz}$
VGA - VBA	$2.0\mu V/\sqrt{Hz}$

In order to demonstrate that VBA before VGA is the better configuration a simple mathematical calculation using the noise figure is calculated as below using the value of noise figure calculated earlier of this chapter and the result plotted in Figure 6.29.

where, $F_{LMH6624} = 5.7$, $F_{LMH6732} = 14$, $F_{AGC} = 27$

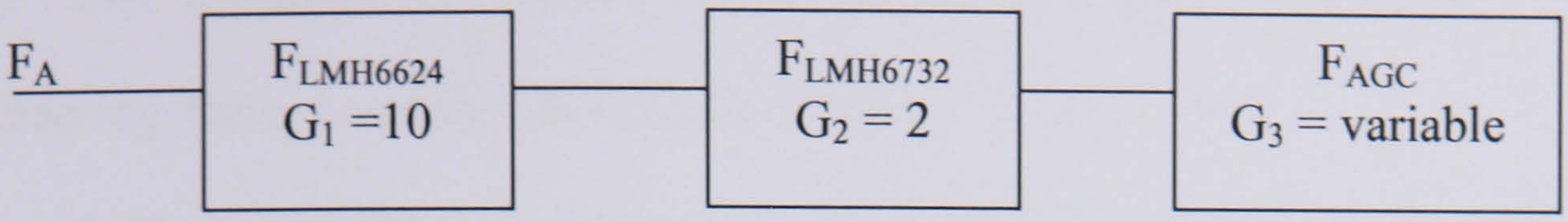

$$F_A = F_{LMH6624} + \frac{F_{LMH6732}}{G_1} + \frac{F_{AGC}}{G_1 G_2} = 5.7 + \frac{14-1}{10} + \frac{27-1}{(10)(2)} = 8.3$$

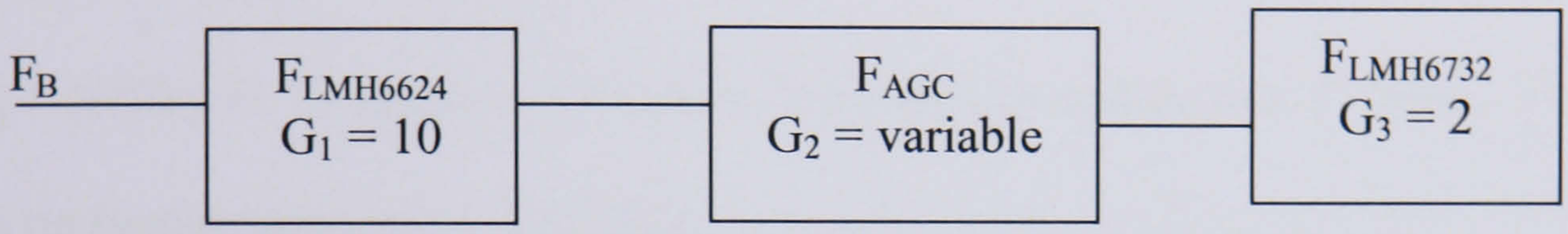

$$F_A = F_{LMH6624} + \frac{F_{AGC}}{G_1} + \frac{F_{LMH6732}}{G_1 G_2} = 5.7 + \frac{27-1}{10} + \frac{14-1}{(10)(10)} = 8.43 \quad (\text{Assume } G_2 = 10)$$

$$= 5.7 + \frac{27-1}{10} + \frac{14-1}{(10)(1)} = 9.6 \qquad (\text{Assume } G_2 = 1)$$

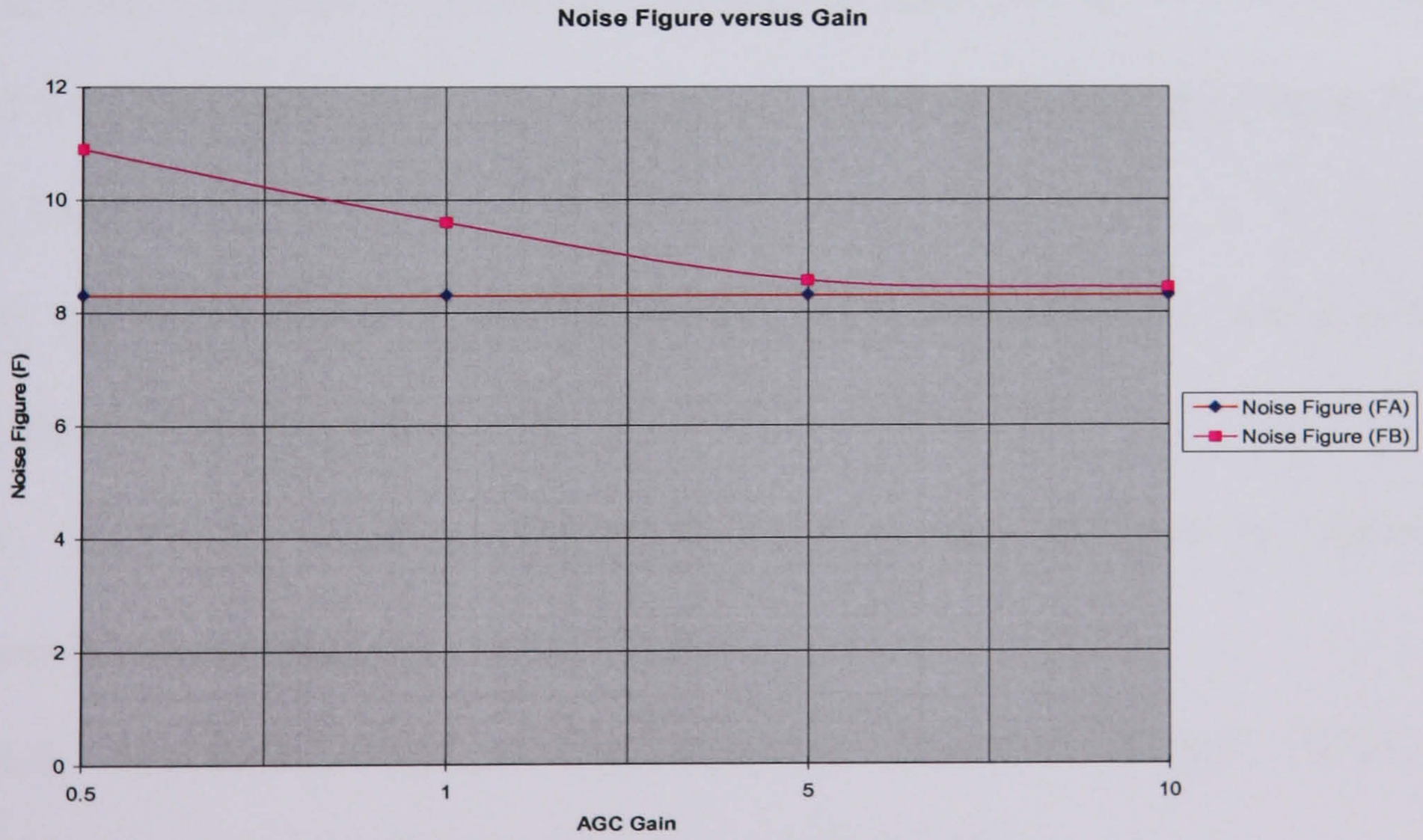

Figure 6.29 Noise Figure, F_A and F_B versus Gain

References

[6.1] S.B. Alexander, "Optical Communication Receiver Design", SPIE Optical Engineering Press, London, UK Chapter 5, 1997.

[6.2] H. Nyquist, "Thermal Agitation of Electricity in Conductors" Physical Review, Vol. 32, No. 1, pp. 110-113, July 1928.

[6.3] R. Jacob Baker, "CMOS : Circuit design, Layout and Simulation" Wiley-Interscience, Chapter 8, 2005.

[6.4] Jeffrey B. Carruthers, "Wireless Infrared Communications" Wiley Encyclopedia of Telecommunications, pp. 1-10, 2002.

[6.5] C. D. Motchenbacher and F. C. Fitchen, "Low noise Electronic design" John Wiler & Sons, Chapter 2, 1973.

[6.6] Z. Bielecki, W. Kolosowski, R. Dufrene, M. Borejko, "Low noise optical receivers" 11th GAAS Symposium, pp. 137-140, 2003.

[6.7] M. Park, "Analysis of sensitivity degradations caused by the flicker noise of GaAs-MESFET's in Fibre Optic Receivers" Journal of Lightwave Technology, Vol. 6, No. 5, pp. 660-667, 1988.

[6.8] C. Su, "1/f Noise in GaAs MESFETs" IEEE Proceedings of the Ineternational Electron Devices Meeting, 1983.

[6.9] T. V. Muoi, "Receiver Design of Optical Fibre Systems in Optical Fibre Transmission" Macmillan, Chapter 12, 1987.

[6.10] S.B. Alexander, "Optical Communication Receiver Design", SPIE Optical Engineering Press, London, UK, Chapter 6, pp. 173-201,1997.

[6.11] T.V.Muoi,"Receiver Design for Optical Fiber Systems" Journal of Lightwave Technology, Vol. LT-2, No. 3, pp. 243-265, 1984.

[6.12] R.G. Smith and S. D. Personick, "Receiver design for optical fiber communication systems, in semiconductor devices for optical communication" H. Kressel, Vol. 39, 2nd edition, pp. 89-160. 1982.

[6.13] S. M. Sze, " Bipolar transistor in Physics of semiconductor devices" John Wiley & Sons, 1981.

[6.14] Datasheet LMH6624, National Semiconductor, 2003

[6.15] Datasheet LMH6732, National Semiconductor, 2004

[6.16] Datasheet LMH6504, National Semiconductor, 2004

[6.17] A.C. Boucovalas, "Indoor ambient light noise and its effect on wireless optical links" IEE Proceeding Optoelectronics, Vol. 143, No.6, pp.334-338, 1996.

[6.18] Adriano J. C. Moreira, Rui T. Valadas, A. M. De Oliveira Duarte, "Characterisation and Modelling of Artificial Light Interference in Optical Wireless Communication Systems" Sixth IEEE International Symposium on Personal, Indoor and Mobile Radio Communications, Vol 1, pp. 326 – 331, 1995.

Chapter 7

Receiver fabrication and practical implementation setup

This chapter discusses the implementation details and presents the experimental results of one of the proposed designs that were implemented to demonstrate the feasibility of the infrared preamplifier receiver approach. The considered design presented is the combination of voltage feedback amplifier (VFA) with current feedback amplifier (CFA) as the bandwidth adjustment amplifier. Connected as a composite amplifier configuration, these amplifiers are then integrated with an automatic gain control (AGC). The signal-to-noise module is also implemented as the module which controls the bandwidth amplifier.

7.1 Hardware design documentation and setup

A simplified block diagram of the transmitter and receiver front-end is shown in Figure 7.1. The signal path consists of a laser diode bias T- PCB and the proposed voltage feedback transimpedance amplifier, followed by the current feedback bandwidth adjustment amplifier integrated with the automatic gain circuit. Additional circuitry is the signal and noise bandpass filter connected to the signal-to-noise ratio module which is linked to an AC-DC converter. The output of the AC-DC converter is converted to a negative voltage by the inverting amplifier. The output of this amplifier is connected to the current feedback bandwidth adjustment amplifier, via pin 8.

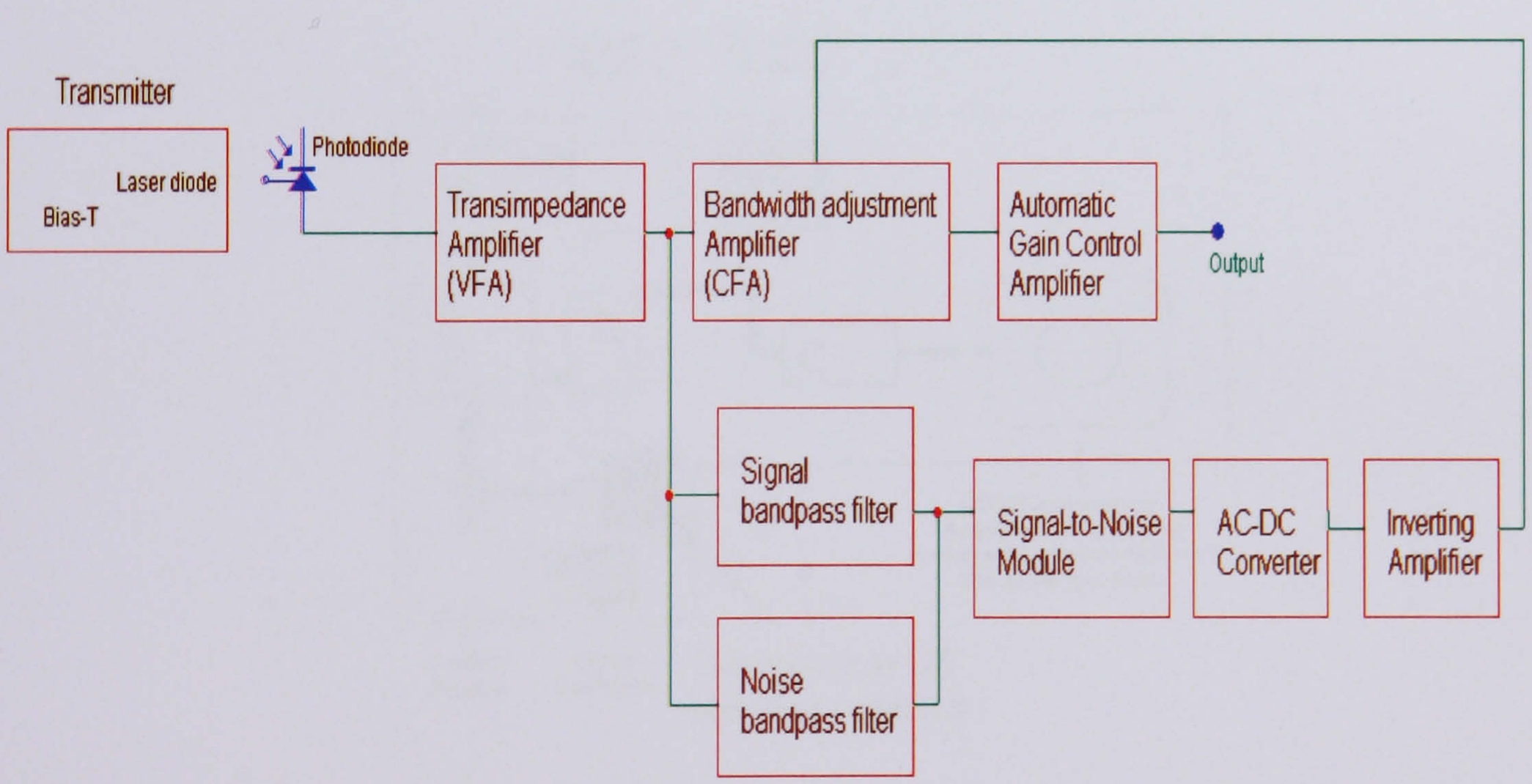

Figure 7.1 Simplified block diagram of the transmitter-receiver frond-end

Transmitter

The transmitter consisted of a red laser diode, operating at a wavelength 635nm with a light output power of 6mW. The laser diode was first connected to a laser diode constant current driver, the LD1255. The LD1255 function is to get the laser to operate in CW mode. Then the laser diode was disconnected from the LD1255, and connected to the laser diode bias T-PCB circuit. The bias-T PCB superimposes a modulation current onto the laser diode DC supply current for modulation frequencies in the range of 100Hz to 1GHz. However, the actual frequency range is also determined by the properties of the impedance network surrounding the laser diode. The circuit also has a DC blocking capacitor and a reverse bias protection diode included to protect the laser diode. Figure 7.2 shows the laser diode bias-T PCB layout.

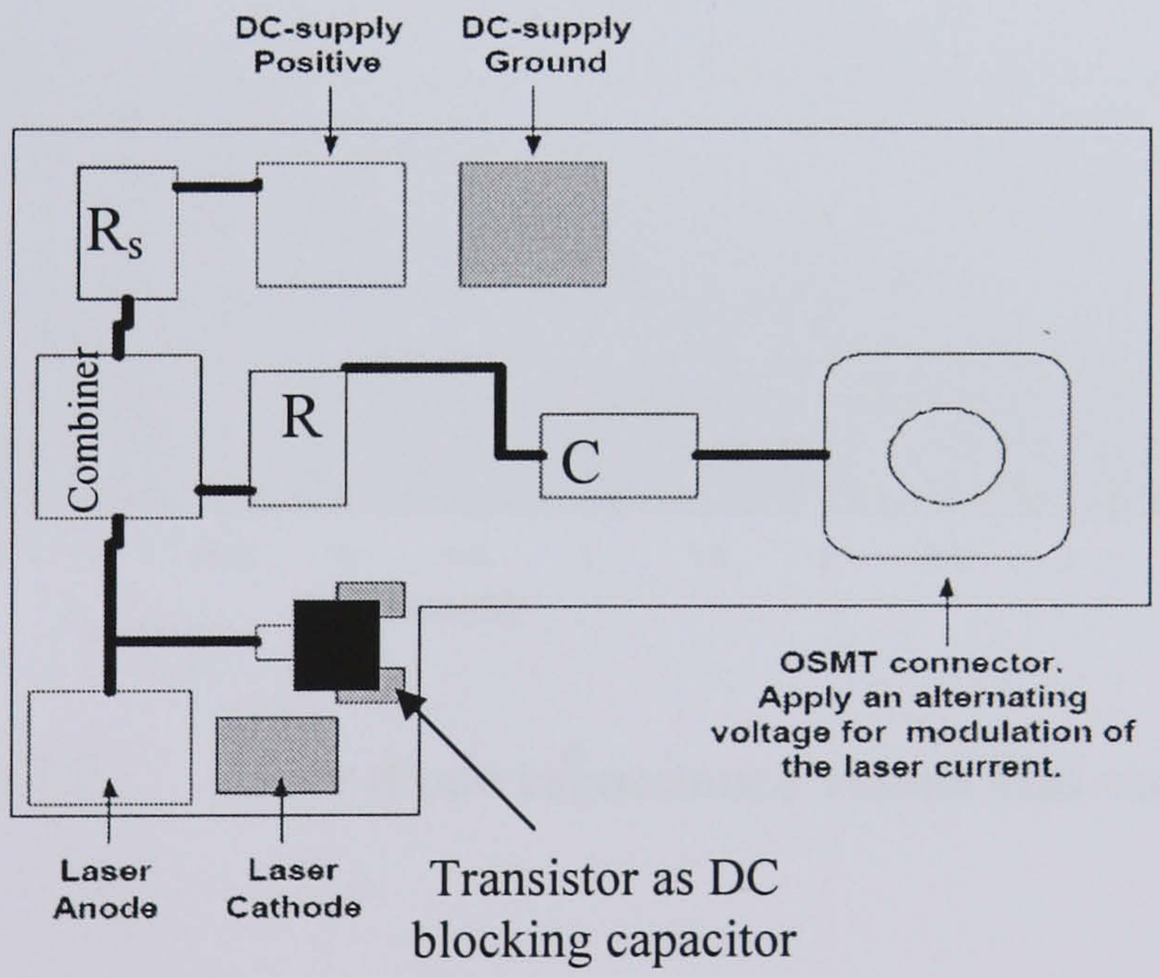

Figure 7.2 Laser diode bias-T PCB

The DC supply will generate a laser current of :

$I_{Laser}(A)$ = [(Supply voltage-voltage over the laser diode)/100Ω]

$I_{Laser}(A)$ = [(5-2.4)/100] = 26mA

The measurement of the laser diode capacitance, C_D versus reverse bias voltage is plotted in Figure 7.3. The measurement shows that, as the voltage increases the capacitance of the laser diode increases to 400pF at input bias voltage, 3.5V.

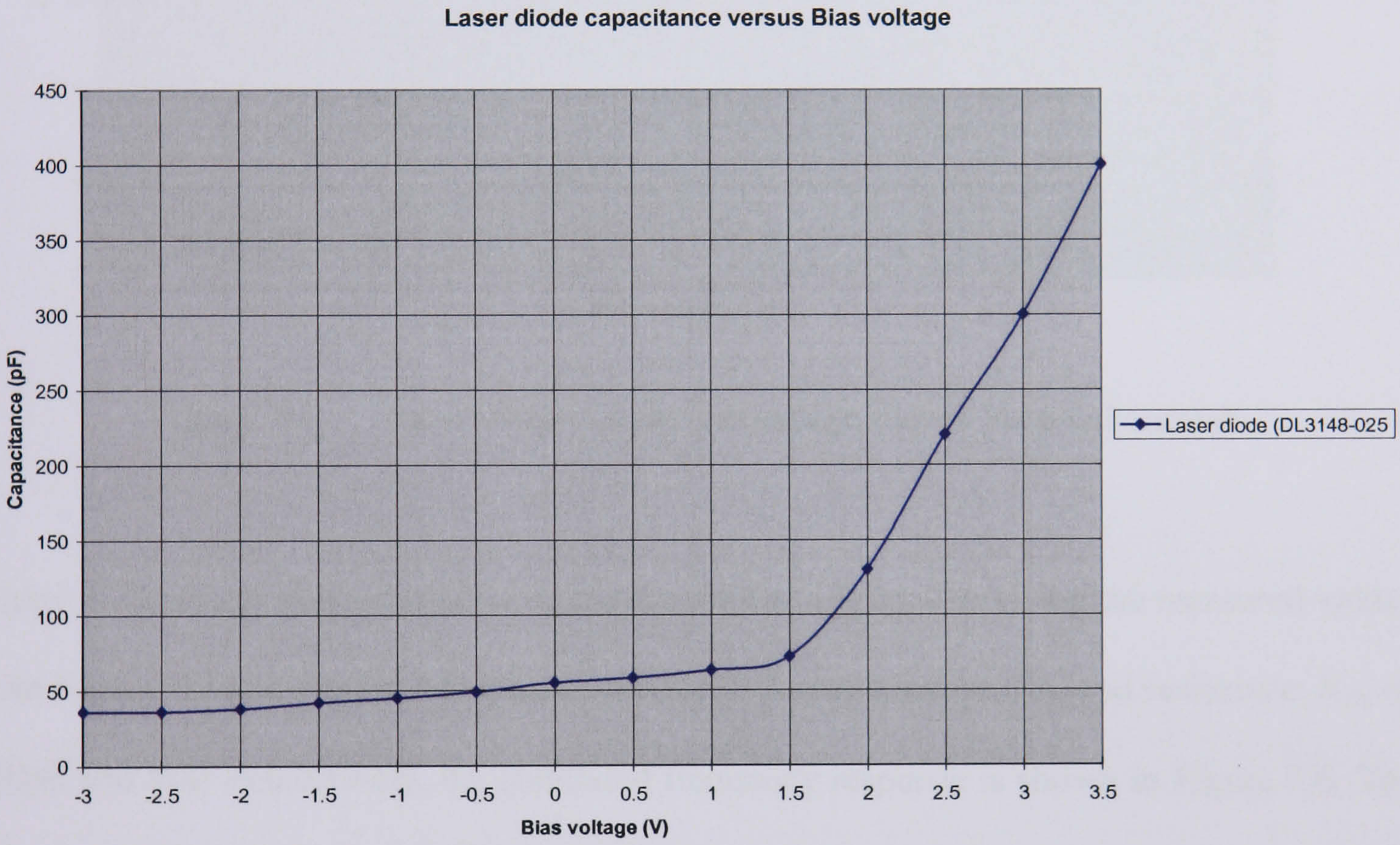

Figure 7.3 Laser diode capacitance versus bias voltage

The measurement of the laser diode forward current versus forward voltage is plotted in Figure 7.4. The measurement shows that at around 1.5V the laser diode starts to operate. The laser diode resistance during forward voltage, 2V is calculated using Figure 7.4 to be 80Ω.

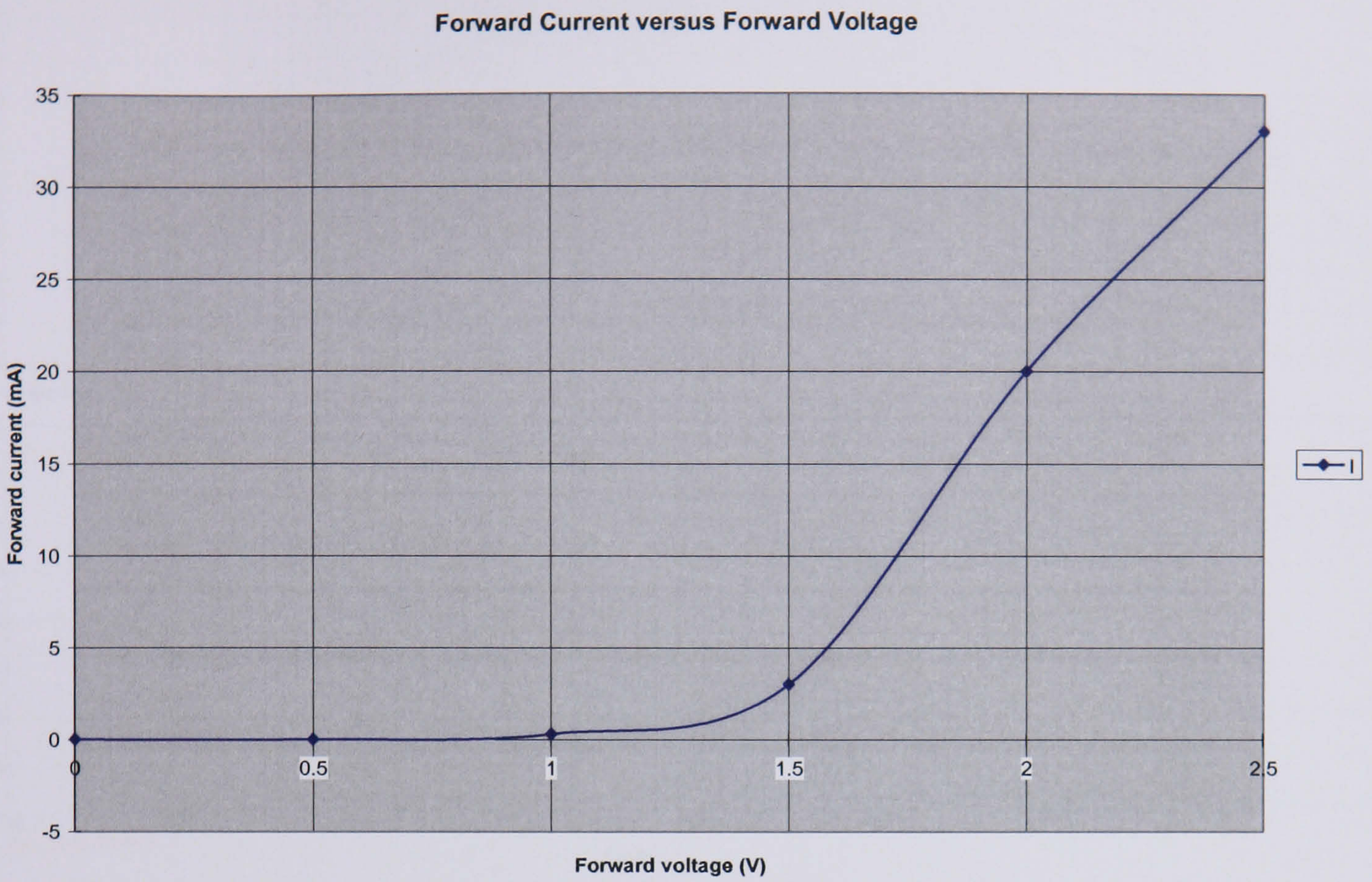

Figure 7.4 Laser diode : Forward voltage versus Forward current

Figure 7.2 was simulated as shown in Figure 7.5 and Figure 7.6. Using the measured values from Figure 7.3 and Figure 7.4, the laser diode has a capacitance, C_D, and resistance, R_D, of 130pF and 80Ω respectively, the simulated frequency response is shown in Figure 7.6. The frequency response shows the transmitter has a bandwidth between 3k Hz to 45MHz.

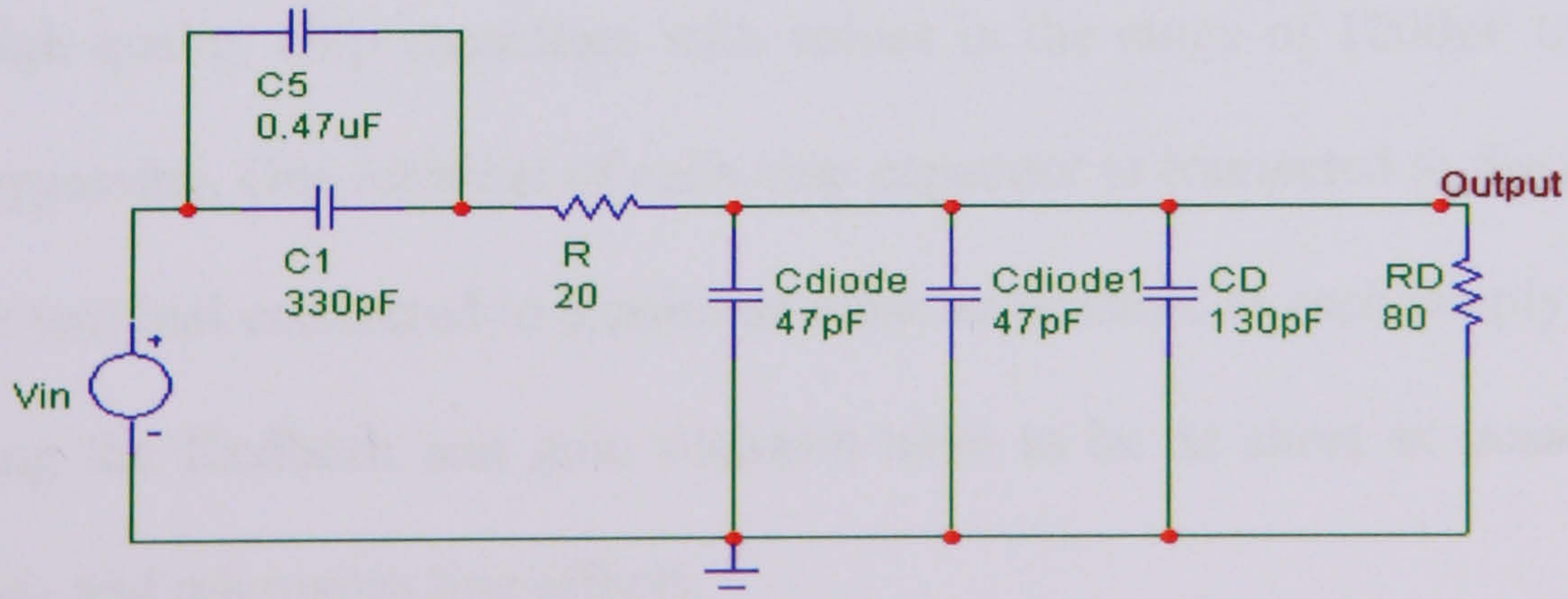

Figure 7.5 Model of Figure 7.2

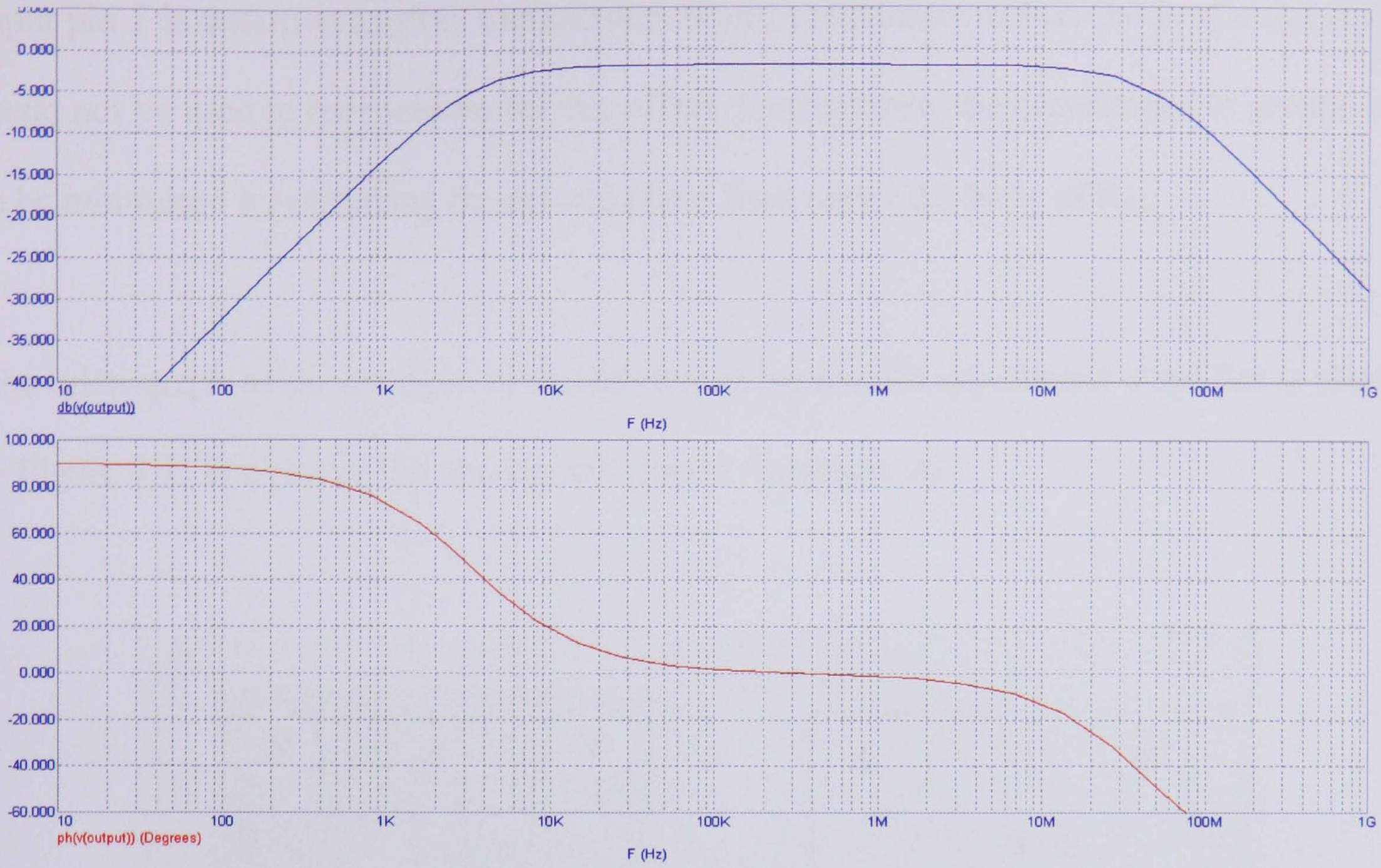

Figure 7.6 Frequency response of the transmitter

PCB layout is very important with high-speed amplifiers. Therefore the PCB fabrication for this circuit has taken into consideration a few general points of layout design [7.0-7.1]. A good high frequency layout exhibits a separation of power supply and ground traces from the inverting input and output pins. Parasitic capacitances between these nodes and ground may cause frequency response peaking and possible circuit oscillations. It is recommended to use high quality chip capacitors with values in the range of 1000pF to 0.1F for power supply bypassing. One terminal of each chip capacitor is connected to the ground plane and the other terminal connected to a point as close as possible to each supply pin. Signal lines connecting the feedback and gain resistors have to be as short as possible to minimise inductance and microstrip line effects.

For the layout consideration of the AGC circuit, the node trace area has to be small, as input pin 7 is sensitive to stray capacitance. Shunt capacitance across the feedback resistor could not be used to compensate for this effect. Furthermore, the capacitance to ground has to be minimised by removing the ground plane from under the body of R_G.

The micrograph of an example of the fabricated bandwidth adjustment amplifier is shown in Figure 7.7. The rest of the micrographs are in Appendix A.

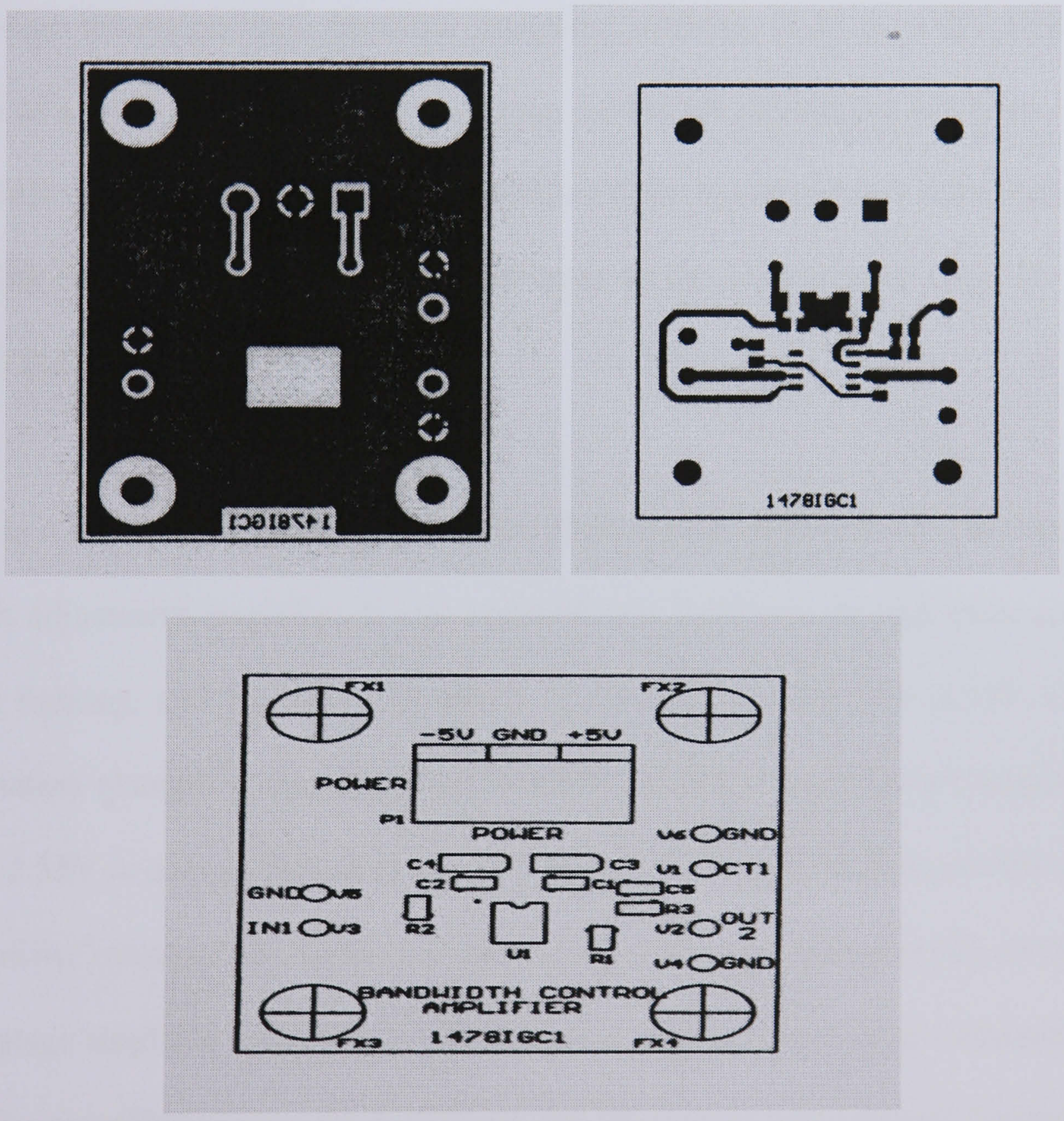

Figure 7.7 Micrographs of the bandwidth adjustment amplifier

7.2 Experimental results

The measured frequency response of the system was determined with two different settings. The first was to measure the frequency response of the whole system without the SNR module, which means that $V_{control}$ for the bandwidth adjustment of the current feedback amplifier was set to zero. The frequency responses were taken at the output of the transimpedance amplifier (VFA), the output of the bandwidth adjustment amplifier (CFA), and at the output of the AGC. The frequency response is shown in Figure 7.8. The gain at the first stage transimpedance amplifier fluctuated between 42dB to 40dB, with a cut-off frequency at around 85MHz. The second stage bandwidth adjustment amplifier had a gain around 46dB with a cut-off frequency of 40MHz, while the third stage amplifier has a gain of 50dB. Its cut-off frequency is almost the same as the second stage amplifier, which is around 38.2MHz.

The second measurement was taken with the SNR module connected to the control of the bandwidth adjustment amplifier. It was assumed that there was normal room temperature and room lighting, and the measured output of the SNR module was -2.55V. Due to the small variation changes at the output of the SNR module, the frequency response, when $V_{control}$ = -2.55V is only plotted as shown in Figure 7.9. The gain and bandwidth at the first stage amplifier remained the same, but there was an increase of bandwidth for the second and third stage amplifier, whereas the gain for the second and third stage remained the same as well. The cut-off frequency for the second and third stage was centered between 50MHz to 60MHz.

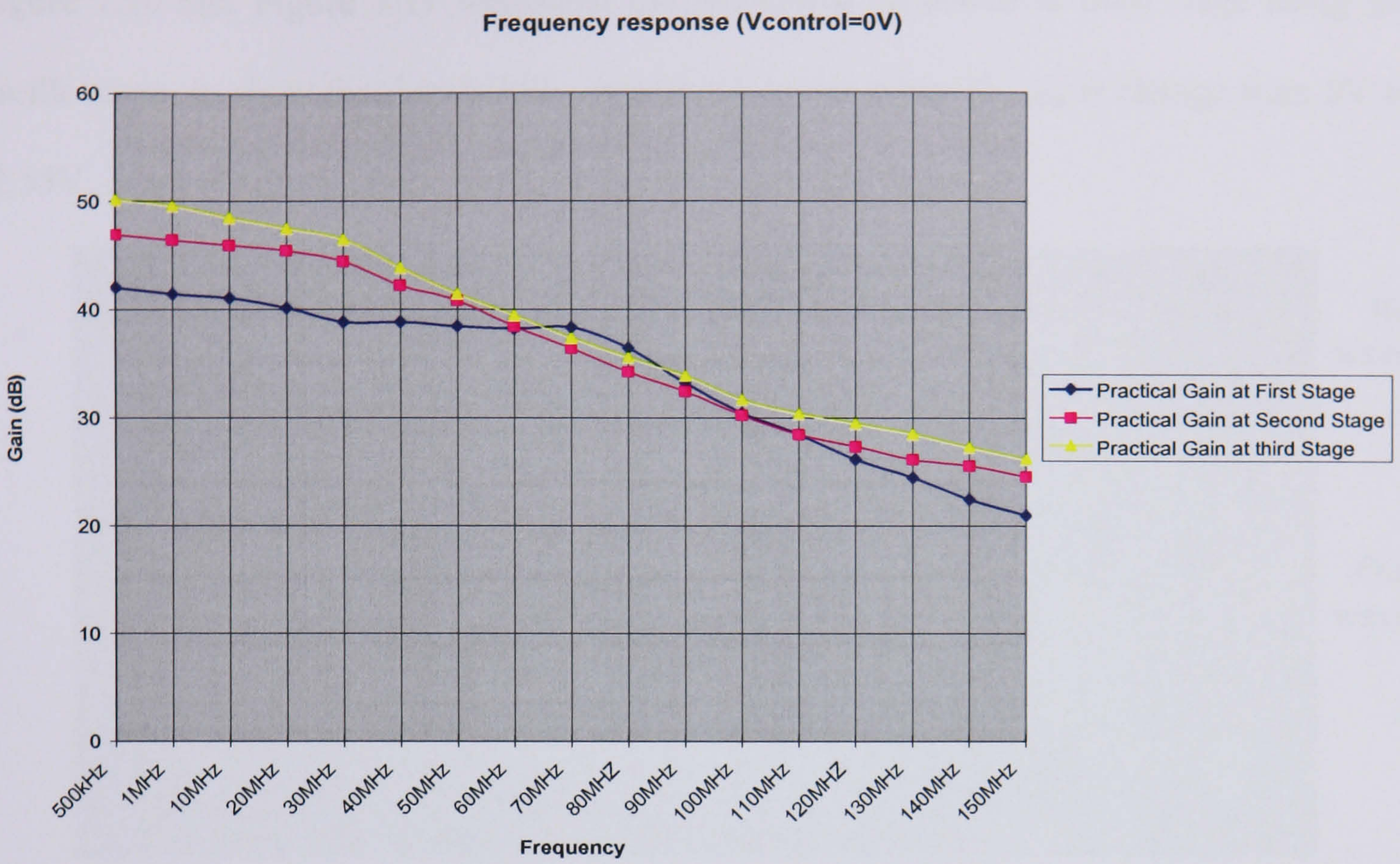

Figure 7.8 Frequency response when $V_{control}$ =0V

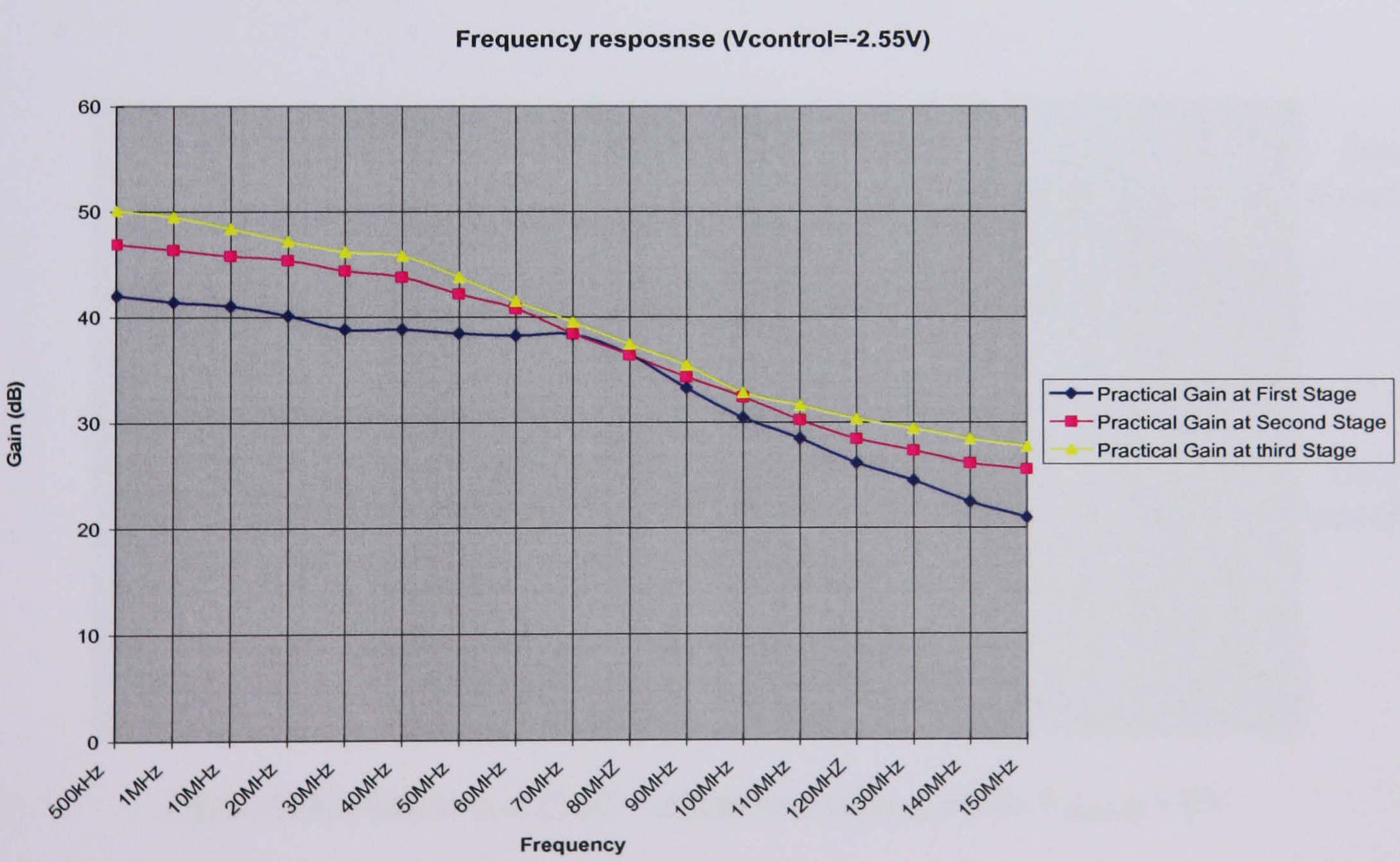

Figure 7.9 Frequency response when $V_{control}$ = -2.55V

Figure 7.10 and Figure 7.11 illustrated the waveform measured at third stage using the oscilloscope, to show that bandwidth adjustment occurs when $V_{control}$ is change from 0V to -2.55V.

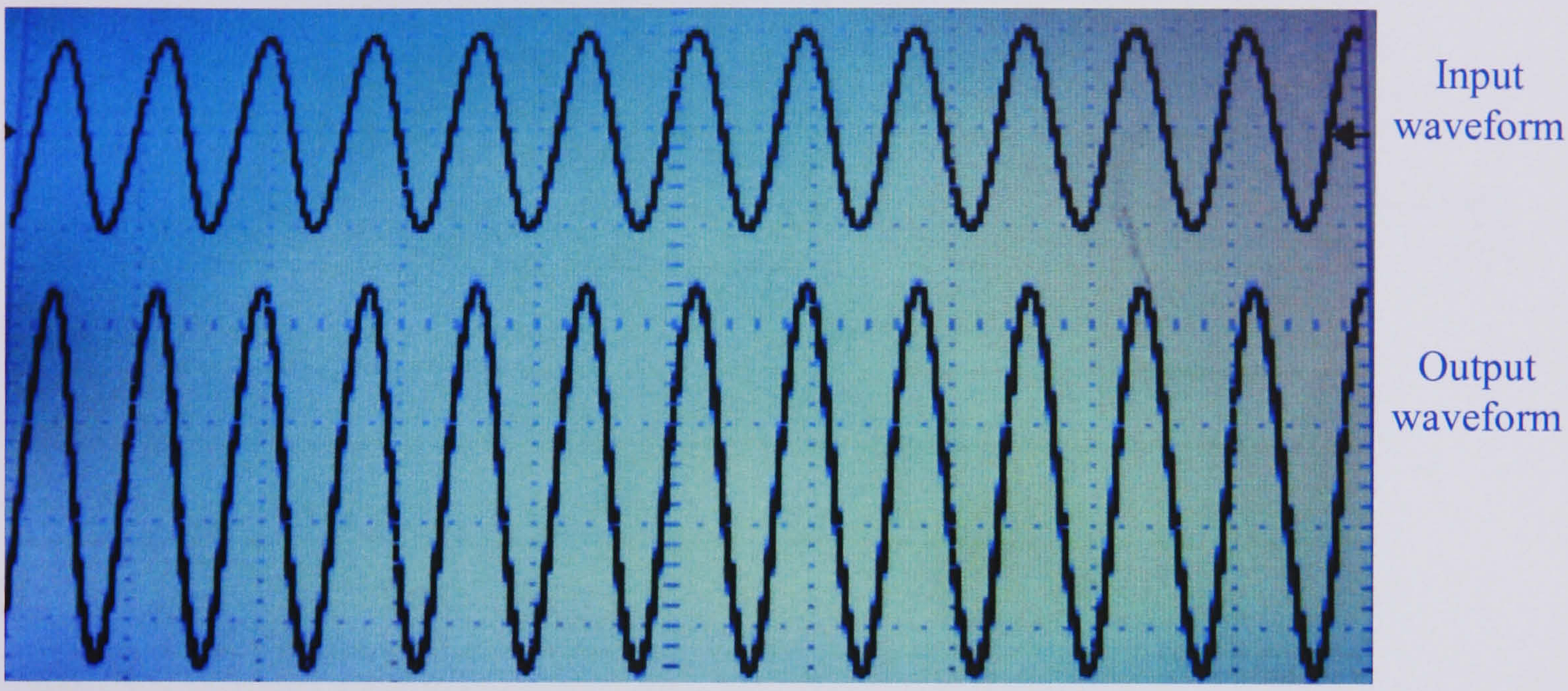

CH1=100mV/division CH2 = 200mV/division, when $V_{control}$ = -2.55V

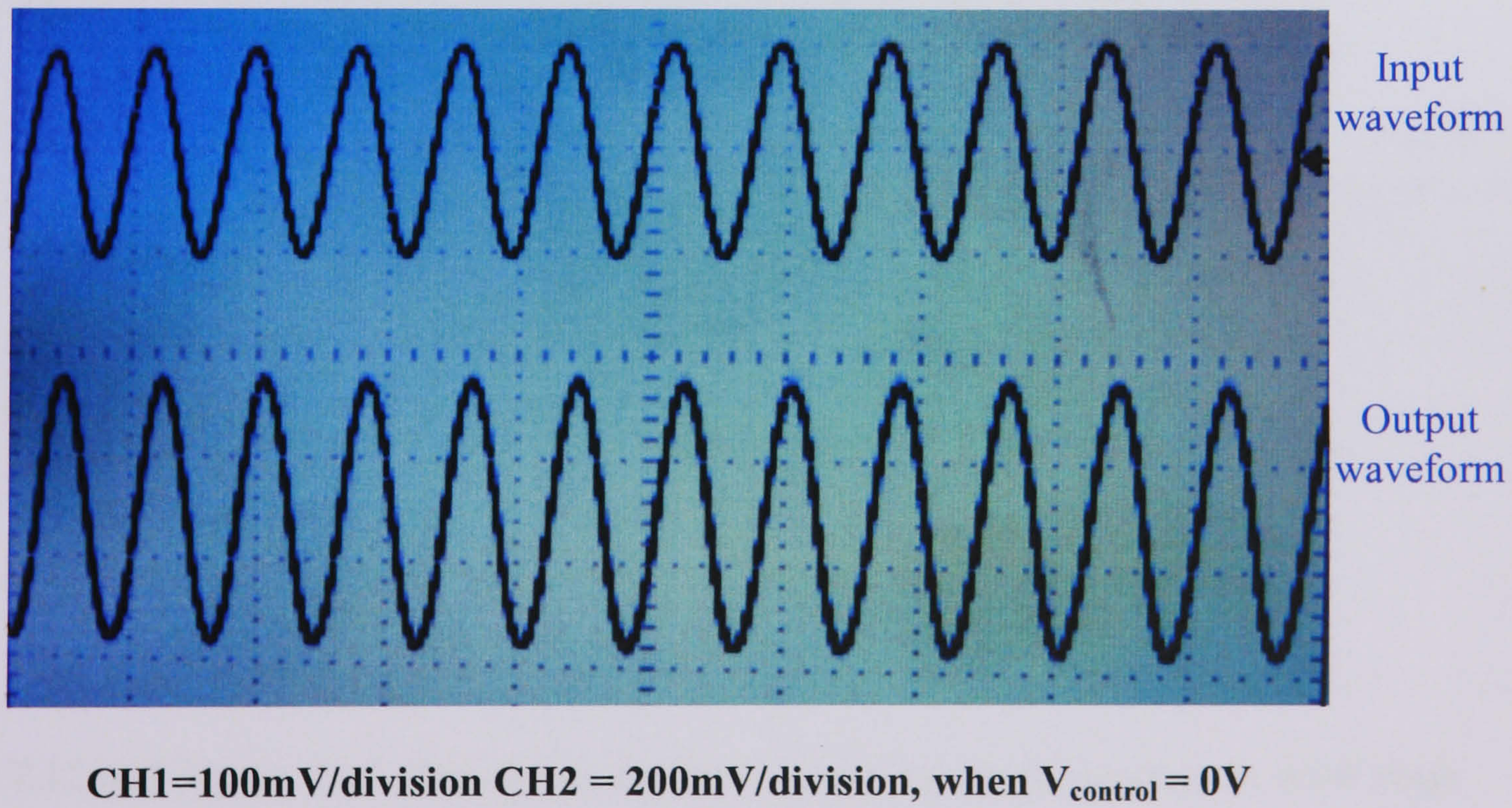

CH1=100mV/division CH2 = 200mV/division, when $V_{control}$ = 0V

Figure 7.10 Output waveform from oscilloscope when F = 50MHz

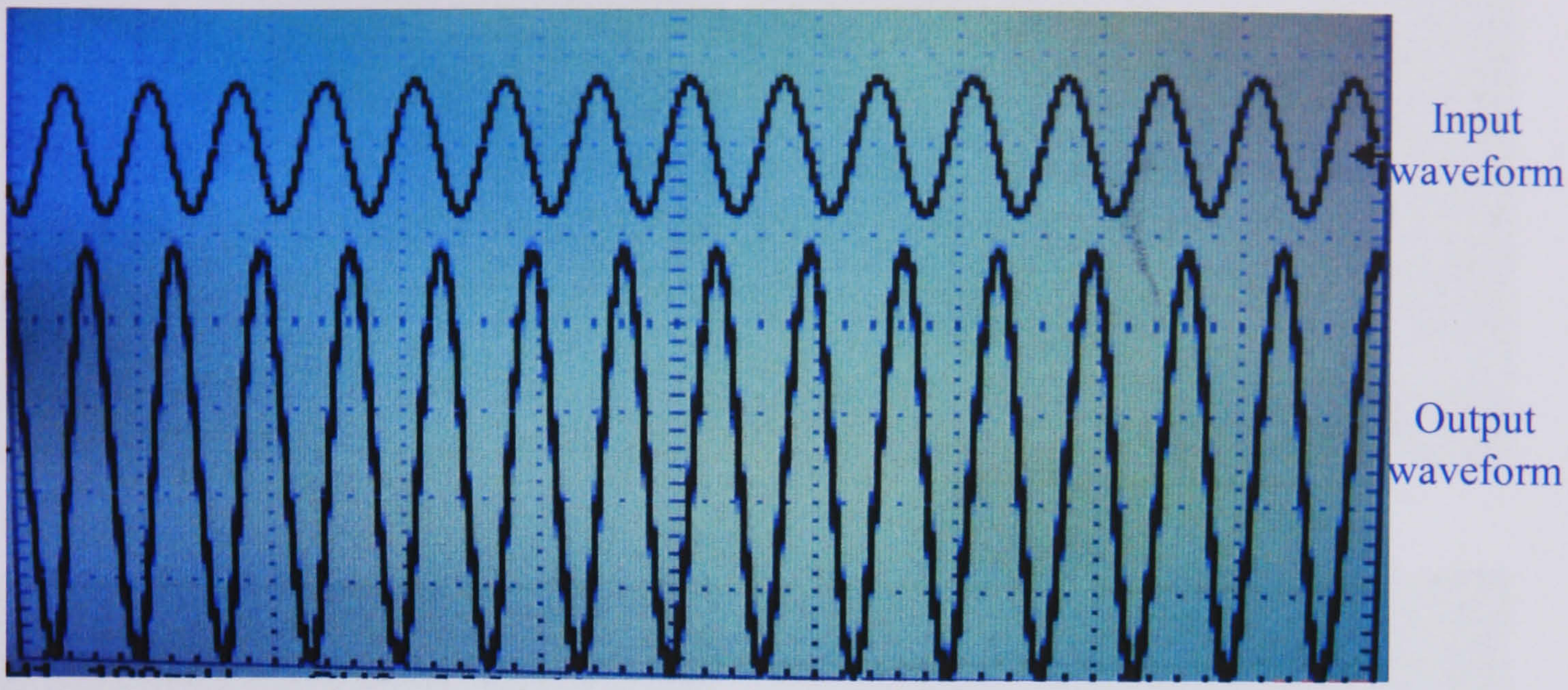

CH1=100mV/division CH2 = 200mV/division, when $V_{control}$ = -2.55V

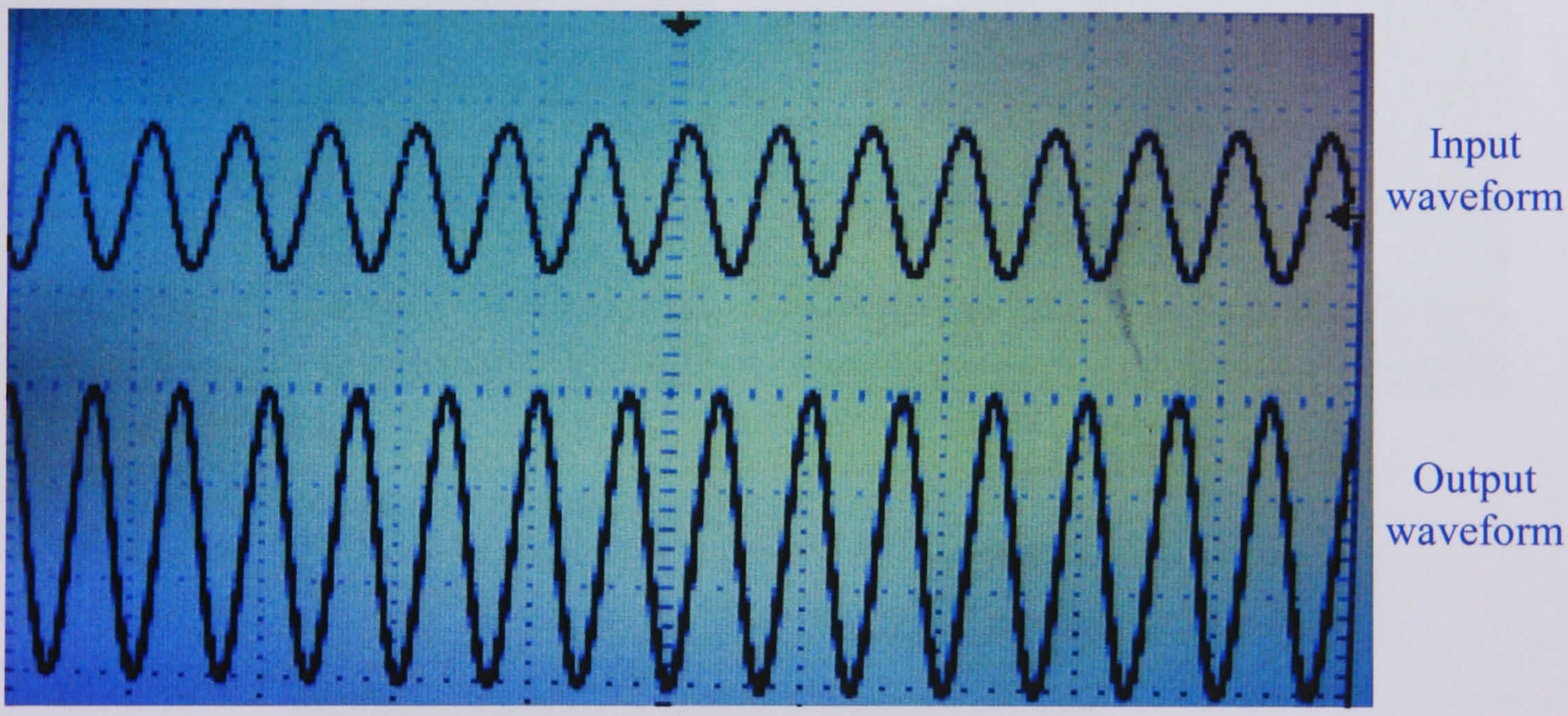

CH1=100mV/division CH2 = 200mV/division, when $V_{control}$ = 0V

Figure 7.11 Output waveform from oscilloscope when F = 60MHz

Figure 7.12 and Figure 7.13 illustrates a series of output spectrum measure at third stage using a spectrum analyser for the frequency range of 50MHz to 90MHz, to demonstrate that bandwidth adjustment occurs when $V_{control}$ is change from 0V to -2.55V.

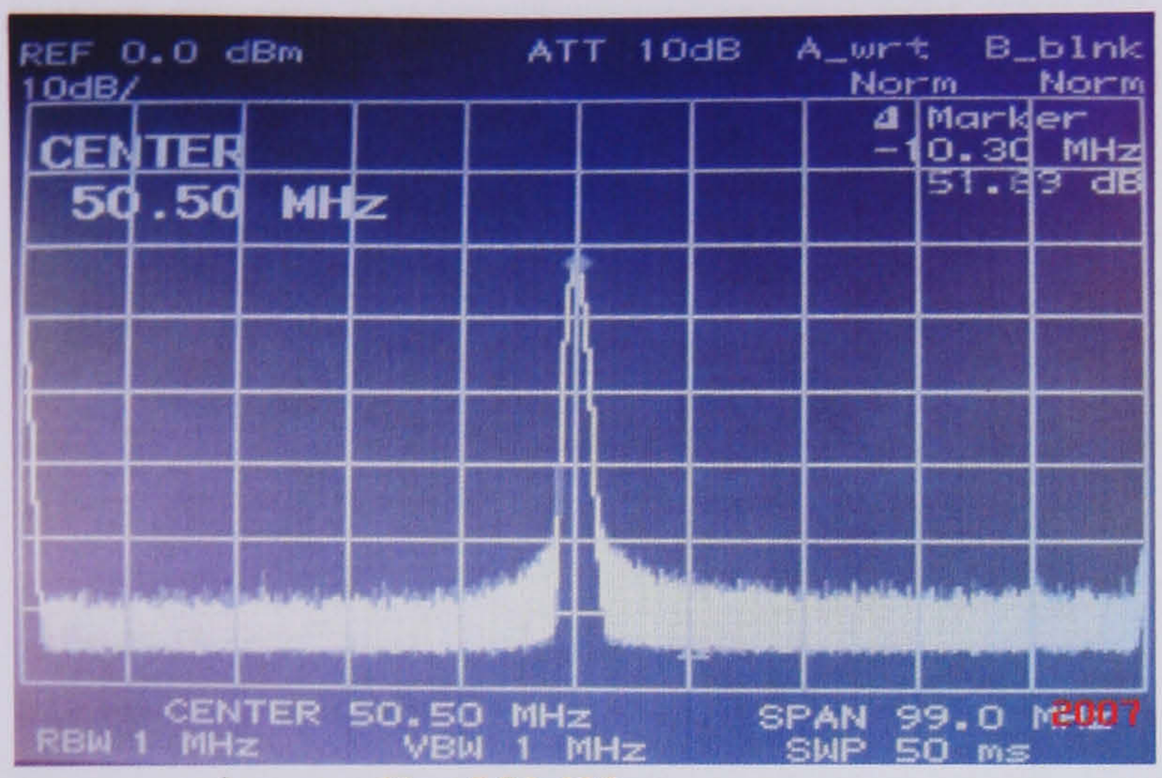

a) F= 50MHz

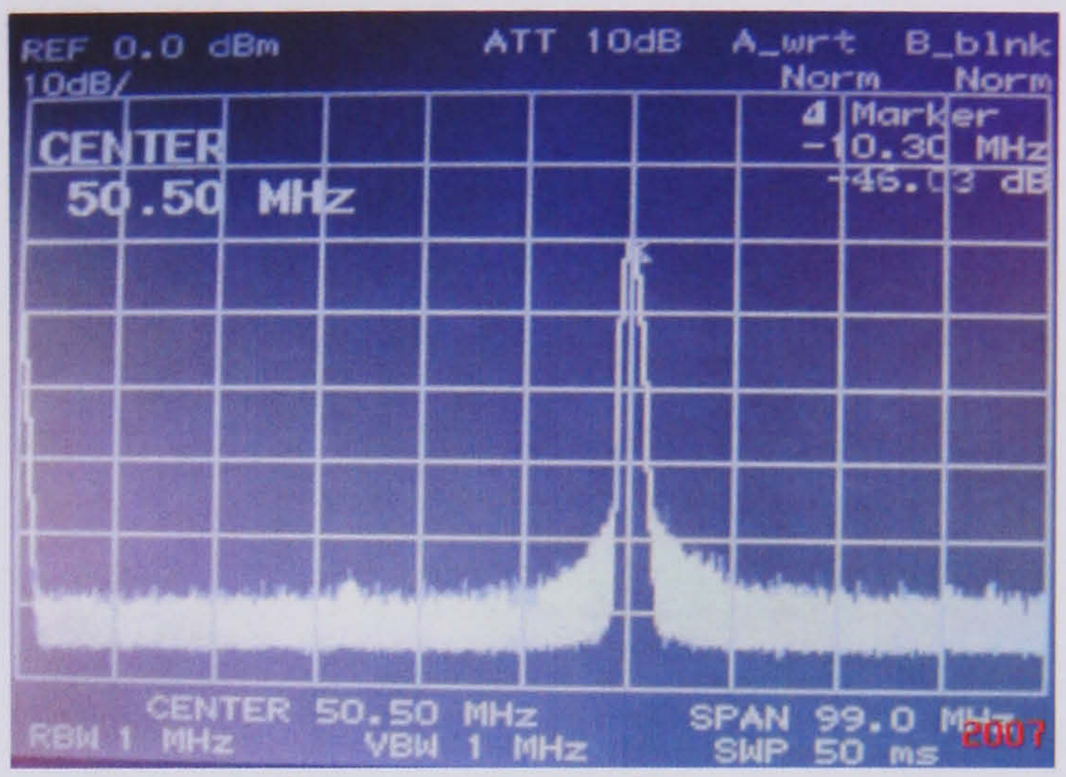

b) F=60MHz

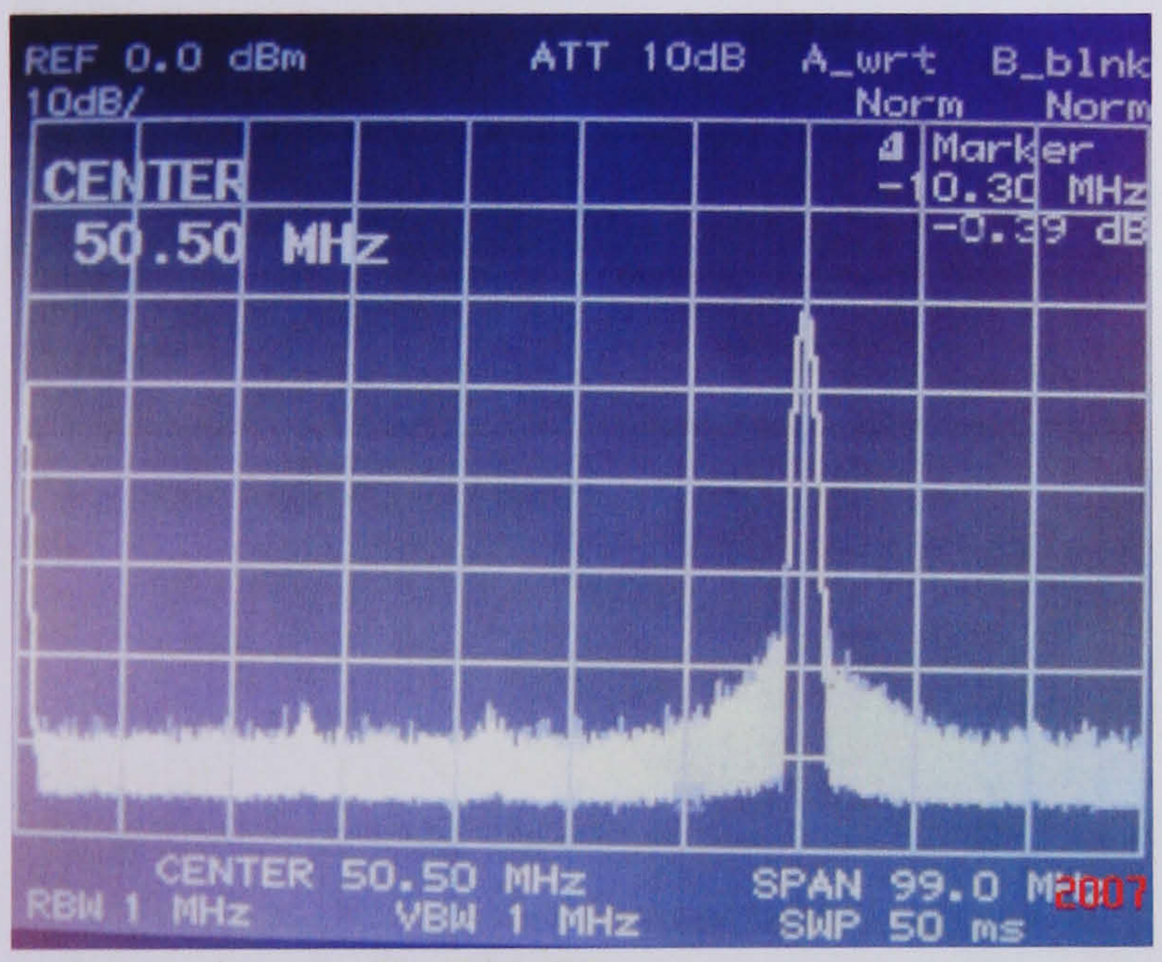

c) F=70MHz

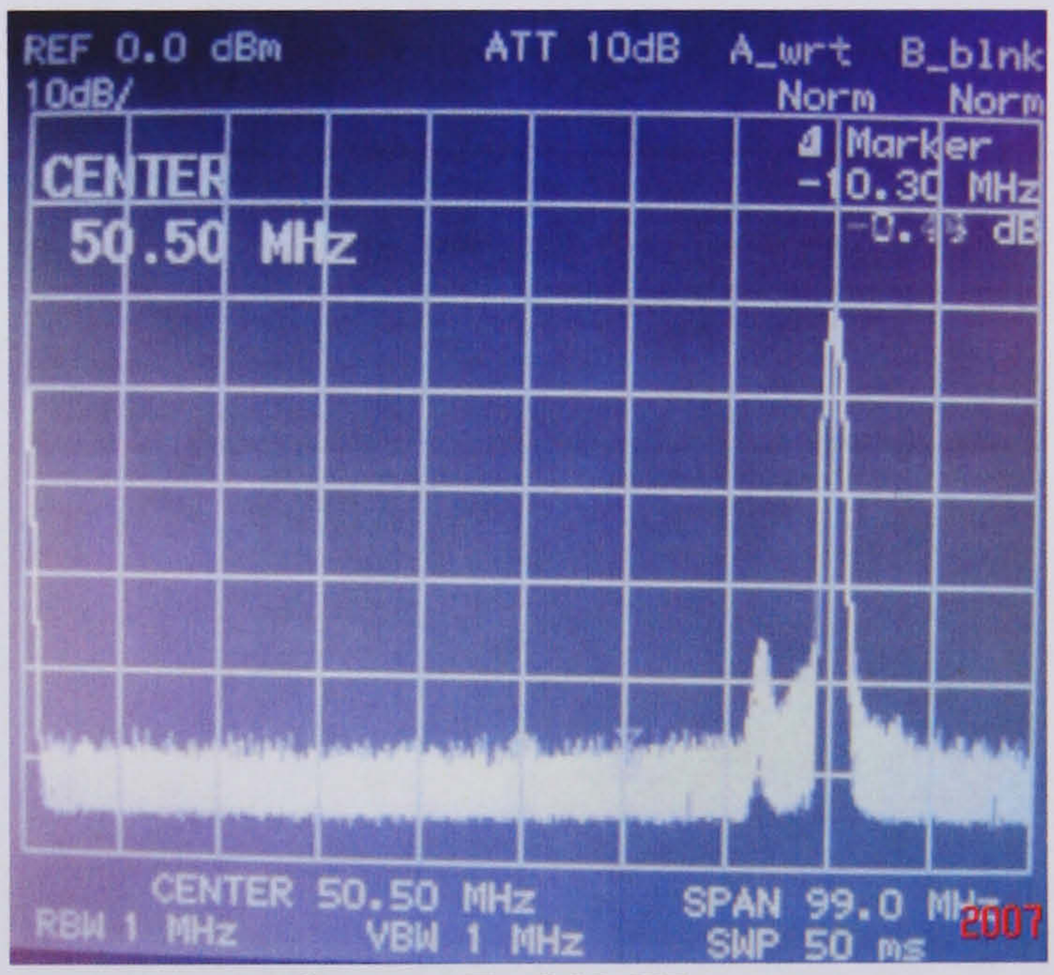

d) F=80MHz

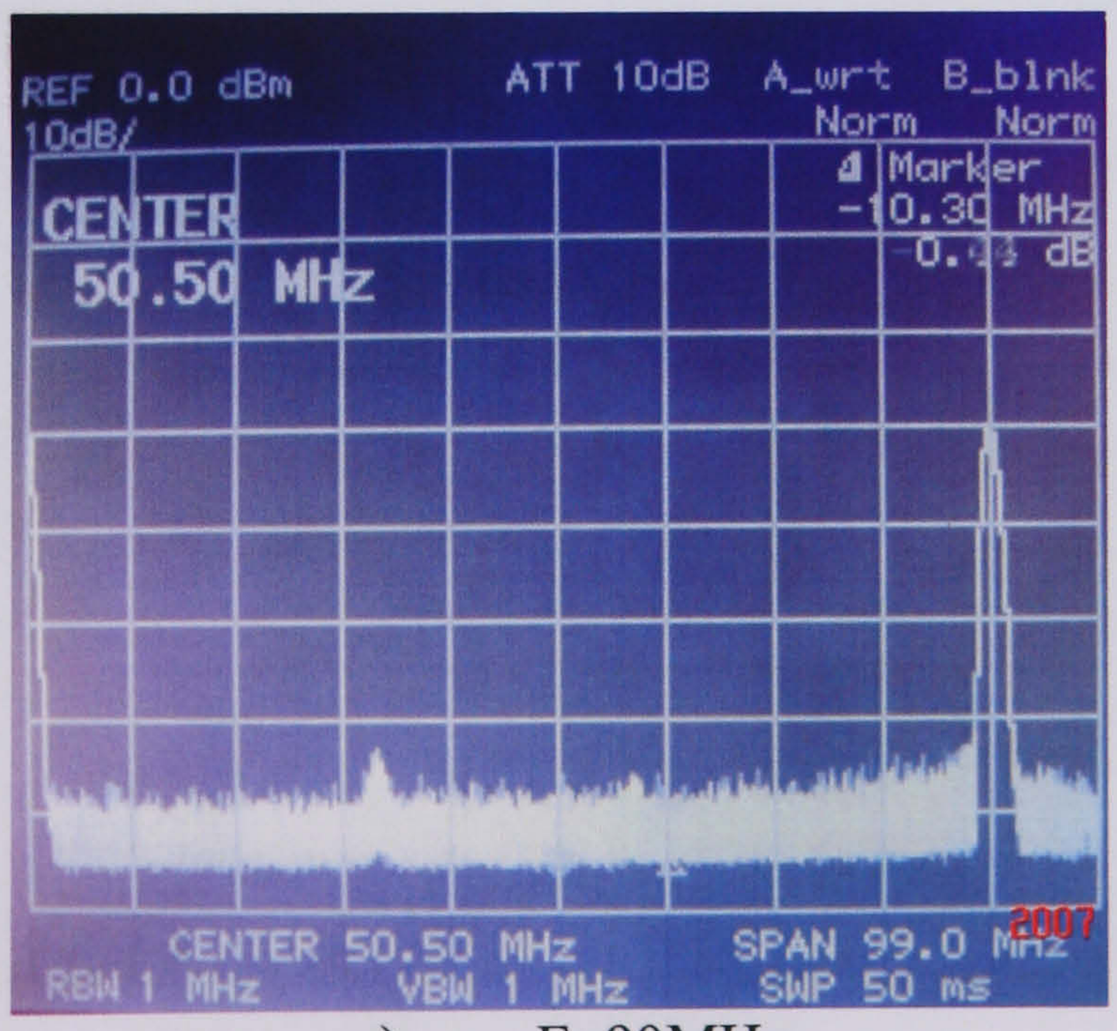

e) F=90MHz

Figure 7.12 Output spectrum when $V_{control}$ = -2.55V

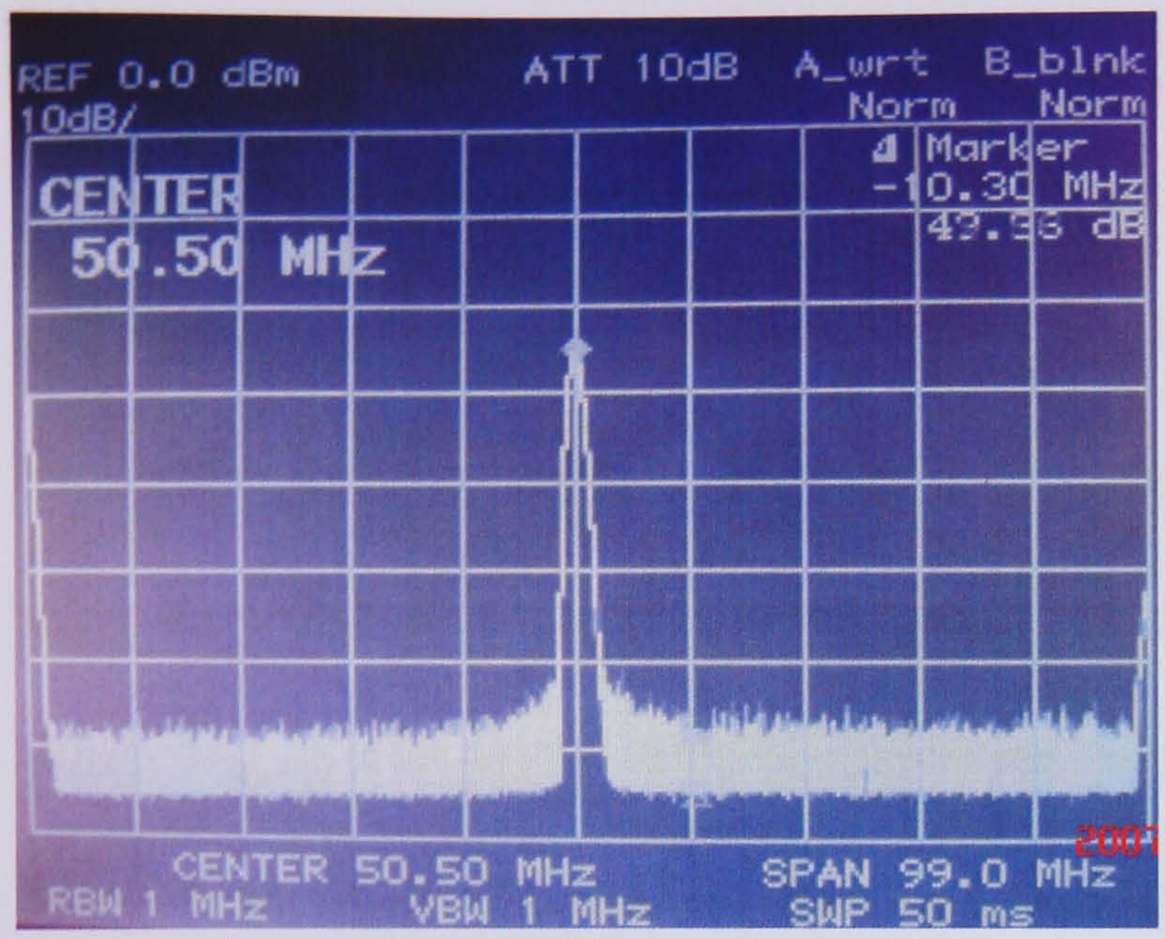

a) F= 50MHz

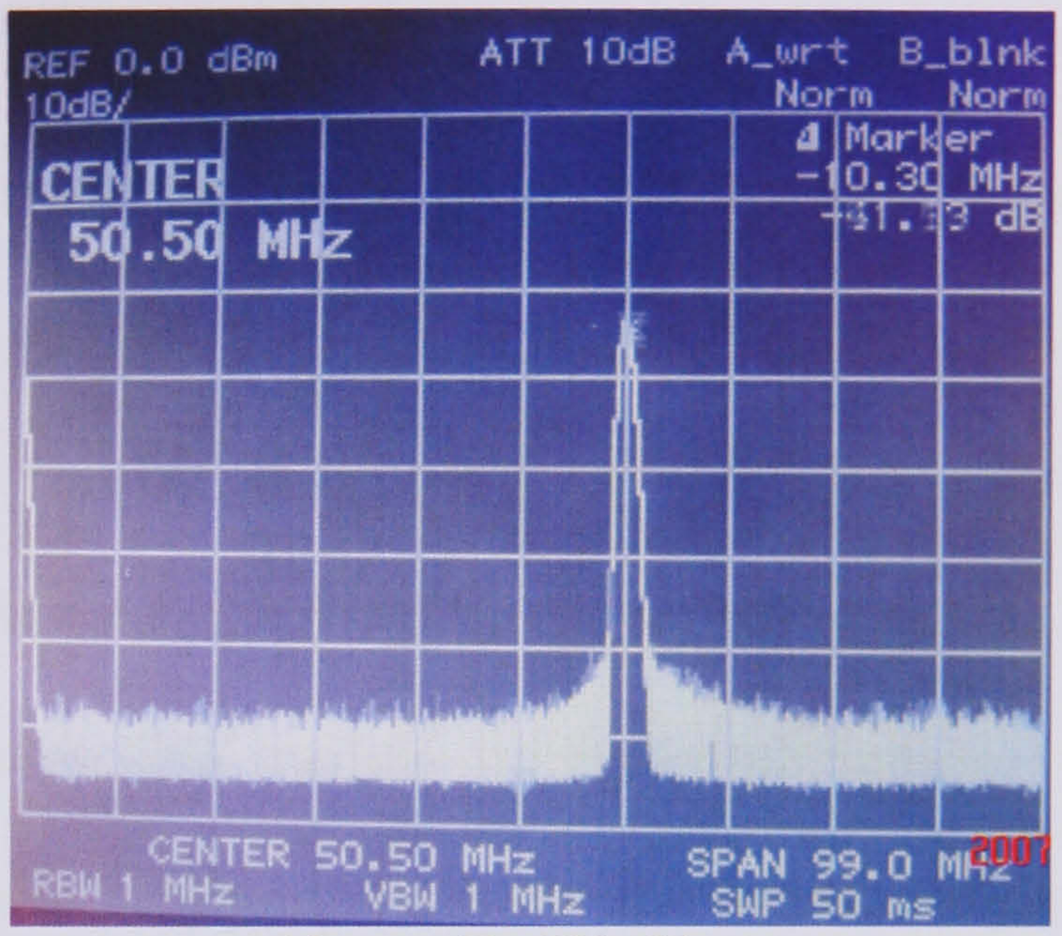

b) F=60MHz

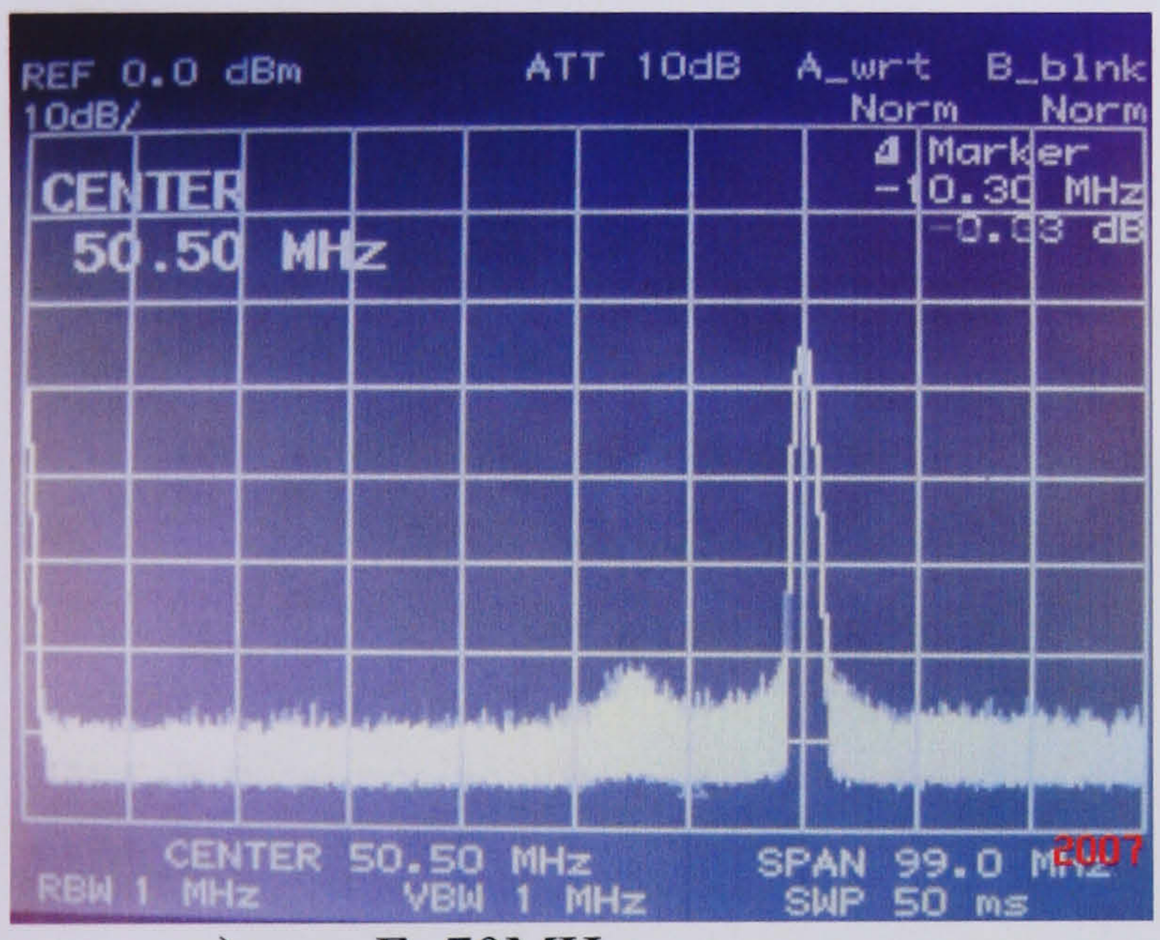

c) F=70MHz

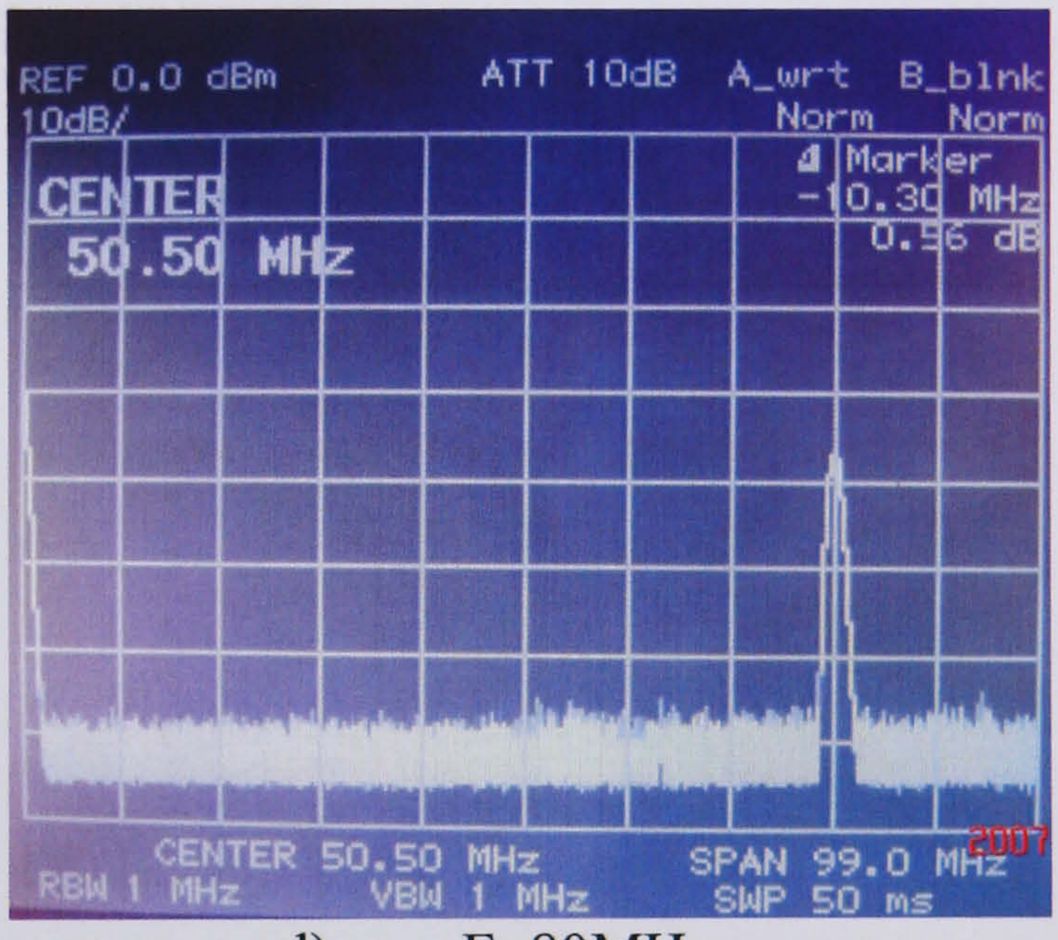

d) F=80MHz

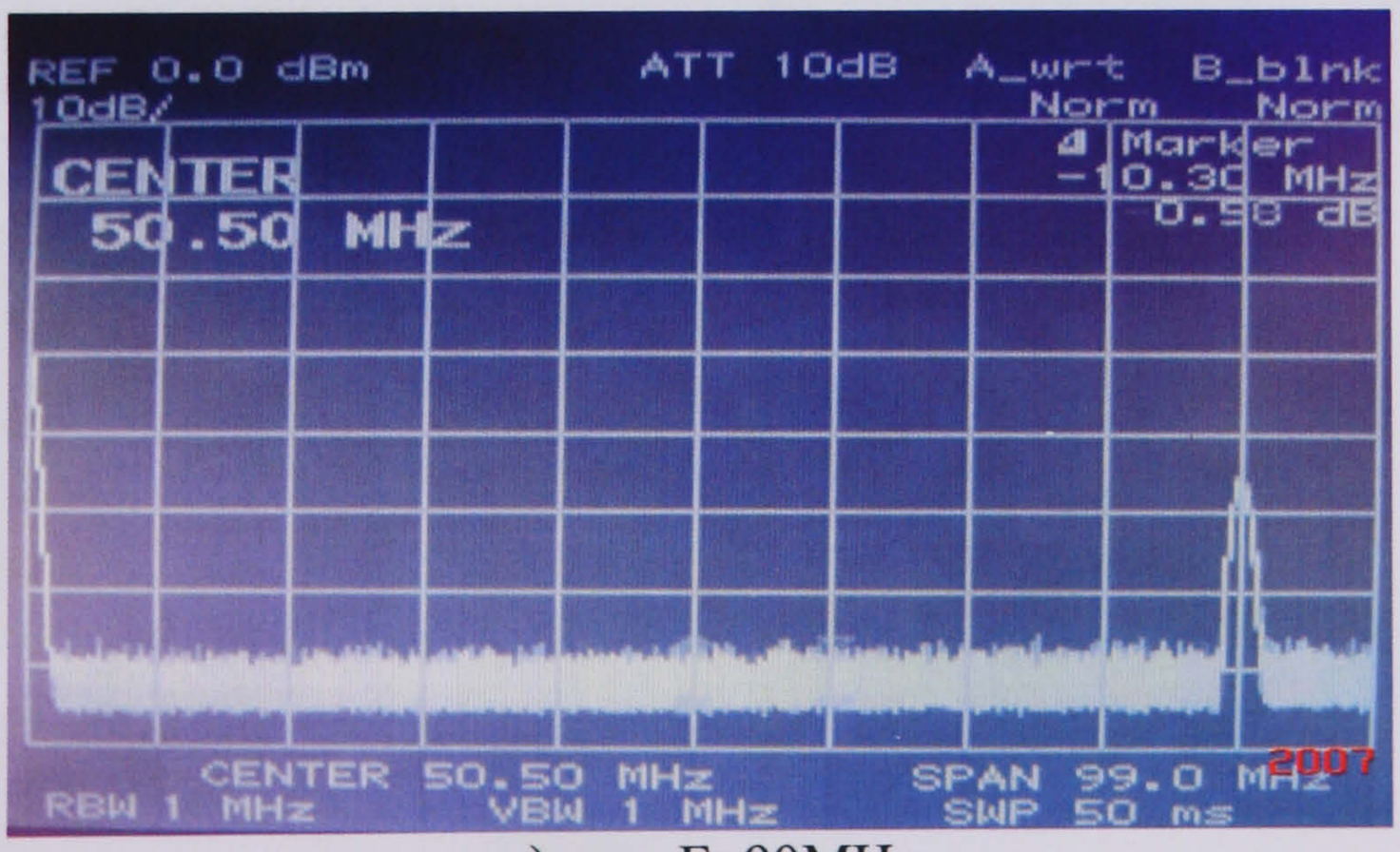

e) F=90MHz

Figure 7.13 Output spectrum when $V_{control}$ = 0V

Comparisons between the practical results and simulated results are shown in Figure 7.14 and Figure 7.15. Figure 7.14 shows that there is a difference in at least 2 - 4dB in gain and bandwidth difference of 31MHz for first stage, 10MHz for second stage and 4.8MHz for third stage between the measured frequency response compared to the simulated results. When $V_{control}$ was set to -2.55V, generated from the SNR module, the measured frequency response in Figure 7.15 shows that there was also a bandwidth variation of 31MHz for first stage, 23MHz for second stage and 14MHz for third stage compared to the simulated results, whilst the gains remain unchanged.

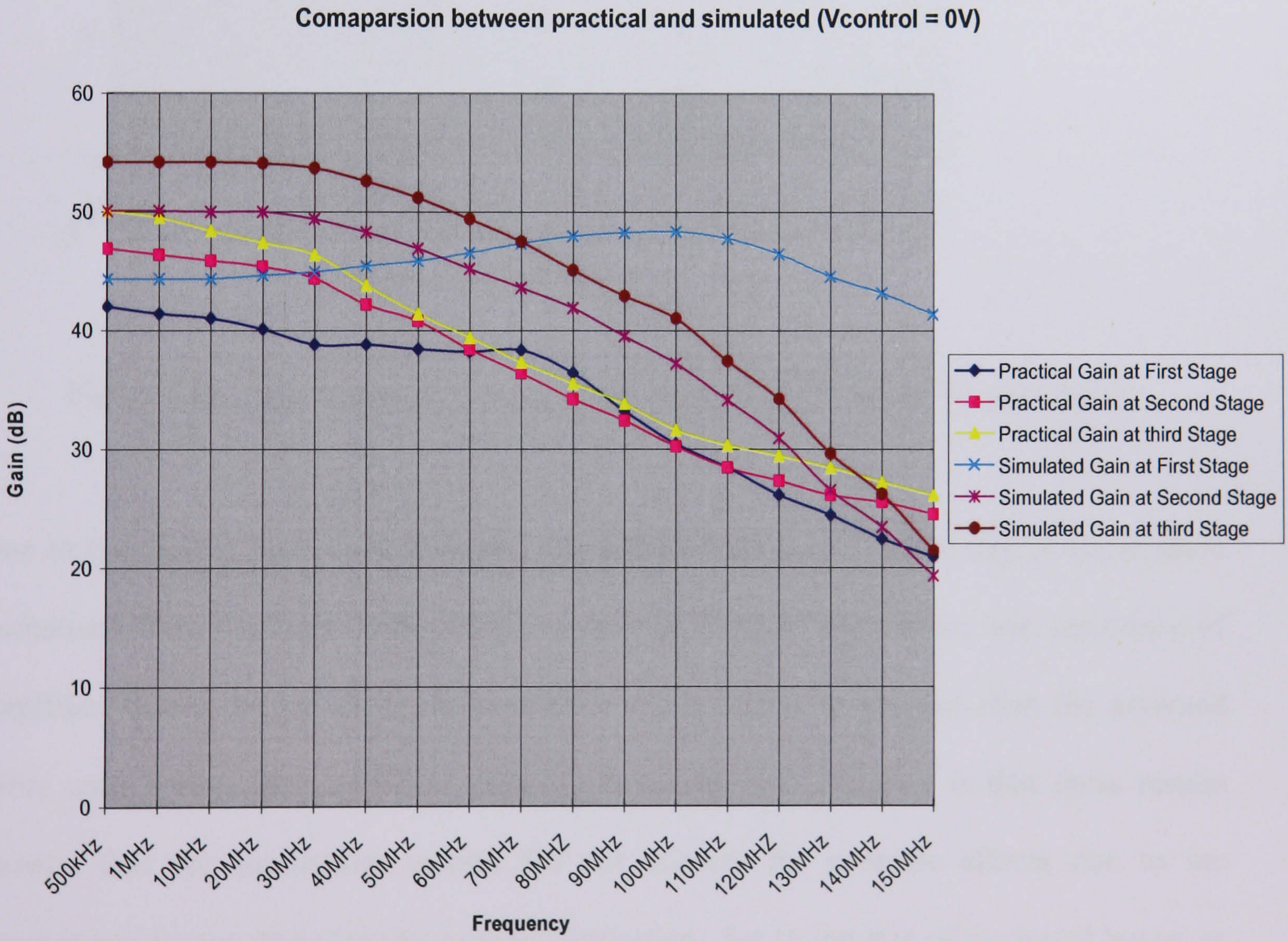

Figure 7.14 Comparison between simulated and practical for $V_{control}$=0V

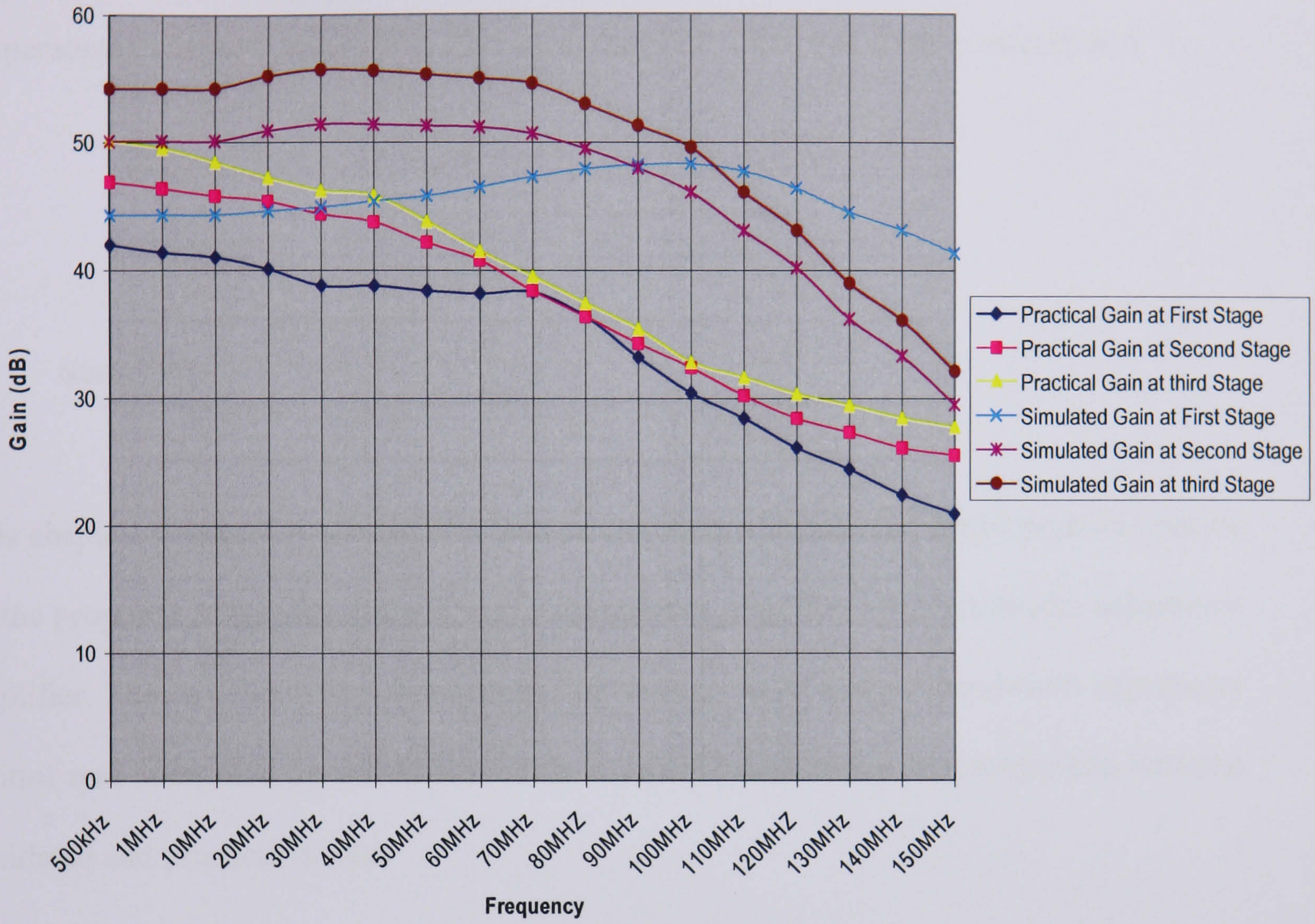

Figure 7.15 Comparison between simulated and practical for $V_{control}$=-2.55V

One of the factors that could have severely affected the bandwidth is due to capacitance limitations from the laser diode and photodetector, internal capacitance and resistance of amplifier, where the values could have been much higher in practice than the assumed value used during the simulation. Another factor for this variation is that these results showed that the simulations results did not account for parasitic effects due to the components layout, trace lengths ground connection, due to the size of the board layout as recommended by National Semiconductor for the integrated chip to operate at full

performance should be 1.5" x 1.5", wires connection had high parasitic inductance that limits the amplifier's bandwidth at high frequencies, mismatch of SMA connectors and capacitive loading from test probes will change circuit performance drastically or temperature variations, and so it is likely that the bandwidth was quite overestimated.

7.3 Summary

This chapter presented a comparison between simulated results and tested practical results on the proposed composite technique transimpedance amplifier with bandwidth adjustment amplifier. The two amplifiers were integrated with an AGC and the bandwidth adjustment control was controlled by the SNR module. Table 7.1 summarise the comparison between simulated and practical results.

Table 7.1 Comparison between simulated and practical results

	$V_{control}$ =(0V)				$V_{control}$=(-2.55V)			
	Simulated		Practical		Simulated		Practical	
	Gain	Bw	Gain	Bw	Gain	Bw	Gain	Bw
First Stage	44dB	116MHz	42dB	85MHz	44dB	116MHz	42dB	85MHz
Second Stage	50dB	50MHz	46dB	40MHz	50dB	75MHz	46dB	52MHz
Third Stage	54dB	43MHz	50dB	38MHz	54dB	72MHz	50dB	58MHz

The measured gain is consistent with the simulated results for $V_{control}$ = 0V and $V_{control}$ = -2.55V which is predicted ranging from 40dB to 55dB. The results showed a slight variation of 4dB compared to the simulated results. In contrast the bandwidth measurement showed a variation of around 4.8MHz to 31MHz compared to the simulated results for $V_{control}$ = 0V, but a higher variation of around 14MHz to 31MHz was observed when compared the simulated results for $V_{control}$ = -2.55V. This variation is due to the fact that the simulation results had not taken into account capacitances and inductances generated from layout aspects, which limited the frequency response. Despite the techniques taken into account in the fabrication process to minimise the capacitances produced around the circuits, stray capacitances still existed.

References

[7.0] "Single High Speed Operational Amplifier evaluation boards" (SOIC and SOT), National Semiconductor, 2003

[7.1] LMH6504, SOIC-8 evaluation boards, National Semiconductor, 2004.

Chapter 8

Conclusions and Further Work

8.1 Summary of the work

As portable computers and communication terminals become more powerful and are more widely deployed, the demand for high-speed wireless networks is increasing. An optical wireless transmission technique represents an attractive choice for many indoor and outdoor applications. Its advantages include the availability of a wide bandwidth that is unregulated worldwide, and that can be reused in a very dense fashion, immunity to eavesdropping, the ability to achieve very high bit rates, low signal-processing complexity, and potentially very low cost. However, some problems remain which need to be solved in this field. This thesis has discussed the design of transimpedance amplifiers for use in

infrared optical wireless, in particular being concerned with how to be able to adjust the bandwidth of a receiver properly according to the dynamic service quality of the incoming signals. The approach to the discussion had been from two perspectives, firstly that of the circuit, and second by that of the input current and voltage noise analysis.

In terms of the circuit perspective, this thesis looked at alternative topologies and a combination of mixed techniques to achieve the receiver criteria: wide dynamic range, bandwidth enhancement and low noise operation. The receiver designed has two parameter adjustment characteristics. The first is an automatic bandwidth adjustment which is controlled by the signal to noise ratio of the input signal. The output from the bandwidth adjustment amplifier is considered to have a low noise level. The benefit of controlling the bandwidth is that it improves receiver sensitivity by rejecting out-of-band noise without the need for additional filtering. The second element taken into consideration is the variable gain adjustment, which automatically monitors and level adjusts any changes from the input signal of the receiver front-end.

In terms of bandwidth enhancement, this thesis shows that the bootstrap transimpedance amplifier exhibits the highest range of bandwidth adjustment and gain. The dual feedback loop amplifier with VFA, and VFA with CFA also produces high bandwidth adjustment, but have the lowest gain. This thesis has also taken an detailed look at the analysis and design process itself. The discussion includes mathematical modeling of the transfer function for each of the proposed transimpedance amplifier structures. The transimpedance amplifier serves as an excellent vehicle for this discussion because of its demanding

requirements and complex design trade-offs typify the challenges faced in analogue circuit design.

In the perspective view of noise analysis, this thesis has taken into consideration all the major noise affecting an infrared optical wireless receiver. It has shown that the relatively rapid increase of noise, due to the terms proportional to the square and cube of the receiver bandwidth, is the limiting factors in achieving low-noise performance. Simulated results of output noise spectral density show that the design using a bootstrapped transimpedance amplifier exhibits the lowest noise level. Unfortunately this configuration exhibits highest noise when working together with an AGC circuit. This shows that each circuit technique has its own best capabilities, and integration with other circuit functions could reduce the best performance obtained.

8.2 Applications of this research

Integration of radio and optical technology, and integration of wired and wireless communication technology, will increasingly progress in future. In next generation high-speed all-digital networks, an optical wireless communication technique will be more important than now. Optical wireless communication is attractive in many indoor and outdoor applications, such as short-range high speed data transmission, telemetry, video broadcasting, fixed wireless access networks, inter-satellite links, and so on. For example, a

future "all-intelligent" optical home network concept is shown in Figure 8.1 and the principles of wireless optical in seat entertainment shown in Figure 8.2.

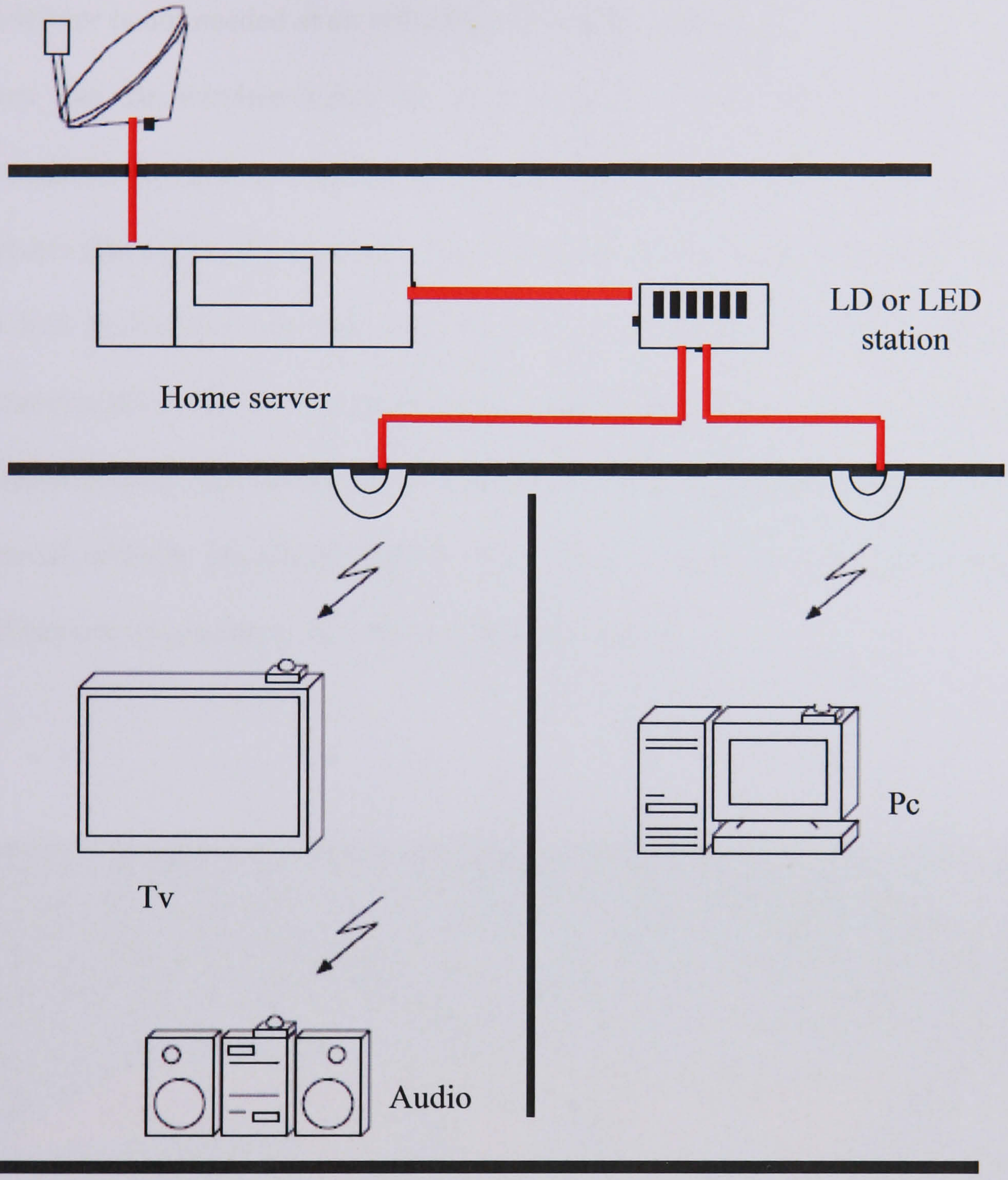

Figure 8.1 Suggested intelligent indoor all-optical home networks

The digital data from an external network are stored in a home server, which has an optical modulation unit, composed of many LEDs or LDs. The required data are modulated at a home server and are distributed in each room using the diffuse method. In a room, optical

signals are amplified with an optical preamplifier and are emitted into the air. Therefore, in all optical home networks, optical access points in each room are simple because a modulator is not needed at an optical access point. Therefore, all electrical appliances in the home can be wireless-linked to each other in future. These wireless systems exist throughout our home, ranging from short-distance point-and-shoot systems to cellular systems that cover whole rooms. These devices automatically select the link which offers the best performance at that time. As we roam through our home taking our portable communicator with us, it remains linked to the network by seamlessly switching between different rooms. All rooms are interconnected within our home and linked to the high-speed external network via plastic optical fibre. Thus, optical wireless communication systems will become increasingly important in the near future.

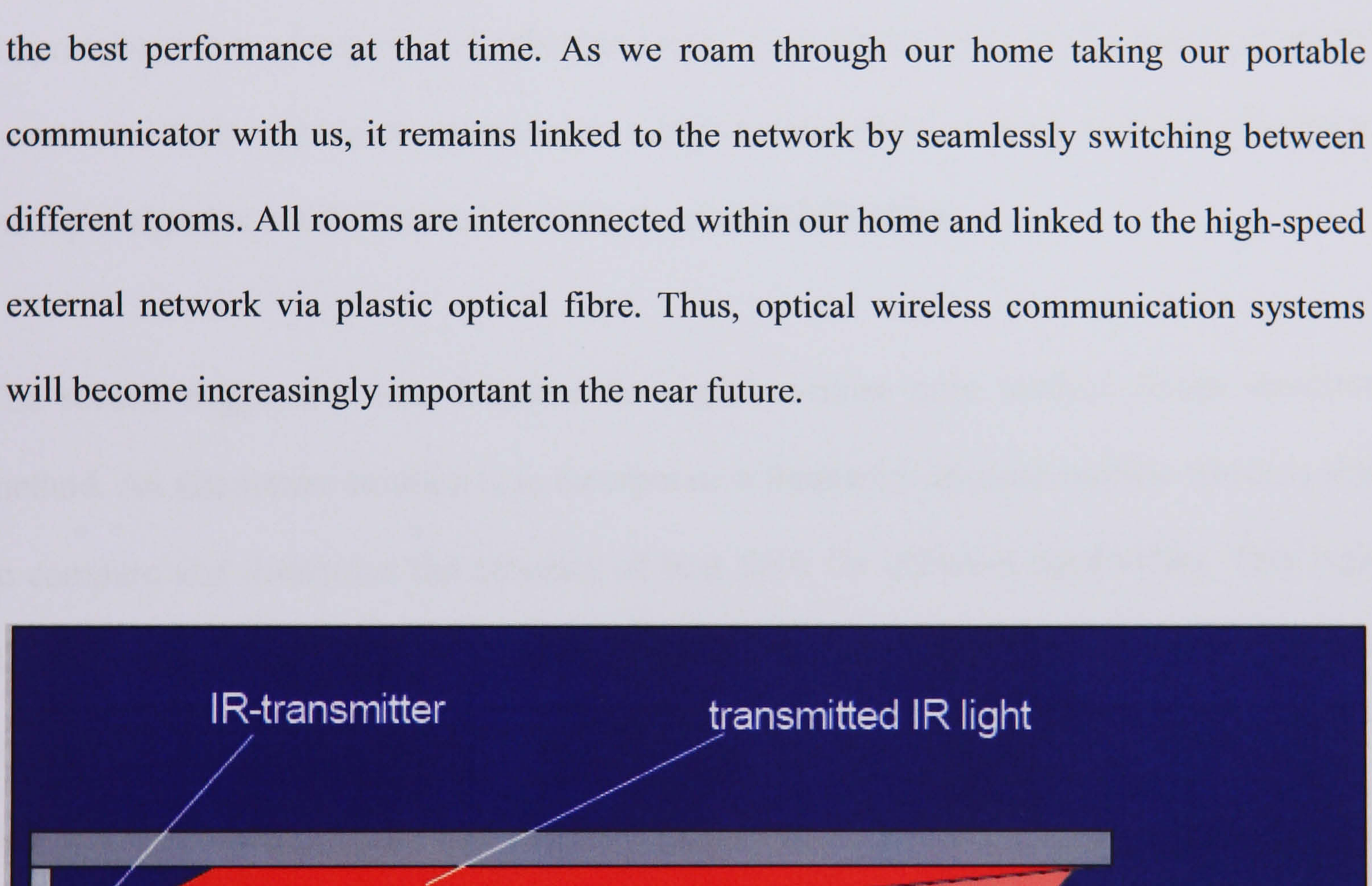

Figure 8.2 Principles of wireless optical in seat entertainment [8.1]

8.3 Future improvements and suggestions for further work

There are numerous directions for future work concerning the discussed designs of transimpedance amplifiers receivers with automatic bandwidth adjustment and AGC. The first suggestion is to look into the differential transimpedance amplifiers topologies with automatic bandwidth adjustment. The advantages of using differential topologies are its suppressing effect of supply and substrate noise, since photodiodes produce a single-ended current and their cathode is connected to a high voltage to allow high quantum efficiency, the input signal is not differential, leading to several difficulties.

The second suggestion is to improve the signal-to-noise ratio module design detection method. An alternative solution is to incorporate a frequency decision module which is able to compare and determine the category of best SNR for different bandwidths. This logic decision from the module would then be able to activate different voltage control sources that set the bandwidth adjustment amplifier. The only concern with this method is the fact that the bandwidth adjustment amplifier can have a minimum of five differences of bandwidth range according to its voltage control switching capability. Therefore, there would be the need to have at least five different bands of possible measured SNR.

The third suggestion is to look into the types of modulation techniques suitable for the discussed receivers, in addition to looking into the design of an intelligent transmitter that is capable of communicating with the designed receiver. For example, when the data

transmission is low, the transmitter will send a signal to the receiver to reduce its bandwidth and vice-versa.

The fourth suggestion is to design and develop a transimpedance amplifier capable of low voltage operation, for example 1V operation, without the use of low threshold devices. The idea is to maximise both the output signal swing and the bias voltage for the photodiode. A suggested topology exists is to use a sub 1V current mirror suggested by Rijins and Peluso [8.2-8.3], as shown in Figure 8.3. The current mirrors differ from a normal mirror circuit with the additional device M_1 at the input. The advantage of this circuit is much lower impedance and adjustable input voltage.

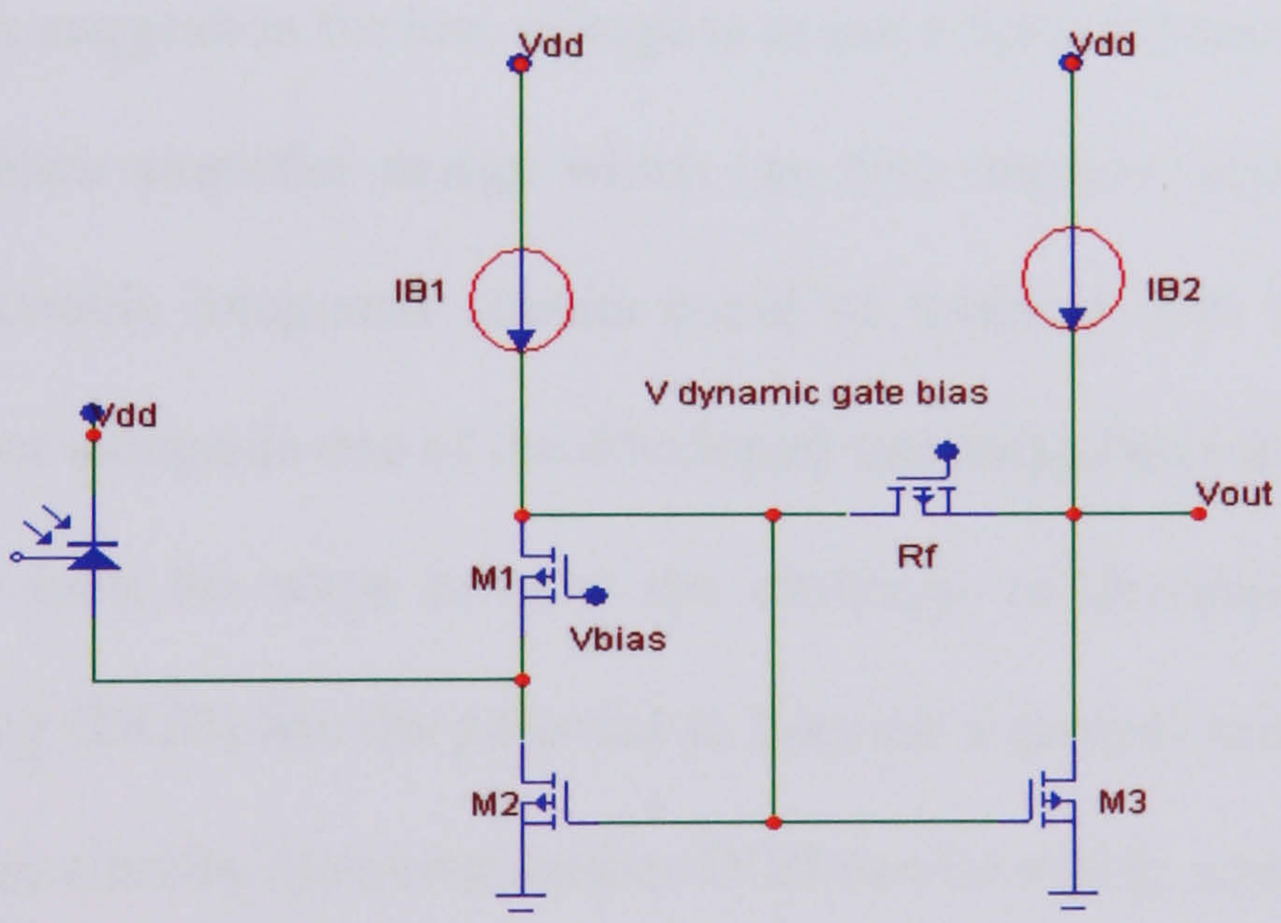

Figure 8.3 A low voltage transimpedance amplifier

An alternative topology exists in which the feedback resistor is placed directly across the input and output terminals of the current mirror as shown in Figure 8.4 [8.4]. The advantage

of this topology, however is the much lower input impedance seen by the photodiode which may potentially improve speed.

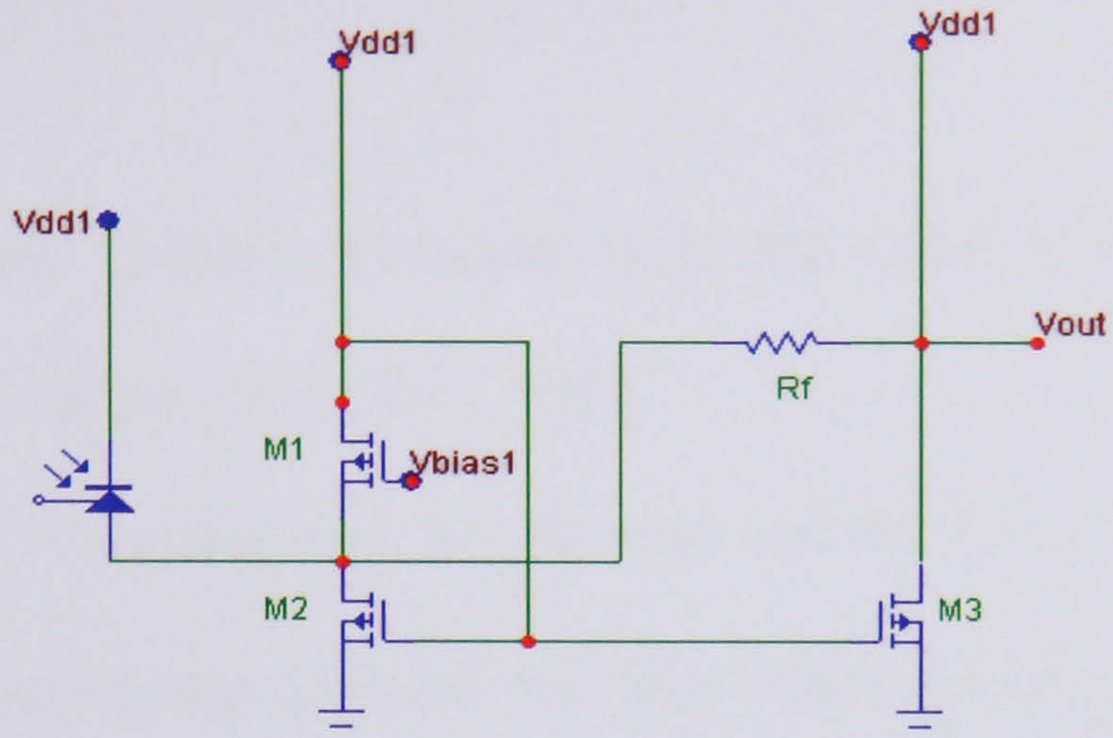

Figure 8.4 An alternative low voltage transimpedance amplifier

The final alternative suggestion for low voltage is to use a fully-differential implementation for the transimpedance amplifier design which can also improve supply noise rejection. Work into optoelectronic integrated circuits could be initiated with the integration of a CMOS photodetector alongside one of the developed transimpedance amplifier designs. As analogue designers look for ways to meet the challenge of decreased supply voltages, dynamic gate biasing (DGB) has the potential to become a general technique for realizing low voltage analogue circuits. However, before DGB can be widely applied, designers need a better understanding of the effects of charge injection and clock feed-through on circuit performance. Future work should focus on developing methods of reducing such transient effects. One example would be its use in tunable, low voltage, continuous-time filters.

References

[8.1] Nikolaus P. Schmitt, "Wireless optical NLOS communication in aircraft cabin for in flight entertainment distribution" DTI-Workshop on Photonic Wireless Communication, 2005.

[8.2] J. J. F. Rijins, "54MHz switched capacitor video channel equalize" Electronics Letters, Vol. 29, No. 25, pp. 2181-2182, 1993.

[8.3] V. Peluso, P. Vancorenland, M. Steyaert and W. Sansen,"900mV differential class AB OTA for switched opamp applications" Electronics Letters, Vol. 33, No. 17, pp. 1455-1456, 1997.

[8.4] K. Phang, "CMOS optical preamplifier design using graphical circuit analysis", Thesis, 2001.

APPENDIX

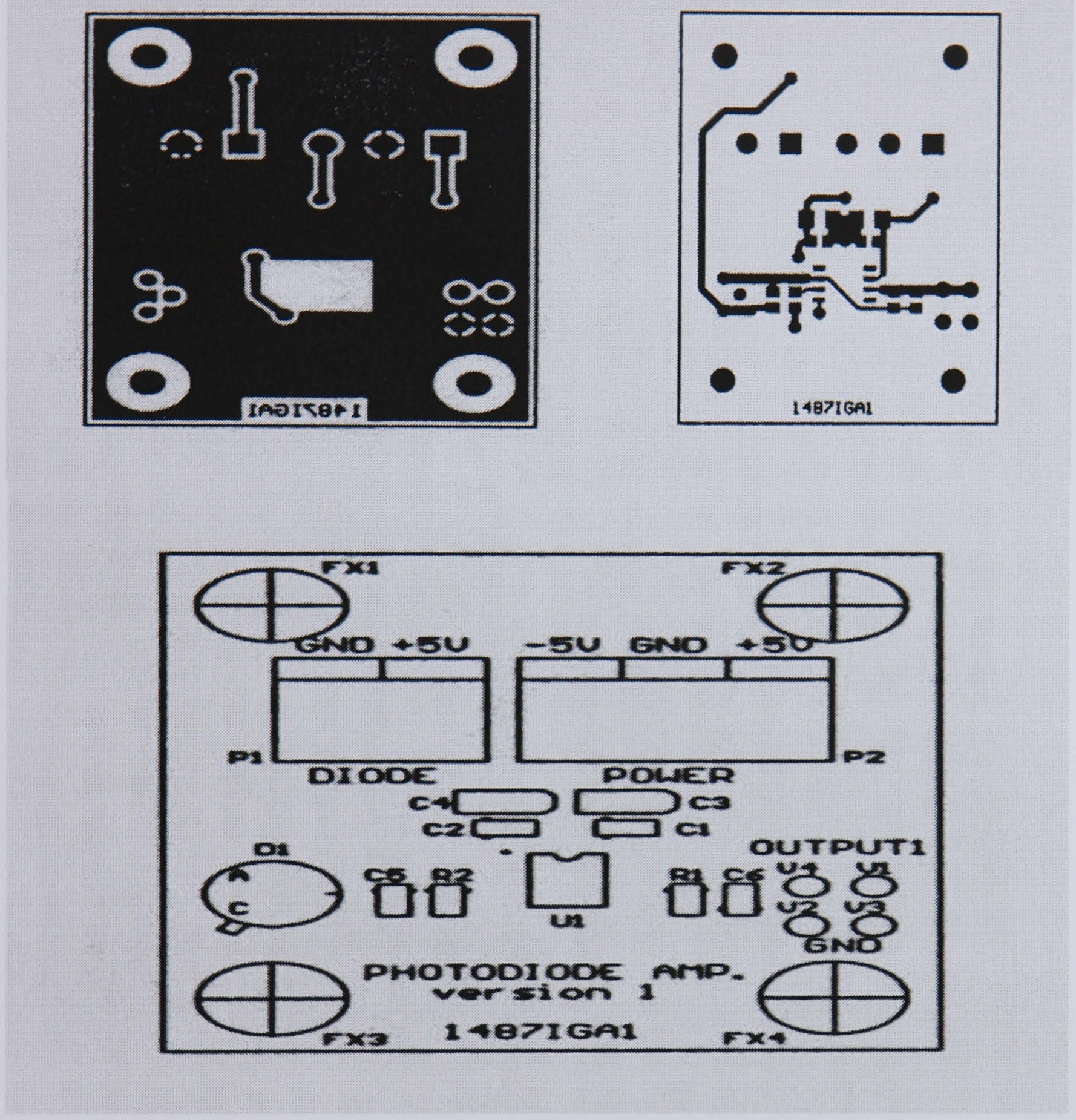

Figure : Photodiode with transimpedance amplifier

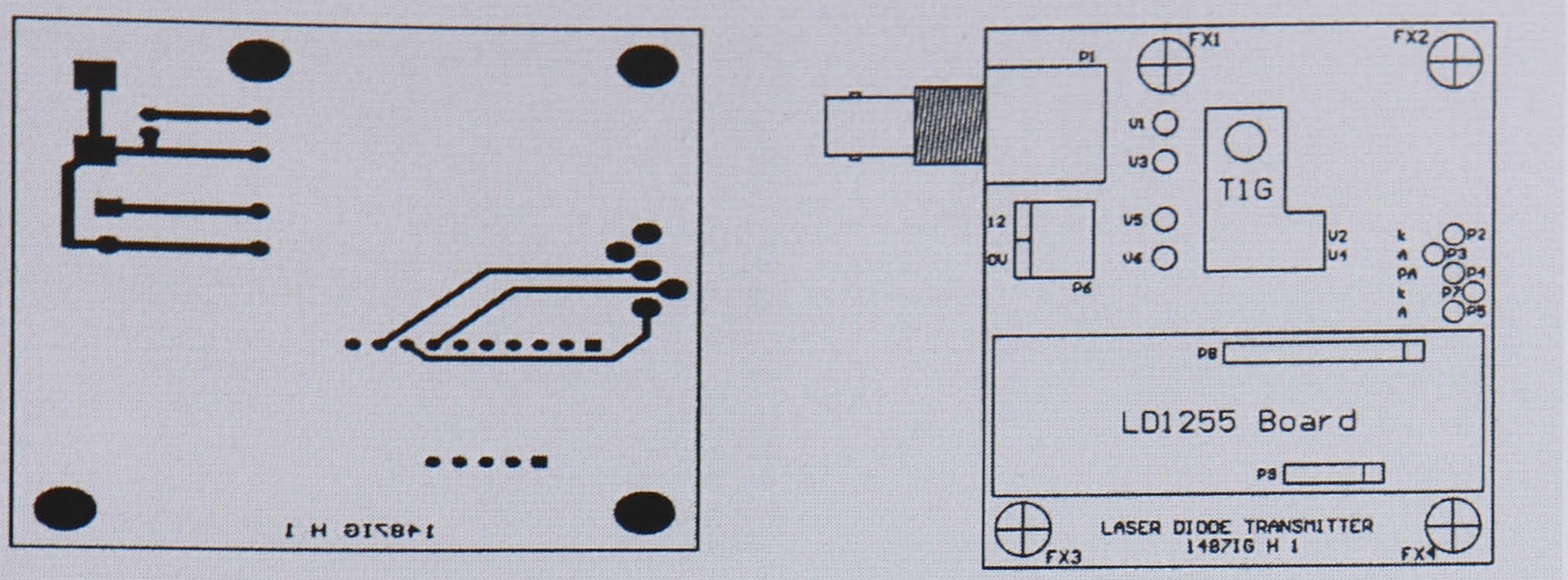

Figure : Transmitter layout

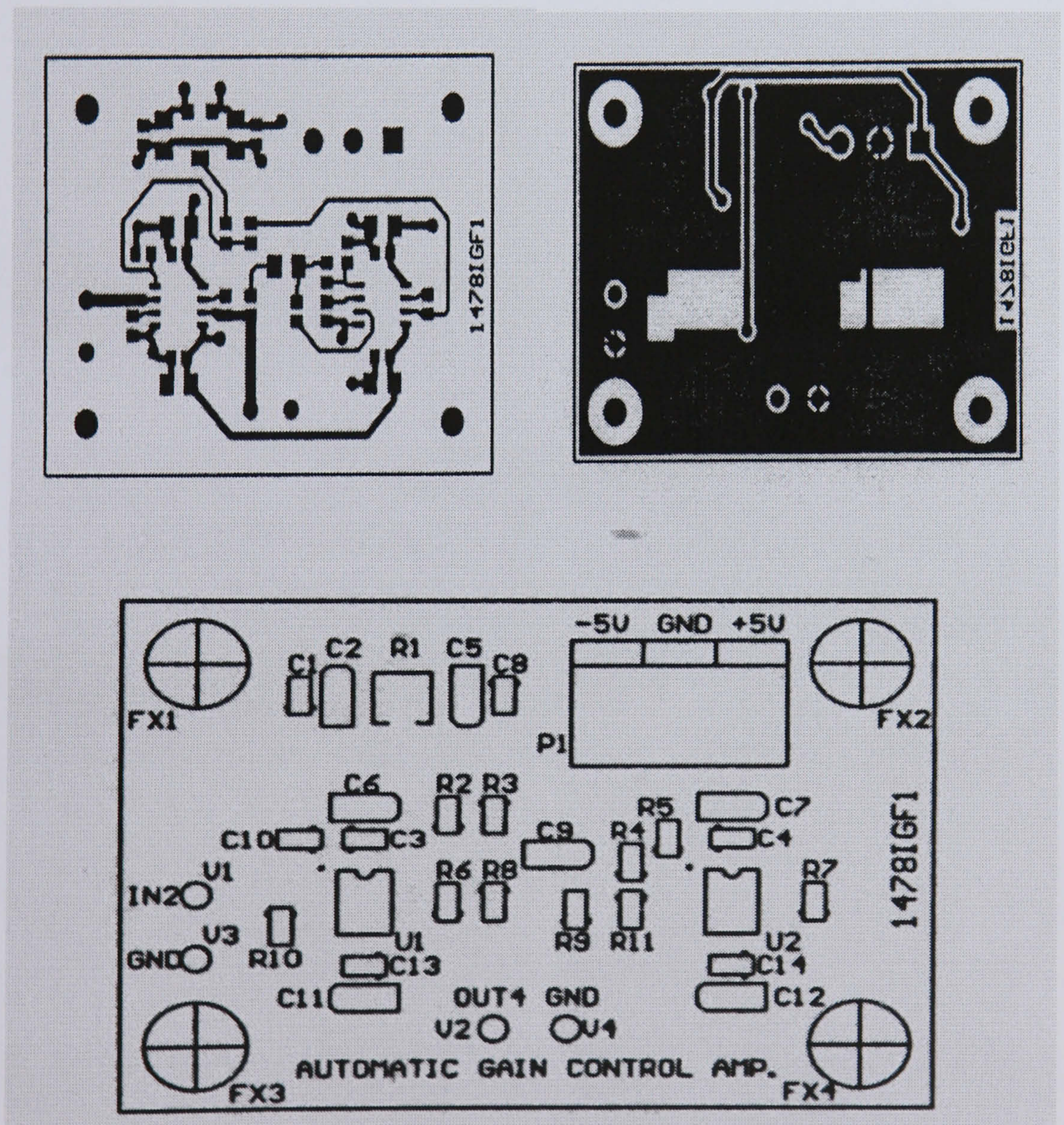

Figure : AGC circuit

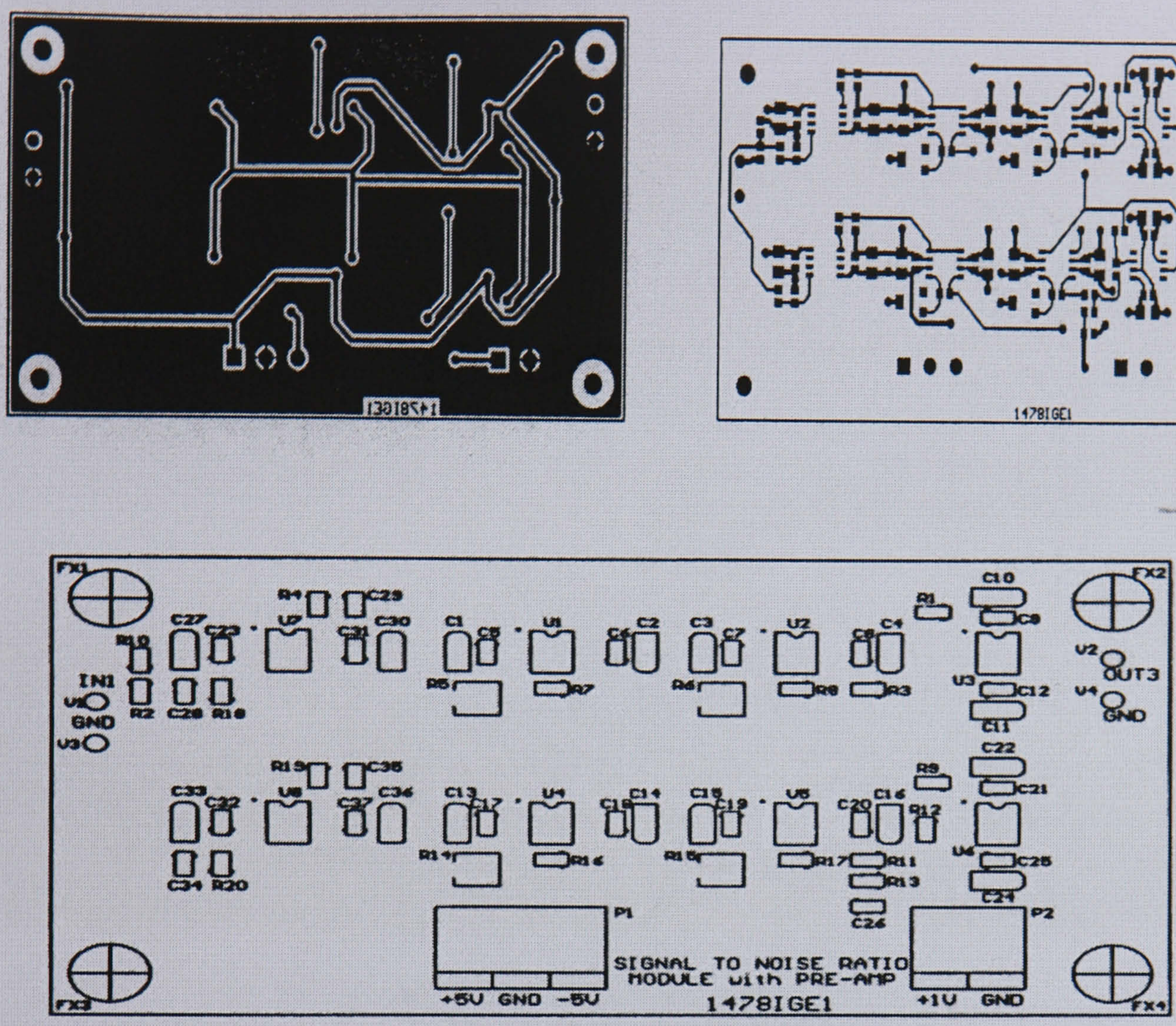

Figure : SNR circuit

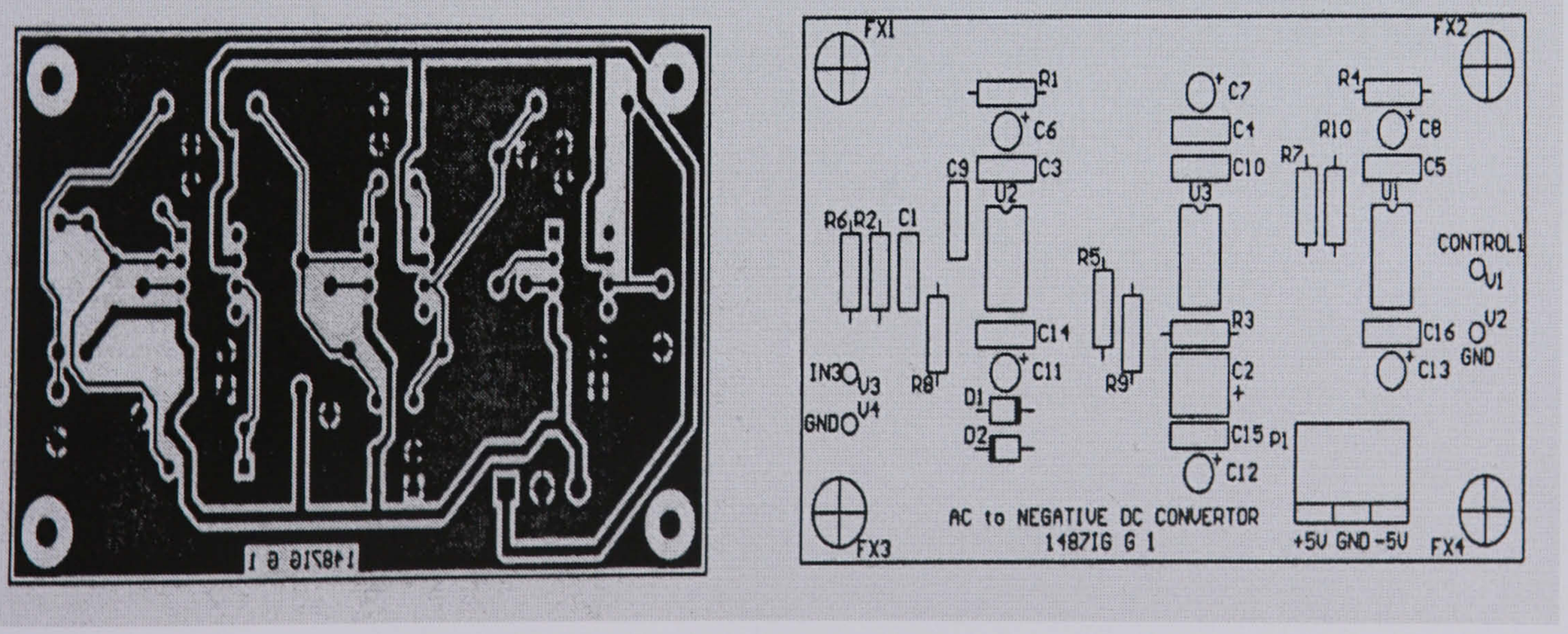

Figure : AC to DC circuit

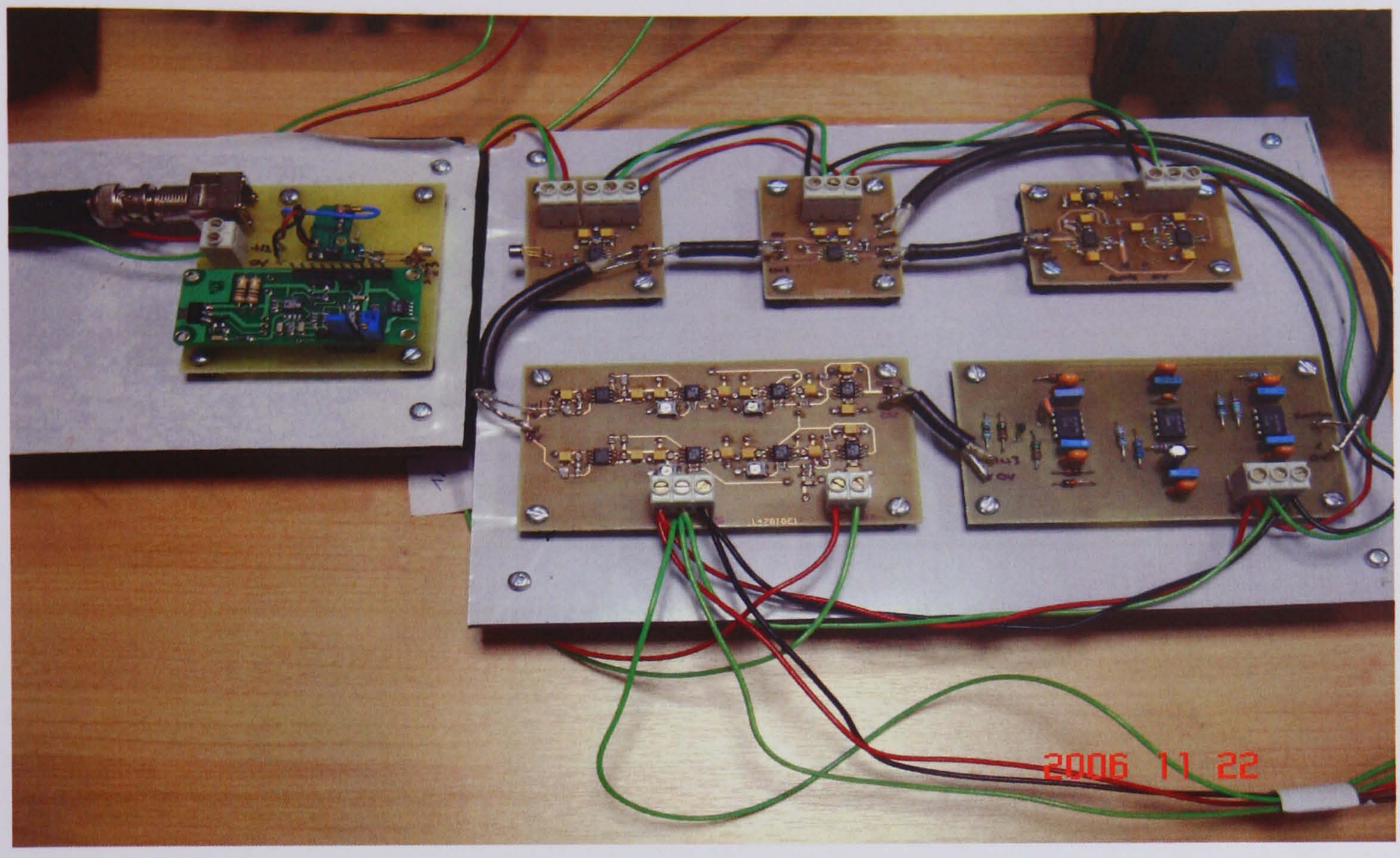

Figure : Design circuit layout

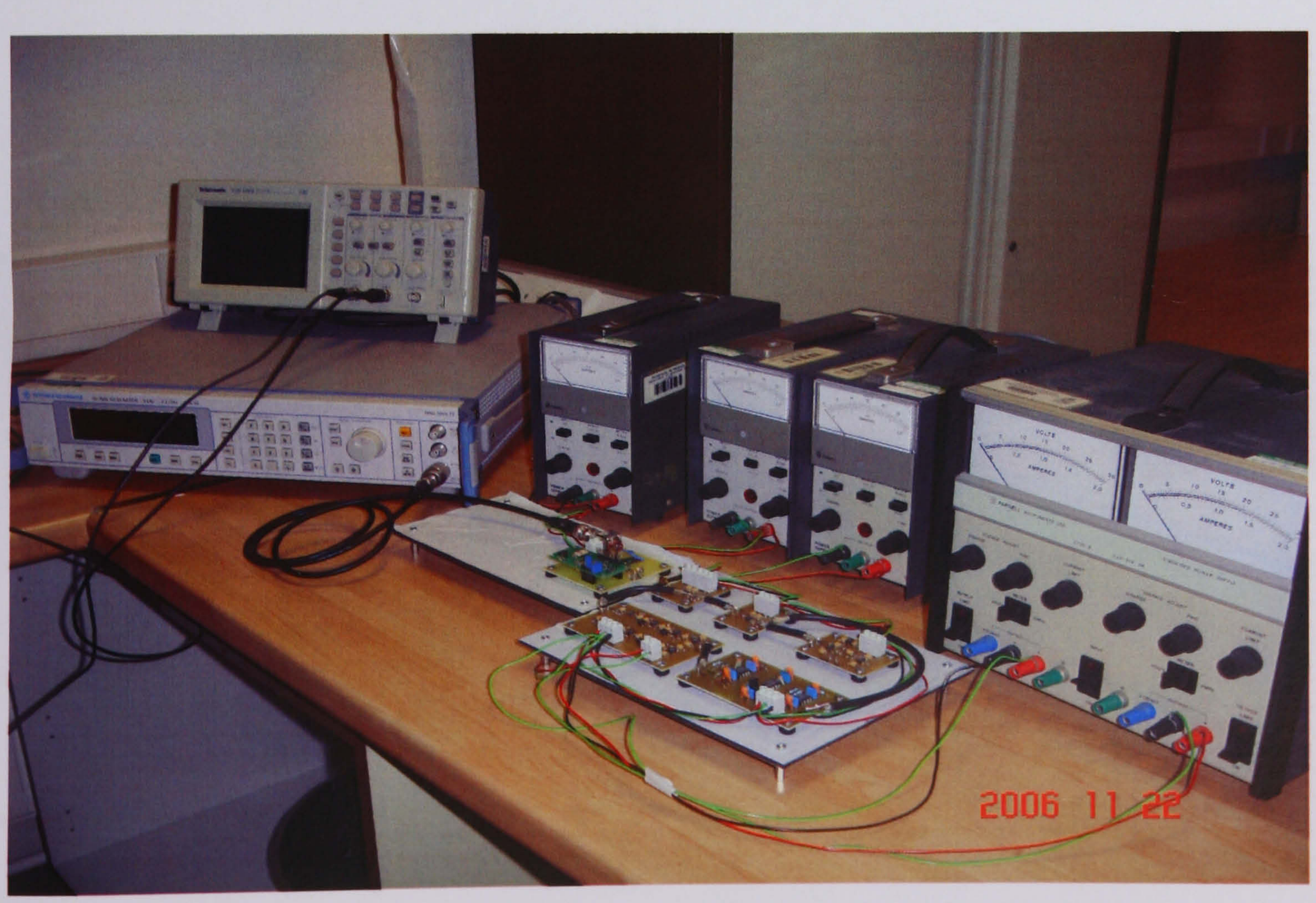

Figure : Experimental setup